Department of Chemical and
Environmental Engineering



University of Nottingham
UK | CHINA | MALAYSIA

Development of an artificial metalloenzyme from a nicotinamide-dependent enzymatic scaffold

Mattias Pascal Fabien Basle

A thesis submitted to the University of Nottingham
For the degree of Doctor of Philosophy

September 2019





Acknowledgment

Firstly, I would like to heartfully express my gratitude to my supervisors; Dr. Anca Pordea and Dr. Sebastiaan Winkler. Their constant support and patience throughout my PhD, alongside with their impressive knowledge, helped me to pursue my studies and research in the best possible conditions. Their guidance during my time at the University of Nottingham and during the writing of this thesis was of great help. None of the work presented below could have been done without them, and I am extremely grateful to have them both as supervisors.

Besides my supervisors, I would like to thank Steve, Luca and Andrew for their patience and help regarding experimental work in the lab. I would also like to thank the Pordea group, past and present; Tim, Camille, Alanna, Simone, Floriane, Maria Leticia, Harry and Aziana for all the good moments and all the knowledges we shared throughout this 4-years long journey.

A particular thank you goes to Simone and Floriane who helped me a lot with bioconjugation (section 5.3) and covalent docking (section 4.2) respectively. They avoid me a tremendous amount of problem by taking the time to transfer their knowledge for the benefits of this project.

In a broader range, I would like to thank the whole SPT. It was a constant pleasure to work alongside all these brilliant minds and to share some local beverages with them. A huge thank to the lab technicians, Amy and Rachel, who are constantly making sure I have all the materials required to do my job and kept me on my toes about cleanliness.

I would like to thank all the people I have met through climbing at Nottingham. Their laughs and support allowed me to cope with difficult aspects of this work.

To all my friends at home, I would like to thank you for all the time we spent together, all the laughs and all the food we had. A special thank you goes to Alexandre Chalvet, my best friend, who harassed me with phone calls to make sure I was fine and stayed focus on my research.

Finally, to my family, I thank all and each one of you because you are too many for the individual hug you deserve. But I am glad to have you behind me at all time. A massive thank you goes to my parents; Francoise and Claude, and my two older brothers, Pascal and Arnaud.

To all the other persons I have met but not cited above, feel free to address a formal complaint as I should have mentioned you. Because every single person that I met during the last four years made me who I am today and made the following thesis to be what it is.

Abstract

Transfer hydrogenation reactions can yield a diverse range of chiral products to be used as such, or as building block for the synthesis of more complex molecules. Biocatalysts and artificial metalloenzymes (ArMs) are sustainable alternatives to chemical routes. ArMs are the result of the insertion of a metal ion or complex into a biological scaffold. Most of the ArMs use proteins as a biological hosts to provide a highly functionalised environment where reactants are brought together and activated in very specific ways. The incorporation of the metal catalyst provides a synthetic activity, not necessarily accessible by natural biocatalysts. Most of the ArMs are based on non-enzymatic scaffolds, containing large binding sites generally evolved to accommodate hydrophobic molecules. As such, their design requires efforts to improve the specific chemical reaction targeted.

Here we present the development of new ArMs that could be used as a biocatalytic platform for transfer hydrogenation reactions. In previous work, our group generated an artificial mutant of *Thermoanaerobacter brockii* alcohol dehydrogenase (TbADH) by bioconjugation of a piano-stool rhodium catalyst to cysteine 37 in the active site. In the present work, a computational design approach was used to investigate more suitable positions for the catalyst to be anchored within the catalytic site of the enzyme, using a covalent anchoring strategy. Four positions were found where thiol sidechains would be more accessible than the reported labelled position 37. Single cysteine mutations were prepared at those positions and compared with two other protein variants, where all but one native cysteine residues in the binding pocket were removed.

After optimisation of the bioconjugation process with three different ligands bearing a bidentate N-N motif, two enzymatic scaffolds were identified and used for the development of ArMs, using covalent anchoring of Rh and Ir complexes. Five different ArMs were subsequently created and their activity towards the regeneration of nicotinamide cofactors and derivatives was assessed. One mutant bearing a rhodium complex bound at position 243 showed catalytic activity for the reduction of nicotinamides, with a discrimination between the natural cofactors and their mimics. This ArM could

potentially be used in a cofactor recycling system compatible with both nicotinamide cofactors. Whilst some of the ArMs suffered from the dissociation of the Cp*Rh functionality from its complex, resulting in unspecific binding and catalysis, one of the constructs, possessing a Cp*Rh(bipyridine) catalyst, showed very promising results for the recycling of NADPH and of benzyl nicotinamide.

Besides a covalent anchoring approach, which requires tedious work for the development of ArMs, a supramolecular approach was also investigated, by taking advantage of one feature of ADH, their nicotinamide binding pocket. Benzyl nicotinamide derivatives were synthesised and their capacity to interact with two ADHs, in a similar fashion to their natural cofactor, was assessed with the aim of using these as anchors for synthetic metal catalysts into ADHs. The lack of interactions observed with both enzymes, TbADH and horse liver alcohol dehydrogenase (HLADH), suggested that more hydrophilic structures would be required to yield a suitable supramolecular anchor. To provide initial data for further investigation on the development of ArMs by supramolecular anchoring with ADH enzymatic scaffolds, two separate studies were performed *in silico*. The first one focused on the anchor structure and its capability to mimic interactions within the cofactor binding site and led to the design of three potential supramolecular anchors where the benzyl substituent was replaced with more hydrophilic functionalities. The second study focused on finding enzymatic scaffolds capable of accommodating the hydrophobic benzyl nicotinamide derivatives. This study led to three potential ADH candidates. To assess the validity of the computational models from the 2 studies, experimental work will be required.

Table of Contents

i

Acknowledgment ..... **i**

Abstract ..... **iii**

List of abbreviation ..... **viii**

1 Literature Review **1**

1.1 Artificial metalloenzymes as tools for biocatalysis 1

1.1.1 Background 1

1.1.2 Artificial metalloenzymes by metal substitution 2

1.1.3 Artificial metalloenzymes by dative anchoring 4

1.1.4 Artificial metalloenzymes by covalent binding 7

1.1.5 Artificial metalloenzymes by supramolecular anchoring 14

1.1.6 Conclusion 21

1.2 Transfer hydrogenation reactions 22

1.2.1 Background 22

1.2.2 Chemical catalysts for transfer hydrogenations 22

1.2.3 Biocatalysts for transfer hydrogenations 27

1.2.4 Cofactor recycling systems 34

1.2.5 Conclusion 39

1.3 Alcohol dehydrogenases, a superfamily of biocatalysts 40

1.3.1 Background 40

1.3.2 Mechanism of zinc-dependent alcohol dehydrogenases 42

1.3.3 Conclusion 45

2 Aim and objectives **46**

2.1 Overall aim 46

2.2 Objectives 49

2.2.1 Development of enzymatic scaffolds capable of covalently anchoring versatile ligands 49

2.2.2 Artificial metalloenzymes for the reduction of nicotinamide derivatives 49

2.2.3 Building an artificial metalloenzyme using a supramolecular anchoring approach 49

3 Materials and methods **51**

3.1 Materials 51

3.1.1 Chemical synthesis 51

3.1.2 Protein expression 51

3.1.3 Protein purification 52

3.1.4 Computational Studies 52
3.1.5 Site directed mutagenesis 53
3.1.6 Bioconjugation 53
3.1.7 Enzymatic assays 54
3.2 Methods to design an artificial metalloenzyme through a covalent approach 55
3.2.1 Chemical synthesis of ligands 55
3.2.2 Design of the library of cysteine mutants 58
3.2.3 Site directed mutagenesis 60
3.2.4 Expression and purification of TbADH mutants 62
3.2.5 Bioconjugation of protein with metal free ligands 63
3.2.6 Bioconjugate analysis 64
3.3 Method to build an artificial metalloenzyme using a covalent approach 66
3.3.1 Synthesis of metal complexes 66
3.3.2 Bioconjugation with metal complexes 70
3.3.3 Catalytic reduction of $NADP^+$ 71
3.3.4 Catalytic reduction of nicotinamide derivatives 71
3.4 Methods to design an artificial metalloenzyme through a supramolecular approach 72
3.4.1 Chemical synthesis 72
3.4.2 Expression and purification of wild-type ADHs 75
3.4.3 Determination of the catalytic activity of the enzymes 77
3.4.4 Impact of nicotinamide derivatives on the enzymatic activity 79
3.4.5 Determination of the inhibitory potential of the cofactor mimics 81
3.4.6 Molecular modelling study of ADHs and the cofactor mimics 81
4 Building an artificial metalloenzyme using the covalent binding approach 83
4.1 Background 83
4.2 Creation of a mutant library 85
4.3 Site directed mutagenesis 91
4.4 Expression and purification of single cysteine TbADH variants 91
4.5 Synthesis of brominated bidentate ligands 94
4.6 Bioconjugation of brominated ligands to TbADH mutants 97
4.7 Summary and Conclusions 105
5 Artificial metalloenzymes for the reduction of nicotinamide derivatives 107
5.1 Synthesis of metal-based ligands 107
5.2 Reduction of $NADP^+$ using the metal complexes 108
5.3 Bioconjugation of metal catalysts with the different mutants 109

5.3.1 Ellman's assay of ArMs 111
5.3.2 UV-Vis analysis of ArMs 112
5.3.3 ESI-MS of ArMs 114
5.3.4 ICP-MS of ArMs 116
5.4 Reduction of NADP+ using artificial metalloenzymes 118
5.5 Reduction of hydrophobic nicotinamide derivative compounds using metal complexes 119
5.6 Reduction of nicotinamide derivatives compounds using artificial metalloenzymes 121
5.7 Evaluation of unspecific binding of the metal catalysts 124
5.8 Effect of acids on compounds Bn-NAD and Bn-NAD-Ph 125
5.9 Summary and Conclusions 126
6 Artificial metalloenzyme design by supramolecular binding 129
6.1 Background 129
6.2 Expression and purification of wild-type His-HLADH and TbADH 130
6.3 Determination of the specific activity of His-HLADH and TbADH 131
6.4 Chemical synthesis 132
6.5 Determination of the activity of His-HLADH and TbADH using cofactor mimics 136
6.6 Determination of the inhibitory potential of nicotinamide derivatives 142
6.7 Molecular modelling study of ADHs and the cofactor mimics 143
6.8 *In silico* evaluation of new designs for supramolecular anchors 146
6.9 *In silico* screening of ADHs capable of accommodating anchors 150 and 151 156
6.10 Summary and Conclusions 160
7 Overall discussion 162
8 Summary, conclusions and future work 168
9 References 174
10 Appendices 192

List of abbreviation

(A)TH	(asymmetric) transfer hydrogenation
ADH	Alcohol dehydrogenase
ArM	Artificial metalloenzyme
bipyridine	5-(bromomethyl)-5'-methyl-2,2'-bipyridine
Bn-NAD	Benzyl nicotinamide
Bn-NAD-Ph	*N*-phenyl-benzyl nicotinamide
CmADH	*Candida magnolia* ADH
Cp*	1,2,3,4,5-pentamethylcyclepentadiene
DMSO-d_6	Deuterated dimethyl sulfoxide
DNA	Deoxyribonucleic acid
EDTA	Ethylenediaminetetraacetic acid
ER	Enoate reductase
ESI-MS	Electrospray ionisation mass spectrometry
EtOAc	Ethyl acetate
FMN	Flavin mononucleotide
GC-FID	Gas chromatography - flame ionization detector
Hex	Hexane
His-tag	Hexahistidine tag
HLADH	Horse liver ADH
HPLC	High performance liquid chromatography
IC50	Inhibition concentration 50 %
ICP MS	Inductively coupled plasma MS
ITC	Isothermal titration calorimetry
KpADH	*Kluyveromyces polyspora* ADH
LDR	Long chain reductase
m/z	Mass to charge ratio
MDR	Medium chain reductase
MeCN	Acetonitrile
MeOH	Methanol
Methanol-d_4	Deuterated methanol
MWCO	Molecular weight cut-off
NAD^+/NADH	Nicotinamide adenosine dinucleotide oxidised/reduced form
$NADP^+$/NADPH	NAD phosphate oxidised/reduced form
NMR	Nuclear magnetic resonance
OD (OD_{600})	Optical density (measured at 600 nm)
OH	Hydroxyl group
PDB	Protein data bank
phenanthroline	5-(2'-bromo)-acetamido-1,10-phenantrholine
ppm	Parts per million
Rf	Retardation factor
rpm	Rotation per minute
SDR	Short chain reductase

SDS-PAGE	Sodium dodecyl sulfate - polyacrylamide gel electrophoresis
sulfonamide	*N*(-2-aminoethyl)-4-(bromomethyl)benzenesulfonamide
SyADH	*Sphingobium yanoikuyae* DSM 6900 ADH
TbADH	*Thermoanaerobacter brockii* ADH
TFA	Trifluoroacetic acid
TOF	Turnover frequency
Tris.HCl	Tris(hydroxymethyl)aminomethane chloride
U	Unit of activity = µmol of substrate per minute
U.mg-1	Specific unit of activity = µmol of substrate per minute per mg of enzyme
UV-Vis	Ultraviolet and visible light
WT	Wild-type

1 Literature Review

1.1 Artificial metalloenzymes as tools for biocatalysis

1.1.1 Background

A metalloenzyme is an enzyme that contains at least one metal ion cofactor. The ion can either play a role in the stabilisation of the structure of the enzyme (structural ion) or can be part of the catalytic mechanism of the enzyme (catalytic ion). A good example of the implication of metal ions within enzymes is the carboxypeptidase T (Figure 1.1). Whilst the zinc ion is involved in the catalytic hydrolysis of C-term amino acids of polypeptide, 4 calcium ions are spread throughout each subunit, stabilising the whole structure, thus providing high thermostability.

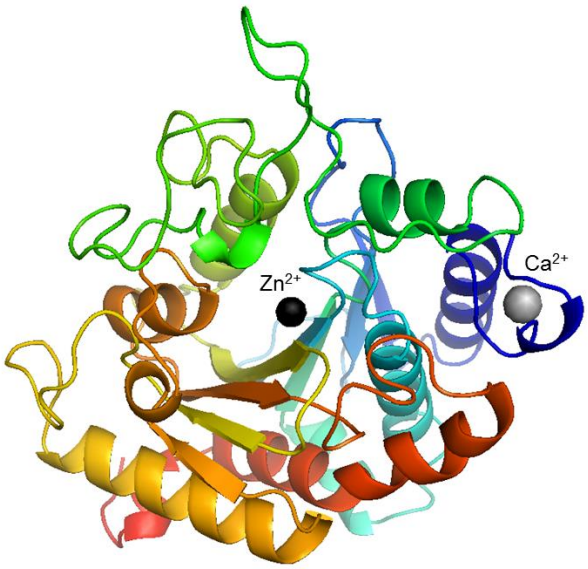


Figure 1.1. Crystal structure of the carboxypeptidase T (PDB entry 1OBR). A structural calcium ion is shown in grey while the catalytic zinc ion is shown in black. This enzyme highlights the two different roles of metal ions within a protein.[1]

Chemical synthesis makes good use of late transition metals to access challenging reactions. On the other hand, natural metalloenzymes mainly contain first row transition metals,[1-6] as depicted with the above example.

Enzymes are valuable catalysts due to their high control over the environment in which the reaction is performed. Metal ions are either coordinated with side chains of specific residues or embedded within a cofactor with non-proteinogenic ligands that are bioconjugated to the protein; in both of these

cases, the coordinating functionalities from the first coordination sphere governing catalytic activity. On the other hand, the precise amino acid sequence of the enzyme surrounding the metal complex provides a chiral environment that acts as a second coordination sphere. The features present in this sphere are directed for a precise control of the interactions involved in the stabilisation of the catalytic species, such as H-bonding or π-staking.

By introducing non-native metal ions in their structure, proteins and enzymes can access new, non-natural chemical reactions. This combinatorial approach makes use of the controlled environment of enzymatic cavities and the reactivity of metal catalysts. The resulting product of such combination is called an artificial metalloenzyme (ArM).[7]

Four different strategies can be applied to insert a non-native metal ion within an enzyme: metal substitution, dative anchoring, covalent binding and supramolecular anchoring (Figure 1.2).[7-9]

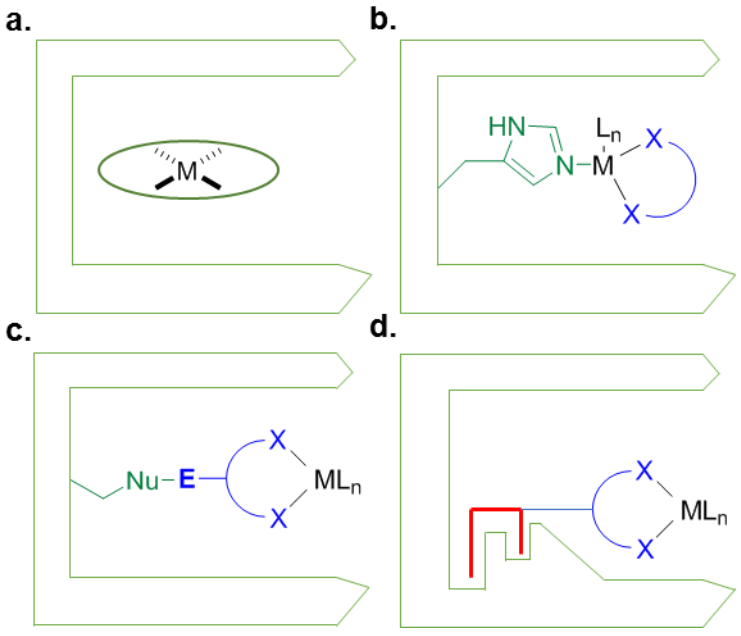


Figure 1.2. Representation of the four strategies to build an artificial metalloenzyme: a. metal substitution, b. dative anchoring, c. covalent binding and d. supramolecular anchoring. The following colour codes were applied: the enzymatic scaffold (green), the supramolecular anchor (red), the spacers and ligands (blue) and the introduced metal centre (black). M: metal centre, L_n: coordinated functional groups, X: coordinated atom from the ligand, Nu: nucleophile and E: electrophile. Modified version from Ward *et al*.[8]

1.1.2 Artificial metalloenzymes by metal substitution

This strategy consists in changing the chemical reaction that will be catalysed by replacing the natural metal ion with another one. This implies, however, that

the scaffold already possesses a metal-binding site. The metal is generally coordinated by side-chain functionalities of amino acids, such as cysteine, histidine, lysine etc.

First, the native metal ion is removed, yielding the metal free protein, called apoprotein. Then the desired metal ion, mainly in a salt form, is mixed with the apoprotein to form the desired ArM. This technique was first reported by Kaiser and co-workers in 1976 using carboxypeptidase A (Figure 1.3).[10] The zinc-containing protein is a natural esterase/peptidase where the zinc acts as Lewis acid to activate the carbonyl functionality for hydrolysis. When the zinc was substituted by a copper ion, the enzyme could no longer exhibit its natural activity towards esters. However, the enzyme could oxidise the ascorbic acid **1** into dehydroascorbic acid **2**. The gain of the oxidase activity came from the copper ion, which was reduced from Cu(II) to Cu(I) in the process.

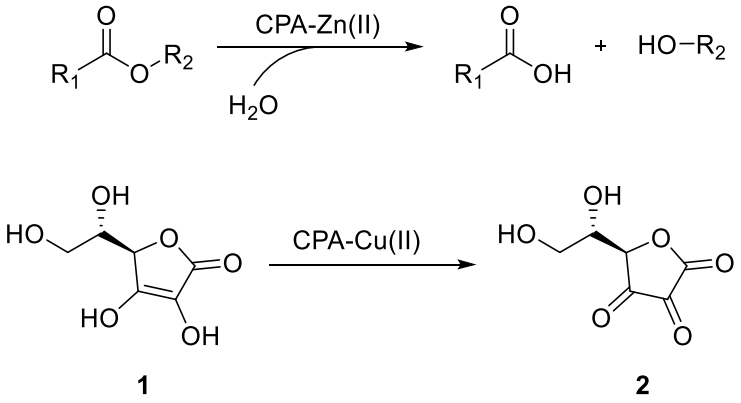


Figure 1.3. Metal substitution on the carboxypeptidase A (CPA) where the esterase activity conferred by the zinc ion was changed into an oxidoreductase activity by the substitution of a copper ion. Reproduced from Kaiser *et al*.[10]

A more recent example of ArM creation by metal substitution is the use of the zinc-dependent carbonic anhydrase (CA) as a scaffold to insert new metal ions. The crystal structure of the ArMs have been solved with Co(II), Cu(II), Ni(II) and Mn(II).[11] Mn(II) and Rh(I) substitution in CA were tested upon non-natural reactions and were able to catalyse alkene epoxidation,[12] alkene hydrogenation,[13] and alkene hydroformylation (Figure 1.4).[14] In these cases, the carbonic anhydrase provided an environment that allowed a control of enantio-, chemo- and regioselectivity that the metal salt complexes could not provide.

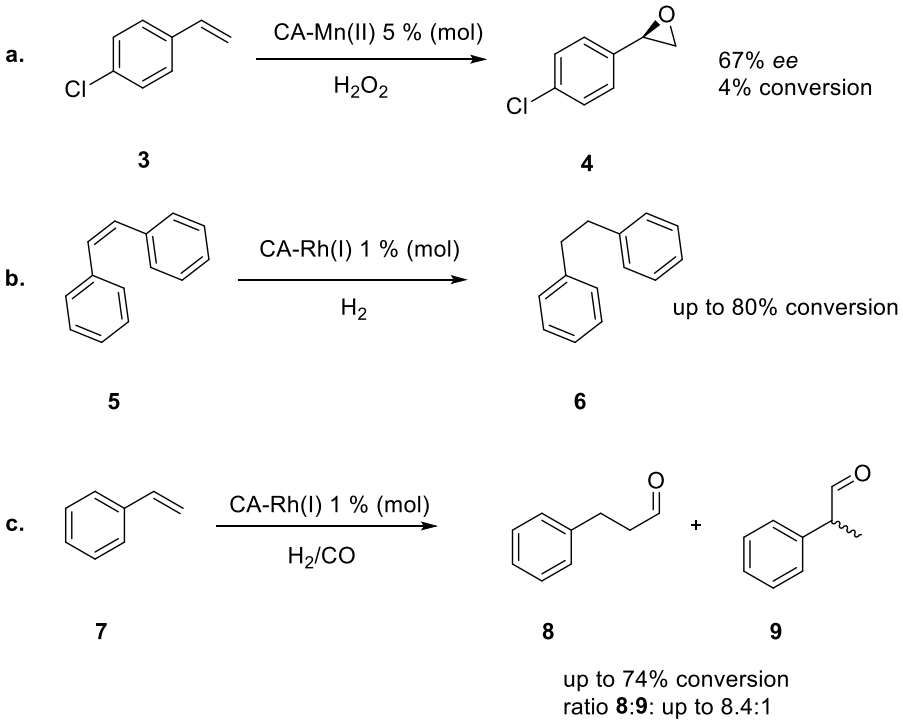


Figure 1.4. Different catalysis carried out with a metal substituted CA. a. Enantioselective epoxidation of *p*-chlorovinylbenzene **3**;[12] b. hydrogenation of *cis*-diphenylethene **5**; [13] and c. hydroformylation of vinylbenzene **7**.[14] Only the main reactions studied in the various published work are shown.

Although challenging reactions were carried out by substituting the native metal of a metalloenzyme, this strategy possesses several limitations. First, this strategy can only be applied to native metalloenzymes, thus reducing the number of available protein scaffolds. Similarly, if the metal ion cannot be removed or if the apoprotein is not stable, the addition of another metal ion is not feasible. Finally, some metal ion can be poisonous for the protein, damaging the integrity of the apoprotein. To circumvent these limitations, other strategies have been developed, starting with dative anchoring.

1.1.3 Artificial metalloenzymes by dative anchoring

This approach to build an ArM is quite similar to metal substitution, however it can be applied to protein others than metalloenzymes. Compared to the previous strategy, introduction of coordinating amino acids to create a metal-binding site is required.

A good example is the work done by Reetz *et al.*[15] In their study, they used the synthase subunit of imidazole glycerol phosphate synthase (tHisF). This thermostable enzyme possesses a TIM-barrel secondary structure that offers a large cleft. Diels-Alder cycloaddition is a reaction that involves large

hydrophobic substrates, and the large cleft made the enzyme suitable to carry out such reaction. The team then engineered a metal-binding site by site-directed mutagenesis. They initially used the aspartic acid in position 11 to act as an oxygen ligand for coordination with the copper ion. From this position they evaluated that leucine 50 and isoleucine 52 were at a suitable distance (ca. 4-5 Å) from position 11 to provide the 2 nitrogen ligands once mutated into histidine. However, to avoid any unspecific binding of the copper ion, they mutated the cysteine in position 9, as well as the 4 histidine residues present in the WT in positions 84, 209, 228 and 244.

The resulting mutant (C9A, L50H, I52H, H84A, H209A, H228A, H244A) was capable of coordinating a copper(II) ion *via* the two histidine (H50 and H52), the aspartic acid 11 and a water molecule, while the cleft offered spatial restrictions that led to improved stereoselectivity. The newly formed ArM was then tested upon the cycloaddition of azachalcone **10** and cyclopentadiene **11**, yielding the cycloadduct **12** mainly in the *endo* configuration (Figure 1.5).

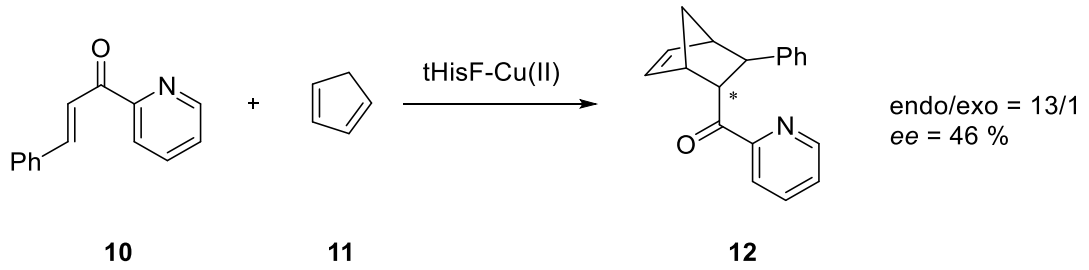


Figure 1.5. Diels-Alder cycloaddition of azachalcone **10** and cyclopentadiene **11** catalysed by tHisF-Cu. Only the main product **12** was depicted.[15]

Another example is the work achieved by Roelfes' team. The team extensively studied the lactococcal multidrug resistant receptor (LmrR) as a protein scaffold for artificial metalloenzymes.[16-25] This receptor is naturally present as a dimer. The interface of this dimer provides a very large hydrophobic pocket that can be finely tuned to accommodate both a metal complex and the desired substrate to perform chemical reactions. Insertion of the unnatural amino acid called bipyridine-alanine (Bpy-Ala, **16**) provides a bidentate ligand to coordinate a Cu(II) ion that can perform Lewis acid catalysis. A recent study of this complex showed the system used to carry out Friedel-Crafts alkylation of indoles (Figure 1.6).[26] The feasibility of this reaction was mainly due to the large available space at the interface (around 1400 $Å^3$), compared to a typical

enzymatic active site (600 Å^3 is considered large)[7, 27], which allows the enone **13** and the various indoles **14a-d** to react with each other.

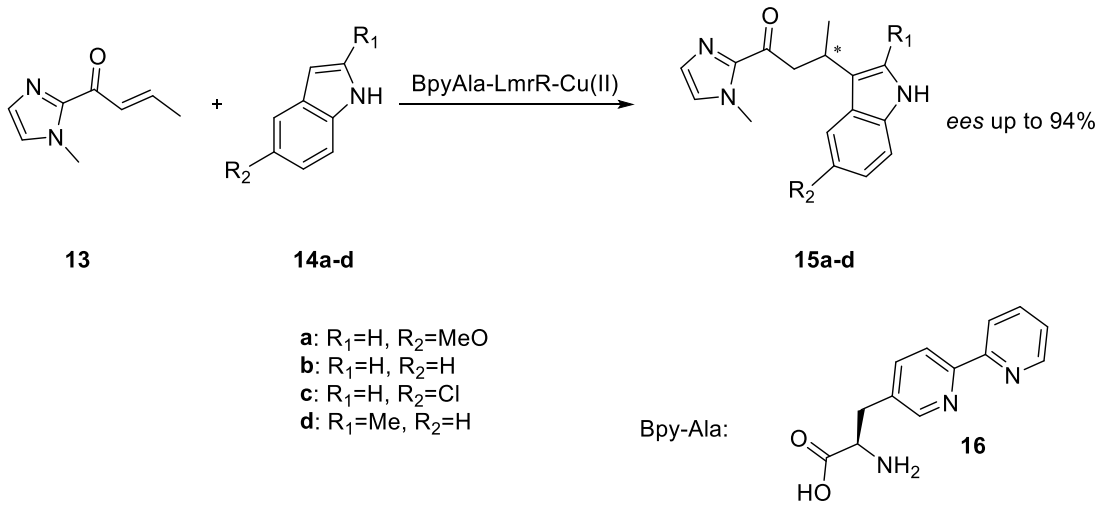


Figure 1.6. Friedel-Crafts alkylation of indoles **14a-d** with enone **13,** catalysed by the ArM BpyAla-LmrR-Cu(II). Reproduced from Drienoska *et al*.[26]

Compared to the metal substitution approach, dative anchoring can be performed on any scaffold. However, the use of metal salts, which are soluble in water and non-poisonous to the protein scaffold, is required. Moreover, the 1st coordination sphere around the metal catalysts is also limited to functionalities that can be encoded genetically, which restricts their reactivity. The complexation of poisonous metal ions before inserting them within the ArM can circumvent this problem. Lewis and co-workers developed an unnatural amino acid, *p*-azido-phenylalanine **17** (Az, Figure 1.7).[28] They used it to insert an azide moiety within the protein cavity. By using a constrained alkyne bearing a metal complex **18**, a metal-free 1,3-cycloaddition (or click reaction) can be carried out, thus incorporating the metal complex within the enzyme.

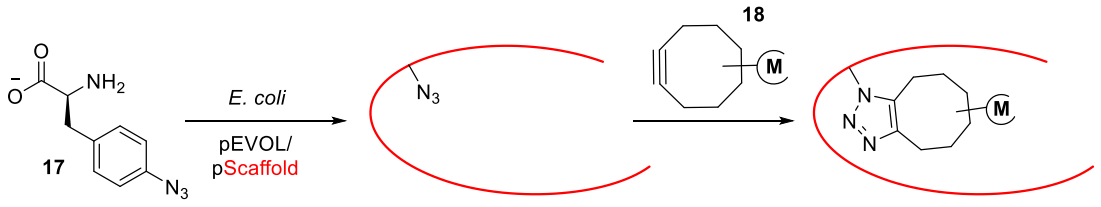


Figure 1.7. Insertion of *p*-azido-phenylalanine **17** into a protein scaffold (red) and the subsequent 1,3-cycloaddition between the azide and the alkyne moieties. This example was inserted in this section based on the modified scaffold where a metal binding site was created prior to any conjugation process, as expected from the dative anchoring strategy. Reproduced from Yang *et al*.[28]

However, to reach a broader range of metal complexes to be inserted within the ArM, two powerful strategies have been developed: covalent binding and supramolecular anchoring.

1.1.4 Artificial metalloenzymes by covalent binding

Some residues such as cysteine or histidine possess nucleophilic substituents in their side chains. By adding an electrophile moiety to a metal complex, a covalent bond can be formed between the electrophile and the nucleophile, locking the metal complex within the enzyme. This strategy is called covalent binding.

Two basic requirements must be fulfilled to use this approach. A uniquely reactive residue must be contained within the protein scaffold to avoid binding of several catalysts in the ArM. Therefore, knowledge about the scaffold structure is crucial. Secondly, to accommodate both the chemical catalyst and the substrate(s), enough space must be provided by the scaffold.

Initial developments have been reported by Kaiser's group on hydrolases, more specifically on the cysteine proteinase papain.[29-31] These well characterized and easy to purify flavin-dependent enzymes naturally possess a single cysteine residue at position 25 in their catalytic site, offering an ideal scaffold to develop the covalent modification of enzyme. Therefore, by developing flavin-derivatives bearing an electrophile moiety, they successfully obtained a papain with a covalently attached cofactor.

The promising results led other teams such as Reetz,[32-33] Salmain[34-35] or Kamer[36] to develop new chemical moieties to conjugate with cysteine residues of other protein scaffolds possessing single cysteines (Figure 1.8).

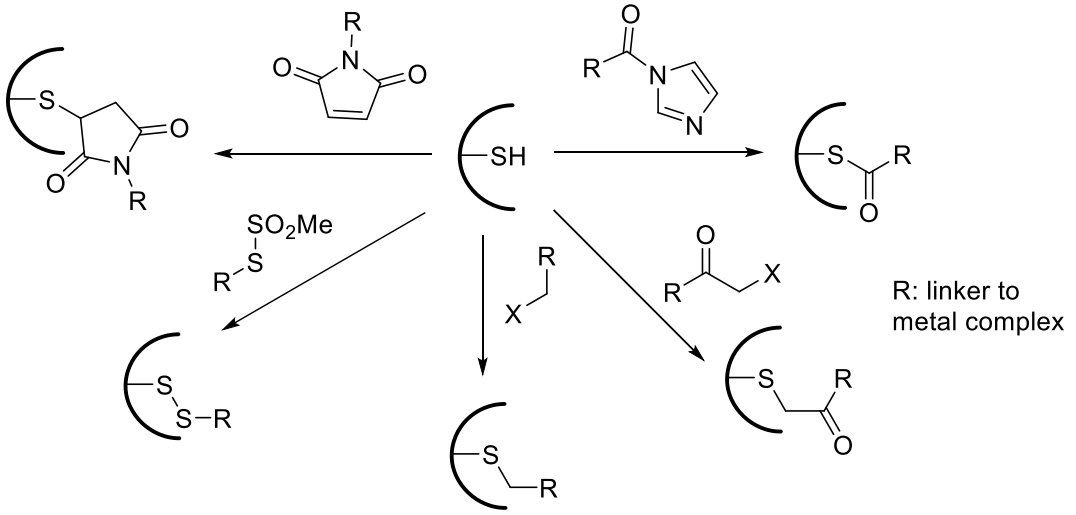


Figure 1.8. Various moieties used to covalently bind to cysteine residues. Reproduced from Pamies *et al*.[9]

Distefano's team was the first one to report the application of such ArMs in catalysis.[27, 37] Their work focused on the adipocyte lipid binding protein (ALBP), a carrier protein for fatty acids. The crystal structure of this protein was solved with various lipid-like structures by Banaszak's team.[38-41] Amongst other features, the carrier protein possesses a relatively large cavity (600 $Å^3$) as well as a single cysteine residue within the cavity at the position 117, making it a suitable candidate for the development of an ArM.

The cysteine residue was targeted by iodoacetamido-1,10-phenanthroline to yield the metal free protein ALPB-Phen (Figure 1.9). The resulting hybrid was then mixed with copper salts to yield the desired ArM. The metalloenzyme was then used to catalyse the hydrolysis of esters and amides. The ArM was capable of binding various esters and amides with great affinity which improved the overall catalytic efficiency of the copper centre by 5-fold towards esters and up to 1 600-fold towards amines. Interestingly, the ArM was also capable of catalysing the hydrolysis of an array of inactivated amino esters **19a-f** into their corresponding amino acids **20a-f** whilst being relatively stereoselective.

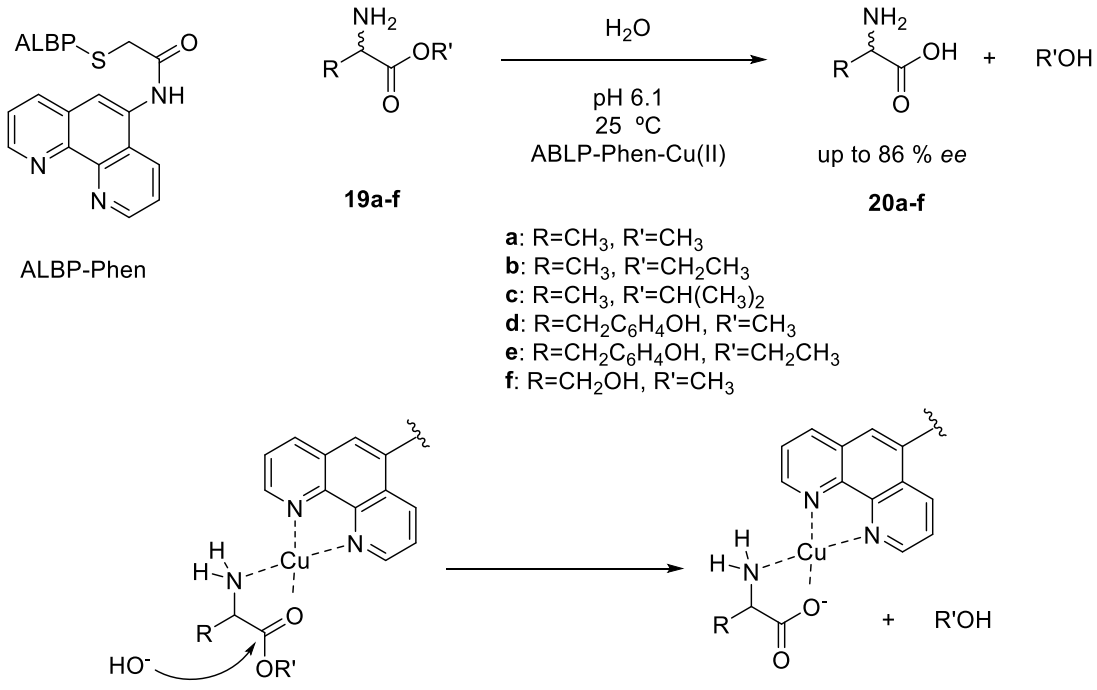


Figure 1.9. Inactivated ester hydrolysis using ALBP-Phen-Cu(II). The mechanism involved in the activation of the ester for subsequent hydrolysis is depicted underneath the reaction scheme. Adapted from Davies *et al.*[37]

The team then developed another ArM based on the same protein scaffold with a different ligand. The resulting ArM displayed transaminase activity.[27] Following the efforts of Distefano's team, Reiner *et al.* later developed an artificial ketoreductase based on papain scaffold (Figure 1.10).[42] The ArM displayed a good substrate scope towards acetophenone derivatives with up to 89 % yield on the reduction of 2,2,2, trifluoroacetophenone **21** into its alcohol counterpart **22**, although with moderate enantioselectivity (24 % (*R*)). This enantioselectivity, however, could be increased at the expense of the yield as proven by the reduction of *p*-chloroacetophenone **23** where 64 % *ee* (*R*) was reached over 12 % yield.

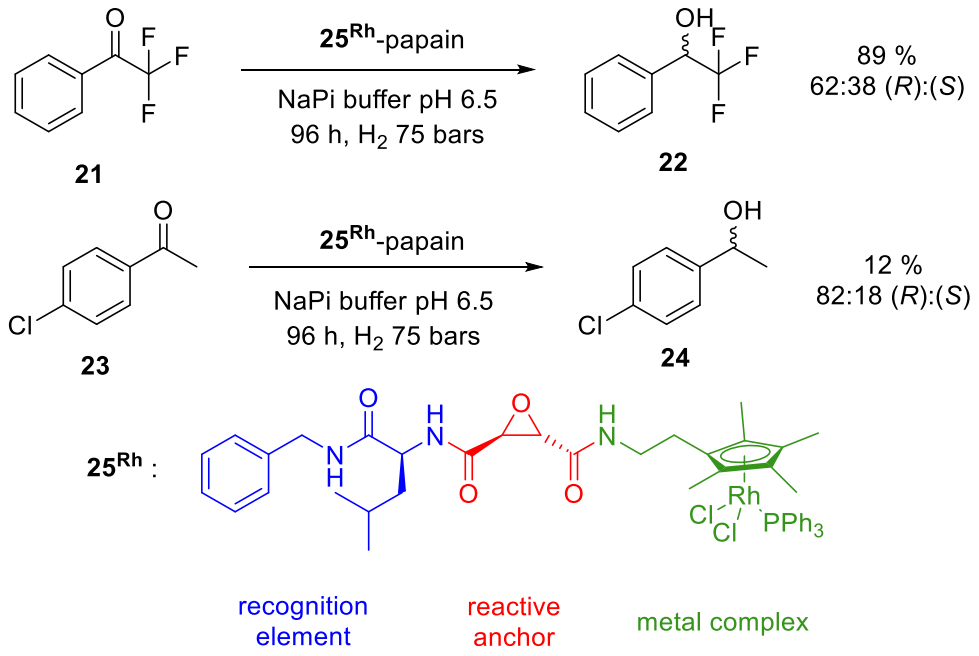


Figure 1.10. Reduction of acetophenone derivatives with Rh-based metallopapain. The two examples depicted are the best results in term of yield (**21**/**22**) and enantioselectivity (**23**/**24**). The three distinct part of the metal catalyst where highlighted in blue for the recognition element, red for the reactive group and green for the metal centre. Reproduced from Reiner *et al.*[42]

These results were achieved due to the innovative system developed by the team called metal-conjugated affinity labels (m-ALs). The m-AL can be split into 3 distinctive parts: 1) an achiral metal complex to bring the catalytic activity, 2) a reactive moiety to anchor the whole structure to the protein and 3) a recognition element to direct the binding orientation of the m-AL, thus improving the stability of the overall system. In the depicted example the achiral metal complex is a half-sandwich rhodium based one, the reactive moiety is the epoxide that will be open by the nucleophilic attack of the sulfur atom and the recognition element is a peptide mimic.

Whilst many efforts have been put into developing ArM in a covalent manner, the research illustrated above take advantage of already existing anchoring point. However, the natural occurrence of a single reactive residue, placed within the catalytic site is limited. To circumvent this limitation, researchers can insert the anchoring point genetically by mutagenesis. Distefano's team used this procedure to modify the position of the reactive cysteine in the intestinal fatty acid binding protein (IFABP) to expand its substrate scope towards ester hydrolysis.[43] More recently, Kamer's team developed a sterol carrier protein type 2 (SCP-2L) bearing a A100C mutation.[44-45] After bioconjugation with the

cysteine residue, the resulting ArMs displayed activity towards the hydroformylation of linear and branched alkenes and the regiospecific oxidation of lignin.

But the main advantage of this procedure is the expansion of the protein scaffold to be used. In this regard, the work performed by Ward's team[46] and Sauer *et al.*[47] on metathesis reactions catalysed by ArM showed the potential of the design and incorporation of non-natural reactive residues (Figure 1.11). Both teams used a second-generation Grubbs-Hoveyda catalyst[48-49] linked to either a bromoacetamide **26** or a maleimide moiety **29a-c** to react with a single cysteine residue, previously added by site-directed mutagenesis.

The former was linked to a small heat shock protein from *Methanocaldococcus jannashii* (MjHSP) by mutating the glycine at the position 41 into a cysteine[50-51] and used into the ring closure metathesis (RCM) of *N,N*-diallyl-4-toluenesulfonamide **27**. The catalyst alone displayed a turnover number (TON) of 33 turnovers but required 20 % (v/v) of *t*-butanol into the buffer to be active. On the other hand, the ArM, under the same conditions, displayed 25 turnovers without supplementation of a co-solvent into the aqueous buffer. At the exception of the use of ultrasound,[52] this system was the first reported as olefin metathesis catalysed without co-solvent.

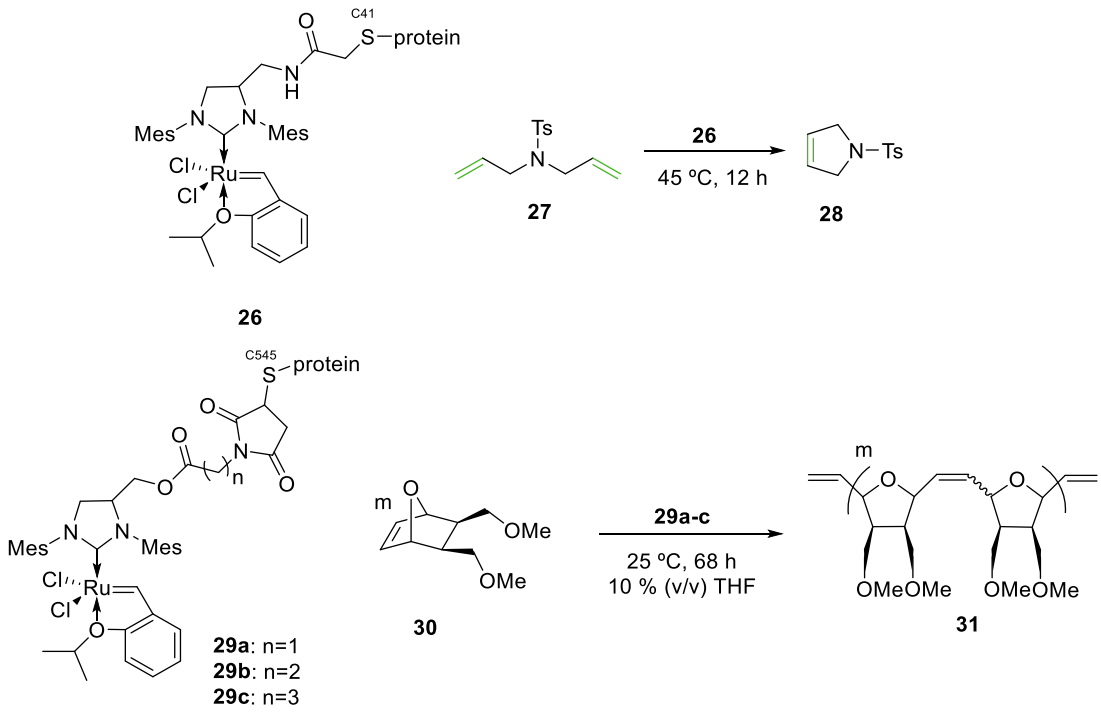


Figure 1.11. 2nd generation of Grubbs-Hoveyda catalyst inserted into protein for metathesis catalysis. The catalyst was used for ring closure metathesis and ring-opening metathesis polymerisation. Reproduced from Mayer *et al*. and Sauer *et al*.[46-47]

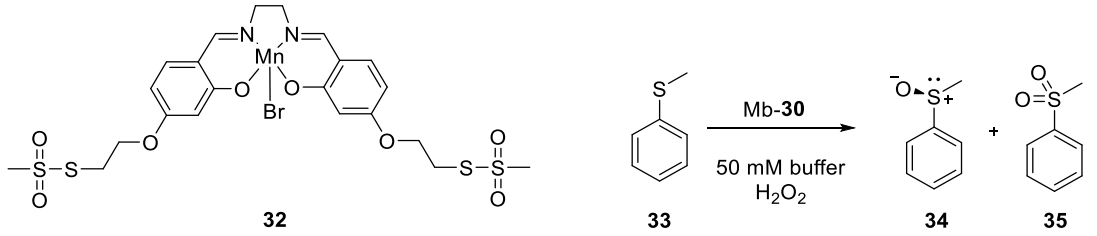
The second catalyst was developed with linkers of different sizes and applied to ring-opening metathesis polymerization (ROMP), using a modified variant of the transmembrane β-barrel protein ferric hydroxamate uptake protein component A (FhuA) from *E. coli* bearing the L545C mutation. This highlighted the importance of the second coordination sphere interactions provided by the protein scaffold. Indeed, the position 545 was chosen based on the hypothesis it would provide a conformationally stable environment.[53] In this context, the catalyst alone yielded a polymer with 50/50 *cis*/*trans* isomers with 990 turnovers. Once embedded, the selectivity went up to 58/42 *cis*/*trans* with 550 turnovers (**29a**).

These two designs showed the versatility of reactions that can be catalysed by ArM built by covalent anchoring, when the anchoring point is selected by rational design and introduced by mutagenesis.

The team of Yi Lu, from the University of Illinois, improved the covalent anchoring approach by developing a system with two anchoring points, to precisely localise the metal centre (Figure 1.12).[54-56] Their work involved the use of manganese salen modified to be covalently bound to two cysteines.

The choices of cysteines position resulted from computational development using Insight III software. Two pairs of positions emerge from the *in silico* study: 72/103 and 39/72. The advantage of such catalyst is the geometrical similarity with the heme centre. The reduced flexibility brought by the 2 anchoring positions improved the selectivity of the system by fixing the location of the metal centre within the protein scaffold.

Using rational design, the team mutated residues within the heme cavity of myoglobin to insert the Mn-salen **32**. Initially, the single position 103 was evaluated and yielded the methyl phenyl sulfoxide **34** 12 % *ee* (*S*) at a rate of $51*10^{-3}$ min^{-1}. This single attachment already showed the importance of the metal location, as the catalyst free in solution yielded the product without selectivity, at a rate of $2.4*10^{-3}$ min^{-1}. Besides, the catalyst alone further oxidised the product into the sulfone **35** due to the lack of selectivity.



32 **33** **34** **35**

Mb-L72C.Y103C: 51% *ee* (*S*)
Mb-T39C,L72C: 60% *ee* (*S*), 100:0 **34**:**35**

Figure 1.12. Sulfoxidation of thioanisole **33** by Mn-salen anchored by two points within different myoglobin (Mb) mutants. Reproduced from Carey *et al.*[54]

When a second anchoring point was added at position 72, the selectivity went up to 51 % *ee* (*S*) at a rate of $390*10^{-3}$ min^{-1}. The additional anchor locked the geometry of the catalyst similarly to the natural heme core. Hence an increase of selectivity and rate was observed. However, some sulfone by-product was still observed. To overcome this problem, the anchoring points were changed to make use of a hydrophobic tunnel that can be used by the substrate. This tunnel was hypothesised to interact more with the thioanisole than with the sulfoxide, therefore preferentially allowing the substrate to reach the cavity occupied by the Mn-salen. The use of the double mutant T39C, L72C led to improved enantioselectivity with 60 % *ee* and full substrate recognition with 0 % overoxidation of the sulfoxide into the sulfone.

Overall, the covalent anchoring strategy allowed researchers to introduce abiotic catalysts to perform non-natural reactions while improving selectivity, rate, substrate scope or even reducing the use of co-solvent. However, this strategy requires the prior purification of the desired protein scaffold, the synthesis of the reactive group of the anchor and the conjugation of the complex within the enzyme. To reduce or avoid these steps, a final approach has been used by utilising intrinsic supramolecular forces between a protein scaffold and a desired chemical.

1.1.5 Artificial metalloenzymes by supramolecular anchoring

The last strategy to develop ArMs is called supramolecular anchoring. In this approach, the metal complex is linked to an anchor that uses supramolecular forces (e.g. hydrophobic forces, H-bonding, π-stacking, etc.) to maintain the whole structure in place within the enzyme. Over the last two decades, two main anchors were used depending on the reaction targeted: porphyrin and biotin.

The use of porphyrin and porphyrin derivatives comes from observation of nature. Heme (or haem) proteins such as haemoglobin possess a supramolecular structure (prosthetic group) within their cavity called protoporphyrin IX (Figure 1.13). This structure can coordinate with metals such as iron to develop a catalytic behaviour.

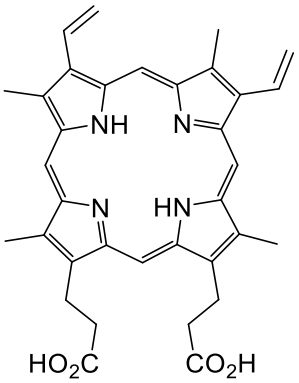


Figure 1.13. Structure of the protoporphyrin IX.

By finely tuning the structure, researchers have developed an array of ArMs based on metalloporphyrinoids inserted into heme proteins. To evaluate the feasibility of such approach, Hayashi and co-workers developed a Zn-based charged porphyrin **36a-b** (Figure 1.14),[57] which they inserted into myoglobin.

By modulating the number of charges held by the supramolecular structure as well as the nature of the charge itself (positive or negative) they showed that such approach yielded a stable ArM with a binding constant of $2.6*10^3$ M^{-1} and $1.5*10^5$ M^{-1} for the negatively (8^-) and positively (4^+) charged complexes, respectively.

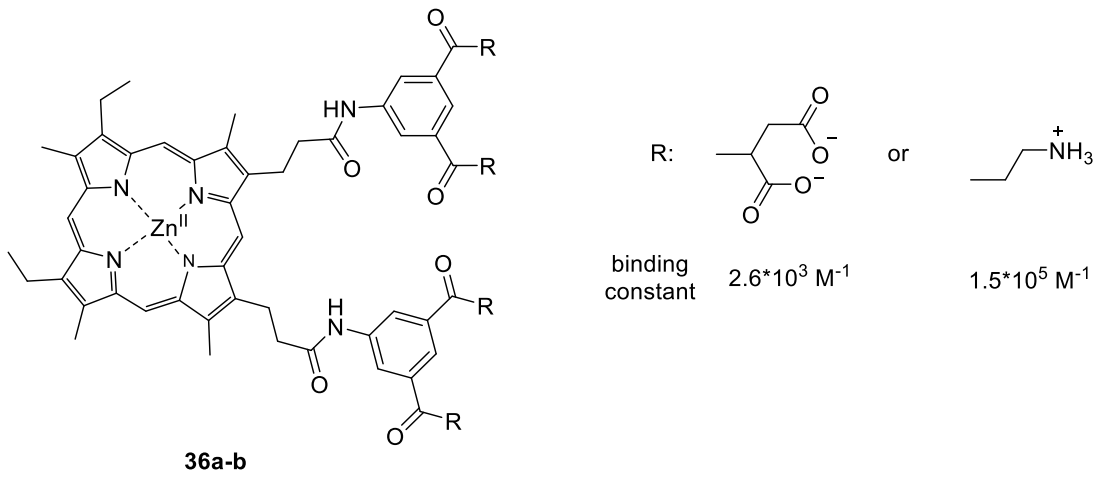


Figure 1.14. Modified porphyrin with charged groups for supramolecular anchoring within a myoglobin biomolecule.[57]

Using myoglobin, Watanabe's team initially focused on the impact of residues within the cavity towards supramolecular interactions.[58] They highlighted two myoglobin double mutants, L29H-H64L and F43H-H64L, which displayed various asymmetric oxidation reactions. Following this work, they decided to put effort into modifying the prosthetic moiety of the mutated myoglobin.[59] Similar to the work done by Carey and co-workers, described in the previous strategy, they synthesized the chromium salophen **37** to mimic the heme cofactor (Figure 1.15). Once inserted into the protein, the ArM was able to selectively oxidise thioanisole into its sulfoxide counterpart with modest turnovers and enantioselectivity.

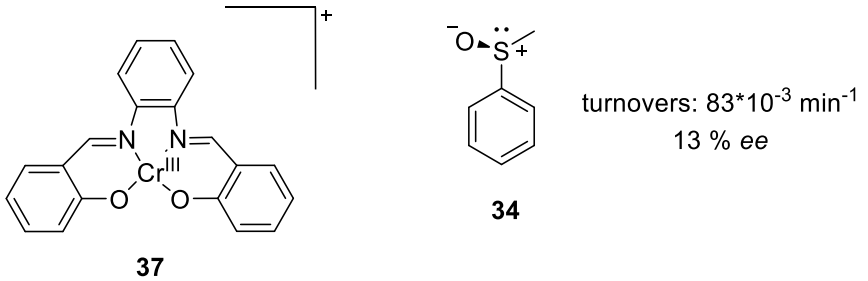


Figure 1.15. Chromium salophen catalyst **37** inserted into myoglobin double mutants to carry out the oxidation of thioanisole. Reproduced from Ohashi *et al*.[59]

More recently, Oohora and co-workers used myoglobin to insert a Mn-containing porphyrin (Figure 1.16).[60] In aqueous solution, the manganese ion within the prosthetic group is preferentially in its Mn^{III} oxidation state. However, using a strong peracid (*m*-chloroperoxibenzoic acid, mCPBA), they were able to oxidise it into Mn^{V}. This oxidation state proved to be stable within the protein and the resulting ArM underwent C-H bond hydroxylation reaction, producing 1-phenylethanol **40** from ethylbenzene **39**, an inert C-H bond bearer.

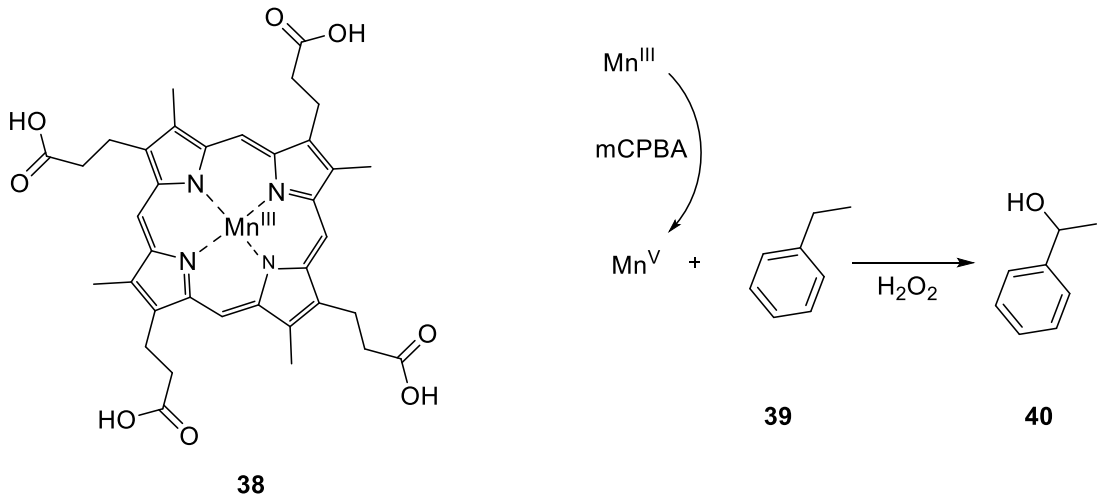


Figure 1.16. Manganese-containing porphyrin and the subsequent C-H hydroxylation of ethylbenzene after activation of the metal ion by the peracid mCPBA. Adapted from Oohora *et al*.[60]

From the viability of the system showed with myoglobin, researchers moved onto other heme-containing proteins. In 2016, Hartwig's team inserted an iridium ion into a protoporphyrin IX and anchored it within a CYP119, a protein from the cytochrome P450 family (Figure 1.17).[61] They used the conversion of diazoester **41** into dihydrobenzofuran **42** as a model reaction for the C-H functionalisation with creation of C-C bonds. Whilst at first the reaction yielded less than 10 % of the desired product, they used directed evolution techniques to improve the ArM efficiency to reach full conversion to **42** with 94 % *ee*. In parallel, they analysed the kinetics of the ArMs and provided evidence that the evolved ArM displayed kinetics similar to those of the natural enzyme.

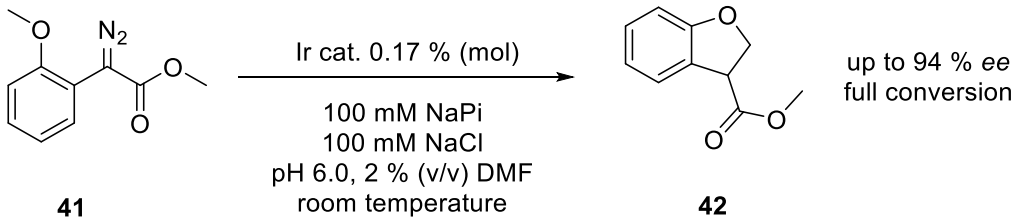


Figure 1.17. Conversion of diazoester **41** into dihydrobenzofuran **42** with Ir-CYP119. Reproduced from Dydio *et al*.[61]

More recently, Lu's team used cytochrome *c* to incorporate a [4Fe-4S] cluster linked to a porphyrin.[62] The resulting ArM catalysed the reduction of sulfite. Zunszain *et al*. and Rousselot-Pailley *et al.* used the human serum albumin (HSA) as a protein scaffold to insert a modified heme. The artificial HSA showed an improved oxidation of thioanisole and other sulfides.[63-64] Ricoux *et al.* developed an artificial xylanase to perform various oxidation reactions.[65-66]

As shown above, porphyrin is a versatile structure to act as a supramolecular anchor. However, this system is rather limited in term of reaction scope. Most of the work described focused on oxido-reduction reactions. A second anchoring structure can be used, biotin (Figure 1.18). Biotin, or vitamin B_7, is a natural cofactor involved in different part of the human metabolism. This cofactor is also known to bond to (strept)avidin with a dissociation constant K_d of around 10^{-15} M, the strongest protein-ligand interaction known to date.[67]

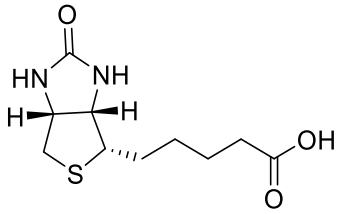


Figure 1.18. Representation of a biotin molecule.

By using the high binding affinity of this system, Wilson and Whitesides, in 1978, reported the introduction of a rhodium catalyst within this non enzymatic scaffold (Figure 1.19).[68] The structure of the reactive complex is divided in three parts: a) the biotin which acts as an anchor, b) a linker to space out the biotin from c) the metal complex that provides the reactivity. They mixed the reactive complex with avidin and applied the mixture to the reduction of α-acetamidoacrylic acid **44**. As they reached full conversion compared to the

metal complex alone in solution, they also observed modest enantioselectivity with 44 % *ee* (*S*) whilst the rhodium catalyst yielded a racemic product.

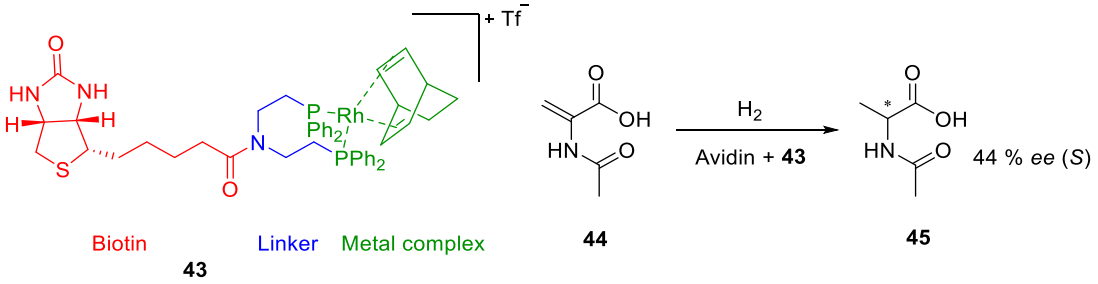


Figure 1.19. First biotin-Rh complex synthesized and its application to the asymmetric reduction of α-acetamidoacrylic acid **44** into α-acetylalanine **45**. Adapted from Wilson and Whitesides.[68]

However, this system did not bring so much attention within the scientific community at that time. The system did reappear in 1999 with the work of Lin and co-workers, using the avidin-biotin binding affinity to develop a new ArM (Figure 1.20).[69] The overall structure remained similar to what had been done two decades earlier, with the three distinctive parts. The team, however, modified the linker moiety. The particularity of the new linker allowed Lin *et al.* to access both enantiomers based on the intrinsic chirality of the phosphines. Although full conversion was achieved, very modest enantioselectivity was observed with 48.1 % and 15.5 % *ees* for the (*R*)- and (*S*)- enantiomer respectively.

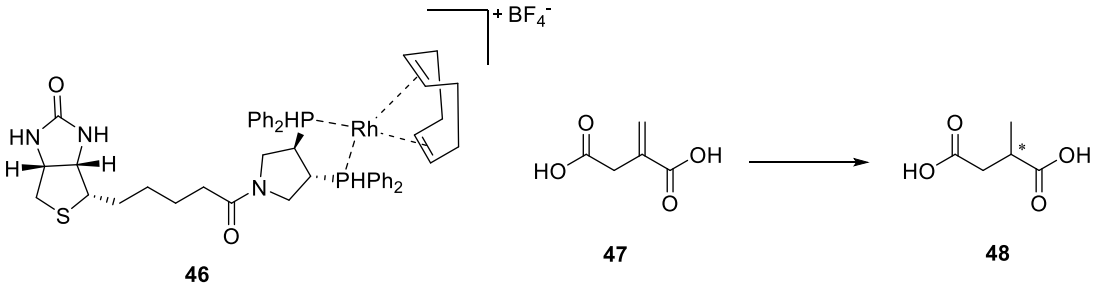


Figure 1.20. Second biotin-Rh complex **46** and its application to the asymmetric reduction of 2-methylenesuccinic acid **47** into 2-methylsuccinic acid **48**. H-source: H_2. Adapted from Lin *et al*.[69]

The most successful work so far with the biotin-(strept)avidin system has been reported by Ward and his team. Initially focusing on improving the Rh-catalysed hydrogenation of activated alkenes, they hypothesized the use of streptavidin would yield better results than the avidin.[70] Their initial thoughts were that streptavidin offers a larger cavity to reduce the steric hindrance around the metal centre. After extensive research the team developed an array

of catalysts and mutants to reach up to 96 % *ee* (*R*) and 91 % *ee* (*S*) with quantitative yields towards the reduction of α-acetamidoacrylic acid derivatives (Figure 1.21).[71-74]

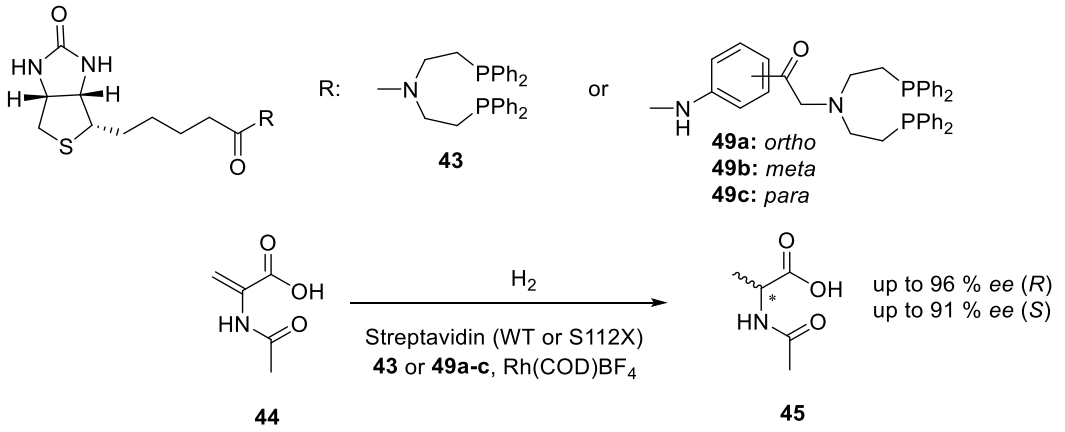


Figure 1.21. The various linker used by Ward's team towards the improvement of the reduction of α-acetamidoacrylic acid **44**. Adapted from Skander *et al.*[71, 73]

To reach such high yield and enantioselectivity, Ward and co-workers used site-saturated mutagenesis to improve the impact of the second coordination sphere on the reaction. Following the advance made in with the system, Ward's team then developed various combinations of mutants and metal complexes that were catalytically active towards different reactions such as allylic alkylation,[75-76] metathesis,[77-78] asymmetric C-H activation,[79] sulfoxidation,[80] and asymmetric transfer hydrogenation (Figure 1.22).[81-82]

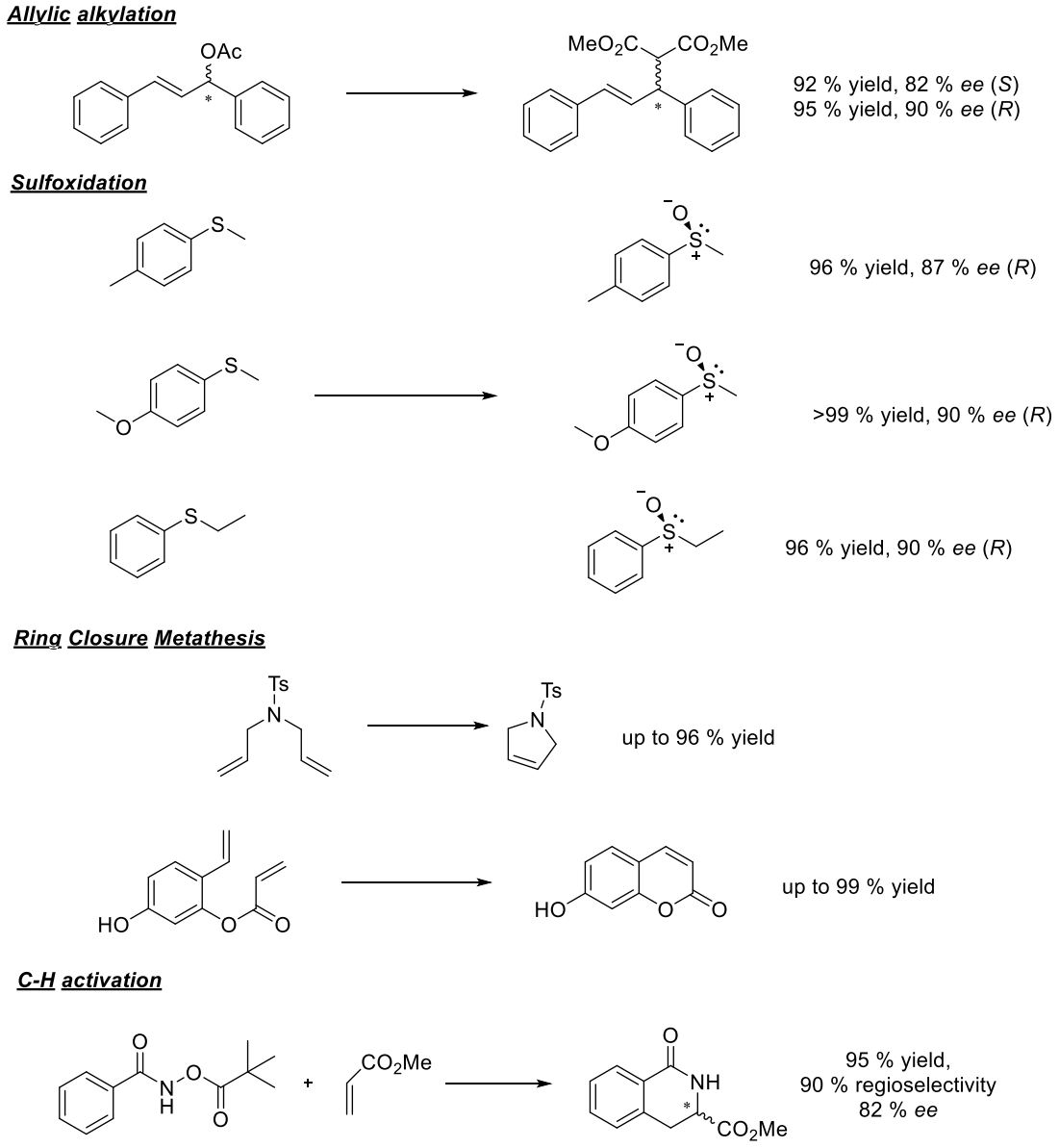


Figure 1.22. Various example of the reaction scope performed using biotin-(strept)avidin technology developed by Ward and co-workers. Adapted from Ward *et al*. [70, 75-79]

Besides developing the substrate scope on the biotin-(strept)avidin system, Ward and co-workers tailored the active site of the host protein to involve the biological scaffold in the activation of C-H bonds.[79] Their best result was obtained with the streptavidin double mutant S112Y-K121E where the aspartic acid acts in concert with the Rh(III) complex to yield dihydroisoquinolones (Figure 1.22) at a rate increased by almost 100-fold to their previously reported system.

Another key contribution of the biotin-(strept)avidin technology was the use of the host protein as a protective shell for cascade reactions. d^6-piano stools are

known to inactivate protein activity.[83] By developing an artificial transfer hydrogenase (ATHase) with a d^6-piano stool embedded within, the host protein act as a shield, allowing the combination with other biocatalysts for cascade reaction.[84] This led to development of various cascade reactions, including the double stereoselective deracemization of amines **51** and **52** (Figure 1.23).

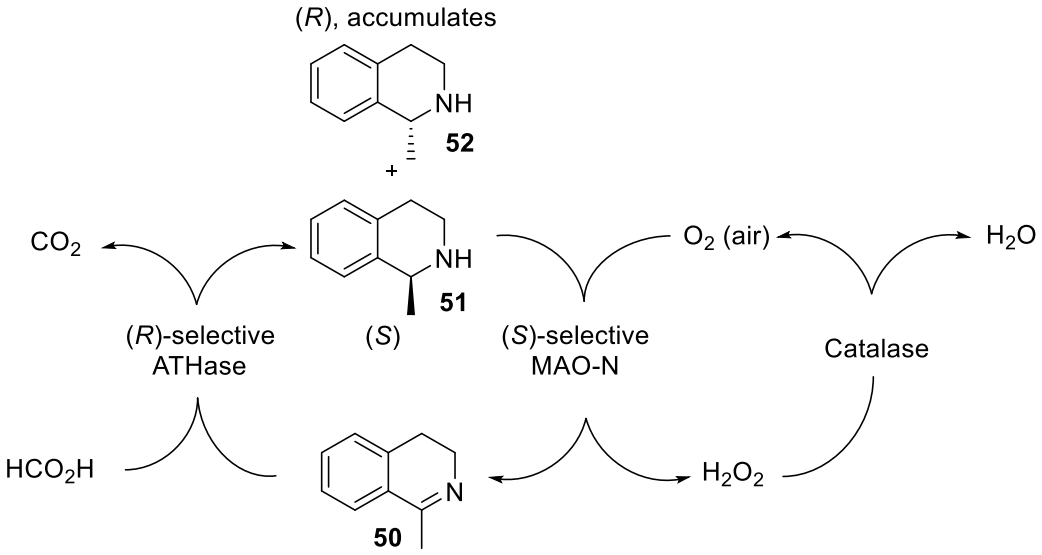


Figure 1.23. Cascade reaction of the double stereoselective deracemization of amines **51** and **52**. ATHase: artificial transfer hydrogenase, MAO-N: artificial monoamine oxidase.

Based on these promising results, the cascade reactions were then applied *in vivo* by compartmentalising the ArMs in the periplasm of cells with catalysts optimised by directed evolution to fit with the requirements of this challenging environment.[85] Directed evolution techniques applied to ArMs has been well described by Reetz, including for the biotin-(strept)avidin system to improve the enantioselectivity of the system for the C=C double bond hydrogenation of α-acetamido-acrylic acid ester.[86]

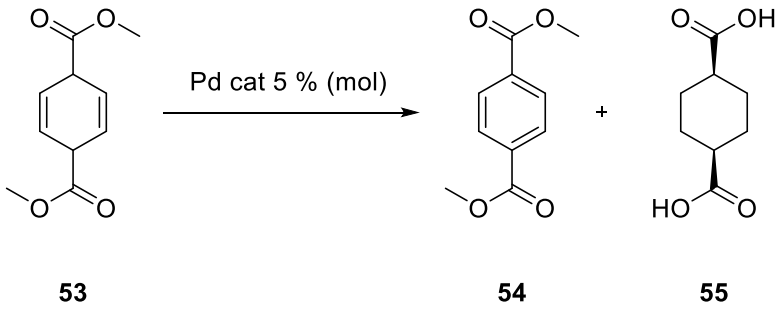
1.1.6 Conclusion

More examples of artificial metalloenzymes are added to scientific knowledge regularly as the research field keeps growing. To build such biocatalysts, one of the four strategies discussed previously can be used. The choice of selection depends on multiple factors, and two major ones can be used as a starting point: the chemical reaction targeted and the protein scaffold to be used.

1.2 Transfer hydrogenation reactions

1.2.1 Background

Transfer hydrogenation (TH) reactions refer to the addition of hydrogen to a molecule from a non-H_2 gas hydrogen source. These reactions offer a convenient and powerful alternative to direct hydrogenation (DH) where H_2 gas is used as hydrogen source. The first TH was reported by Knoevenagel *et al*. in 1903 where they demonstrated the disproportionation of dimethyl-1,4-dihydroterephthalate **53** to dimethylterephthalate **54** and *cis*-hexahydroterephthalate **55** using palladium (Figure 1.24).[87] The reaction occurs between two molecules of substrate exchanging hydrogen atoms through activation by the Pd catalyst.



53 **54** **55**

Figure 1.24. First transfer hydrogenation reported by Knoevenagel *et al*.[87]

Since this initial report, a tremendous amount of research has been done into this fundamental transformation in organic synthesis. Developments have been made using organometallic catalysts, organocatalysts and biocatalysts to improve the selectivity, the substrate scope and the rate of this reaction.

1.2.2 Chemical catalysts for transfer hydrogenations

1.2.2.1 Organometallic catalysts

Compared to the reaction depicted by Knoevenagel, most of the TH reactions studied involved different donor and acceptor units using a large variety of metals.[88] In 1925, Meerwein and Verley independently published the first TH reaction on carbonyl compounds.[89-90] The transfer of the hydrogen to the ketone was promoted by an aluminium alkoxide. A transition state with the formation of a six-membered ring allows the direct transfer of the hydrogen from the donor to the acceptor unit (Figure 1.25).

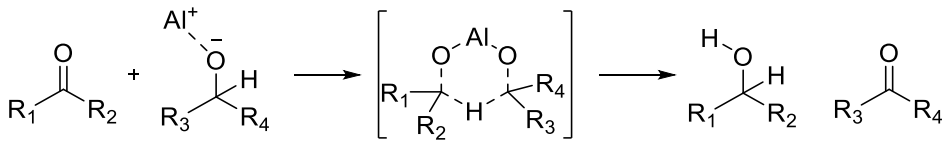


Figure 1.25. Direct hydrogen transfer via a six-membered ring transition state.

The next milestone in the development of THs was the discovery of late transition-metal catalysts. Notably, the pioneering work of Henbest, Mason and co-workers with iridium-based complexes[91-92] and Sasson and Blum on ruthenium-based complexes.[93-95] The extensive research that followed in this area led to the use of such complexes for asymmetric transfer hydrogenation (ATH) where the end product is chiral. The evolution of ATH was awarded by a shared Nobel Prize in 2001 to Noyori and Knowles for their contribution to this ever-growing field (Figure 1.26).[96-99]

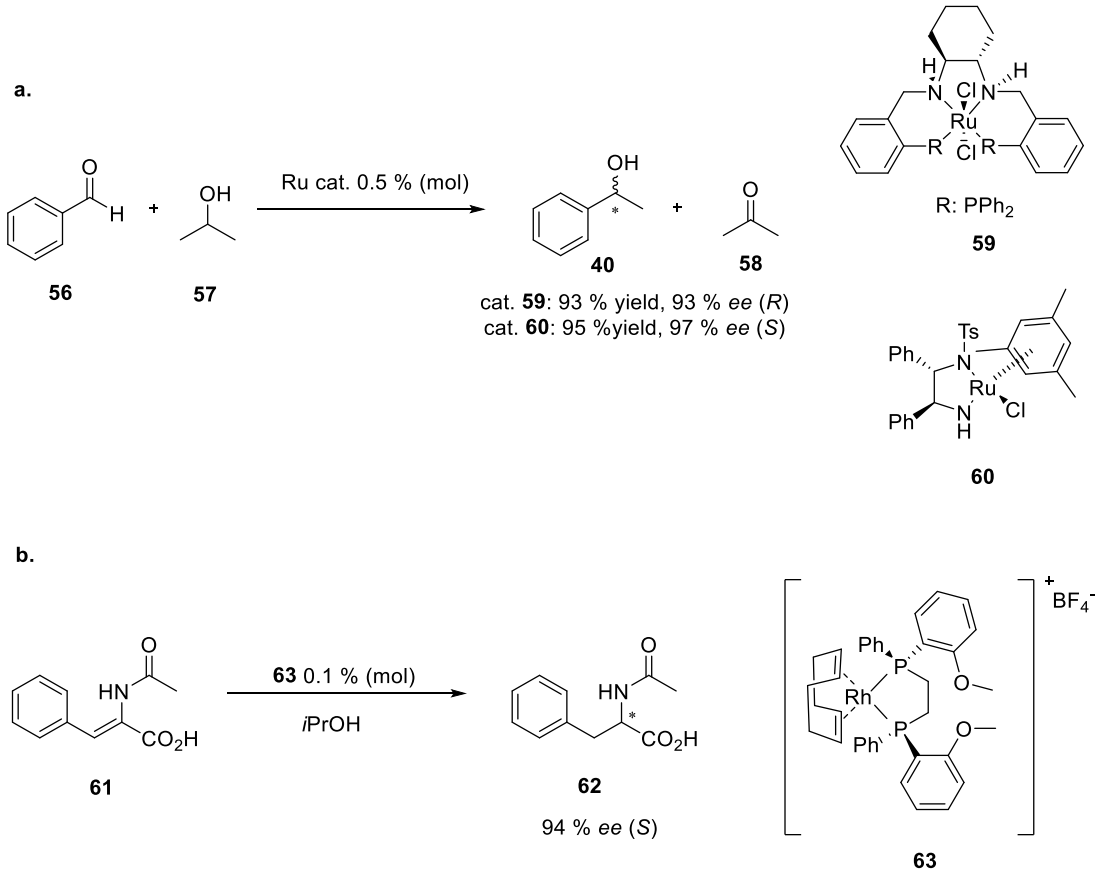


Figure 1.26. Asymmetric transfer hydrogenation developed by a. Noyori *et al.*[96] and b. Knowles *et al.*[99]

Since then, numerous studies were reported on the use of different metal ions and different ligands[88], including studies on ATH performed in water. [100-103] These studies developed ligands, based on Noyori's catalyst, capable of

performing THs with ketones and imines in water, when coordinated with metal complex **64** (Figure 1.27b). All ligands possessed a tosyl moiety linked to one nitrogen of the bidentate NN motif, showed to stabilise the complexes in water. Aside from the ligand used, the studies showed the impact of the hydrogen source and the pH on the outcome of the reactions. Most of the THs performed with these ligands used sodium formate as hydrogen source. It has been proven that higher quantity of formate enhanced the reaction rate. Similarly, depending on the complex used, the pH of the reaction might impact the enantioselectivity of the catalyst, with acidic pH (below 6) demonstrating a drop of selectivity by up to 50 % or impact the conversion yield at pH below 4, where a drop by more than 20-fold was observed. An in-depth study of THs in water with Ru complexes was also carried out, providing a reaction mechanism (Figure 1.27a).

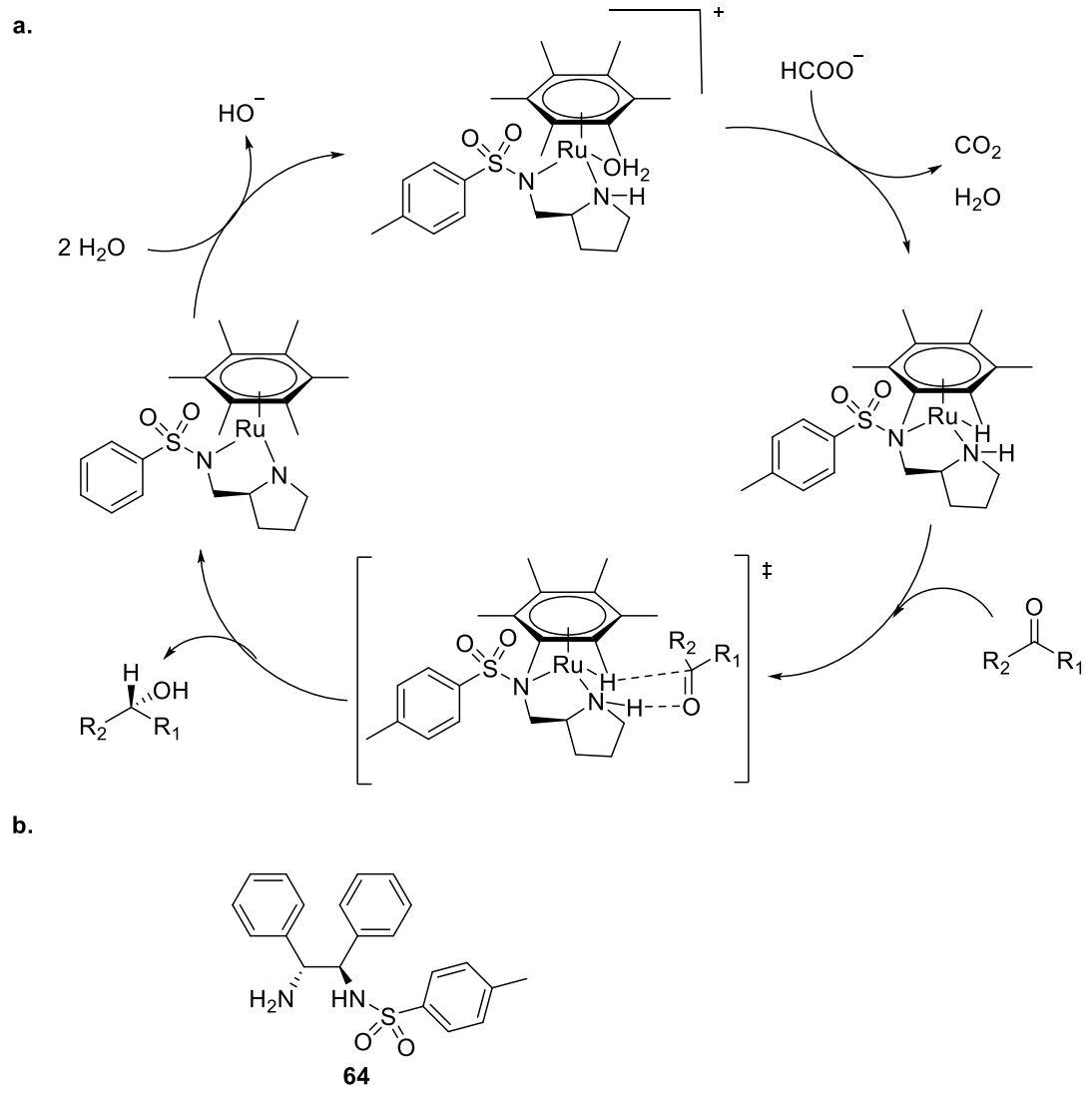


Figure 1.27. a. Postulated mechanism of transfer hydrogenation in water, b. ligands developed for ketones bearing a tosyl moiety. Adapter from Canivet *et al*.[100]

1.2.2.2 Organocatalysts

The recent focus on ATH in water revealed the interest of researchers for greener alternatives. As part of such alternatives, an array of organocatalysts were developed to overcome the use of metal ions in ATH reactions. The most prominent work in this area was reported by List's [104-107] and MacMillan's [108-110] respective groups. They independently used the structural similarity between Hantzsch esters and the nicotinamide ring of the natural cofactor NAD(P)H (Figure 1.28). The ester acts as a cheap sacrificial hydrogen donor.

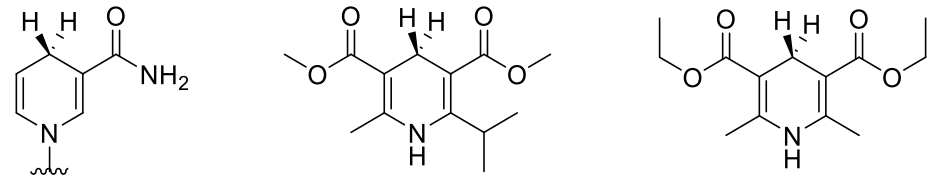


Figure 1.28. Structural similarity between natural cofactor NAD(P)H and Hantzsch esters **65** and **66**, respectively developed by List *et al*. and MacMillan *et al*. Reproduced from Zheng and You.[111]

They both demonstrated that using a chiral secondary amine as a catalyst, aided by an organic acid (trichloro- or trifluoro-acetic acid), hydrogen could be transferred from the ester to α,β-unsaturated aldehydes (Figure 1.29). The substrate scope of the set up was quite broad as aromatic, aliphatic and functionalised α,β-unsaturated aldehydes were tolerated.

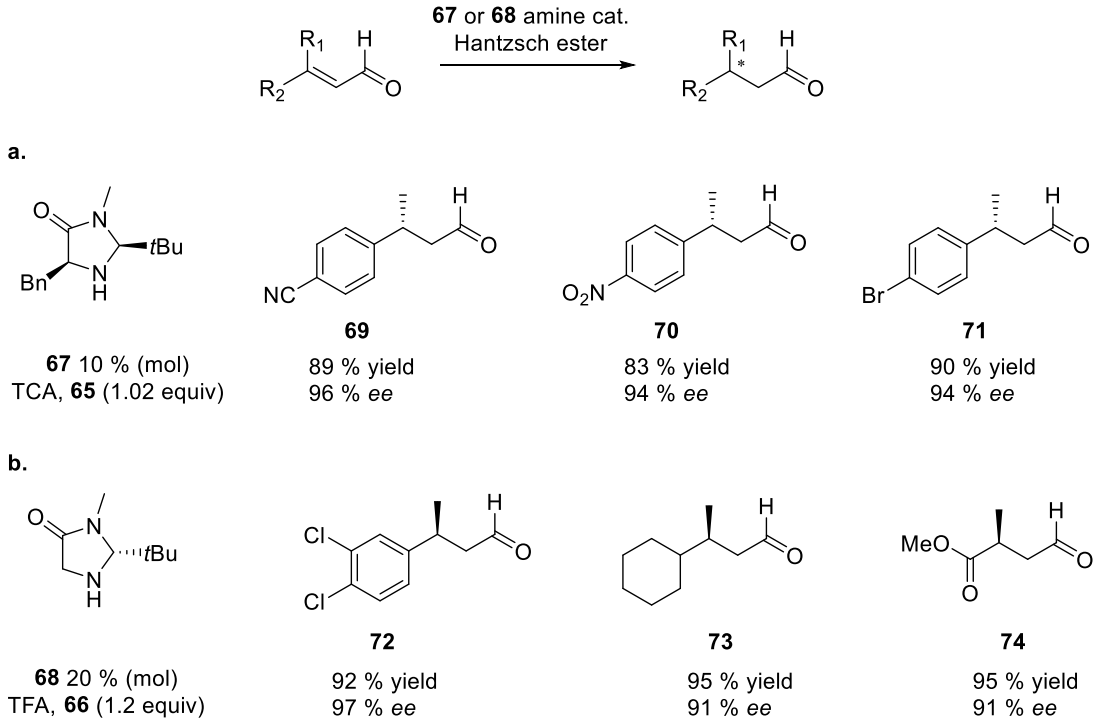
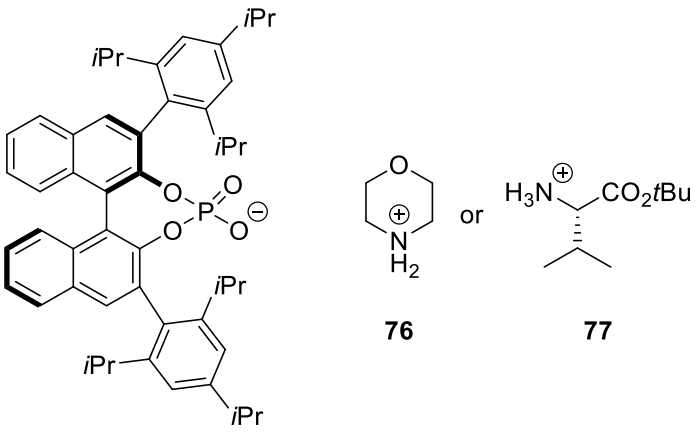


Figure 1.29. Substrate scope of ATH catalysed by secondary chiral amine in the presence of Hantzsch ester. Work performed by a. List's group and b. MacMillan's group. Reproduced from Zheng and You.[111]

Later on, Mayer and List used BINOL-derived chiral phosphoric acids instead of secondary chiral amines.[105] The system, called asymmetric counteranion-directed catalysis (ACDC) improved the enantioselectivities previously obtained and further extended the substrate scope to α,β-unsaturated ketones and ketimines, so far inaccessible with organocatalysts.



75 **76** **77**

Figure 1.30. TRIP anion **75** (TRIP: 3,3'-bis(2,4,6-triisopropylphenyl)-1,1'-binaphtyl-2,2'-diyl hydrogen phosphate) with counterion morpholinium **76** or aminium **77** for ATH using the ACDC system on ketimines and α,β-unsaturated ketones. Reproduced from Zheng and You.[111]

1.2.3 Biocatalysts for transfer hydrogenations

Transfer hydrogenation reaction is one of the most common reactions found in nature. Enzymes capable of reducing C=C, C=N and C=O double bonds were found in a large variety of organisms, often yielding enantiopure products due to the inherent capacity of enzymes to catalyse asymmetric reactions.

1.2.3.1 Enzymatic reduction of C=C double bonds

Enoate (or Ene) reductases (ERs, EC 1.3.1.31) are enzymes capable of reducing alkenes, more specifically α,β-unsaturated ketones and aldehydes, quinones and nitro alkenes. These NAD(P)H-dependent flavin mononucleotide (FMN) containing enzymes are found in bacteria, yeast, plants and eukaryotes.[112-113]

In 2010, Scrutton and co-workers applied directed evolution techniques to the pentaerythritol tetranitrate reductase from *Enterobacter cloacae*.[114] They were able to switch the enantiopreference for 2 substrates α-methyl-*trans*-cinnamaldehyde **81** and (*E*)-2-aryl-1-nitropropene **89** as well as expanding the substrate scope of the enzyme (Figure 1.31). These modifications brought to the enzymes are of great interest for industrial application where wild-type enzymes are often too limited in term of substrate scope or can, sometimes, only provide the undesired enantiomer.

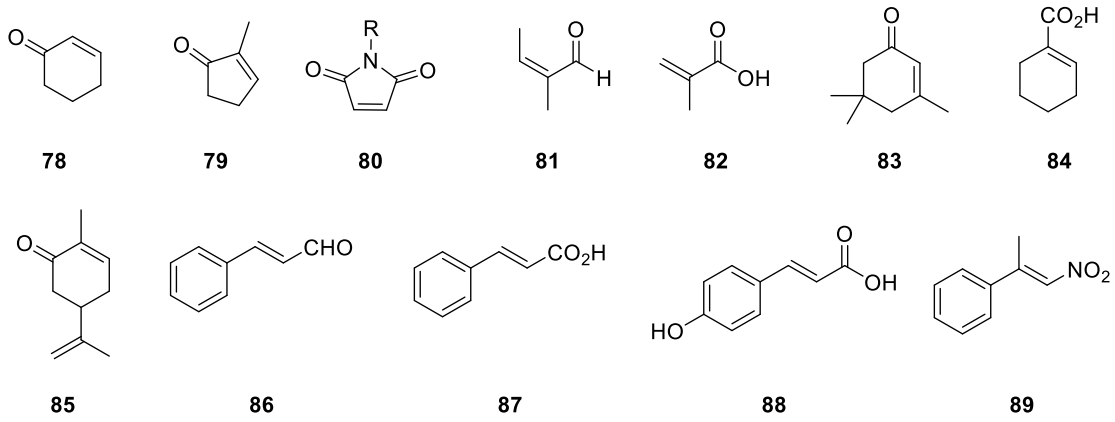


Figure 1.31. Overview of the substrate scope of ERs. Reproduced from Hulley *et al*.[114] and Peters *et al*.[113]

In 2014, Bornscheuer and co-workers identified 3 new ERs from *Pseudomonas putida*, increasing the pool of biocatalysts capable of reducing C=C bonds.[113] One of them, Xenobiotic reductase A (XenA)[115-117] was extensively used by Hollmann's group to develop nicotinamide cofactor mimics (Figure 1.32).[118-120] Nicotinamide mimics aim at offering a cost efficient alternative to the natural cofactors NAD(P). After initial investigation with an ER from *Bacillus subtilis* (YqjM), the group showed that mimic **90** exhibited a similar behaviour as NADH for the reduction of various aromatic and aliphatic enones. This cofactor was then used with XenA and the kinetics displayed were improved compared to the natural cofactor under the same conditions, *i.e.* lower K_M and higher k_{cat}. These promising results led Löw *et al.* to further develop the concept, resulting in mimic **91** that improved product yield on some challenging substrates.[121]

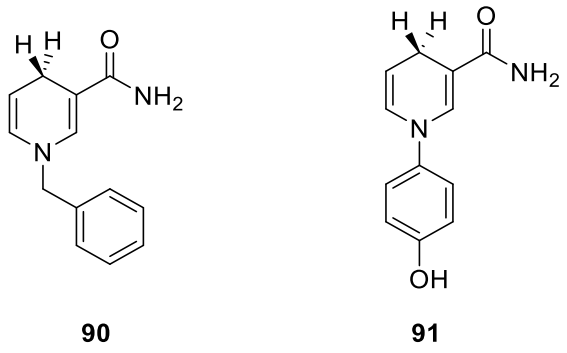


Figure 1.32. Nicotinamide cofactor mimics **90** and **91** developed respectively by Hollmann[118] and Löw.[121]

These mimics are a good example of the promiscuity of enzymes that can be implemented at an industrial scale to decrease the cost of biocatalytic processes.

1.2.3.2 Enzymatic reduction of C=N double bonds

Until the 2010, known enzymes capable of reducing C=N double bonds were highly specific with a narrow substrate scope.[122] Examples of such enzymes are the 1,2-dehydroreticuline synthase (DHRR)[123] and festuclavine synthase (FS)[124] in alkaloid synthesis and Δ^1-pyrroline-5-carboxylate reductase (Pyr5CR) in L-proline synthesis(Figure 1.33).[125]

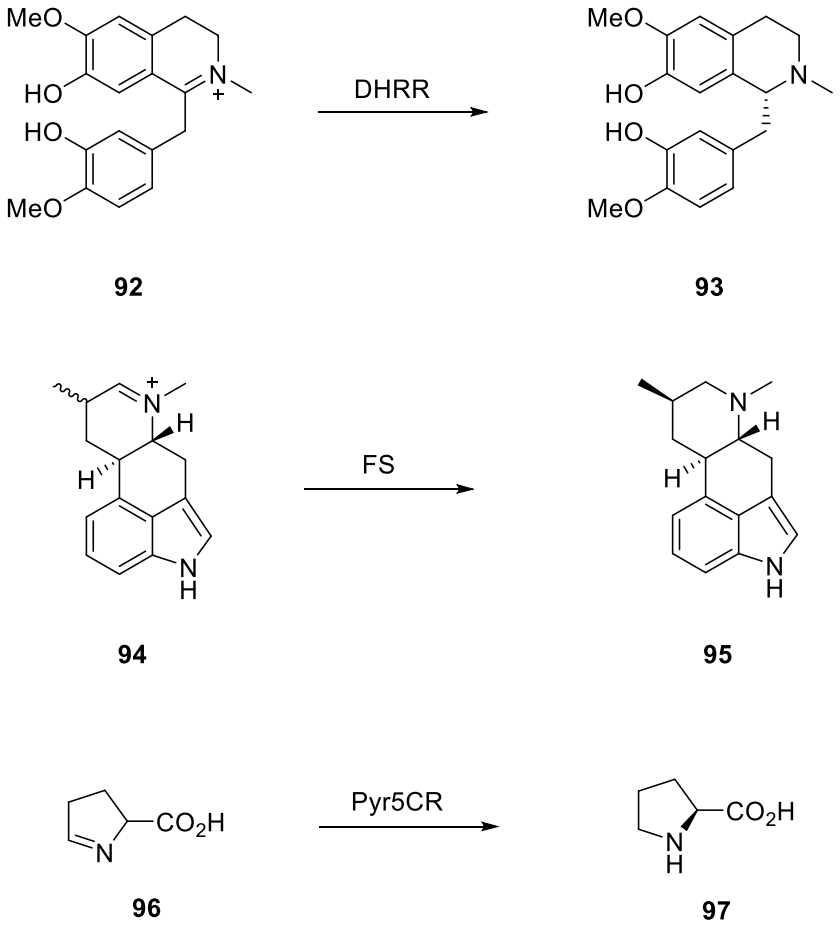


Figure 1.33. Naturally occurring reactions catalysed by 1,2-dehydroreticuline synthase (DHRR), festuclavine synthase (FS) and Δ^1-pyrroline-5-carboxylate reductase (Pyr5CR). Adapted from Schrittwieser *et al*.[122]

Due to their substrate specificity and other inconveniences, natural imine reductases were merely applied in biocatalysis. However, research in whole cell biocatalysis yielded interesting results, one of them being the expanded substrate scope of *Candida parapsilosis* towards arylimines (Figure 1.34).[126]

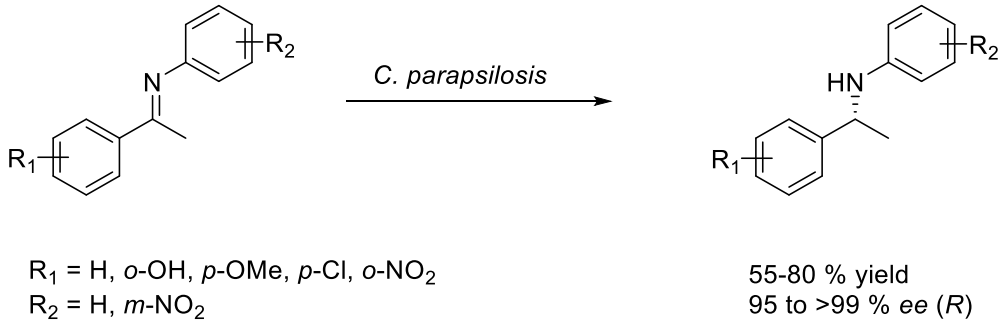


Figure 1.34. Whole cell biocatalysis of arylimines using *C. parapsilosis*. Adapted from Vaijayanthi *et al*.[126]

In 2010 Mitsukura *et al*. used genome mining on 688 microbial strains to highlight 5 cultures from *Streptomyces* sp. that exhibited a reduction activity towards 2-methyl-proline.[127] Enzymes responsible for this activity were then identified, cloned and purified to yield the first members of the imine reductase family (IREDs).[128] The results of this intensive work led Turner and co-workers to explore the potential of these enzymes (Figure 1.35).[129-132] They were able to identify (*S*) and (*R*) specific IREDs and explore the substrate scope in both cases. Computational modelling also improved kinetics of the (*R*) specific IRED by pinpointing the key position 172 as a target for site-directed mutagenesis.

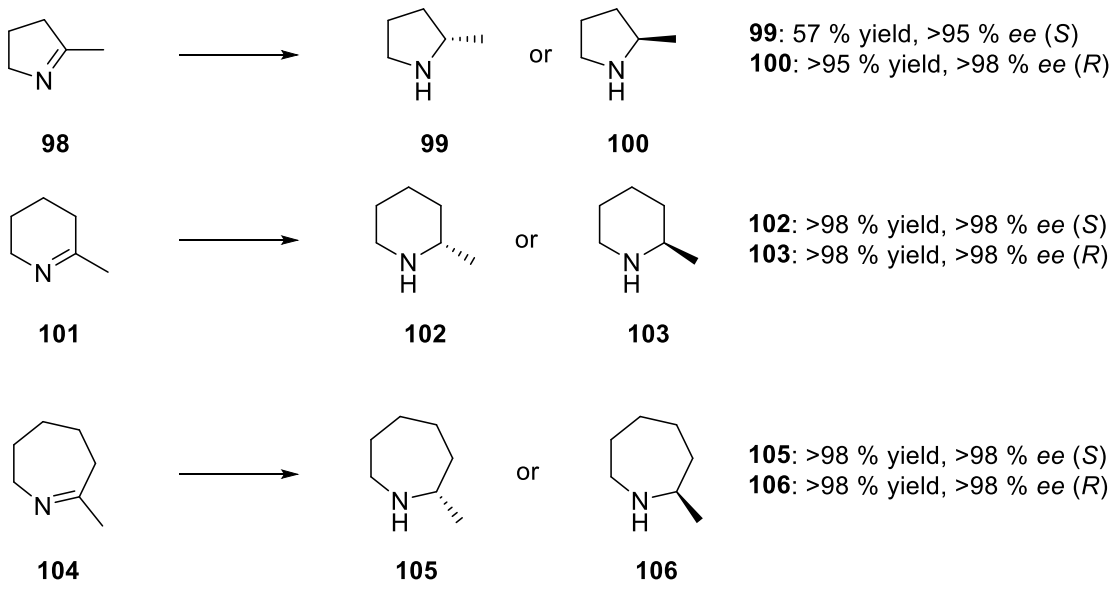


Figure 1.35. Few examples of cyclic imine reductions catalysed by (*S*) and (*R*) specific IRED. Adapted from Schrittweiser *et al*.[122]

Ward and co-workers developed an artificial imine reductase as an alternative to IREDs.[133-135] After comparing various catalysts towards the production of salsolidine, the biotinylated iridium complex **108** exhibited the highest activity

and selectivity. Following is previously described work, Ward and co-workers used site saturation mutagenesis at position 112 of streptavidin to improve the overall activity and selectivity of the system, including the production of the (*S*) enantiomer, so far unreached with this technology. The mutants S112K and S112A displayed the best results (Figure 1.36). Later, the group implemented other mutations to increase enantiomeric excess (*ee*) for both the (*R*) and (*S*) enantiomers as well as increasing the substrate scope.

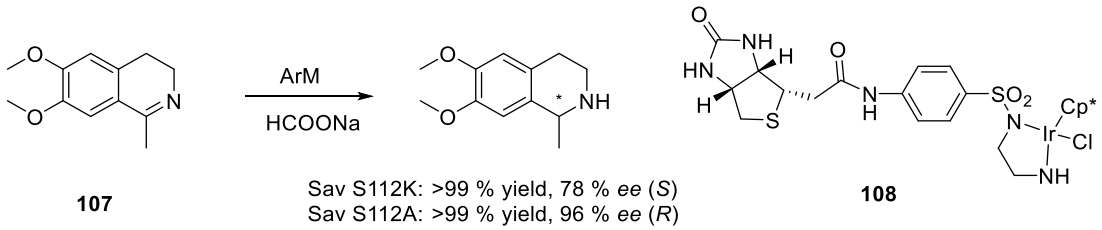


Figure 1.36. Production of both enantiomers of salsolidine using an artificial imine reductase based on biotin-streptavidin technology. Adapted from Dürrenberger *et al*.[133]

Focusing on the same substrate, Duhme-Klair *et al*. developed an ArM based on the iron siderophore of *Campylobacter jejuni* CeuE where an Ir-based complex is anchored to the protein with a siderophore (Figure 1.37).[136] Although the approach yielded a less efficient ArM (36 % *ee* (*R*)), the resulting ArM can be reversibly assemble into the apoprotein and the metal complex **109** apart, a feature that can potentially increase the durability of the system.

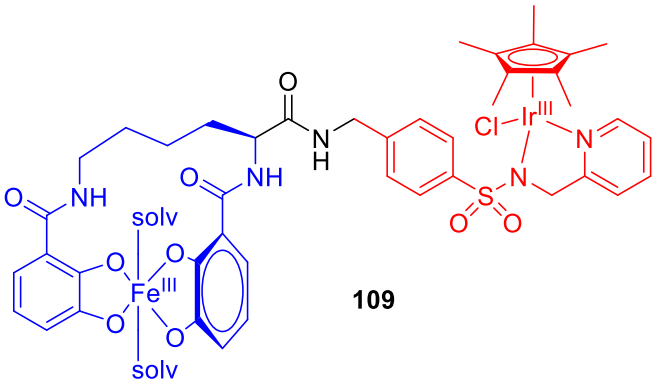


Figure 1.37. Catalyst developed by Duhme-Klair and co-workers for the production of salsolidine with ArMs. The siderophore anchor was highlighted in blue and the Ir-based catalyst in red. Reproduced from Raines *et al*.[136]

1.2.3.3 Enzymatic reduction of C=O double bonds

Amongst the various enzymatic path to reach chiral alcohols, dehydrogenase enzymes (DHs) were considered the most attractive alternative to chemical

synthesis.[137] Some of the attractive features of DHs are their large substrate scope and enantio- and regio-selectivity (Figure 1.38).

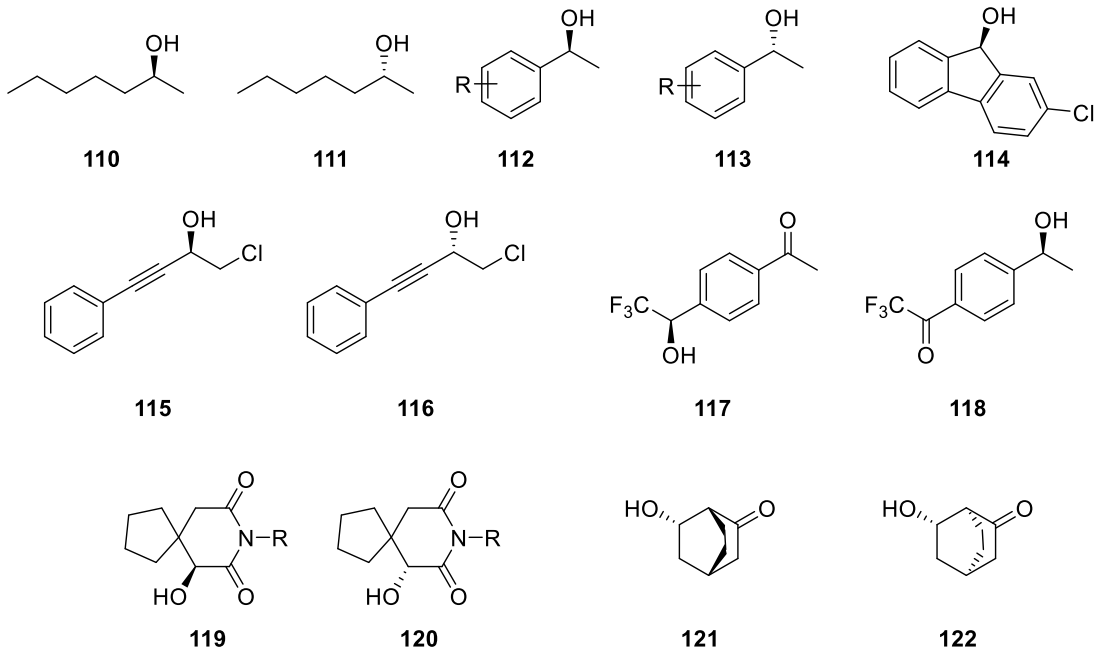
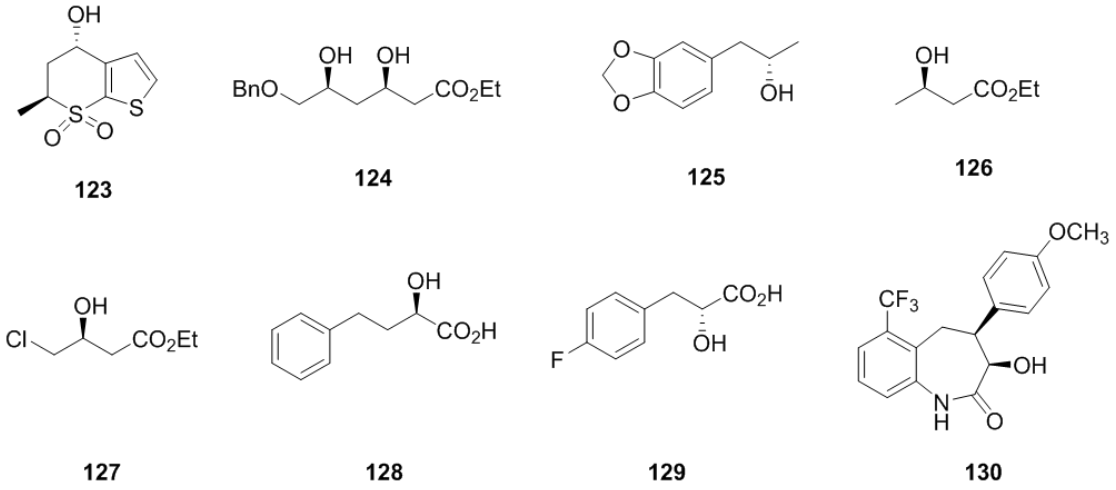


Figure 1.38. Non exhaustive list of products derived from ketone reduction catalysed by DHs. Adapted from Hollmann *et al*.[138]

The depicted substrate scope of DHs allowed these enzymes to be used in biocatalytic process at an industrial scale, competing with synthetic chemistry due to their very high enantioselectivity (Figure 1.39).[138]



Product	Catalyst	Yield (%)	*ee (%)*
123	*Neurospora crassa*	>85	>98
124	*Acinetobacter calcoaceticus (cell extract)*	92	99
125	*Zygosaccharomyces rouxii*	96	>99
126	*Lactobacillus brevis (cell extract)*	96	99
127	*Geotrichium candidum*	95	99
128	*Staphylococcus epidermis (isolated ADH)*	91	99
129	*Staphylococcus epidermis (isolated ADH)*	99	99
130	*Nocardia salmonicolor*	96	99

Figure 1.39. Examples of ADHs used for ketone reduction at an industrial scale. Reproduced from Hollmann *et al*.[138]

Researchers also developed artificial metalloenzymes to reduce C=O double bonds. Ward and co-workers designed a biotin-streptavidin system complexed with ruthenium **134**[139] whilst Salmain and co-workers used papain as a protein scaffold to insert a rhodium-based complexes **135** and **136**.[140] The former ArM was more successful both in term of conversion of ketone to alcohol and in enantioselectivity with up to 94 % *ee* (*R*) and 63 % *ee* (*S*) (Figure 1.40).

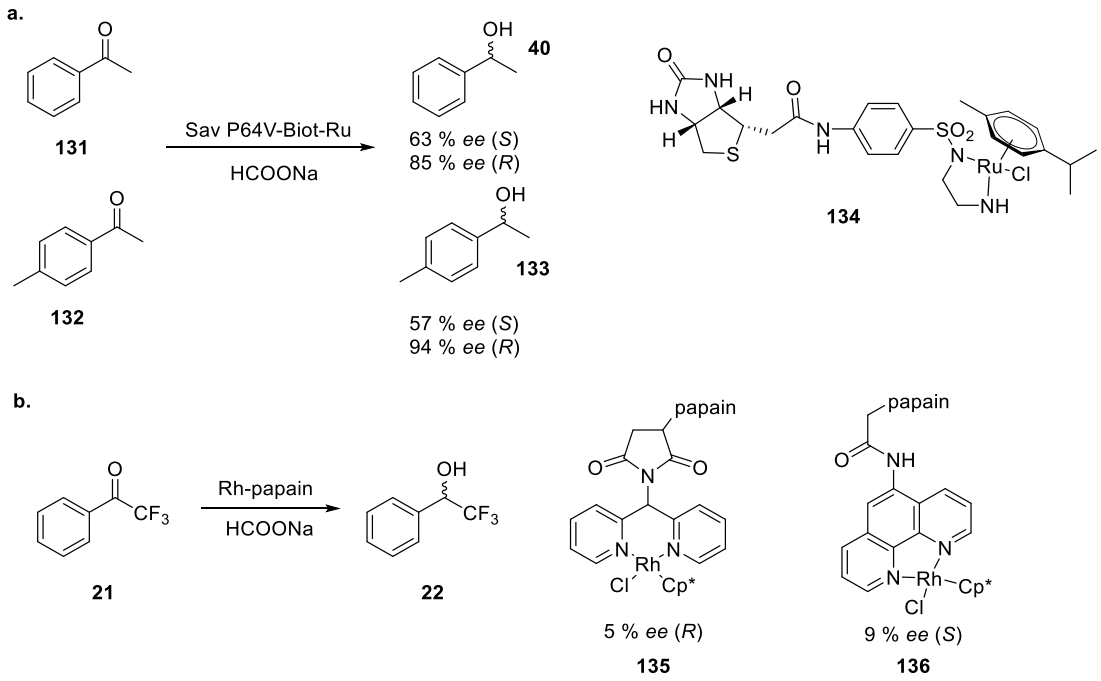


Figure 1.40. Ketone reduction using a. Ru-based and b. Rh-based artificial metalloenzymes. Adapted from Letondor *et al*.[139] and Madern *et al*.[140]

1.2.4 Cofactor recycling systems

As described above, enzymatic catalysis offers an interesting alternative to classic synthetic chemistry. While the enzyme can be loaded to catalytic amount within the reaction, a cofactor is often required as a sacrificial hydrogen donor. In most THs, the cofactor is the expensive NAD(P)H. Therefore, recycling systems to regenerate the cofactor at the expense of a cheap chemical have been developed, the regeneration reaction being a regiospecific C=C double bond reduction yielding the 1,4-dihydronicotinamide cofactor.[141]

1.2.4.1 Electrochemical regeneration

By applying an electrical potential via an electrode, direct reduction or oxidation of the cofactor can be achieved. However, due to the lack of regiospecificity, by products such as 1,2- and 1,6-dihydronicotinamide can be formed.[142-143] To circumvent side reactions, electron mediators (or shuttles) have been developed, resulting in the indirect reduction or oxidation of the cofactor (Figure 1.41).[144-145]

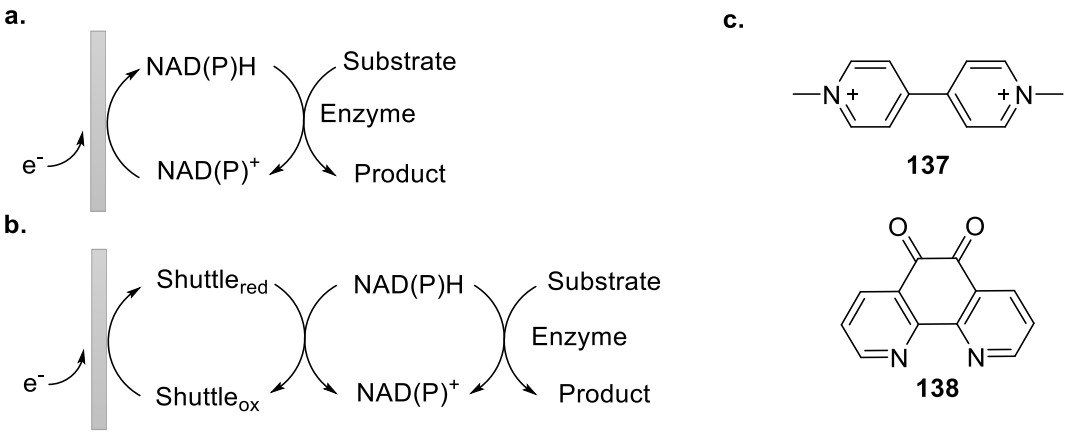


Figure 1.41. Electrochemical cofactor regeneration a. without and b. with electron shuttle. c. Two examples of electron shuttle molecules. Adapted from Truppo.[141]

A plethora of dyes were developed as electron mediators, such as methyl viologen **137** and 1,10-phenantholine-5,6-dione **138**.[146] As an alternative to these dyes, metal complexes capable of transferring hydrides to the nicotinamide cofactor were investigated. One of the most successful complexes was a [Cp*Rh(bpy)]Cl complex (Figure 1.42). The complexation of the Rh with the oxygen of the carbonyl offers a close proximity between the hydride of the hydridorhodium and the C4 position of the nicotinamide ring, allowing a regio-specific transfer to regenerate the cofactor.

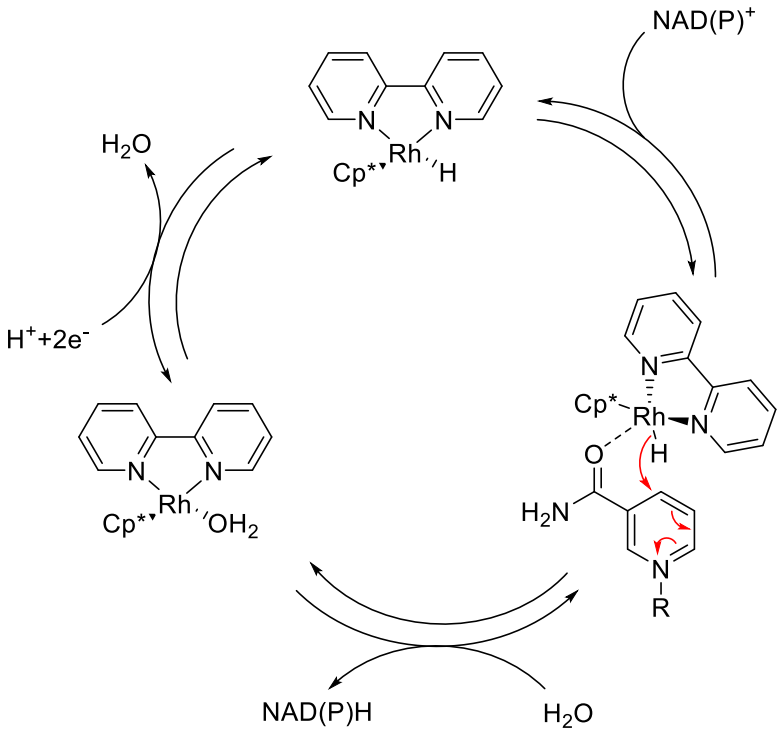


Figure 1.42. Catalytic cycle of the regeneration of nicotinamide cofactors by Rh-based complexes. Reproduced from Wu *et al*.[146]

Although indirect electrochemical regenerations of cofactor are very effective, the difficulties to run an electrochemical reactor at an industrial scale reduced their appeal for extended development.

1.2.4.2 Photochemical regeneration

Compared to the previous method, photochemical regeneration of cofactor uses light as the energy source to reduce the photosensitizer (PS) molecule at the expense of an electron donor species. Willner and Mandler used Ru(III)-*tris*-bipyridine or Zn(II)-*meso*-(*N*-tetramethylpyridinium)porphyrin as PS and ethylene diamine tetraacetic acid (EDTA) as a sacrificial electron donor.[147]

To avoid the use of expensive metal catalysts, Reetz *et al* developed a simpler system where a flavin group is used as a PS in pair with EDTA (Figure 1.43).[148]

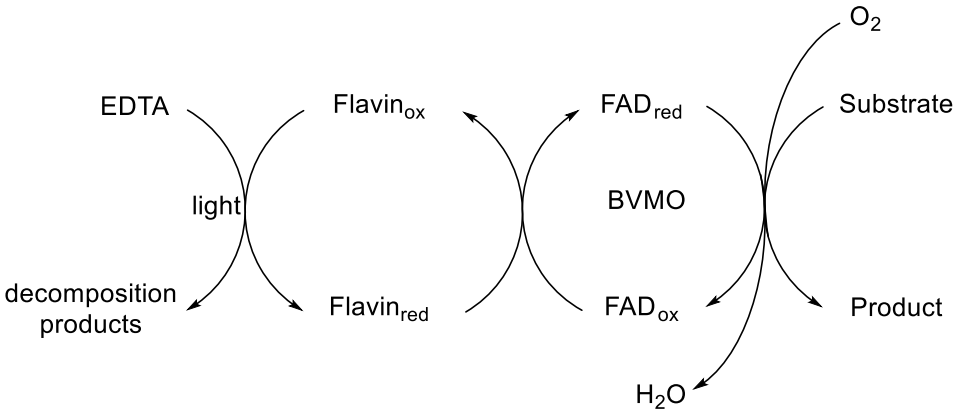


Figure 1.43. Photochemical regeneration of Baeyer-Villiger monooxygenase (BVMO) cofactor using light. Reproduced from Taglieber *et al*.[148]

Another approach was developed by Wangikar and co-workers.[149] By using the natural photosynthetic system of cyanobacteria *Synechococcus elongatus*, they were able to reduce acetophenone into (*R*)-1-phenylethanol with 99 % *ee* using the whole cell, light and 1 % CO_2.

1.2.4.3 Chemical regeneration

Steckhan and co-workers developed a Rh-based catalyst capable of reducing NAD^+ into NADH with albeit moderate activity (Figure 1.44).[150-151] Despite these pioneering results, very few others examples were found due to the intrinsic deactivation of enzyme by late transition metals and their propensity to catalyse the desired enzymatic reaction in a non-selective manner. However, the reported system was further used by Fish *et al*. towards the

reduction of nicotinamide mimics in tandem with an alcohol dehydrogenase for the reduction of ketones.[152-155]

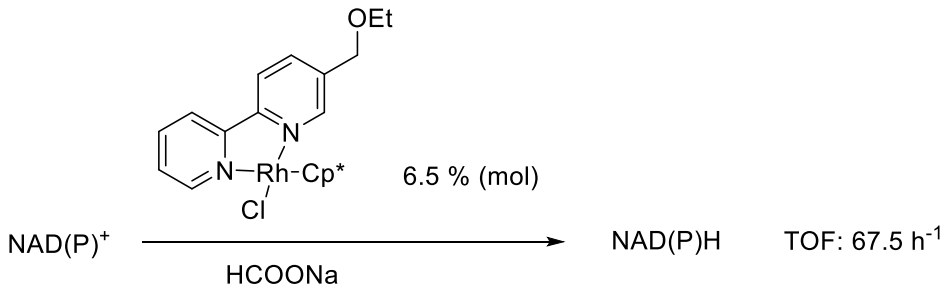


Figure 1.44. Rhodium-based catalyst for the regiospecific reduction of $NAD(P)^+$ into NADPH. Adapted from Steckhan *et al*.[150]

1.2.4.4 Enzymatic regeneration

This method is divided into two approaches: substrate- and enzyme-coupled systems (Figure 1.45). The former consists of using a second substrate accepted by the working enzyme to regenerate the cofactor while the latter consists of using a second enzyme to performing the regeneration of the cofactor independently of the working enzyme.

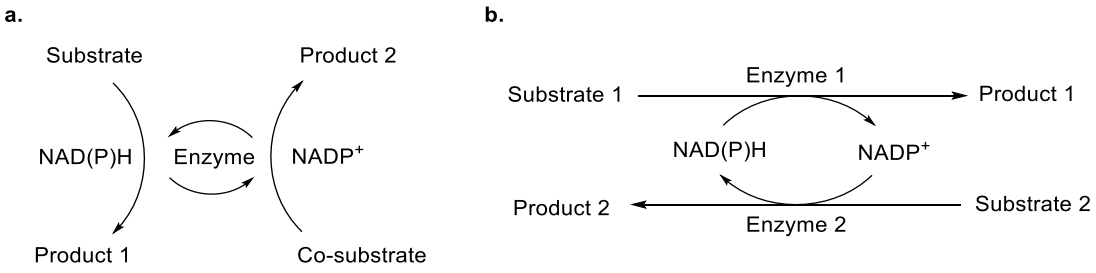


Figure 1.45. Enzymatic regeneration of NAD(P)H. a. substrate-coupled approach. b. enzyme-coupled approach. Reproduced from Truppo.[141]

The substrate-coupled approach offers a simple, single enzyme system in which the working enzyme catalyses two reaction, including the oxidation of a cheap sacrificial co-substrate such as 2-propanol (Figure 1.46).[156-159] This system however is limited to ADHs due to the nature of the alcohol co-substrate. Although simple, this approach is limited by the thermodynamics of the reaction. Indeed, both the oxidation and reduction reactions are competing. To overcome this drawback, high concentrations of co-substrate can be employed to drive the equilibrium towards the regeneration of NAD(P)H and therefore improving the yield of the desired product. Another solution is

the continuous removal of the acetone formed by the regeneration system through distillation.

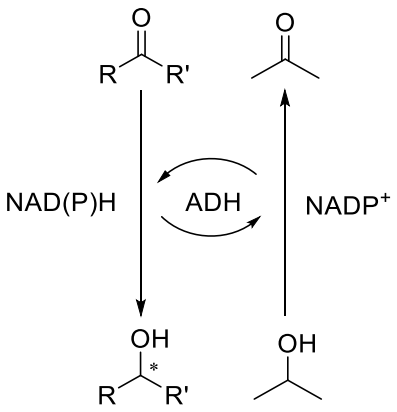


Figure 1.46. Substrate-coupled system using an ADH and 2-propanol as a sacrificial co-substrate.

Recently, an innovative approach was developed by Fraajie and co-workers using fused enzymes technology.[160] By fusing an alcohol dehydrogenase with an NADPH oxidase the resulting dual-enzyme ADH-NOX can catalyse both the oxidation of alcohols and the regeneration of $NADP^+$ using oxygen (Figure 1.47).

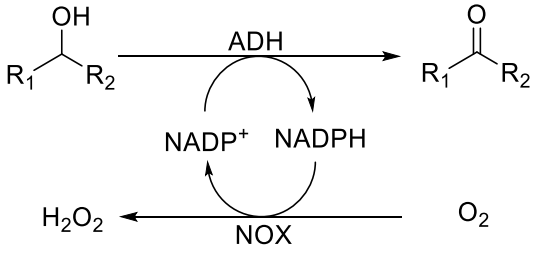


Figure 1.47. Fused ADH-NOX system for the oxidation of alcohol using a single protein containing two enzymatic behaviour. Adapted from Aalbers *et al*.[160]

As an alternative, the enzyme-coupled approach provides a large variety of choices for both the substrate and the enzyme to implement the system, improving the thermodynamics in favour of the desired product. Two of the most applied enzymes are formate dehydrogenase (FDH)[161-164] and glucose dehydrogenase (GDH).[165-167] The first one catalyses the reduction of formate to CO_2, making use of the volatility of CO_2 driving the equilibrium towards the required product. The second enzyme catalyses the reduction of glucose into gluconic acid using $NAD(P)^+$ as a cofactor (Figure 1.48).

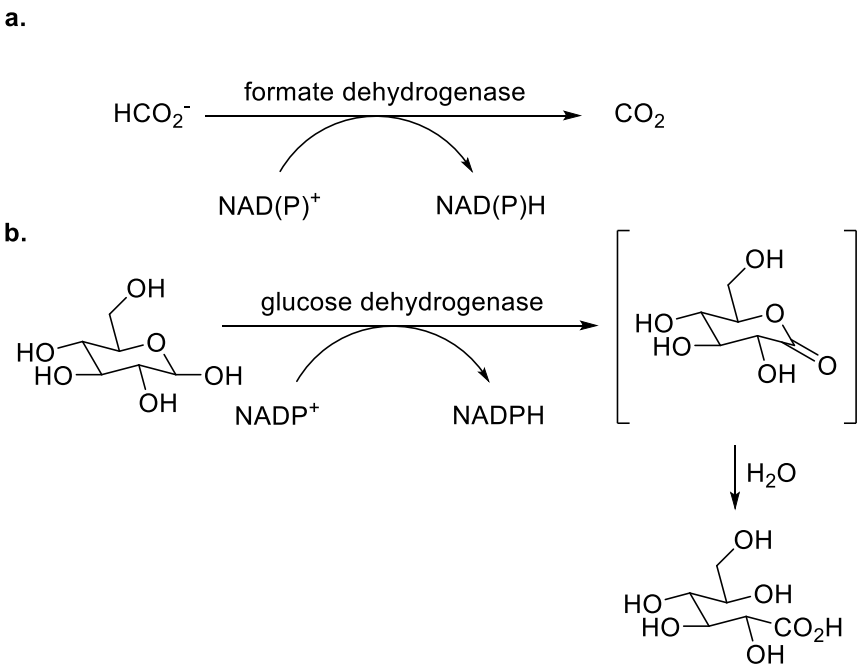


Figure 1.48. Reactions catalysed by a. the formate dehydrogenase and b. the glucose dehydrogenase as part of a cofactor regeneration system.

Following the same methodology, other systems have been developed using for example phosphite dehydrogenase (PTDH) or hydrogenase.[168-169] A recent use of the enzyme-coupled recycling system was published by Kara and co-workers.[170] Their approach made use of the co-substrate to yield the desired product, yielding the convergent catalysis of ε-caprolactone **141** (Figure 1.49).

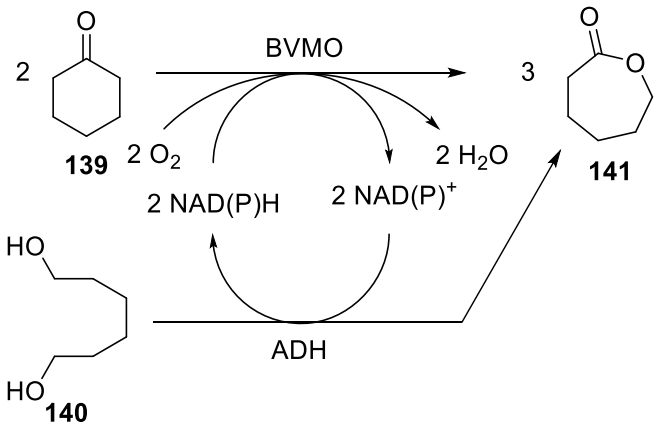


Figure 1.49. Convergent production of ε-caprolactone **141** from cyclohexanone **139** and 1,6-hexanediol **140** using an enzyme-coupled recycling system composed of a Baeyer-Villiger monooxygenase (BVMO) and an alcohol dehydrogenase (ADH). Reproduced from Bornadel *et al*.[170]

1.2.5 Conclusion

Transfer hydrogenation reactions are quite versatile and offer a wide range of asymmetric products that can further be used as building block for subsequent

synthesis. As an alternative to chemical syntheses, biocatalysts and artificial metalloenzymes were developed, offering a broad range of substrates. The main drawback of these systems is the requirement of expensive cofactor as sacrificial hydrogen donors. Thus, recycling systems were investigated and yielded valuable regeneration rates to circumvent the drawback.

1.3 Alcohol dehydrogenases, a superfamily of biocatalysts

1.3.1 Background

Alcohol dehydrogenases (ADHs, E.C 1.1.1.1) are enzymes that belong to the oxidoreductases. They constitute a superfamily of enzymes that can catalyse the reversible oxidation of alcohols into their corresponding aldehydes or ketones at the expense of the coenzyme nicotinamide adenine (phosphate) NAD(P) (Figure 1.50).

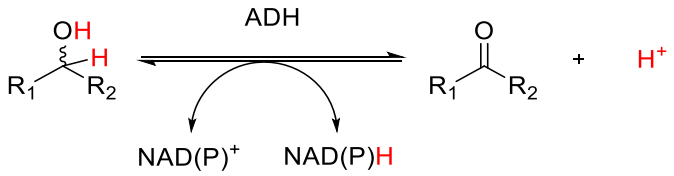


Figure 1.50. Oxido-reduction catalysed by ADHs at the expense of the coenzyme nicotinamide adenine (phosphate).

ADHs are present in a multitude of organisms. Yeasts,[171-174] plants[175-177] and bacteria[178-179] are mainly using the enzymes as part of the fermentation process. This process allows the organism to regenerate the coenzyme NAD(P) to its oxidised form for further use in their metabolism. On the other hand, the enzyme is involved in the detoxification process of alcohols in humans and other animals.[180-183]

Based on their sequence length, cofactor dependency and other structural features, 3 subfamilies were used to classified them: 1) the short-chain dehydrogenase / reductase (SDR), 2) the medium-chain zinc-dependent dehydrogenase / reductase and 3) the long-chain iron activated dehydrogenase / reductase (LCR). [184-186]

1.3.1.1 Short-chain ADHs

These ADHs possess a sequence of around 250 amino acids. Whilst the enzyme from *Drosophilia lebanonesis* was the most studied from this subfamily,[187-188] SDRs displayed very different sequences due to the large

variety of organisms in which they have been found.[189-191] Despite the heterogeneity of the sequences, the catalytic behaviour and the interactions of the proteins with the cofactor are very similar due to highly conserved residues. These residues are a tyrosine, a lysine, a serine and an asparagine, acting as a catalytic tetrad to perform acid/base catalysis.[192-193] In contrast, the substrate binding site of these enzymes exhibit the least conserved sequences, offering variation in their substrate scope.

1.3.1.2 Medium-chain ADHs

These zinc-dependent ADHs have a sequence of around 350 amino acids. They constitute a large part of the ADH family and have been studied extensively. The two most studied enzymes of this category are from horse liver (HLADH) and from yeast (ScADH, Figure 1.51a), representing the dimeric (mammalian) and tetrameric (microbial) forms in which they were found. Each subunit contains a cofactor binding domain, a substrate binding domain and a metal binding site at the edge of the previous two.

Depending on the enzyme, the cofactor binding domain can interact with NAD or NADP in either their reduced or oxidised forms. At the exception of two thermostable enzymes *Thermoanaerobacter brockii* and *Thermoanaerobacter ethanolicus*,[194] MDRs contain two zinc ions per subunit: a structural zinc, tetracoordinated to 4 cysteine residues, and a catalytic zinc, coordinated to an histidine and 2 cysteine residues (Figure 1.51b and c).

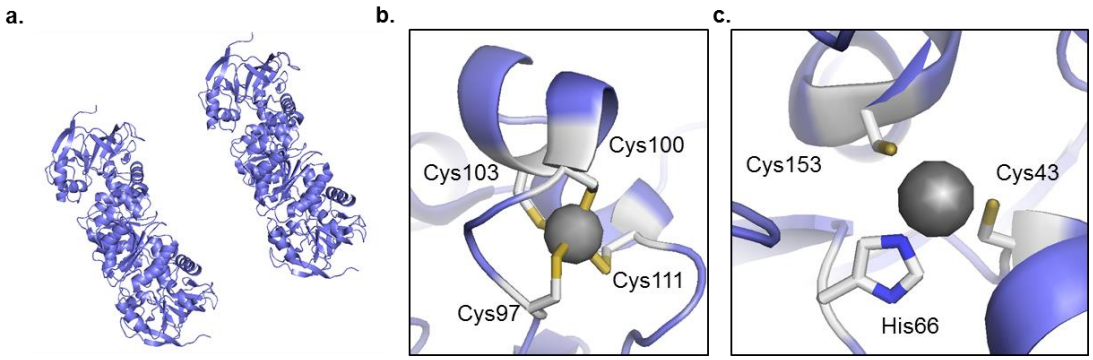


Figure 1.51. a. Tetrameric structure of ADH from *Saccharomyces cerevisiae* (PDB 4W6Z), b. close view of the structural zinc coordinated with 4 cysteine residues, c. close view of the catalytic zinc coordinated with 1 histidine and 2 cysteine residues. [195]

1.3.1.3 Long-chain ADHs

The sequence of these ADHs contains 385 or more amino acids per subunit. The most studied enzymes from this category are the ADHs from *Zymomonas mobilis* (bacterial)[196-198] and *Saccharomyces cerevisiae* (fungal).[199] Besides their larger structures, these enzymes are coordinating an iron atom for catalytic purposes. A tetrad is involved in the coordination of the metal where 3 highly conserved histidines (H198, 263 and 277) are supplemented by an acidic residue to display an acid/base catalytic behaviour.

1.3.2 Mechanism of zinc-dependent alcohol dehydrogenases

1.3.2.1 Horse liver alcohol dehydrogenase

HLADH was the most studied MDR and therefore used as a model to understand the mechanism of action of these enzymes.[200-202] The suggested mechanism was based on kinetic, spectroscopic and crystallographic data (Figure 1.52). In the substrate oxidation process, NAD^+ binds to the cofactor binding domain of HLADH. This binding enacts a conformational change to the active form of the enzyme and the subsequent formation of the substrate binding pocket.

The alcohol substrate then coordinates with the zinc through its oxygen atom, displacing a molecule of water. The Lewis acid character of the zinc draws electrons away from the oxygen, resulting in a weaker O-H bond. The proton from the alcohol moiety is then removed via a proton relay system engaged by His51 and followed by the 2' hydroxyl of the cofactor and Ser48. The system lead to the formation of a negatively charged alkoxide ion.

A hydride transfer from the ion to the C4 position of the pyridinium ring is then performed, yielding the carbonyl product and the cofactor in its reduced form. The product is then released, followed by NADH. The reduced form of the cofactor having a stronger affinity for the enzyme than its oxidised counterpart, the release of NADH is considered the rate-limiting step in alcohol oxidation.

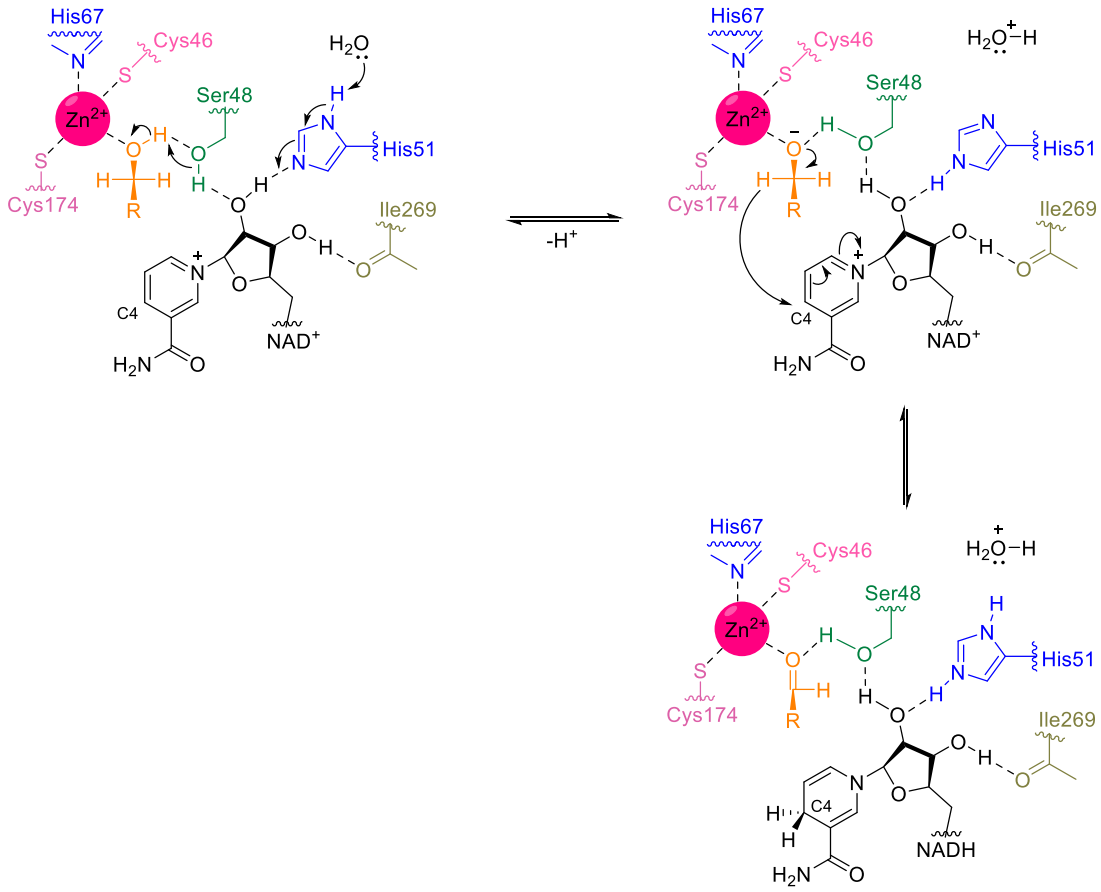


Figure 1.52. Mechanism of alcohol oxidation in HLADH using a proton relay system. Reproduced from Lee *et al*.[203]

In the reverse reaction, the coordination of the oxygen atom of the carbonyl moiety to the zinc ion increases the electrophilicity of the α-carbon. This facilitates the hydride transfer from the C4 position of NADH to this carbon, generating the NAD^+ species. A proton relay from a water molecule then yield the corresponding alcohol product.

1.3.2.2 Thermoanaerobacter brockii alcohol dehydrogenase

Compared to the previously described mechanism, *Thermoanaerobacter brockii* alcohol dehydrogenase (TbADH) uses a pentacoordinated zinc during the catalytic process instead of a proton relay system (Figure 1.53).[194, 204] In the oxidation process, the catalytic cycle starts by the binding of $NADP^+$ to the enzyme. In the holoenzyme, the zinc is in a tetrahedral arrangement with residues Cys37, His59, Glu60 and Asp150. The first pentacoordination is due to the addition of a water molecule leading to the first intermediate(denoted Int. 1). This is quickly followed by the dissociation of Glu60 to yield a new tetrahedral zinc ion. The subsequent addition of the alcohol substrate leads to

the second intermediate (Int. 2). During this stage, the water molecule is not displaced by the arrival of the substrate as it is in the proton relay system.

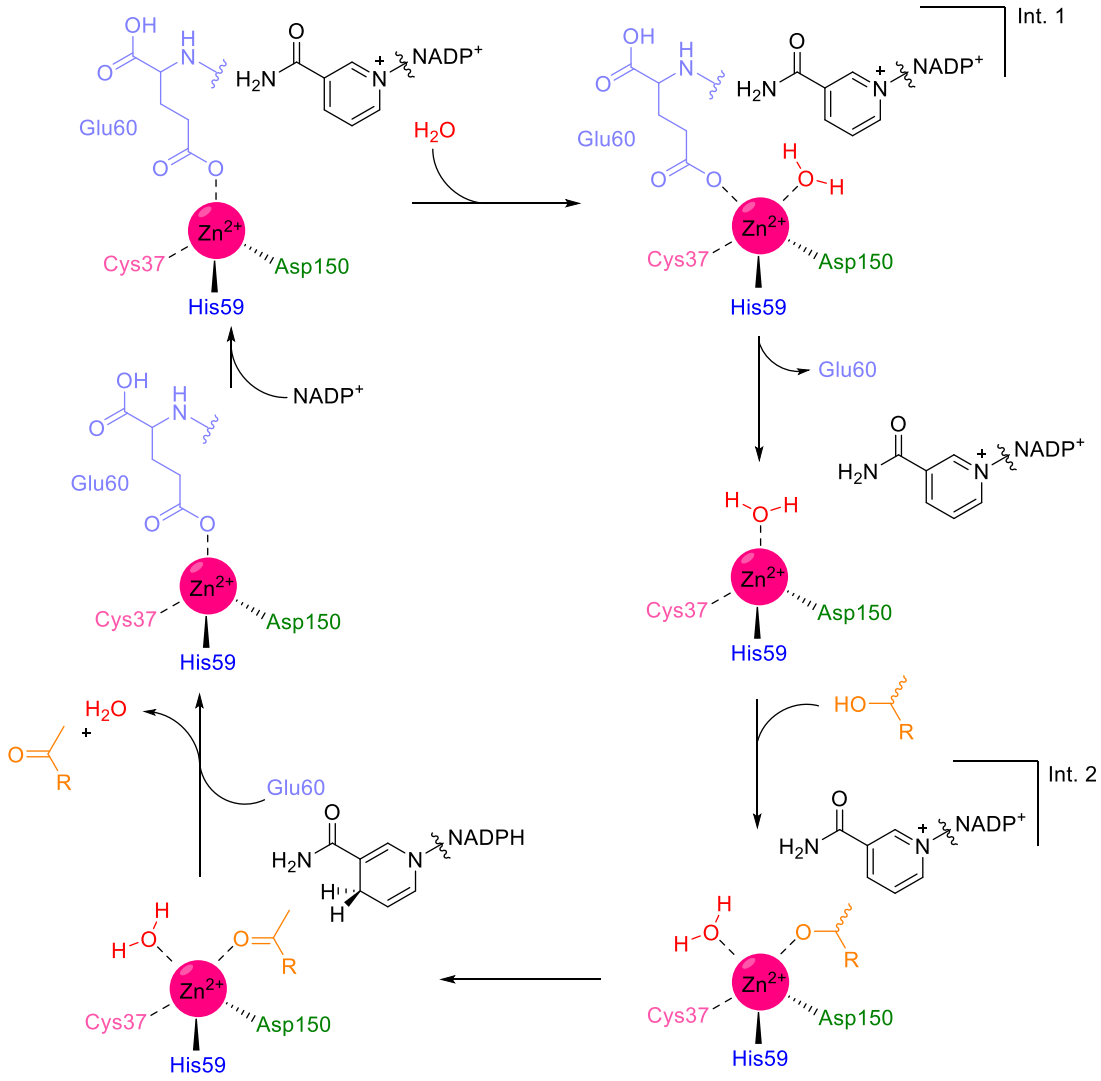


Figure 1.53. Mechanism of alcohol oxidation in TbADH using a pentacoordinated zinc species. Reproduced from Lee *et al.*[203]

The hydride transfer to the C4 position of the pyridinium ring of the cofactor then leads to the formation of the product and the reduced form of the cofactor. The reinstatement of the tetrahedral conformation of the zinc is due to the dissociation of the product and a water molecule, followed by the coordination of Glu60 and removal of NADPH to yield the WT state of the enzyme, concluding a full catalytic cycle.

1.3.2.3 Stereoselectivity of zinc-dependent alcohol dehydrogenases

In the reduction of ketones and aldehydes, the carbonyl substrates can be prochiral, yielding different enantiomers. Depending of the hydride used from

the C4 position of the nicotinamide ring of NAD(P)H, the product yielded will be the (*S*)- or (*R*)-alcohol. Due to evolutionary pressure, ADHs evolved to be stereospecific towards one enantiomer.[205] If the hydride transfer takes place from the *re*-face of the nicotinamide ring, the pro-*R* hydride is transferred, resulting in the (*S*)-alcohol by following the Cahn-Ingold-Prelog priority rule (CIP rule, Figure 1.54).[206] If the pro-*S* hydride is transferred, then the (*R*)-alcohol will be produced, following the anti-CIP rule. An estimation by Kaplan *et al*. revealed that half of the ADHs transferred the pro-*S* and the other half the pro-*R*.[207]

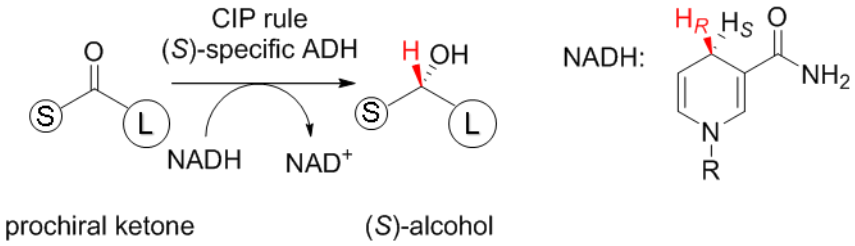


Figure 1.54. Illustration of the Cahn-Ingold-Prelog rule in the reduction of a prochiral ketone by a (*S*)-specific ADH. L: large group, the most prioritised according to the CIP rule. S: small group.

1.3.3 Conclusion

ADHs are robust biocatalysts used in asymmetric TH of prochiral ketones and aldehydes. The MDR subfamily possess a metal binding site, an additional feature compared to SDRs. This feature can be exploited to introduce metal complexes within the cavity of the enzymes and develop new ArMs. These ArMs can take advantages of the already evolved substrate binding pocket to enhance the substrate scope of the natural ADHs, e.g. towards imine and alkene reduction. Furthermore, ADHs are nicotinamide-dependent enzymes. By mimicking the interactions of the nicotinamide cofactor, supramolecular anchors could be developed in order to insert the desired metal complexes.

2 Aim and objectives

2.1 Overall aim

As presented in the literature review, artificial metalloenzymes (ArMs) are a powerful alternative to access challenging chemical reactions. The most versatile ArMs are currently based on non-enzymatic scaffolds. This is the case for the biotin-(strept)avidin technology developed by Ward's team or the use of the LmrR receptor by Roelfes' team.

Enzymatic scaffolds were also reported, such as P450s, CA etc. Compared to the non-enzymatic scaffolds, they offer an already evolved substrate activation pocket, leading to great control of the reaction. The main drawback of this type of scaffold is the limited promiscuity, inherent to the evolved enzymatic structure. However, the lack of promiscuity can be overcome by finely tuned the catalytic site to allow access to versatile metal catalyst and to extend the substrate scope.

So far, no enzymatic chassis has been reported with substrate promiscuity comparable to their non-enzymatic homologues. At the exception of P450s, there are very few examples of ArMs where the ability of enzyme to stabilise a particular transition state was exploited to insert non-natural activity.

Therefore, developing a method to design an ArM from a cofactor-dependent enzymatic scaffold that can be further tuned at will is of great interest. This would offer a suitable alternative to current high-throughput techniques that yield single purpose scaffolds, where the whole process needs to be carried out for each new purpose/chemical target.

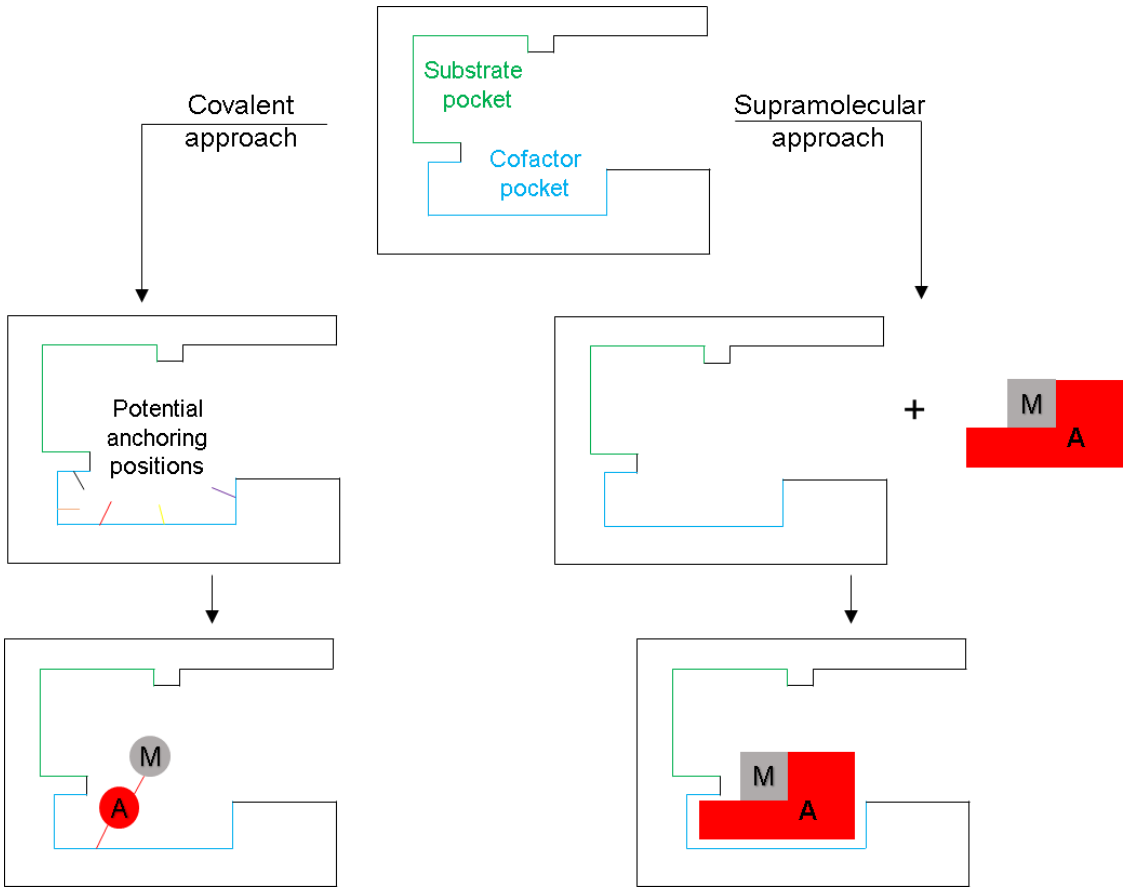


Figure 2.1. Overall representation of the approaches used in this study to build an ArMs from a cofactor-dependent scaffold. A: anchor, M: metal. The inserted metal is facing the already evolved substrate pocket, untouched, where the desired substrate molecules could fit into.

This study aims at designing an artificial metalloenzyme from a cofactor-dependent enzymatic scaffold. Medium chain alcohol dehydrogenases (MDRs) were picked as a starting point for modification, because of their interesting features. They possess a cofactor binding site that can be targeted by supramolecular anchors, a substrate binding site which is already evolved for interactions with various substrate molecules, and a metal binding site that can accommodate a metal ion.

ADHs are one of the most studied and widely used biocatalysts, after hydrolases. A plethora of information on kinetics, mechanism of action, substrate scope and crystallography are readily available as a starting point for designing an ArM. Moreover, the two distinct pockets for substrate and cofactor binding offer space for the insertion of a metal complex and a non-natural substrate to react with. Besides, our group recently published the use of this scaffold in the creation of an ArM capable of regenerating NADPH

cofactor, an important reaction for economic sustainability at an industrial scale.

Two ADHs were chosen in this study for the knowledge gathered by researchers throughout the years: horse liver alcohol dehydrogenase (HLADH) and *Thermoanaerobacter brockii* alcohol dehydrogenase (TbADH). The latter will be used as a scaffold using a covalent approach to design an ArM. The enzyme will be modified after rational design and probe for promiscuity for the regiospecific C=C double bond reduction of $NADP^+$.

The two enzymes will also be tested upon supramolecular anchoring of nicotinamide cofactor mimics with the objective to build an artificial transfer hydrogenase with a tuneable substrate scope beyond their current C=O double bond reduction.

2.2 Objectives

2.2.1 Development of enzymatic scaffolds capable of covalently anchoring versatile ligands

This objective aims at evaluating the position of a targeted cysteine residue within the catalytic site of TbADH, on its ability to accommodate a non-natural functionality. TbADH was previously used as a scaffold to develop an artificial metalloenzyme capable of reducing C=C double bonds in a regiospecific manner. First, the position of the cysteine within the active site will be evaluated *in silico* to generate a small mutant library based on the orientation of a chosen ligand within the cavity. Then the selected mutants will be engineered, transformed into *E. coli*, expressed and purified. Finally, each mutant will be tested upon incorporation of different ligands to evaluate their own capacity to create the desired chemo-enzymatic hybrid.

2.2.2 Artificial metalloenzymes for the reduction of nicotinamide derivatives

Following the previous results, mutants which can successfully react with the different ligands will be further evaluated with the corresponding metal complexes. The addition of metals into the mutants will be investigated and characterised. Once properly characterised by spectrophotometry and mass spectrometry, all metal-based catalysts will be assessed for their ability to reduce nicotinamide cofactors and their mimics.

2.2.3 Building an artificial metalloenzyme using a supramolecular anchoring approach

This objective involves the investigation of two ADHs (dimeric HLADH and tetrameric TbADH) for their ability to interact with supramolecular anchors in their cofactor-binding pocket in a supramolecular manner. HLADH was selected as it was the most studied protein from the ADH family. Supramolecular anchors will be designed based on the nicotinamide structure, targeting similar interactions to NAD(P) cofactors with the enzymes. Once synthesized, anchors will be evaluated both *in vitro* and *in silico*. Finally, based on the results of the first generation of anchors, optimisation of the binding will be investigated further, using docking. Two paths will be considered: the first one is the development of a second generation of anchors, putting an

emphasis on the chemical optimisation aspect of the design of ArMs; and the second is the assessment of more suitable proteins within the ADH family to accept the first generation of anchors, focusing on the biological optimisation of the design of ArMs.

3 Materials and methods

3.1 Materials

3.1.1 Chemical synthesis

Unless otherwise stated, all chemicals and solvents were purchased from Sigma Aldrich. Silica (60 Å) was used for column chromatography. Evaporation of solvents under reduced pressure was performed using a bench rotary evaporator (Büchi).

All compounds were analysed using a Bruker AV400 or DPX300 (400 or 300 MHz ^{1}H frequency, 100 or 75 MHz ^{13}C frequency) and a microTOF 61 Mass Spectrometer using Electron Spray Ionisation (ESI-MS, Bruker Corp) (Appendix 11).

NMR spectra were recorded at 298 K. Chemical shifts were quoted in parts per million (ppm), referenced to the residual deuterated solvent quoted in text as internal standard. When applicable, coupling constants J were quoted in Hz. Multiplicity of each signal was designated with the following abbreviations: s, singlet; d, doublet; t, triplet; q, quartet; m, multiplet; dd: doublet of doublet. Except otherwise stated, all ESI-MS analysis of chemical compounds were performed in methanol.

3.1.2 Protein expression

All biological experiments were conducted under aseptic conditions using a laminar flow cabinet level 1, MSC Advantage (Thermo Scientific). All media and flasks were sterilised using a Prestige Classic 2100 benchtop autoclave (Medstore Medical) or an AMB420 (Astell), at operating temperatures and pressures of 126 ˚C and 1.4 bar.

E. coli BL21 (DE3), BL21 (DE3) pLys and DH5α competent cells were purchased from Novagen (Germany). Protein genes were already available in our laboratory, inserted into pET21a (TbADH) and pRSETb (His-HLADH) vectors.

Plasmids were transformed into cells by electroporation using a GenePulser Xcell (Interface v3.15, BioRad). Super Optimal broth with Catabolite

repression (SOC, containing 2 % tryptone, 0.5 % yeast extract, NaCl 10 mM, KCl 2.5 mM, $MgCl_2$ 10 mM and glucose 20 mM) and Luria-Bertani (LB, containing 1 % tryptone, 0.5 % yeast extract and NaCl 170 mM) media were used for transformation and expression respectively.

Cultures were grown in 250 mL or 2 L Erlenmeyer flasks, in New Brunswick Scientific Innova 40 Incubator Shakers (Eppendorf).

Cells were harvested using an Avanti J-26 XP centrifuge (Beckman Coulter) and a 5810R centrifuge (Eppendorf,) and then stored at -80 ˚C in a DW-86L828J freezer (Haier Biomedical).

3.1.3 Protein purification

One Shot Cell Disruptor (Constant System Ltd.) or a Model 120 Sonic Dismembrator (Fisherbrand) were used to physically lyse the cells. If required, a water bath (TC 120, Grant) was used to heat shock cell lysates. AKTA Fast Liquid Protein Chromatography System (GE Healthcare) was used to purify the protein. Proteins were loaded onto a HisTrap FF crude 1 mL and StrepTrap HP 5 mL affinity columns for protein purification (GE Healthcare). Precast SDS-PAGE (12 % Tris-Glycine, BioRad) and Vivaspin 20 (10.000 MWCO) centrifugal concentrators (Sartorius Stedim Biotech) were used to analyse and concentrate the purified proteins, respectively.

Bradford assay for protein concentration assay was purchased from Bio-Rad Laboratories Inc. (UK), prepared on 96-well plate (Corning Inc.) and assays were monitored on a FLUOstar OPTIMA (BMG Labtech).

3.1.4 Computational Studies

3.1.4.1 Protein preparation

Protein sequences and crystal structures were used from the RSCB Protein Data Bank (PDB). Structures were prepared either using AutoDockTools4 (version 1.5.6) or Maestro Protein Preparation Wizard (Schrödinger, version 11.6). PyMol (version 1.7.4.5) was used to visualize the results of the prepared structure as well as to compute residue mutations. Theorical protein masses were calculated based upon their amino acid sequences using the ExPASy Resource Portal.

3.1.4.2 Ligand preparation

All chemical structures were constructed in 3D using Chem3D HotLink interface from ChemDraw Professional 16.0, then translated into the appropriate format using AutoDockTools4 (version 1.5.6). Alternatively, ligands were computed using the Ligprep tool from the Schrödinger suite.[208]

3.1.4.3 Classical and covalent docking

AutoDock Vina[209] software was used to model and compute docking assays. The Glide SP software[210] was used to perform covalent docking. All computational work using the Maestro software (covalent docking) was performed by Floriane Martins.

3.1.4.4 Sequence alignment

Sequence alignments were performed online, using the Basic Local Alignment Search Tools (BLAST) from the National Center for Biotechnology Information (NCBI).

3.1.5 Site directed mutagenesis

The different primers were design in both forward and reverse directions using SnapGene. GenElute™ Plasmid MiniPrep Kit (Sigma-Aldrich) and QuickChange Lightning Site-Directed Mutagenesis Kit (Agilent Technologies) were used to extract DNA and performed site directed mutagenesis respectively. Mastercycler personal (Eppendorf) was used to perform polymerase chain reaction (PCR) to amplify the mutated genes prior to transformation. XL10- Gold cell line was provided with the mutagenesis kit (Agilent) to transform the newly mutated genes.

µLITE+ (BioDrop) was used to determine DNA concentration after extraction. DNA sequencing was performed by Integrated DNA Technologies (IDT) and Source BioScience.

3.1.6 Bioconjugation

PD-10 Desalting Columns (GE Healthcare) were used to purify and prepare labelling products for subsequent analysis. Agilent UV-Vis spectrophotometer (Agilent Technologies) was used to discriminate purified fractions. Vivaspin 6 (10,000 MWCO) centrifugal concentrators (Sartorius Stedim Biotech) were

used to concentrate labelling products. ESI-MS experiments were conducted on a Brucker impact II spectrometer (Brucker Corp). Inductively coupled plasma mass spectrometry (ICP-MS) experiments were conducted on an iCAP-Q (Thermo-Fisher Scientific) equipped with CCTED (collision cell technology with energy discrimination).

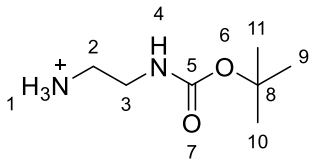
3.1.7 Enzymatic assays

NAD^+ and NADH were purchased from Apollo Scientific Ltd (UK). UV mini-1240 UV-Vis spectrophotometer (Shimadzu), 1220 Affinity LC (Agilent) with Chiracel OD column (4.6 mm* 250mm, PS 10 µm) and 7820A GC-FID System (Agilent) equipped with a HP-5 column (30 m* 0.32 mm, film thickness: 0.25 microns, carrier: helium) were used to analyse protein assays and products of catalysis.

3.2 Methods to design an artificial metalloenzyme through a covalent approach

3.2.1 Chemical synthesis of ligands

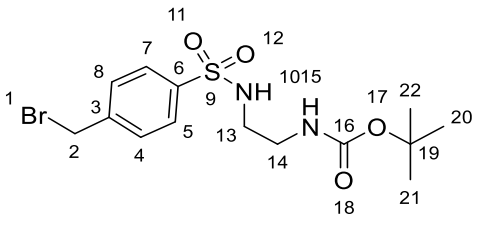
<u>*N*-(*tert*-butyl carbamate)-ethylenediamine (143)</u>



Ethylenediamine **142** (4 mL, 60 mmol) was dissolved in $CHCl_3$ (100 mL) and the solution was cooled down to -15 ˚C. To this solution was added dropwise di-*tert*-butyl dicarbamate (7.5 mL, 30 mmol) in $CHCl_3$ (30 mL). The resulting mixture was stirred overnight and allowed to warm up to room temperature. The crude mixture was washed with brine supplemented with 1 M NaOH (5 % v/v, 80 mL three times), brine (80 mL) then distilled water (80 mL). The organic phase was then dried over $MgSO_4$, filtered and the solvent was removed under reduced pressure to yield the product **143** as an off-white solid (4.798 g, 29.9 mmol, >99%).[211]

Rf (MeOH) 0.25; **^{1}H NMR** ($CDCl_3$, 300 MHz) δ (ppm) 5.20 (s, 1H, H^4) 3.10 (t, 2H, H^2, J=6.3 Hz) 2.73 (t, 2H, H^3, J=6.3 Hz) 1.39 (s, 9H, $H^{9\text{-}11}$) 1.31 (s, 2H, H^1); **^{13}C NMR** ($CDCl_3$, 75 MHz) δ (ppm) 28.3; **ESI-MS$^+$** calculated for $(C_7H_{17}N_2O_2)^+$ 161.13, found 161.1291 ($M + H^+$).

<u>*N*-(*N'*-(*tert*-butyl carbamate)-2-aminoethyl)-4-(bromomethyl) benzenesulfonamide (145)</u>

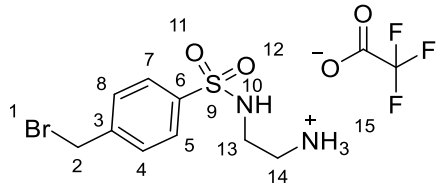


In a solution of *N*-(*tert*-butyl carbamate)-ethylenediamine **143** (300 mg, 1.88 mmol) in CH_2Cl_2 (5 mL) was added triethylamine (280 µL, 2.0 mmol). The solution was cooled to 0 ˚C, then a solution of 4-(bromomethyl)-benzenesulfonyl chloride **144** (542 mg, 2.02 mmol) in CH_2Cl_2 (2 mL) was

added dropwise. After few minutes the solution was washed with a sat. $NaHCO_3$ solution (10 mL twice) then with brine (10 mL). The organic layer was then dried over $MgSO_4$, filtered and the solvent was evaporated under reduced pressure. The crude solid was purified by glass column chromatography (CH_2Cl_2/MeOH, gradient from 100/0 to 95/5, v/v), yielding the pure compound **145** as a white powder (500 mg, 1.26 mmol, 67%).[212]

Rf (EtOAc/Hexane, 6/4) 0.8; **^{1}H NMR** ($CDCl_3$, 300 MHz) δ (ppm) 7.85 (d, 2H, $H^{4,8}$, J=6.0 Hz) 7.55 (d, 2H, $H^{5,7}$, J=6.0 Hz) 5.26 (s, 1H, H^{10}) 4.84 (s, 1H, H^{15}) 4.52 (s, 2H, H^{2}) 3.26 (q, 2H, H^{13}, J=4.2 Hz) 3.11 (q, 2H, H^{14}, J=4.2 Hz) 1.60 (s, 9H, $H^{20\text{-}22}$) **^{13}C NMR** (methanol-d_4, 100 MHz) δ (ppm) 157.19, 143.11, 140.14, 129.56, 127.02, 42.41, 39.95, 30.93, 29.79, 27.40 **ESI-MS$^+$** calculated for ($C_{14}H_{21}{}^{79}BrN_2O_4S$) 392.04 and for ($C_{14}H_{21}{}^{81}BrN_2O_4S$) 394.04, found 415.0309 and 417.0292 ($M + Na^+$).

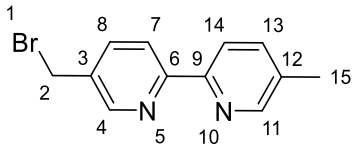
***N*-(2-aminoethyl)-4-(bromomethyl) benzenesulfonamide (L1)**



To a solution of *N*-(*N'*-(*tert*-butyl carbamate)-2-aminoethyl)-4-(bromomethyl) benzenesulfonamide **145** (200 mg, 0.51 mmol) in CH_2Cl_2 (10 mL) on ice was added trifluoroacetic acid (400 µL, 5.1 mmol). The crude mixture was stirred overnight. The resulting solution was evaporated under reduced pressure to yield the desired compound as a light orange TFA salt (200 mg, 0.49 mmol, 97%).[212]

Rf (EtOAc/Hex, 6/4) 0; **^{1}H NMR** (DMSO-d_6, 300 MHz) δ (ppm) 7.80 (d, 2H, $H^{4,8}$, J=4.6 Hz) 7.71 (d, 2H, $H^{5,7}$, J=4.8 Hz) 4.79 (s, 2H, H^{2}) 2.96 (q, 2H, H^{13}, J=6.0 Hz) 2.87 (q, 2H, H^{14}, J=4.8 Hz) **^{13}C NMR** (DMSO-d_6, 100 MHz) δ (ppm) 143.41, 139.64, 130.65, 127.55, 69.03, 62.61, 33.17 **ESI-MS$^+$** calculated for $(C_9H_{14}{}^{79}BrN_2O_2S)^+$ 293.00 and for $(C_9H_{14}{}^{81}BrN_2O_2S)^+$ 295.00, found 292.9957 and 294.9938 (M^+).

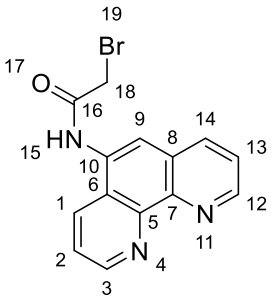
5-(bromomethyl)-5'-methyl-2,2'-bipyridine (L2)



Under inert atmosphere were dissolved 5,5'-dimethyl-2,2'-dipyridine **146** (250 mg, 1.4 mmol) and *N*-bromosuccinimide (250 mg, 1.4 mmol) in CCl_4 (10 mL). Azobisisobutyronitril (25 mg, 0.14 mmol) was then added and the resulting mixture was refluxed at 77 ˚C overnight. The suspension was then filtered, and the filtrate was left at room temperature for 48 h, until full precipitation of the di-brominated by-product was observed. The by-product was then filtered, and the resulting solution was purified by glass column chromatography (isocratic, CH_2Cl_2/MeOH, 98/2, v/v) yielding the desired mono-brominated chemical as an off-white solid (131 mg, 0.49 mmol, 36 %).[213]

Rf (CH_2Cl_2/MeOH, 9/1) 0.6 **^{1}H NMR** ($CDCl_3$, 300 MHz) δ (ppm) 8.68 (s, 1H, H^4) 8.52 (s, 1H, H^{11}) 8.38 (d, 1H, H^8, J=8.2 Hz) 8.30 (d, 1H, H^{13}, J=8.0 Hz) 7.85 (dd, 1H, H^7, J=8.1, 1.9 Hz) 7.65 (dd, 1H, H^{14}, J=8.0, 1.8 Hz) 4.55 (s, 2H, H^2) 2.42 (s, 3H, H^{15}) **^{13}C NMR** (CDCl3, 300 MHz) δ (ppm) 156.37, 153.15, 149.86, 149.38, 137.63, 133.87, 133.38, 120.89, 120.86, 29.90, 18.53 **ESI-MS$^+$** calculated for $(C_{12}H_{12}{}^{79}BrN_2)^+$ 262.02 and for $(C_{12}H_{12}{}^{79}BrN_2)^+$ 264.02, found 263.0174 and 265.0151 ($M + H^+$)

5-(2'-bromo)-acetamido-1,10-phenanthroline (L3)



Under inert atmosphere 5-amine-1, 10-phenanthroline **147** (195 mg, 1 mmol) was added to 30 mL of $CHCl_3$ (anhydrous). Bromoacetyl bromide **148** (104 µL, 1.2 mmol) was then gently added. The resulting mixture was heated to reflux overnight. The resulting suspension was then filtered while hot and the solid

was recrystallized from hot MeOH yielding the desired compound as orange-red crystals (147 mg, 0.47 mmol, 47%).[16]

Rf (MeOH) 0; **^{1}H NMR** (DMSO-d_6, 400 MHz) δ (ppm) 10.94 (s, 1H, H^{15}) 9.35 (dd, 1H, H^{3}, J=4.6, 1.3 Hz) 9.24 (dd, 1H, H^{12}, J=5.0, 1.4 Hz) 9.18 (d, 1H, H^{1}, J=8.3 Hz) 9.09 (d, 1H, H^{14}, J=15 Hz) 8.60 (s, 1H, H^{9}) 8.25 (dd, 2H, $H^{2,13}$, J=8.2, 5.0 Hz) 4.38 (s, 2H, H^{18}); **^{13}C NMR** (DMSO-d_6, 100 MHz) δ (ppm) 172.88, 149.50, 145.92, 143.52, 138.78, 135.62, 133.79, 130.00, 126.29, 125.84, 119.86, 62.45 **ESI-MS^{+}** calculated for $(C_{14}H_{11}{}^{79}BrN_3O)^{+}$ 316.01 and for $(C_{14}H_{11}{}^{81}BrN_3O)^{+}$ 318.01, found 316.0099 and 318.0084 ($M + H^{+}$)

3.2.2 Design of the library of cysteine mutants

3.2.2.1 Protein preparation

From the crystal structure of WT TbADH (PDB 1YKF), the following mutations were created using PyMol: H59A, D150A, C203S, C283A and C295A. Additionally, the zinc ion, naturally coordinated with C37, H59 and D150 was removed from the file. This yielded the structure of TbADH 5M. The cysteine in position 37 was mutated in an alanine to provide the cysteine-free scaffold 6M. The scaffold was then used to introduce, *in silico*, single cysteine mutations at positions 175, 178, 203 and 266.

Each mutant was prepared by using the Maestro Protein Preparation Wizard in the Schrödinger suite.[214] The structure integrity was analysed, missing hydrogen atoms and residues side chains were added to the structure by Prime-refinement throughout the pre-processing. During the refinement, water molecules with less than three hydrogen bonds to other atoms were removed, which resulted in no more water in the binding site. Selection of the position of hydroxyl and thiol hydrogen, the protonation/tautomer states and the “flip” assignment of Asp, Glu, Arg, Lys and His were adjusted at pH = 7.0 using PROPKA.[215] Finally, the structures were minimized using the OPLS3 force field[216] with a RMSD = 0.3 Å displacement of non-hydrogen atoms as convergence parameter.

3.2.2.2 Ligand preparation

Ligand **L1** was prepared using Ligprep from Schrödinger suite, with OPLS3 force field. Generation of all possible protonation and ionisation states combinations was performed by using Epik in aqueous solution at pH of 7.0 +/- 2.0.

3.2.2.3 Grid preparation

In order to define the pocket of interest for the docking, a grid was set around the defined docking site. The enclosure box was defined from the optimized protein structure at the centroid of the active site (10 Å radius around the co-crystallized ligand). No constraints were added. The standard settings of a van der Waals scaling factor of 1.0 for nonpolar atoms was conserved. Nonpolar atoms were defined with absolute value of partial atomic charges ≤ 0.25.

3.2.2.4 Covalent docking

The prepared ligand **L1** was covalently docked into the receptor grid using Glide SP procedure, within the five single cysteine mutants containing C37, C175, C178, C203 and C266. In this method, the receptor was kept rigid. Glide docking uses a technique of exhaustive systematic search to predict orientation, conformation and binding position of a ligand inside a receptor pocket. The following steps were undertaken during a Glide docking procedure:

- Determination of the chemical reaction to apply. In this study, a nucleophilic substitution
- Determination of the reagent of the reaction. In this study, the alkyl bromide from ligand **L1** and the thiol for the single cysteine residue
- Collection of ligand conformations (from exhaustive enumeration of ligand torsions)
- Minimization of ligand poses with full flexibility. A Monte Carlo procedure analysed nearby torsional minima and selected the minimum energy poses.

3.2.2.5 Assessment of the results

The covalently docked ligand **L1** was visualised in PyMol for each mutant. The space around the ligand was then expanded to 4 Å^3. Each amino acid contained within the expanded space was listed for each mutant. From this list were discarded the prolines, the residues placed on a secondary structure and the residues in which the side chain was not pointing towards the catalytic site of the enzyme. From the remaining residues, the positions that were shared in all the mutation were chosen for experimental work.

Single cysteine mutants were also prepared at these selected positions, and the covalent docking procedure was repeated, as above, to assess the position of the ligands within the mutants.

3.2.3 Site directed mutagenesis

Methods provided with GenElute^{TM} Plasmid MiniPrep Kit (Sigma-Aldrich) and QuickChange Lightning Site-Directed Mutagenesis Kit (Agilent Technologies) were used to extract DNA and set up the mutagenesis reaction respectively. DNA from the TbADH 5M mutant was extracted and sequenced using T7 forward and T7-term primers. The sequence was used to design the primers for the mutations (Table 3.1).

Table 3.1 Primer sequences and denomination of the different mutations performed. The codons responsible for the mutations were underlined in all sequences.

Mutation	Template	Primers	Mutant name
C37A	5M	Forward: cgctgctgtgcgcgcactctgacatccatac Reverse: gtatgatgtcagagtgcgcgcacagcagcg	6M
G174C	6M	F: gcaaccgttgcggttctgtgcatcggtccggttggcctga R:tcaggccaaccggaccgatgcacagaaccgcaacggttgc	7M-C174
G198C	6M	F: ggtcgtatcatcgcggtttgctctcgtccggtgagcgttg R:caacgctcaccggacgagagcaaaccgcgatgatacgacc	7M-C198
S203C	6M	F: gttggttctcgtccggtgtgtgttgatgctgctaaatact R: agtatttagcagcatcaacacacaccggacgagaaccaac	7M-C203
A242C	6M	F: gtggacgcagcgattatctgcggtggtaacgcggatatca R: tgatatccgcgttaccaccgcagataatcgctgcgtccac	7M-C242
G243C	6M	F: gacgcagcgattatcgcatgcggtaacgcggatatcatgg R: ccatgatatccgcgttaccgcatgcgataatcgctgcgtc	7M-C243

Each mutant DNA was prepared by mixing 1 µL of template DNA with, in order, 5 µL of reaction buffer provided by the supplier, 1.5 µL of each primer (forward and reverse), 1 µL of dNTPs mix, 1.5 µL Quick solution, 37.5 µL of molecular biology grade water and 1 µL of Quick enzyme for a final volume of 50 µL. The mixture was then placed into a thermocycler and the following PCR sequence was rum:

- segment 1, 1 cycle, 95 °C, 2 minutes
- segment 2, 18 cycles, 95 °C (20 seconds), 60 °C (10 seconds), 68 °C (3 minutes 20 seconds)
- segment 3, 1 cycle, 68 °C, 5 minutes

The PCR product was transformed into XL10 Gold, the solution was dispersed onto plate of LB and Agar supplemented with carbenicillin (100 µg.mL^{-1}) and were incubated overnight at 37 °C.

Colonies resulting from the incubation were handpicked (3 colonies per mutation), resuspend into LB with carbenicillin (100 µg.mL^{-1}), incubated overnight, the DNA was subsequently extracted then sequenced. Only one mutant plasmid stock was stored at -20 °C and used for subsequent experiments, whilst the others were discarded. Plasmids containing the mutated genes were then transformed into *E. coli* BL21 (DE3). On ice, in a conical bottom Eppendorf tube were mixed 1 µL of DNA with 25 µL of competent cells. The mixture was left on ice for 5 min then transferred into a GenePulser cuvette (0.1 cm electrode gap, BioRad). A single pulse of 1.8 kV was applied through the cuvette then 500 µL of SOC medium was added for resuspension. The medium was transferred into Eppendorf tubes and incubated at 37 ˚C for 1.5 h. After incubation, the cells were dispersed onto LB plates with carbenicillin (100 µg.mL^{-1}).

Single colonies were handpicked for each mutant and transferred into a 5 mL liquid culture of LB media with carbenicillin (100 µg.mL^{-1}). They were incubated overnight at 37 ˚C, 250 rpm. Then, 200 µL of the liquid culture was aliquoted and mixed with 800 µL of glycerol solution (50 % v/v) and the cell stocks were stored at -80 ˚C.

3.2.4 Expression and purification of TbADH mutants

3.2.4.1 Expression of TbADH mutants

The following procedure was performed with every mutant regardless of the mutations. A seed culture (6 mL in LB supplemented with carbenicillin 100 µg.mL^{-1}) was prepared into a 50 mL sterile Falcon tube from cryostock (6 µL) and used to inoculate 500 mL LB medium supplemented with carbenicillin (100 µg.mL^{-1}). The culture was grown at 37 ˚C, 200 rpm until an OD_{600} = 0.6 - 0.8 was reached (approximately 2 h). Expression was then induced using isopropyl-β-D-1-thiogalactopyranoside (IPTG) at 1 mM and cells were grown overnight at 30 ˚C, 120 rpm to an OD_{600} = 4-5. A sample was taken for SDS-PAGE analysis while the remaining cells were harvested by centrifugation (4

˚C, 20 min, 5000 g). The supernatant was then removed, and, on ice, the cells were resuspended in cold Tris HCl 100 mM, NaCl 150 mM buffer pH 8.0. The suspension was transferred into 50 mL Falcon tubes, centrifuged (4 ˚C, 10 min, 5000 g) and stored at -80 ˚C until further use.

3.2.4.2 Purification of TbADH mutants

The cell pellet was thawed on ice for 1h while the lysis buffer was prepared as follows: proteases inhibitors cocktail (1 tablet), lysozyme from chicken egg (1 $mg.mL^{-1}$) and benzonase nuclease (1 $\mu L.mL^{-1}$) were dissolved in 15 mL of 100 mM Tris.HCl, 150 mM NaCl buffer pH 8.0. The pellet was then resuspended in the fresh lysis buffer and the suspension was stirred on ice for 1h. The suspension was sonicated on ice (5 min, 35% power, 30 sec ON, 59 sec OFF) then centrifuged (25 000 g, 15 min, 10 ˚C). The cleared lysate was transfer into a water bath at 60 ˚C for 15 min then cooled on ice for 10 min to induce precipitation of mesophilic proteins. The resulting white suspension was centrifuged (16 900 g, 15 min, 4 ˚C) and the supernatant was collected and purified by affinity chromatography.

Affinity chromatography was performed on an AKTA FPLC system using StrepTrap HP column (5 mL) with a flow rate of 3 $mL.min^{-1}$. The column was equilibrated with buffer Tris.HCl 100 mM, NaCl 150 mM pH 8.0 (buffer W), the sample was then loaded (10-15 mL) and pure TbADH was recovered with the elution buffer (buffer W supplemented with 2.5 mM desthiobiotin). Fractions containing protein were analysed by SDS-PAGE. The pure fractions were pooled, and a buffer exchange was carried out using Vivaspin 20 (10,000 MWCO) and Tris.HCl 100 mM buffer pH 8.0 was used to remove the presence of NaCl and desthiobiotin. Once the buffer exchanged, the amount of protein was then quantified *via* Bradford method before storage at -20 ˚C.

3.2.5 Bioconjugation of protein with metal free ligands

3.2.5.1 Optimisation of the bioconjugation procedure

TbADH 5M (25 µM, 1 $mg.mL^{-1}$) and ligand **L1** (100 µM) were mixed in Tris.HCl 100 mM buffer pH 8.0 for 1 h at room temperature. For subsequent experiments the parameters were varied as follows: a) time, either 1 or 4 h, b) temperature, either room temperature or 37 °C, c) protein concentration, either

1 or 4 mg.mL^{-1} and d) ligand concentration, either 25 or 100 µM. Once the bioconjugation was finished, the resulting mixture was purified through PD10 desalting column, previously equilibrated with molecular biology grade water. Fractions resulting from the purification were analysed by UV-Vis. The fractions of interest were pooled and concentrated using Vivaspin 6 (10 000 MWCO). The final concentration was assayed by the Bradford method. Ellman's assay was performed to evaluate the ratio of free thiol available within each protein sample.

3.2.5.2 Optimised bioconjugation procedure

Ligands **L1**, **L2** and **L3** (100 µM) were individually mixed with TbADH 5M, TbADH 6M, 7M-C174, 7M-C198, 7M-C203, 7M-C242 or 7M-C243 (25 µM, 1 mg.mL^{-1}) in Tris.HCl 100 mM buffer pH 8.0 for 4 h at 37 °C. Once completed, each bioconjugation product was purified and analysed by Ellman assay and ESI-MS. The protein concentration was determined by Bradford assay.

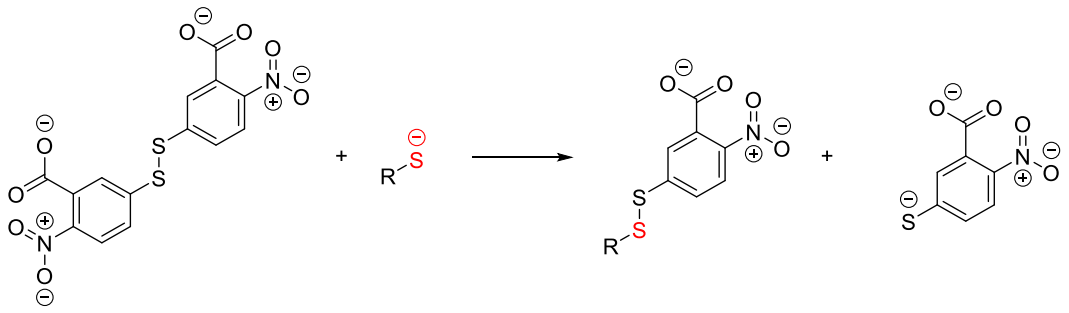
3.2.6 Bioconjugate analysis

3.2.6.1 Bradford assay

A set of standard protein concentrations ranging from 0.25 to 1 mg.mL^{-1} was prepared using bovine serum albumin (BSA) diluted in the required solvent from a stock solution of 5 mg.mL^{-1}. If the samples were expected to be out of range, appropriate dilutions were made using the same solvent as for the standards. Using a 96-well plate, 10 µL were placed at the bottom of each well, followed by 300 µL of Bradford reagent (BioRad). The reaction mixtures were incubated for 15 min at room temperature, placed into a plate reader and the absorbance was recorded at 525 nm.

3.2.6.2 Ellman assay

Ellman's reagent (5, 5'-dithiobis (2-nitrobenzoic acid), DTNB) was solubilised in a buffer solution (sodium phosphate 100 mM, EDTA 1 mM pH 8.0), at a concentration of 4 mg.mL^{-1}. The determination of free thiols in proteins was achieved in accordance with the following reaction:



DTNB^{2-} mixed disulfide TNB^{2-} absorbance at 412 nm

Samples were prepared as follows: 445 µL of buffer, 45 µL of protein sample (or protein buffer for negative control) and 10 µL of Ellman's reagent solution were mixed together. The reaction was left at room temperature for 15 min then absorbance was monitored at 412 nm. Concentration of free thiols were then calculated using the following equation:

$$[free\ SH] = \frac{Abs\ protein - Abs\ control * 1\ 000\ 000 * 500}{14\ 500 * 45}$$

Where [free SH] correspond to the concentration of free thiol (in µM), Abs protein is the absorbance of the protein sample at 412 nm, Abs control is the absorbance of the control cuvette at 412 nm, 500 and 45 are the volume of the reaction and the sample respectively, 1,000,000 is the conversion factor from M to µM and 14500 M^{-1} cm^{-1} is the coefficient of molar extinction of TNB^{2-} at 412 nm under the assay's conditions. A cuvette of path length 1 cm was used for each experiment.

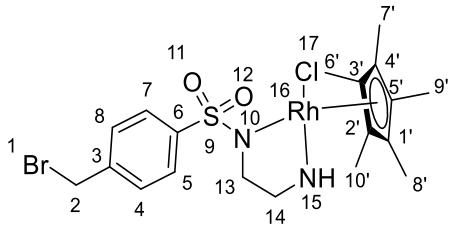
3.2.6.3 ESI-MS

Protein samples for injection into ESI-MS were prepared as follows: 40 µL of sample were added to 40 µL of 0.1 % (v/v) formic acid in acetonitrile. The preparation was then spun for 1 min at 16900 g in a benchtop centrifuge and the supernatant was injected into the calibrated ESI-TOF (detector: micro channel plate, MCP) for analysis.

3.3 Method to build an artificial metalloenzyme using a covalent approach

3.3.1 Synthesis of metal complexes

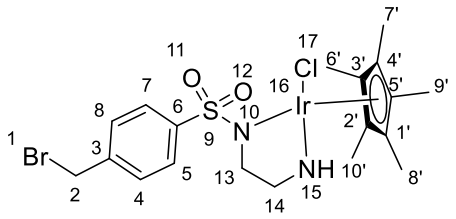
Cp*Rh (*N*-(2-aminoethyl)-4-(bromomethyl)benzenesulfonamide) chloride (M1a)



This compound was synthesized by adapting a previously described protocol.[217] Working under nitrogen, pentamethylcyclopentadienyl rhodium(III) chloride dimer (87 mg, 0.14 mmol) was suspended in methanol (2 mL). To this suspension was added *N*-(2-aminoethyl)-4-(bromomethyl) benzenesulfonamide **L1** (114 mg, 0.28 mmol) then 1 mL of methanol was added to improve the particle dispersion. Upon addition of 100 µL of triethylamine (TEA), the mixture immediately turned into a yellow/orange clear solution, indicating the formation of the rhodium-sulfonamide complex. The resulting mixture was filtered to remove any unreacted reagent. The desired product was precipitated by adding the mixture dropwise into cold *n*-hexane (10 volumes), collected by filtration and dried, to obtain a bright orange powder (66.7 mg, 0.11 mmol, 42%).

Rf (MeOH) 0.21 **^{1}H NMR** (methanol-d_4, 300 MHz) δ (ppm) 7.94 (t, 2H, $H^{5, 7}$, J = 7.8 Hz), 7.39 (d, 2H, $H^{4, 8}$, J = 8.3 Hz), 4.59 (s, 1H, H^{2}), 4.49 (s, 1H, H^{2}, Cl replacement), 2.69 (m, 4H, $H^{13, 14}$) 1.81 (s, 15H, $H^{6'\text{-}10'}$) **^{13}C NMR** (methanol-d_4, 100 MHz) δ (ppm) 128.21, 128.02, 126.89, 125.99, 94.14, 63.20, 49.53, 45.40, 8.28 **ESI-MS^{+}** calculated for $(C_{19}H_{27}{}^{79}Br^{35}ClN_2O_2RhS)^{+}$ 564.98, found 529.0032 (M + H^{+} - ^{35}Cl), 564.9793 (M + H^{+}) and calculated for $(C_{19}H_{27}{}^{81}Br^{35}ClN_2O_2RhS)^{+}$ 566.98, found 532.0015 (M + H^{+} - ^{35}Cl) and 566.9772 (M + H^{+}).

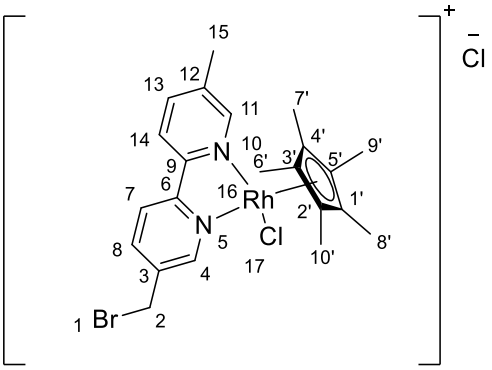
Cp*Ir (*N*-(2-aminoethyl)-4-(bromomethyl) benzenesulfonamide) chloride (M1b)



Following the procedure used for the synthesis of **M1a**, pentamethylcyclopentadienyl iridium(III) chloride dimer (87 mg, 0.11 mmol) was suspended in methanol (2 mL). To this suspension was added N-(2-aminoethyl)-4-(bromomethyl) benzenesulfonamide **L1** (90 mg, 0.22 mmol) then 1 mL of methanol was added to improve the particle dispersion. Upon addition of 100 µL of triethylamine (TEA), the mixture immediately turned into a yellow/orange clear solution, indicating the formation of the iridium-sulfonamide complex. The resulting mixture was filtered to remove any unreacted reagent. The desired product was precipitated by adding the mixture dropwise into cold *n*-hexane (10 volumes), collected by filtration and dried, to obtain a bright yellow powder (113.5 mg, 0.16 mmol, 72%).

Rf (MeOH) 0.21 **^{1}H NMR** (methanol-d_4, 300 MHz) δ (ppm): 7.99 (t, 2H, $H^{5, 7}$, J = 8.4 Hz), 7.49 (d, 2H, $H^{4, 8}$, J = 8.2 Hz), 4.68 (s, 1H, H^{2}), 4.60 (s, 1H, H^{2}, Cl replacement), 2.61 (m, 2H, H^{13}), 2.50 (m, 2H, H^{14}), 1.78 (s, 15H, $H^{6'\text{-}10'}$) **^{13}C NMR** (methanol-d_4, 100 MHz) δ (ppm) 128.57, 128.23, 128.08, 85.63, 50.96, 46.49, 44.63, 8.21 **ESI-MS^{+}** calculated for $(C_{19}H_{27}{}^{79}Br^{35}ClN_2O_2IrS)^{+}$ 655.04, found 577.1080 (M + H^{+} - ^{79}Br), 619.0598 (M + H^{+} - ^{35}Cl), 655.0336 (M + H^{+}) and calculated for $(C_{19}H_{27}{}^{81}Br^{35}ClN_2O_2IrS)^{+}$ 657.04, found 575.1092 (M + H^{+} - ^{81}Br), 621.0586 (M + H^{+} - ^{35}Cl) and 657.0340 (M + H^{+}).

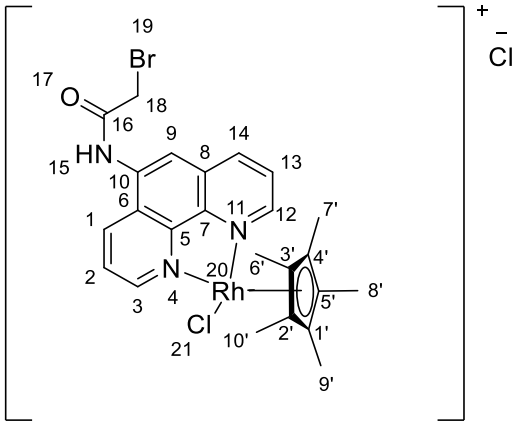
Cp*Rh (5-(bromomethyl)-5'-methyl-2,2'-bipyridine) chloride (M2)



Following the procedure used for the synthesis of **M1a**, pentamethylcyclopentadienyl rhodium(III) chloride dimer (154 mg, 0.25 mmol) was suspended in methanol (2 mL). To this suspension was added 5-(bromomethyl)-5'-methyl-2,2'-bipyridine **L2** (131 mg, 0.49 mmol) then 1 mL of methanol was added to improve the particle dispersion. The mixture immediately turned into a yellow/orange clear solution, indicating the formation of the rhodium-bipyridine complex. The resulting mixture was filtered to remove any unreacted reagent. The desired product was precipitated by adding the mixture dropwise into cold *n*-hexane (10 volumes), collected by filtration and dried, to obtain a bright yellow powder (127.4 mg, 0.24 mmol, 48%). After ^{1}H-NMR analysis, the ratio of Br:Cl at position 1 was 51:49.

Rf (MeOH) 0.0 **^{1}H NMR** (methanol-d_4, 400 MHz) δ (ppm) 9.01 (d, 1H, H^{7}, J = 10.54 Hz), 8.79 (d, 1H, H^{14}, J = 11.54 Hz), 8.51 (dd, 1H, H^{4}, J = 8.41, 4.14 Hz), 8.47 (dd, 1H, H^{11}, J = 8.53, 3.51 Hz), 8.35 (t, 1H, H^{8}, J = 7.15 Hz), 8.15 (t, 1H, H^{13}, J = 6.78 Hz), 5.02 (m, 1H, H^{2}), 4.98 (m, 1H, H^{2}, Cl replacement), 2.63 (s, 3H, H^{15}), 1.80 (s, 15H, $H^{6'\text{-}10'}$) **^{13}C NMR** (methanol-d_4, 100 MHz) δ (ppm) 152.26, 151.78, 151.34, 140.68, 140.15, 123.25, 122.94, 97.57, 41.12, 16.96, 7.47 **ESI-MS^{+}** calculated for $(C_{22}H_{26}{}^{79}Br^{35}ClN_2Rh)^{+}$ 535.00, found 457.0839 (M^{+} - ^{79}Br), 493.0512 (M^{+} - ^{79}Br + ^{35}Cl), 535.0034 (M^{+}) and calculated for $(C_{22}H_{26}{}^{81}Br^{35}ClN_2Rh)^{+}$ 537.00, found 455.0748 (M^{+} - ^{81}Br), 491.0546(M^{+} -^{81}Br + ^{35}Cl) and 537.0025 (M^{+}).

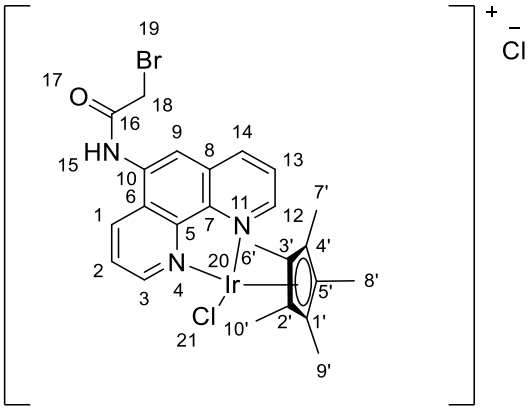
Cp* Rh (5-(2'-bromo)-acetamido-1,10-phenanthroline) chloride (M3a)



Following the procedure used for the synthesis of **M1a**, pentamethylcyclopentadienyl rhodium(III) chloride dimer (50 mg, 0.08 mmol) was suspended in methanol (2 mL). To this suspension was added 5-(2'-bromo)-acetamido-1,10-phenanthroline **L3** (64 mg, 0.16 mmol) then 1 mL of methanol was added to improve the particle dispersion. The mixture immediately turned into a yellow/orange clear solution, indicating the formation of the rhodium-phenanthroline complex. The resulting mixture was filtered to remove any unreacted reagent. The desired product was precipitated by adding the mixture dropwise into cold *n*-hexane (10 volumes), collected by filtration and dried, to obtain a bright orange powder (47.7 mg, 0.11 mmol, 71%).

Rf (MeOH) 0.0 **^{1}H NMR** (methanol-d_4, 400 MHz) δ (ppm) 9.41 (d, 1H, H^3, J = 4.4 Hz), 9.33 (d, 1H, H^{12}, J = 5.3 Hz), 8.95 (dd, 1H, H^1, J = 8.5, 1.2 Hz), 8.83 (dd, 1H, H^{14}, J = 8.3, 1.1 Hz), 8.47 (s, 1H, H^9), 8.23 (dd, 1H, H^2, J = 8.4, 5.1 Hz), 8.17 (dd, 1H, H^{13}, J = 8.2, 5.2 Hz), 4.48 (s, 2H, H^{18}), 1.87 (s, 15H, $H^{6'-10'}$) **^{13}C N MR** (methanol-d_4, 100 MHz) δ (ppm) 167.74, 152.74, 152.05, 145.60, 143.64, 138.58, 134.72, 132.91, 130.16, 126.81, 126.28, 121.48, 97.81, 42.40, 7.90 **ESI-MS$^+$** calculated for $(C_{24}H_{25}{}^{79}Br^{35}ClN_3ORh)^+$ 588.00 found 587.9949 (M^+) and calculated for $(C_{24}H_{25}{}^{81}Br^{35}ClN_3ORh)^+$ 590.00, found 589.9918 (M^+).

Cp*Ir (5-(2'-bromo)-acetamido-1,10-phenanthroline) chloride (M3b)



Following the procedure used for the synthesis of **M1b**, pentamethylcyclopentadienyl iridium(III) chloride dimer (152 mg, 0.19 mmol) was suspended in methanol (2 mL). To this suspension was added 5-(2'-bromo)-acetamido-1,10-phenanthroline **L3** (100 mg, 0.38 mmol) then 1 mL of methanol was added to improve the particle dispersion. The mixture immediately turned into a yellow/orange clear solution, indicating the formation of the iridium-phenanthroline complex. The resulting mixture was filtered to remove any unreacted reagent. The desired product was precipitated by adding the mixture dropwise into cold *n*-hexane (10 volumes), collected by filtration and dried, to obtain a bright yellow powder (198 mg, 0.29 mmol, 76%).

Rf (MeOH) 0.09 **^{1}H NMR** (methanol-d_4, 400 MHz) δ (ppm) 9.42 (t, 1H, H^{3}, J = 6.58 Hz), 9.33 (t, 1H, H^{12}, J= 7.02 Hz), 8.96 (t, 1H, H^{1}, J = 9.79 Hz), 8.83 (t, 1H, H^{14}, J = 9.5 Hz), 8.54 (s, 1H, H^{9}), 8.23 (m, 1H, H^{2}) 8.16 (m, 1H, H^{13}), 4.50 (s, 2H, H^{18}), 1.84 (s, 15H, $H^{6'\text{-}10'}$) **^{13}C NMR** (methanol-d_4, 100 MHz) δ (ppm) 167.73, 152.40, 151.61, 138.60, 134.77, 130.44, 127.48, 127.18, 126.65, 121.36, 89.95, 42.39, 7.52 **ESI-MS^{+}** calculated for $(C_{24}H_{25}{}^{79}Br^{35}ClN_3OIr)^{+}$ 678.05, found 678.0478 (M^{+}) and calculated for $(C_{24}H_{25}{}^{81}Br^{35}ClN_3OIr)^{+}$, found 680.0469 ($M^{+}$).

3.3.2 Bioconjugation with metal complexes

3.3.2.1 Rhodium catalysts

Following the published procedure developed in our laboratory,[217] complexes **M1a**, **M2** and **M3a** were individually mixed with TbADH 5M, TbADH 6M, 7M-

C174 or 7M-C243 during 1h at room temperature. The protein concentration was 4 mg.mL^{-1}, and 4 equivalents of ligands (400 µM) were used. After completion, each bioconjugation product was purified and analysed as previously described in section 3.2.6. ICP-MS analysis were performed to evaluate the metal content of each protein sample.

3.3.2.2 Iridium catalysts

In the initial procedure, complexes **M1b** and **M3b** were individually mixed with TbADH 5M, TbADH 6M, 7M-C174 or 7M-C243 during 1h at room temperature. The protein concentration was 4 mg.mL^{-1}, and 4 equivalents of ligands (400 µM) were used. Optimisation was performed by varying the following parameters: a) protein concentration, 1 mg.mL^{-1} and b) ligand concentration, 1 equivalent (25 µM).

3.3.2.3 ICP-MS

Protein samples were diluted as required to reach 80 ppb of metal content in 2% (v/v) nitric acid in molecular biology grade water. The solutions were heated to 95 ˚C for 30 min then cooled to room temperature. The cooled solutions were centrifuged at 4000 g for 15 min. The supernatants were then analysed by ICP-MS at the Sutton Bonington campus.

3.3.3 Catalytic reduction of NADP$^+$

Following a published procedure, the following reagents were added into a 1 mL quartz cuvette: NADP$^+$ (0.42 mM final concentration), sodium formate (500 mM final concentration), metal catalysts (25 µM, final concentration) or artificial metalloenzyme (12.5 µM of protein, final concentration) in sodium phosphate 100 mM buffer pH 7.0. The increase of absorbance was monitored at 340 nm at 50 °C for 120 seconds (metal catalysts) or 1020 seconds (artificial metalloenzymes). The reaction was initiated by the addition of the catalyst. Each experiment was run in triplicate. The concentration was determined by weight for the free catalysts, and by Bradford for the artificial metalloenzymes.

3.3.4 Catalytic reduction of nicotinamide derivatives

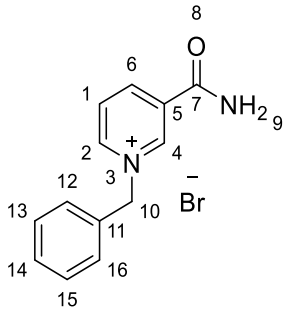
Following the previously described procedure, the following reagents were added into a 1 mL quartz cuvette: nicotinamide derivatives NAD$^+$, Bn-NAD or Bn-NAD-Ph (0.42 mM final concentration), sodium formate (500 mM final

concentration), metal catalysts (25 µM, final concentration) or artificial metalloenzyme (12.5 µM of protein, final concentration) in sodium phosphate 100 mM buffer pH 7.0. The increase of absorbance was monitored at 340 nm (or 380 with Bn-NAD-Ph) at 50 °C for 120 seconds (metal catalysts) or 1020 seconds (artificial metalloenzymes). The reaction was initiated by the addition of the catalyst. Each experiment was run in triplicate.

3.4 Methods to design an artificial metalloenzyme through a supramolecular approach

3.4.1 Chemical synthesis

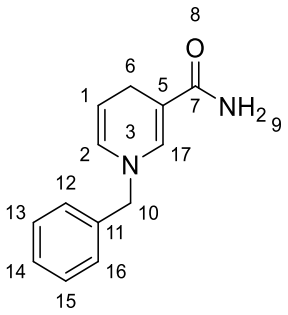
1-benzyl-3-carboxamidepyridinium , Bn-NAD oxidised form (150)



This compound was prepared according to a previously reported procedure. To a solution of nicotinamide **148** (500 mg, 4.09 mmol) in acetonitrile (10 mL) was added benzyl bromide **149** (160 µL, 1870 mg, 10.9 mmol) at room temperature. After 24 h, the reaction was heated to 40 ˚C for an additional 24h. The mixture was cooled and diethyl ether (10 mL) was added to the mixture to precipitate the pyridinium salt. The reaction was cooled to room temperature and the crude mixture was triturated with diethyl ether to give the title compound as an off-white powder (841.5 mg, 3.77 mmol, 94%).[218]

Rf (100% MeOH) 0.12; **NMR ^{1}H** (CD_3OD, 300 MHz) δ (ppm) 9.53 (s, 1H, H^4) 9.17 (d, 1H, H^2, J=5.2 Hz) 9.01 (d, 1H, H^6, J=8.0 Hz) 8.23 (t, 1H, H^1, J=14.2 Hz) 7.51 (m, 5H, $H^{12\text{-}H16}$) 5.93 (s, 2H, H^{10}); **NMR ^{13}C** (MeOD, 75 MHz) δ (ppm) 161.77, 143.92, 132.79, 129.80, 129.39, 128.99, 128.19, 64.74; **ESI-MS$^+$** calculated for $(C_{13}H_{13}N_2O)^+$ 213.10 found 213.1027 (M^+)

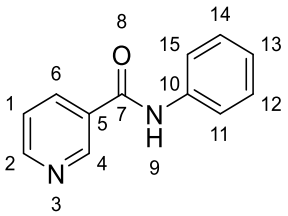
1-benzyl-3-carboxamide-1,4-dihydropyridine, Bn-NAD reduced form (151)



Under nitrogen atmosphere 1-benzyl-3-carbamoylpyridinium **150** (100 mg, 0.47 mmol) was dissolved into a 2/1 (v/v) mixture of water and CH_2Cl_2 (15 mL). $NaHCO_3$ (235 mg, 2.8 mmol) was added and the flask was placed and stirred in an ice bath. Sodium dithionite (327 mg, 1.88 mmol) was then added portion wise over a period of 5 minutes and the resulting solution was kept stirring for 4 h whilst on ice. The aqueous layer was then removed by phase separation and the organic layer was washed three times with cold water (10 mL each time) then dried over magnesium sulphate. The solvent was removed under reduced pressure to yield the title compound (62.2 mg, 0.29 mmol, 62 %) as yellow crystals.[218]

Rf (100% MeOH) 0.85; **NMR ^{1}H** ($CDCl_3$, 300 MHz) δ (ppm) 7.33 (m, 5H, H^{12}-H^{16}) 7.16 (s, 1H, H^{17}) 5.73 (dd, 1H, H^{2}, J=8.1, 1.7 Hz) 5.17 (s, 2H, H^{9}) 4.75 (m, 1H, H^{1},) 4.29 (s, 2H, H^{10}) 3.17 (q, 2H, H^{6}, J=1.7 Hz); **NMR ^{13}C** ($CDCl_3$, 75 MHz) δ (ppm) 170.1, 140.1, 137.2, 128.9, 128.8, 127.8, 127.2, 103.2, 98.5, 57.4, 22.8; **ESI-MS^{+}** calculated for $(C_{13}H_{15}N_2O)^{+}$ 215.12 found 215.1181 (M + H^{+}).

***N*-phenylnicotinamide (154)**

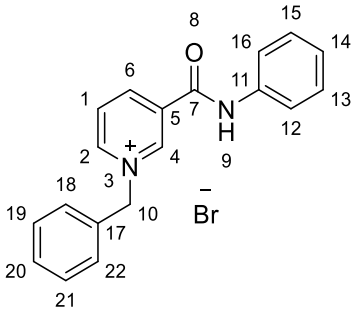


To a solution of nicotinic acid **152** (500 mg, 4.06 mmol) in chloroform (10 mL) at 0 ˚C were added propylphosphonic anhydride (1.594 g, 1.5 mL, 5.01 mmol), diisopropylethylamine (1.046 g, 1.4 mL, 8.1 mmol) and aniline **153** (190 mg,

185 µL, 2.03 mmol). The solution was stirred overnight and allowed to warm up to room temperature. After completion, the crude mixture was washed three times with brine (10 mL each time) then twice with distilled water (10mL each time), dried over sodium sulphate and evaporated under reduced pressure. The crude solid was then purified by silica gel chromatography (isocratic, CH_2Cl_2/MeOH, 9/1) to yield the title product as a yellow solid (293.2 mg, 1.47 mmol, 73%).

Rf (CH_2Cl_2 with 10% MeOH) 0.5; **NMR ^{1}H** (methanol-d_4, 300 MHz) δ (ppm) 9.08 (s, 1H, H^4) 8.73 (d, 1H, H^2, J=4.9 Hz) 8.34 (d, 1H, H^6, J=8.6 Hz) 7.71 (d, 2H, H^{11}-H^{15}, J=8.5 Hz) 7.58 (m, 1H, H^{13}) 7.37 (t, 2H, H^{12}-H^{14}, J=8.1 Hz) 7.17 (t, 1H, H^1, J=7.4 Hz); **NMR ^{13}C** (methanol-d_4, 75 MHz) δ (ppm) 151.3, 147.9, 135.9, 128.4, 124.50, 123.7, 120.8; **ESI-MS$^+$** calculated for $(C_{12}H_{11}N_2O)^+$ 199.09 found 199.0872 ($M + H^+$)

<u>*N*-phenyl-1-benzyl-3-carboxamide-pyridinium, Bn-NAD-Ph oxidised form (155)</u>

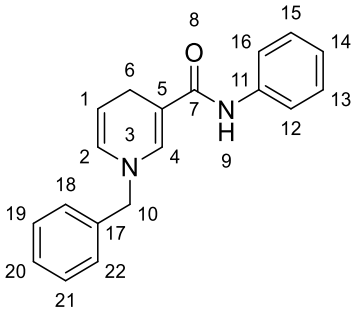


To a stirred solution of *N*-phenylnicotinamide **154** (293.2 mg, 1.47 mmol) in methanol (10 mL) was added benzyl bromide (514 mg, 360 µL, 3 mmol) at room temperature. The resulting mixture was stirred at 50 ˚C overnight. After reaction completion, the solution was cooled to room temperature and diethyl ether (10 mL) was added to precipitate the pyridinium salt. The reaction mixture was left for 1h to allow complete precipitation, the product was then collected by filtration as white crystals (419.5 mg, 1.45 mmol, 98%).

Rf(CH_2Cl_2/MeOH, 9/1) 0.31; **NMR ^{1}H** (DMSO-d_6, 300 MHz) δ (ppm) 10.87 (s, 1H, H^9) 9.75 (s, 1H, H^4) 9.31 (d, 1H, H^2, J=5.7 Hz) 9.10 (d, 1H, H^6, J=7.4 Hz) 8.34 (t, 1H, H^1, J=7.2 Hz) 7.75 (d, 2H, H^{12}-H^{16}, J=8.2 Hz) 7.60 (m, 2H, H^{13}-H^{15}) 7.45 (m, 5H, $H^{18\text{-}22}$) 7.20 (t, 1H, H^{14}, J=7.5 Hz) 5.95 (s, 2H, H^{10}); **NMR ^{13}C**

(DMSO-d_6, 75 MHz) δ (ppm) 152.3, 129.4, 125.2, 124.7, 120.9, 19.8; **ESI-MS$^+$** calculated for $(C_{19}H_{17}N_2O)^+$ 289.13 found 289.1364 (M^+)

<u>*N*-phenyl-1-benzyl-3-carboxamide-1,4-dihydropyridine, Bn-NAD-Ph reduced form (156)</u>



Under nitrogen atmosphere, *N*-phenyl-1-benzyl-3-carboxamide-pyridinium **155** (100 mg, 0.35 mmol) was dissolved into a 2/1 (v/v) mixture of water and CH_2Cl_2 (15 mL). $NaHCO_3$ (168 mg, 2 mmol) was added and the flask was placed and stirred in an ice bath. Sodium dithionite (240 mg, 1.38 mmol) was then added portion wise over a period of 5 minutes and the resulting solution was stirred overnight and allowed to warm up to room temperature. The aqueous layer was then removed by phase separation and the organic layer was washed three times with cold water (10 mL each time), then dried over magnesium sulphate. The solvent was removed under reduced pressure to yield the title compound (64.5 mg, 0.22 mmol, 64 %) as an orange solid.

Rf (CH_2Cl_2/MeOH, 9/1) 0.8; **NMR ^{1}H** ($CDCl_3$, 300 MHz) δ (ppm) 11.67 (s, 1H, H^9) 10.10 (s, 1H, H^4) 8.83 (d, 1H, H^2, J=8.4 Hz) 8.38 (d, 1H, H^1, J=7.0 Hz) 7.54 (m, 5H, H^{18}-H^{22}) 7.08 (m, 5H, H^{12}-H^{16}) 4.80 (m, 2H, H^{10}) 3.36 (q, 2H, H^6, J=1.7 Hz); **NMR ^{13}C** ($CDCl_3$, 75 MHz) δ (ppm) 226.9, 218.6, 191.1, 162.8, 146.8, 138.5, 120.0, 19.8; **ESI-MS$^+$** calculated for $(C_{19}H_{19}N_2O)^+$ 291.15 found 291.1497 ($M + H^+$)

3.4.2 Expression and purification of wild-type ADHs

3.4.2.1 Expression and purification of His-HLADH

A seed culture (20 mL) previously grown overnight from a cryostock was used to inoculate Luria-Bertani (LB) medium (800 mL) containing carbenicillin (50 $\mu g.mL^{-1}$) and chloramphenicol (34 $\mu g.mL^{-1}$). The culture was grown at 37 ˚C,

250 rpm, up to an OD_{600} = 0.6-0.8. Expression was then induced using isopropyl-β-D-1-thiogalactopyranoside (IPTG) at 0.4 mM and cells were grown overnight at 30 ˚C, 250 rpm to an OD_{600} = 4-5. A sample was taken for SDS-PAGE analysis while the remaining cells were harvested by centrifugation (4 ˚C, 20 min, 5 000 g) and stored at -80 ˚C.

The harvested cell pellets were resuspended in sodium phosphate 100 mM buffer NaCl 150 mM pH 7.0 (binding buffer). A protease inhibitor cocktail tablet and benzonase nuclease (0.1 $\mu g.mL^{-1}$) were added to the solution prior to two passages through the cell disruptor (20 bars). The resulting sample was centrifuged (4 ˚C, 20 min, 10 000 g). The supernatant was then purified by affinity chromatography.

Affinity chromatography was performed on an AKTA FPLC system using His Trap FF crude column (1 mL). The column was equilibrated using the binding buffer, the sample was then loaded (c.a. 10-15 mL) and pure His-HLADH was eluted with the elution buffer (binding buffer supplemented with imidazole 500 mM) using a linear gradient (0-100 %). Fractions containing protein were analysed by SDS-PAGE. The pure fractions were pooled and dialysed two times for 2 h followed by an overnight dialysis in 200 volumes of sodium phosphate 100 mM buffer pH 7.0. The resulting samples were concentrated, subjected to protein analysis and stored at –80 ˚C until further use.

3.4.2.2 Expression and purification of WT TbADH

A seed culture (6 mL) was prepared into a 50 mL sterile Falcon tube from cryostock (6 µL) supplemented with carbenicillin (100 $\mu g.mL^{-1}$). It was used to inoculate 500 mL LB medium supplemented with carbenicillin (100 $\mu g.mL^{-1}$) and $ZnCl_2$ (136.3 $\mu g.mL^{-1}$). The culture was grown at 37 ˚C, 200 rpm until an OD_{600} = 0.6 - 0.8 was reached (approximately 2 h). Expression was then induced using isopropyl-β-D-1-thiogalactopyranoside (IPTG) at 1 mM and cells were grown overnight at 30 ˚C, 120 rpm to an OD_{600} = 4-5. A sample was taken for SDS-PAGE analysis while the remaining cells were harvested by centrifugation (4 ˚C, 20 min, 5 000 g). The supernatant was then removed, and, on ice, the cells were resuspended in cold Tris HCl 100 mM, NaCl 150

mM buffer pH 8.0. The suspension was transferred into 50 mL Falcon tubes, centrifuged (4 ˚C, 10 min, 8 000 g) and stored at -80 ˚C until further use.

The cell pellet was thawed on ice for 1h while the lysis buffer was prepared (buffer W supplemented with a protease inhibitor cocktail tablet and benzonase nuclease (0.1 µg.mL^{-1})). The pellet was then resuspended in the fresh lysis buffer and the suspension was stirred on ice for 1h. The suspension was sonicated (5 min, 35% power, 30 sec ON, 59 sec OFF) then spun down by centrifugation (25 000 g, 15 min, 10 ˚C). The cleared lysate was transfer into a water bath at 60 ˚C for 15 min then put back on ice for 10 min to induce precipitation of mesophilic proteins. The resulting white suspension was split into Eppendorf tubes and spun down by centrifugation (16 900 g, 15 min, 4 ˚C). The supernatants were collected, pooled and purified by affinity chromatography.

Affinity chromatography was performed on an AKTA FPLC system using StrepTrap HP column (5 mL) with 3 mL.min^{-1} flow rate. The column was equilibrated using the buffer W, the sample was then loaded (10-15 mL) and pure Strep-TbADH was recovered with the elution buffer (buffer W supplemented with 2.5 mM desthiobiotin). Fractions containing protein were analysed by SDS-PAGE. The pure fractions were pooled, and a buffer exchange was carried out using a Vivaspin 20 (10,000 MWCO) and Tris.HCl 100 mM buffer pH 8.0 was used to remove the presence of NaCl and desthiobiotin. Once the buffer exchanged, the amount of protein was then quantified via Bradford method before storage at -80 ˚C.

3.4.3 Determination of the catalytic activity of the enzymes

3.4.3.1 Enzymatic assays of His-HLADH

For the oxidation of the ethanol substrate, the following reagents were added into a 1 mL quartz cuvette: NAD^+ (200 µL, 1.5 mM final concentration), ethanol (100 µL, 200 mM final concentration) and His-HLADH (10 µg) in sodium phosphate 100 mM buffer pH 8.8. The reaction was initiated by the addition of the enzyme. The increase of absorbance was monitored at 340 nm for 400 seconds at 25 ˚C.

For the reduction of the acetaldehyde substrate, the following reagent were added into a 1 mL quartz cuvette: NADH (200 µL, 1.5 mM final concentration), acetaldehyde (100 µL, 200 mM final concentration) and His-HLADH (10 µg) in sodium phosphate 100 mM buffer pH 7.0. The reaction was initiated by the addition of NADH. The decrease of absorbance was monitored at 340 nm for 400 seconds at 25 ˚C.

To a solution of 4-phenyl-2-butanone (10 µL, 5 mM final concentration) and NADH (200 µL, 20 mM final concentration) in sodium phosphate 100 mM buffer pH 7.0 (500 µL final volume) was added His-HLADH (100 µL, 3 $mg.mL^{-1}$ final concentration) and the solution was stirred at room temperature. After 24h, the reaction was quenched by addition of 10 M NaOH (20 µL). The substrate and products were extracted with hexane (500 µL) and analysed by HPLC using a Chiracel OD column (1 µL/injection, hexane/ isopropanol 94/6, 25 ˚C, 18 min). Retention times: ketone; 7.05 minutes, (*R*)-alcohol; 8.3 minutes and (*S*)-alcohol; 11.8 minutes.

3.4.3.2 Enzymatic assays of TbADH WT

For the oxidation of the 2-butanol substrate, the following pre-heated (40 ˚C) reagents were added into a 1 mL quartz cuvette: $NADP^+$ (200 µL, 1 mM final concentration), 2-butanol (100 µL, 20 mM final concentration) and TbADH WT (1 µg) in Tris.HCl 50 mM buffer pH 9.0. The reaction was initiated by the addition of the enzyme and monitored at 340 nm for 150 seconds at 40 ˚C.

For the reduction of the 2-butanone substrate, the following reagents were added into a 1 mL quartz cuvette: NADPH (200 µL, 1 mM final concentration), 2-butanone (100 µL, 20 mM final concentration) and TbADH WT (1 µg) in Tris.HCl 50 mM buffer pH 6.0. The reaction was initiated by the addition of the enzyme and monitored at 340 nm for 150 seconds at 40 ˚C.

To a solution of 4-phenyl-2-butanone (10 µL, 5 mM final concentration) and NADPH (200 µL, 20 mM final concentration) in Tris.HCl 50 mM buffer pH 6.0 (500 µL final volume) was added TbADH WT (100 µL, 0.2 $mg.mL^{-1}$ final concentration) and the solution was stirred at room temperature. After 24h, the reaction was quenched by addition of 10 M NaOH (20 µL). The substrate and

products were extracted with hexane (500 µL) and analysed by HPLC using a Chiracel OD column (1 µL/injection, hexane/ isopropanol 94/6, 25 ˚C, 18 min).

3.4.4 Impact of nicotinamide derivatives on the enzymatic activity

3.4.4.1 Determination of the catalytic activity of His-HLADH using cofactor mimics

The evaluation of His-HLADH activity with cofactor mimics was performed in both substrate oxidation and reduction directions. In a 1 mL quartz cuvette were added the NAD mimic (200 µL, 1 mM final concentration), the substrate (100 µL, 10 mM final concentration) and His-HLADH (10 µg) in sodium phosphate 100 mM buffer. The reaction buffer was at pH 8.8 for the oxidation of ethanol and at pH 7.0 for the reduction of acetaldehyde, both supplemented with MeCN 5% (v/v). The reactions were initiated by addition of the enzyme for the oxidation reaction and by addition of the NADH mimic for the reduction reaction. The assays were monitored at 340 nm with Bn-NAD (**150**/**151**), and at 380 nm with Bn-NAD-Ph (**155**/**156**) for 400 seconds at 25 ˚C.

The catalytic assay of His-HLADH (3 $mg.mL^{-1}$) was also carried out by reducing 4-phenyl-2-butanone (10 µL, 5 mM final concentration) with **151** or **156** (200 µL, 20 mM final concentration) in sodium phosphate 100 mM buffer pH 7.0 (500 µL final volume), with magnetic stirring at room temperature over 24h. The reaction was quenched by addition of 10 M NaOH (20 µL). The substrate and compounds were extracted with hexane (500 µL) and analysed by HPLC using a Chiracel OD column (1 µL/injection, hexane/ isopropanol 94/6, 25 ˚C, 18 min).

3.4.4.2 Determination of the catalytic activity of TbADH WT using cofactor mimics

The evaluation of TbADH WT activity with cofactor mimics was performed in both substrate oxidation and reduction directions. In a 1 mL quartz cuvette were added the NAD mimic (200 µL, 1 mM final concentration), the substrate (100 µL, 20 mM final concentration) and TbADH WT(1 µg) in Tris.HCl 50 mM buffer. The reaction buffer was at pH 9.0 for the oxidation of 2-butanol and at pH 6.0 for the reduction of 2-butanone, both supplemented with MeCN 5% (v/v). The reactions were initiated by addition of the enzyme. The assays were monitored at 340 nm with Bn-NAD (**150**/**151**), and at 380 nm with Bn-NAD-Ph (**155**/**156**) for 400 seconds at 40 ˚C.

The catalytic assay of TbADH WT (0.2 mg.mL^{-1}) was also carried out by reducing 4-phenyl-2-butanone (10 µL, 5 mM final concentration) with **151** or **156** (200 µL, 20 mM final concentration) in Tris.HCl 50 mM pH 6.0 (500 µL final volume) at 40 ˚C over 24h. The reaction was quenched by addition of 10 M NaOH (20 µL). The substrate and compounds were extracted with hexane (500 µL) and analysed by HPLC using a Chiracel OD column (1 µL/injection, hexane/ isopropanol 94/6, 25 ˚C, 18 min).

3.4.4.3 Comparative enzymatic assay with His-HLADH and TbADH WT, and cofactor mimics

Cyclohexanol (1 mM final concentration) in sodium phosphate 100 mM buffer pH 8.8 or 2-butanol (1.8 mM final concentration) in Tris.HCl 50 mM buffer pH 9.0 were used as internal standards with His-HLADH and TbADH WT experiments respectively. Calibration was performed based on the relative area for each dilution of substrates and products combined with the internal standards. Following the calibration, each treated sample was injected (1 µL) and its relative area was measured. Yields were calculated based on the ratio of the area product obtained with respect to the internal standard.

For His-HLADH: To a solution of (±) 4-phenyl-2-butanol (100 µL, 1.34 mM final concentration) and β-nicotinamide mononucleotide or NAD$^+$ (100 µL, 2 mM final concentration) in sodium phosphate 100 mM buffer pH 8.8 (500 µL final volume) was added His-HLADH (10 µL, 0.5 µM final concentration). After 24 h, the reaction was quenched by the addition of 10 M NaOH (20 µL) and the internal standard cyclohexanol (10 µL, 1 mM final concentration) was added. The substrate, the product and the standard were extracted with hexane (500 µL) and analysed by GC-FID (1 µL/injection, 1:10 split, isothermal 110 ˚C for 10 min).

For TbADH WT: To a solution of (±) 2-pentanol (100 µL, 1.8 mM final concentration) and β-nicotinamide mononucleotide or NAD$^+$ (100 µL, 2 mM final concentration) in Tris.HCl 50 mM buffer pH 9.0 (500 µL final volume) was added TbADH WT (10 µL, 0.5 µM final concentration). After 24 h, the reaction was quenched by the addition of 10 M NaOH (20 µL) and the internal standard 2-butanol (10 µL, 1.8 mM final concentration) was added. The substrate, the

product and the standard were extracted with hexane (500 µL) and analysed by GC-FID (1 µL/injection, 1:10 split, isothermal 110 ˚C for 10 min).

3.4.5 Determination of the inhibitory potential of the cofactor mimics

The inhibition of His-HLADH activity by the cofactor mimics was assessed in a 1 mL quartz cuvette under the following conditions: acetaldehyde (10 µL, 10 mM final concentration), His-HLADH (10 µg), **150**/**151** (concentration range from 10^{-7} to 10^{-2} M) or **155**/**156** (concentration range from 10^{-10} to 10^{-2} M) and NADH (200 µL, 0.3 mM final concentration) in phosphate buffer 100 mM pH 7.0. The reaction was initiated by the addition of NADH and followed at 340 nm.

The inhibition of TbADH WT activity by the cofactor mimics was assessed in a 1 mL quartz cuvette under the following conditions: 2-butanone (10 µL, 10 mM final concentration), TbADH WT (1 µg), **150**/**151** (concentration range from 10^{-7} to 10^{-2} M) or **155**/**156** (concentration range from 10^{-10} to 10^{-2} M) and NADPH (200 µL, 0.3 mM final concentration) in Tris.HCl buffer 50 mM pH 6.0. The reaction was initiated by the addition of NAPDH and followed at 340 nm.

The data points were then fitted against a sigmoidal curve resulting in IC_{50} values, which correspond to the concentration required to reach 50% reduction of the initial enzymatic activity.

3.4.6 Molecular modelling study of ADHs and the cofactor mimics

3.4.6.1 Protein preparation

The crystal structures of HLADH (PDB entry 1HLD) and TbADH (PDB entry 1YKF) were cleaned and utilized as rigid receptors using AutoDock Tools4 (version 1.5.6). The cleaning process consisted of removing the cofactors contained in the PDB files to free the space for further docking. The accuracy of the algorithm was ensured by docking back the removed NADH and NADPH. Prior to any docking, Gasteiger charges were computed to ensure partial charges were maintained for all charged amino acids. All the other ADH crystal structures used for docking were prepared in a similar fashion.

3.4.6.2 Ligand preparation

The mimics **150**/**151** and **155**/**156** as well as NADH and NADPH were constructed in 3D using Chem 3D HotLink interface from ChemDraw Professional 16.0. Similarly, new structures for potential supramolecular were designed in ChemDraw Professional 16.0 then their 3D structure were extracted through the Chem 3D HotLink interface.

3.4.6.3 Docking study of HLADH and TbADH with Bn-NAD and Bn-NAD-Ph

After minimization of rotatable bonds, the compounds Bn-NAD and Bn-NAD-Ph were docked into HLADH and TbADH as flexible ligands using AutoDock Vina. The best fitted results of each docking were selected and then superimposed against the original crystal structure of the protein using PyMol.

3.4.6.4 In silico evaluation of new designs for supramolecular anchors

After minimization of rotatable bonds, the different compounds were docked into the proteins as flexible ligands using AutoDock Vina. The best fitted results of each docking were selected and then superimposed against the original crystal structure of the protein using PyMol.

3.4.6.5 In silico screening of ADHs capable of accommodating anchor Bn-NAD

After minimization of rotatable bonds, compounds **150** and $NADP^+$ were docked into the proteins as flexible ligands using AutoDock Vina. The best fitted results of each docking were selected and then superimposed against the original crystal structure of the protein using PyMol.

4 Building an artificial metalloenzyme using the covalent binding approach

4.1 Background

A recent study by Dr. S. Morra from our group, using TbADH as a host protein for rhodium-based catalysts showed that these complexes remained active when covalently anchored to the enzyme.[217] The aim of this study was to regenerate NADPH *in situ* using a TbADH-based artificial metalloenzyme in a coupled system with WT TbADH (Figure 4.1). The system, mimicking a formate dehydrogenase recycling system,[161-162] aimed at reducing the input of expensive cofactor in the reduction reaction of 4-phenylbutan-2-one into its corresponding chiral (*S*)-alcohol.

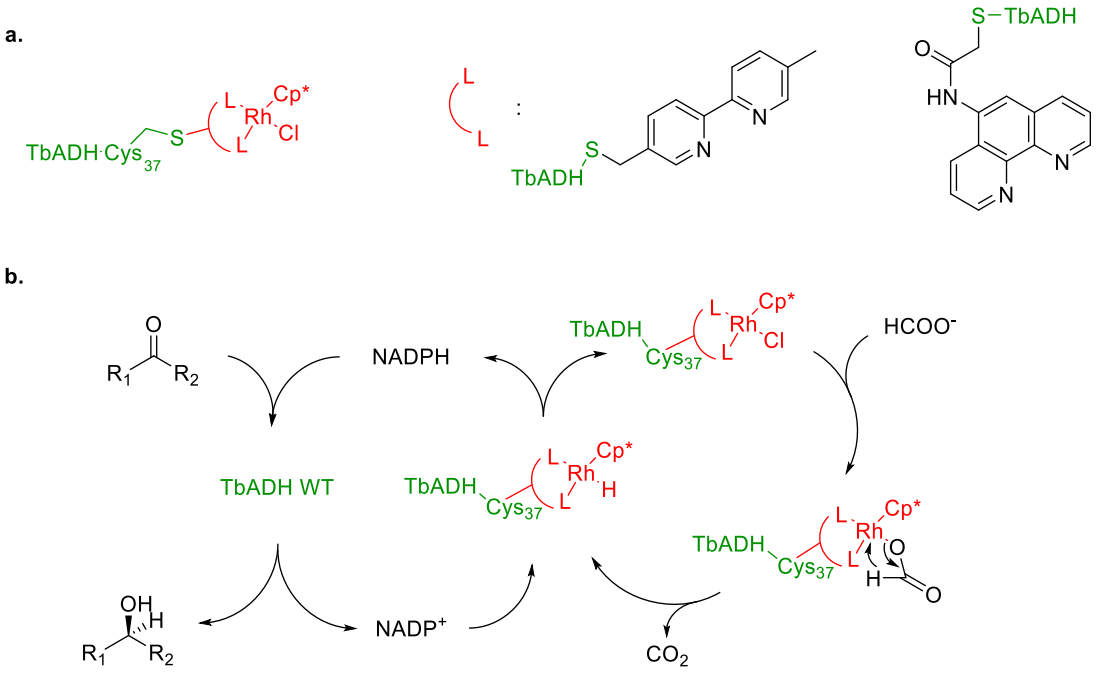


Figure 4.1. Artificial formate dehydrogenase based on ADH a. as a schematic representation of the covalent anchoring system with the two different ligand and b. cofactor recycling system in tandem with the natural enzyme for asymmetric ketone reduction. Adapted from Morra *et al*.[217]

The artificial metalloenzyme was developed using a covalent binding approach. The wild-type TbADH naturally possesses 4 cysteines residues at positions 37, 203, 283 and 295. Position 37 was used as the anchoring point of metal complexes while the three other positions were mutated into alanine or serine. Two other mutations were introduced at positions 59 and 150 in order to remove the interaction with the catalytic zinc ion and free the space for the insertion of rhodium-based catalysts.

Once the mutant developed (called TbADH 5M), bioconjugation was performed and the resulting hybrids were assessed within a coupled system with the wild-type version of TbADH to carry out the reduction of 4-phenyl-2-butanone. Compared to the results with the free catalysts, the protein shell of the artificial metalloenzyme acted as a shield, preventing mutual inactivation between the ADH and the rhodium catalyst. The relative activity of the wild-type enzyme became more stable through time by up to 5-fold (Figure 4.2), allowing the biocatalysis to proceed for longer.

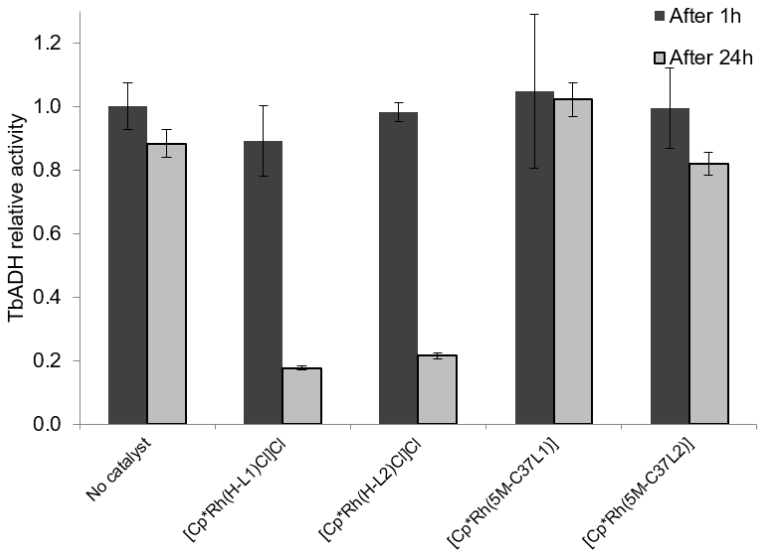


Figure 4.2. Effect of the free and bioconjugated rhodium catalysts on 2- butanone reduction by WT TbADH. WT TbADH (1 µM) was incubated with the corresponding Rh catalyst (5 µM) in sodium phosphate buffer (100 mM, pH 7.0). In the absence of the Rh catalyst, the specific activity of WT TbADH (2-butanone reduction coupled to NADPH oxidation) after 1 h heating was 4.95 ± 0.37 $U.mg^{-1}$. Reproduced from Morra *et al*.[217]

In the published work, the covalent bioconjugation of the Rh complexes to C37 resulted in mixtures of labelled and non-labelled protein, suggesting that the thiol alkylation was not complete. This could be due to the inaccessibility of the active site cysteine and/or to the lack of space around the position 37.

The conversion of 4-phenylbutan-2-one into its corresponding alcohol remained modest - up to 71% coupled with $[Cp^*Rh(5M\text{-}C37L2)]^{2+}$. Therefore, further improvement can be envisaged. Furthermore, given the overall vision of repurposing this enzyme for the catalysis of non-native reactions, the question arose whether nicotinamide derivatives other than $NADP^+$ could be accepted by this ArM system.

Previous work by Bersellini and Roelfes[19] demonstrated the importance of the anchoring position within the protein. In their work, they evaluated 3 positions to introduce a cysteine residue that could be alkylated by a bromo acetamide derivative of 2,2'-bipyridine. After the alkylation, late-first row transition metals were incorporated into the mutants. The activity of the resulting artificial metalloenzymes were then tested towards a Friedel-Crafts reaction and variations of activity were observed depending on the anchoring position.

It was therefore hypothesized that the position of the cysteine within the catalytic site of TbADH would also play an important role in the efficiency of the embedded catalyst, which could thus be improved. Furthermore, the use of more versatile metal complexes, such as those based on sulfonamide ligands (in addition to bipyridine and phenanthroline) would expand the activity spectrum of the ArM (Figure 4.3). If achieved, the enzyme could serve as a biocatalytic platform for transfer hydrogenation reactions by solely modifying the metal-catalyst.

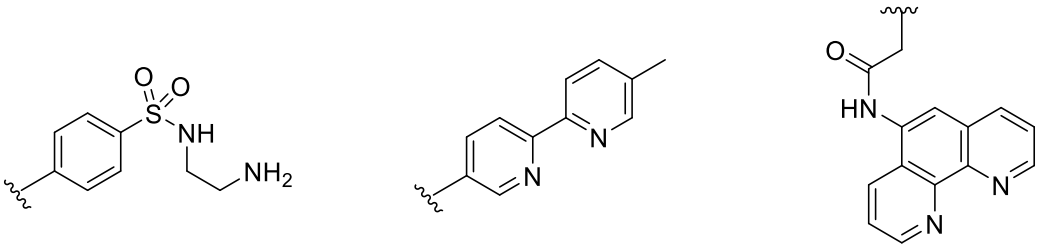


Figure 4.3. *N*-sulfonylethylene diamine, bipyridine and phenanthroline ligands chosen in this study to develop ArMs by covalent binding.

Therefore, as a starting point of this study, it was decided to use the covalent approach to build new ArMs, with TbADH as a protein scaffold, where the position of the anchoring point was modified. To do so, a mutant library was developed *in silico* to investigate positions, within the cofactor binding site, more suitable for this approach. Moreover, the investigation was carried out with a sulfonamide-based ligand, more versatile than those based on bipyridine or phenanthroline.

4.2 Creation of a mutant library

The optimisation process was initiated by the creation of a small mutant library *in silico* (Figure 4.4). This was performed by repositioning the cysteine residue within the active site, to evaluate the impact of its position on the

bioconjugation efficiency and on the resulting catalytic activity. The objective is to use the cofactor binding pocket to accommodate the metal complex, leaving the substrate binding cavity untouched to grant access to various substrate molecule for transfer hydrogenation, as the TbADH enzyme already evolved to perform the reaction on C=O double bonds.

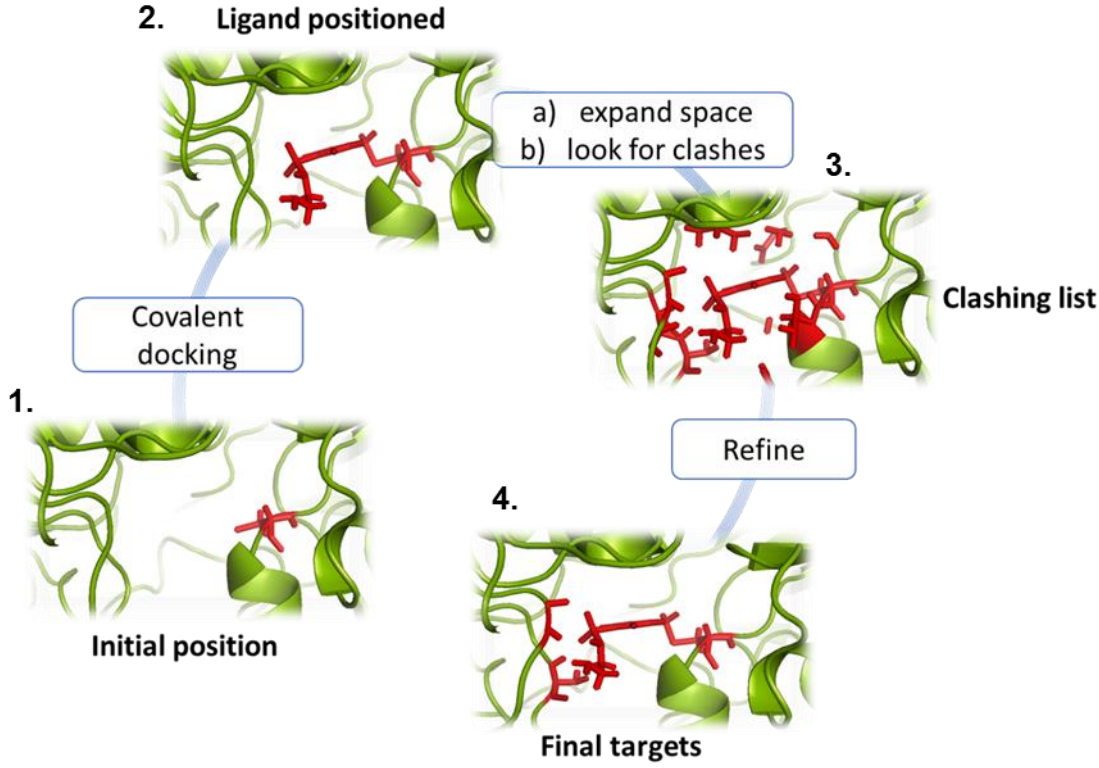


Figure 4.4 The creation of a mutant library was performed in 4 consecutive steps: 1. Initial positions were picked throughout the cofactor binding pocket and *in silico* mutation into cysteines were performed 2. The ligand **L1** was covalently docked at these mutated positions, 3. A sphere of 4 Å in radius was created around **L1** at each position yielding a list of residues that sterically clashed with the sphere, 4. The list was refined to give the final candidate residues by removing prolines and residues on secondary structure as well as residue with a side chain pointing away from the catalytic site.

The *N*-sulfonyl-ethylenediamine ligand **L1** was selected for this study, because it can catalyse a broad range of hydrogen transfer reactions with high activity, thus offering the highest chance to turn the artificial metalloenzyme into a biocatalytic platform. For example, metal complexes (Ru, Rh, Ir) of this ligand have been shown to perform the reduction of nicotinamide cofactors, ketones and imines.[96-98, 100-103, 219-221] This ligand was covalently docked into the protein, at different initial positions chosen by visual inspection of the cofactor binding site, from the PDB structure 1YKF.[194] A total of 5 positions were initially chosen, which possessed a strong interaction with the NADPH

cofactor and were dispersed throughout the cofactor pocket: C37, C203, N266, I175 and V178 (Figure 4.5).

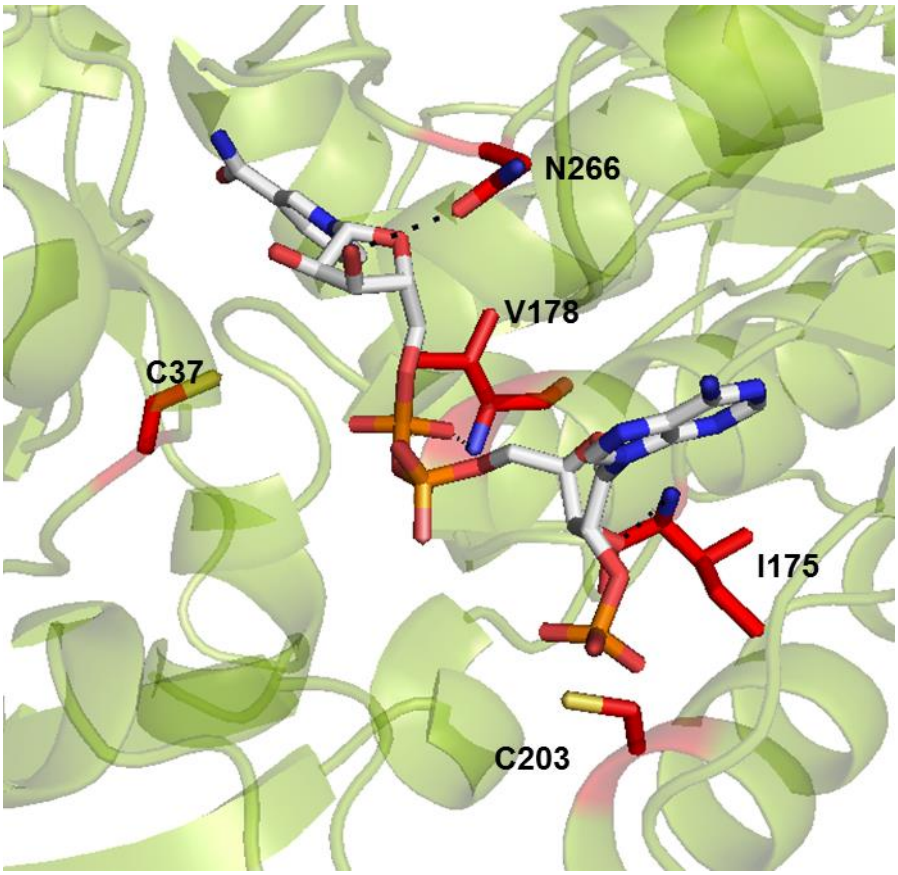


Figure 4.5. Zoom in the active site of TbADH (PDB 1YKF). [194] The different positions used to initiate the *in silico* study are highlighted around the centred nicotinamide cofactor. Colour chart: nitrogen atoms in blue, oxygen atoms in light red, sulphur atoms in yellow, and carbon in white (NADP) or dark red (residues).

Five TbADH mutants were created *in silico*, containing mutations H59A, D150A, C283A and C295A, as well as single cysteines at position C37, I175C, V178C, C203 or N266C. Mutations C37A and C203S were used to remove these cysteines when necessary. Then ligand **L1** was covalently docked within TbADH and linked to each cysteine residue. The covalent docking simulation was run by Floriane Martins, a competent computational chemist within our group.

Once the ligand was covalently attached to the 5 different positions, potential amino acid candidates were identified within a radius of 4 Å from the space occupied by the ligand, which interfered with the ligand through steric clashes. This led to 12 candidates for the positions 37, 178 and 266, and up to 17 for the position 175 and 203, for a total of 70 candidates. Without accounting for

redundancy between the different positions, the number of residues was yet too large to be dealt with through experimental work.

Hence, the list of candidates was refined to a smaller set for which experimental work could be reasonably achieved. The refinement was performed as follows: a) all prolines and residues placed on a helix or a sheet were discarded to avoid affecting the folding of the protein and b) the side chains of the remaining candidates were chosen to point towards the cofactor binding site, therefore increasing the probability of a possible interaction between the ligand and the mutated cysteine at the selected position.

This process led to 13 candidate residues. However, only 4 out of those 13 were repeatedly found with all the docked structures: G174, G198, A242 and G243 (Figure 4.6).

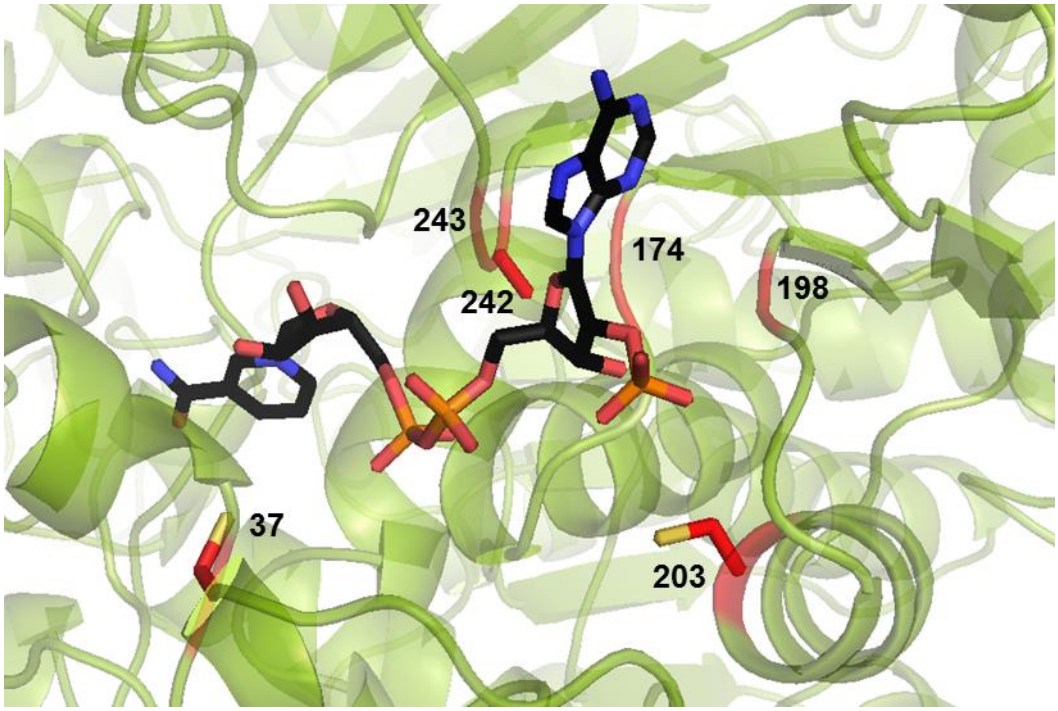


Figure 4.6. Zoom in the catalytic site of TbADH (PDB 1YKF). The selected targets for experimental mutation, bioconjugation and catalysis were highlighted in red. The nicotinamide was highlighted with a carbon backbone in black.

At the exception of the native position 37, none of the targeted positions were close to the nicotinamide ring of NADPH, and thus to the active site in TbADH. This proximity was important for the design, because the metal complex anchored to the targeted cysteines should be able to act as the hydride transfer agent to a substrate or cofactor bound to the enzyme. However, the

residue position itself was not necessarily informative on the final position of the attached metal complex. Thus, after preparing the cysteine mutations at those positions with Pymol, ligand **L1** was covalently docked to the corresponding thiol on the side chain (Figure 4.7). In addition to the four side-chains selected above, position 37 and 203 were also used for covalent docking, as they were the two native cysteine residues from the cofactor and substrate binding pocket of TbADH. The aim was to get a better understanding at the positioning of the ligand based on the position of the cysteine within the cofactor pocket.

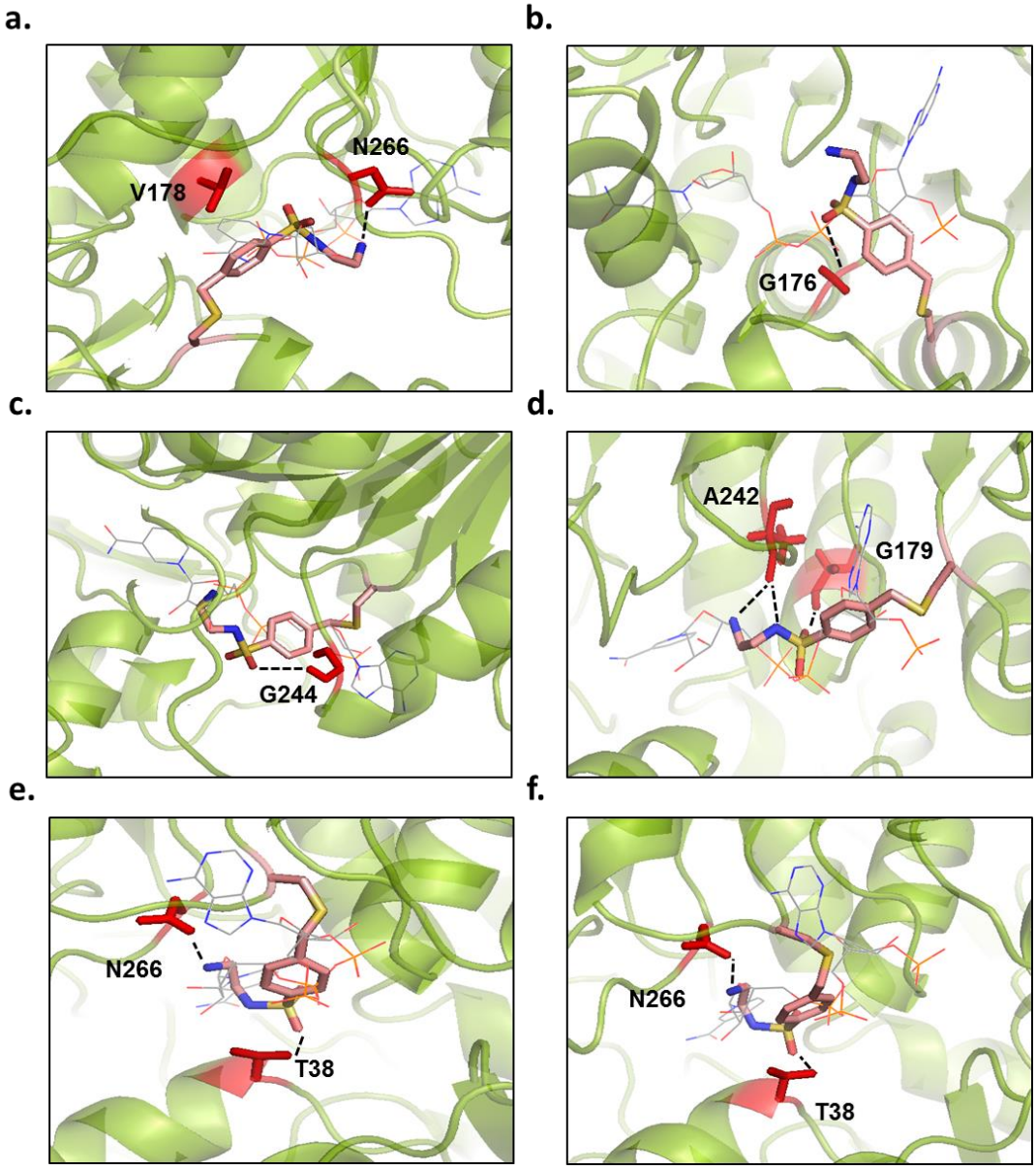


Figure 4.7. Catalytic site of TbADH (1YKF) with covalently docked *N*-sulfonyl ethylenediamine ligand **L1** at position a) 37, b) 203, c) 174, d) 198, e) 242 and f) 243.

Three distinct positionings of ligand **L1** were identified based on the interactions of the diamine and the sulfone with the residues within the cavity. The first one was the result of the docking at positions 37, 242 and 243. In all these cases, a H-bonding interaction was formed between the diamine moiety and asparagine 266. This residue was described to interact via polar interactions with one of the hydroxyl groups of the ribose connected to the nicotinamide ring.[194] Besides, the sulfone group also formed H-bonding interactions with tyrosine 38 for the positions 242 and 243. Interestingly, the position T38 was similarly described to interact with $NADP^+$, using polar interactions with one of the pyrophosphate groups. Additionally, valine 178 seems to provide some stabilization via non-polar interaction to the benzene ring of ligand **L1** in the docking position 37. Once again, this residue displayed hydrophobic interactions with the nicotinamide of $NADP^+$ in the wild type version of the enzyme.

The second positioning was the result of the docking at positions 174 and 203. A single interaction was detected between the diamine moiety and the backbone carbonyl of glycine 244 and 176, respectively. The reason why the sulfone did not interact with any residues was that it sat at the place of the pyrophosphate group linked to the second ribose moiety of $NADP^+$. This pyrophosphate group was shown to lack interactions with the native enzyme.

Finally, the results of the docking at position 198 revealed interactions between the diamine and the backbone carbonyl of alanine 242, and between the sulfone and the backbone carbonyl of the glycine 176. None of these positions were described to interact with $NADP^+$. However, the side chain of G198 sat at the opposite side of the cofactor binding cavity, when compared to position 37. Therefore, the added distance to reach the interacting residues in the native enzyme might be too high.

Based on the results obtained from the covalent docking study, single cysteine mutants were designed at positions 174, 198, 242 and 243 starting from the TbADH 5M variant. The wild-type cysteine position 37 was used as a comparison with already published work, while position 203 was also

investigated and mutated as a second point of comparison between native and mutated cysteine positions.

4.3 Site directed mutagenesis

The TbADH 5M gene (5M-C37), which has already been reported in previous work in our lab, was used to create a template without any cysteine, from which single cysteine mutants were subsequently created. The gene was available within the pET21a vector. The new template, called TbADH 6M (C37A, H59A, D150A, C203S, C283A and C295A), was successfully achieved by site directed mutagenesis using a commercial kit (QuickChange), as demonstrated by sequencing data (Appendix 1).

From this new, cysteine-free chassis, five mutants were developed, named 7M-C174, 7M-C198, 7M-C203, 7M-C242 and 7M-C243 according to the respective position of the cysteine residue inserted within the TbADH 6M sequence. The different mutants were all successfully obtained according to DNA sequencing analysis. The different plasmids were transformed into commercially available BL21(DE3) cells through electroporation. This cell line was engineered to improve expression efficiency by allowing large number of copies of the transformed plasmid within each cell.

4.4 Expression and purification of single cysteine TbADH variants

All mutants were expressed in *E. coli* BL21(DE3) according to a previously described method (section 3.2.3). After overexpression, each pool of cells was harvested, then purified. Each mutant, including the initial 5M-C37 and the cysteine-devoid TbADH 6M, were purified with up to 95 % purity according to SDS-PAGE (Appendix 2).

The results of the purification were listed in Table 4.1 below. The amount of protein purified was similar to the data reported in the literature concerning both the wild type and the TbADH 5M mutant.[217, 222] An Ellman's assay was then performed for each mutant to evaluate the accessibility of the cysteine residue.[223]

Table 4.1 Protein expression yield and cysteine availability through Ellman's assay, for single cysteine TbADH mutants.

Mutant	Free thiols /monomer	Protein yield (mg protein/ 0.5L culture)
5M-C37	0.69 ± 0.01	20-30
6M	0.03 ± 0.01	~ 20
7M-C174	0.63 ± 0.01	~ 22
7M-C198	0.52 ± 0.04	~ 22
7M-C203	0.48 ± 0.03	~ 22
7M-C242	0.61 ± 0.03	~ 22
7M-C243	0.51 ± 0.01	18-25

Mutant 5M-C37 showed an accessibility of 70 % for the 5,5'-dithio-bis-(2-nitrobenzoic acid), the chemical probe used in the assay. This value was already reported by Morra *et al.* and emphasises the limitation of this assay, namely the accessibility of the cysteines targeted by the reagent. Nonetheless, the assay provided a quick estimate of the ratio of accessible cysteines per mutant, which was used to confirm the sequencing results. For example, the results obtained with the cysteine free mutant TbADH 6M showed only 3 % accessibility, which corroborate with the lack of cysteine residue in this mutant. The non-zero result might be explained by a slight self-oxidation of the dye when exposed to light during the process.

The accessibility varied when the mutation location changed from position 37 to the other newly designed mutants, from 48 % with 7M-C203, up to 63 % with 7M-C174. The variations in cysteine accessibility were however expected, as some positions were less exposed to solvent than others. Nonetheless, the results were far from the expected 100 %, and bioconjugation results could suffer from the lack of thiol availability observed. These results could be due to the oxidation of some thiols, unable to react with the reagent. Addition of a reducing agent might be required. However, these chemicals tend to interfere with bioconjugation processes.

Whilst every mutant was considered viable for bioconjugation with ligands, an aliquot was kept from each purification and stored at -20 °C. A month after the

purification, an SDS-PAGE was run (Figure 4.8). The gel revealed that two mutants, 7M-C174 and 7M-C243, were starting to degrade when stored at -20 °C.

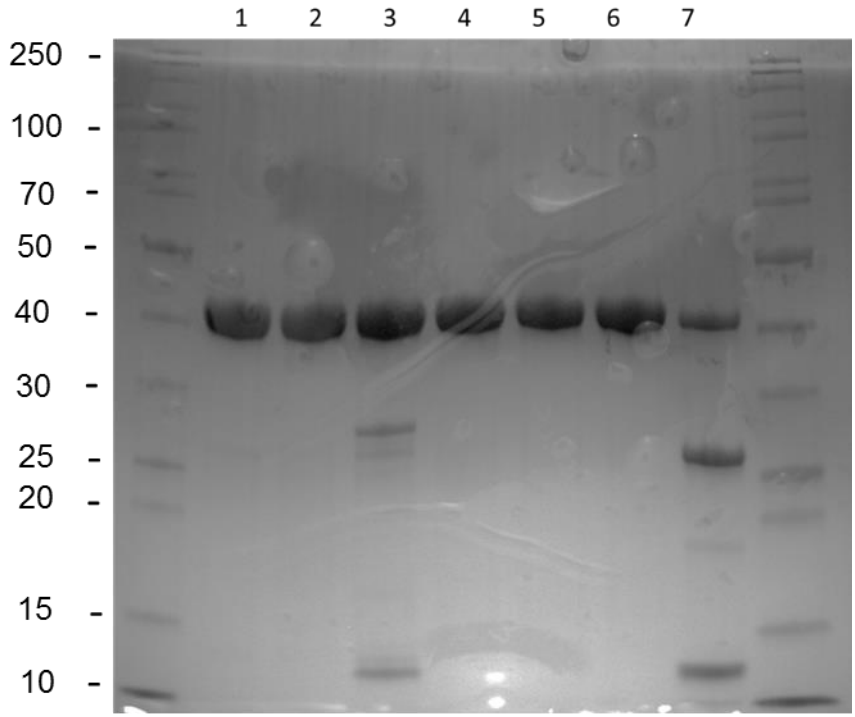


Figure 4.8. SDS-PAGE of the proteins TbADH 5M (lane 1), TbADH 6M (lane 2), 7M-C174 (lane 3), 7M-C198 (lane 4), 7M-C203 (lane 5), 7M-C242 (lane 6) and 7M-C243 (lane 7), sided by a ladder.

In the two cases, two extra bands at around 13 and 27 kDa were found. Those bands were adding up to 40 kDa, further confirming the hypothesis of a degradation rather than contamination. Further stability tests were then performed with the two mutants 7M-C174 and 7M-C243 (Figure 4.9). Each mutant was purified and then stored for 24 h at different temperatures, to evaluate the impact of storage upon protein degradation.

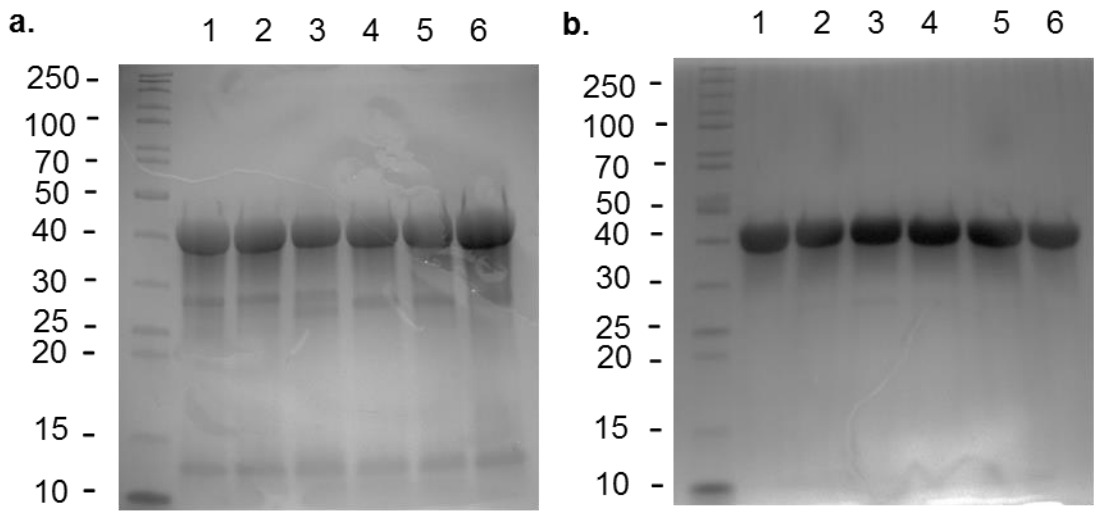


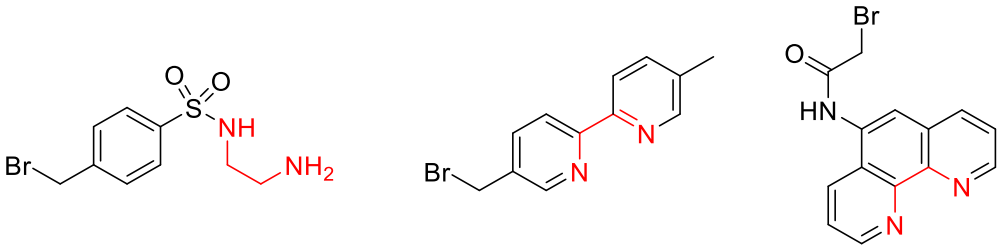
Figure 4.9. SDS-PAGE of the proteins a) 7M-C174 and b) 7M-C243 after 24h of storage at 1) -80 °C, 2) -20 °C, 3) 4 °C, 4) room temperature, 5) 37 °C or 6) 50 °C.

The test showed degradation after 24 h for 7M-C174, regardless of the temperature of storage. However, no difference in intensity were observed between 24 h and a month of storage (Figure 4.8). It could therefore be assumed that a small amount of protein undergoes a degradation process that cannot be circumvented under the conditions used. Nonetheless, the vast majority of the protein remained intact. For the mutant 7M-C243, no degradation was observed after 24 h, regardless of the temperature of storage. The temperature did not seem to have an effect on the degradation of these mutants. Nevertheless, in order to limit any supplementary degradation, both mutants were thereafter stored at -80 °C.

Once all mutants were obtained in the purest form available, different bidentate ligands were synthesized to evaluate the bioconjugation performance of the chemicals based on the position of the cysteine residue within the active site.

4.5 Synthesis of brominated bidentate ligands

Three ligands were chosen for the development of the artificial metalloenzyme: *N*-sulfonyl-ethylenediamine **L1**, bipyridine **L2** and phenanthroline **L3** (Figure 4.10). All the ligands contained a bromide functionality linked either to an alkyl or an acetamide moiety. The bromide is a well-known leaving group for nucleophilic substitution, the reaction targeted to create a covalent bond with the thiol of the cysteine residue.



L1 **L2** **L3**

Figure 4.10. Chemical structure of the different ligands used for the experimental study. The bidentate NN motif used for metal coordination was highlighted in red.

The first one was the ligand used to perform covalent docking and was used to compare accuracy of the *in silico* method with experimental results. The two other ligands were tested as they also possessed the nitrogen-based bidentate structure to coordinate metal ions. They were also reported in various catalysis involving transition metals,[34-35, 140, 224] in particular the recycling of nicotinamide cofactors and their mimics. Their respective syntheses are shown below (Figure 4.11).

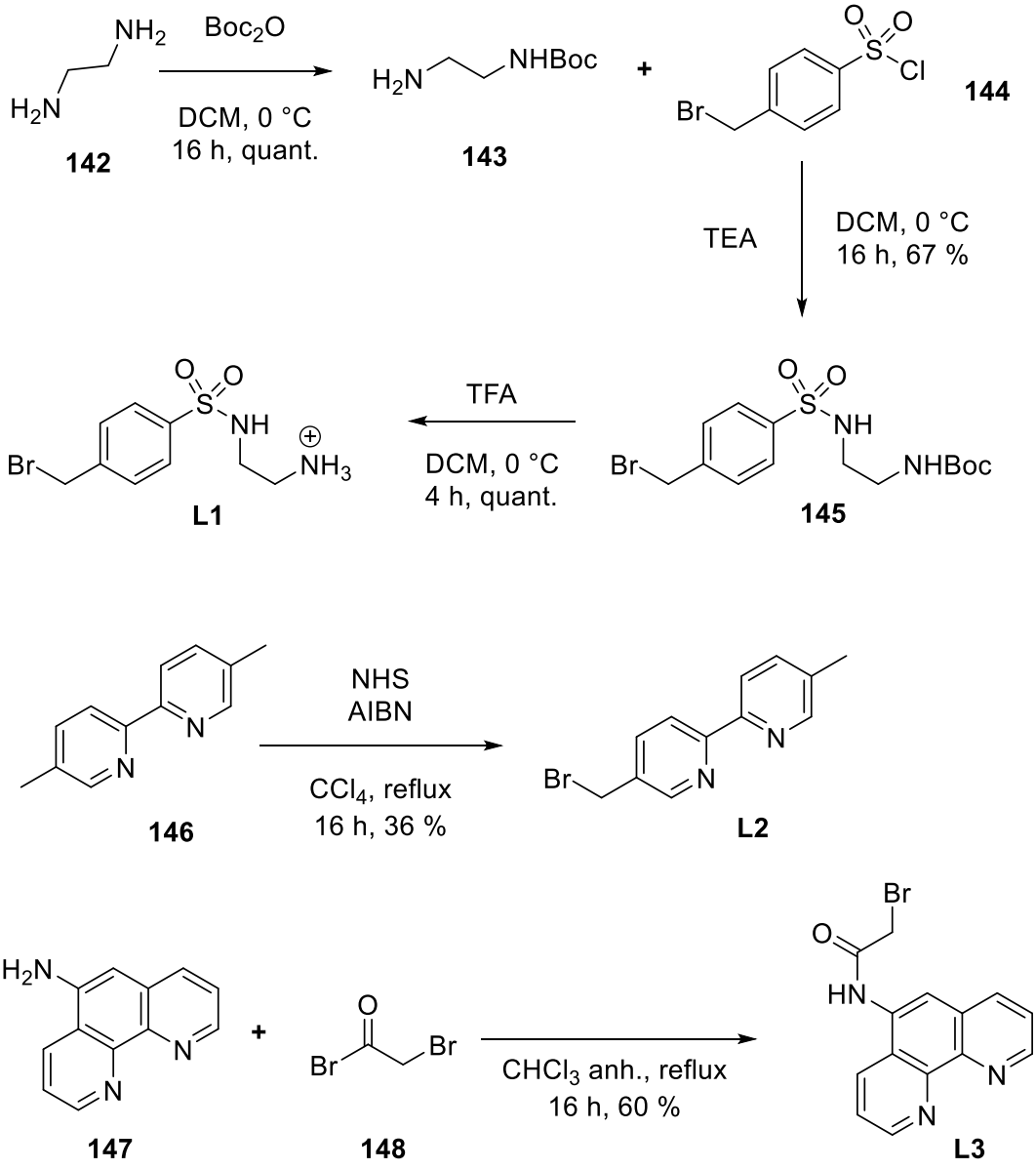


Figure 4.11. Synthetic routes towards the different ligands.

The synthetic route to reach the *N*-sulfonyl-ethylenediamine ligand **L1** was the longest, but also the most efficient with 67 % yield over 3 steps. This was explained by the protection/deprotection steps being quantitative. The limiting step was the creation of the sulfonamide bond. Compared to the other two ligands, the final step of the synthesis of ligand **L1** yielded the desired compound as a trifluoroacetate salt.

The synthesis of the bipyridine ligand **L2** was the most challenging. Although the chemical was produced in a single step, the reaction involved the radical activation of a methyl moiety by the addition of a very reactive bromine. Side reactions are very common with this set up which was successfully reported

twice in the last two decades with 34 % and 70 % yield. [213, 225] The main by-products of this reaction were the non-brominated succinimide and the dibrominated bipyridine, hence the low yields observed.

Finally, the synthesis of the phenanthroline ligand **L3** yielded the desired ligand with 60 %. The electron deficient primary amine, substituent of the phenanthroline, reacted with the highly active carbonyl of bromoacetyl bromide, therefore no other chemical was required to activate the nucleophile nor the electrophile. This set up allowed the performance of a crystallization after completion of the reaction without any further separation steps.

Once all three ligands were fully synthesized and characterized, bioconjugation was performed with the different mutants.

4.6 Bioconjugation of brominated ligands to TbADH mutants

The bioconjugation was a two-step process. The first one was the labelling, where the desired protein and chemical were mixed together. The following step was the purification of the labelled product using a PD10 desalting column. While little could be done on the second step toward improving the overall process, optimisation was carried out on the labelling side.

The optimisation was performed with the TbADH 5M mutant, as this variant was already proven to accept both the bipyridine and phenanthroline ligands. The *N*-sulfonyl-ethylenediamine ligand **L1** was chosen for this optimisation as it was the chemical used during the *in silico* study. The nucleophilic substitution reaction between the thiol of the cysteine and the bromide anchor of the ligand was monitored through Ellman's assay, by assessing the amount of remaining thiol after labelling. Ellman's assay was previously shown to underestimate the thiol content in the mutants and was used as a tool to determine the concentration of thiols available for the bioconjugation reaction by comparing the amount of thiols available after bioconjugation with those initially available (around 70 %). An assessment of the thiol reactivity towards nucleophilic substitution with the brominated ligand **L1** was obtained.

The conditions evaluated during the optimisation were the time and temperature of the labelling, as well as the concentration of protein (Figure

4.12a, entries 1 to 4). Additionally, the amount of chemicals to be added was also assessed (Figure 4.12a, entries 5 and 6).

a.

Entry	Time (h)	Temperature (˚C)	Protein concentration (mg/ml)	Ligand addition (equiv)
1	1	r.t.	1	4
2	4	r.t.	1	4
3	1	37	1	4
4	1	r.t.	4	4
5	4	37	1	4
6	4	37	1	1

b.

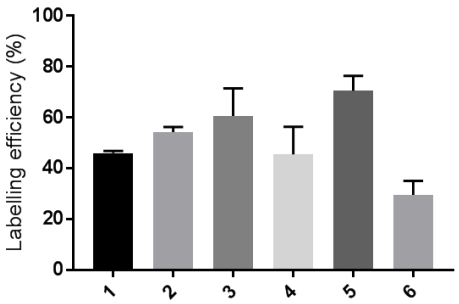


Figure 4.12. a. Description of the different conditions used during the optimisation process. b. results of labelling efficiency with TbADH 5M, normalized to Ellman's thiol availability.

The initial conditions consisted of a labelling time of 1 h, at room temperature with a protein concentration of 1 mg.mL^{-1} (or 25 µM). Once the labelling was complete, the resulting mixture was purified through a PD10 desalting column previously equilibrated with molecular biology grade water. The use of water during the purification process was due to the specific requirement of protein mass spectrometry later used for further analysis. These initial bioconjugation conditions (Figure 4.12a, entry 1) resulted in slightly less than 46 % of protein labelled after the bioconjugation. With the initial conditions, less than half of the available cysteine residues reacted with the alkyl halide.

To optimise this result, both the duration of the labelling and the temperature were varied (Figure 4.12a, entry 2 and 3). The increased time of contact from 1 h up to 4 h led to a slight increase in labelling with 54 % protein labelled. The increased time allowed more reactions to occur between the ligand and the cysteine. The raise of temperature to 37 ºC yielded 60 % protein labelled. This improvement by 25 % of the initial conditions proved this variation to be more efficient.

Another parameter evaluated was the protein concentration (Figure 4.12a, entry 4). However, the increase from 1 mg.mL^{-1} (25 µM) to 4 mg.mL^{-1} (100 µM) did not lead to any improvement as the labelling yielded 45 % of labelled protein. Therefore, it was decided to maintain a concentration of 1 mg.mL^{-1}

until the end of the optimisation process, to reduce the amount of biomaterial used. If later required, the concentration could be increased to 4 mg.mL^{-1}.

From the results described above, the optimum conditions were 1 mg.ml^{-1} of protein at 37 °C for 4 h. The ligand was added in excess at 4 molar equivalents. An additional experiment was performed with an equimolar ratio of ligand. The first conditions were set at 4 equivalents, similar to all the previous conditions, with all the other parameters optimized (Figure 4.12a, entry 5). This set up allowed to compare each individual optimum formerly developed with the overall one as well as providing a reference for the next conditions where the quantity was decrease to an equimolar ratio (Figure 4.12a, entry 6).

The equimolar ratio provided the less efficient conditions with close to 30 % protein labelled, less than obtained with the initial conditions. This put the emphasis on the importance of the ligand quantity. This was further proved with the astonishing results where 4 equivalents were used. More than 70 % of the proteins were labelled at the end of the bioconjugation using these conditions. Cysteines residue and their thiols were locked in the protein structure and embedded within the active site of the protein. Hence, increasing the amount of chemical to react with these residues also increased the probability of the reaction to occur.

Once the optimum conditions developed, i.e. 1 mg.mL^{-1} of protein mixed with 100 µM (4 equivalents) of ligands during 4 h at 37 ˚C, the different mutants were labelled with the ligands. Instead of solely using the Ellman's assay as a monitoring source, a complete quantitative analysis was performed using an ESI-MS to discriminate the results of the different bioconjugations.

Initially, a negative control of each mutant without ligand was performed (Figure 4.13). These experiments were carried out to identify the exact mass of the protein and compare it against the theorical mass obtained using ExPASy tool (referred as calculated value). If the results were alike, they were providing an additional argument towards the success of the mutation. Besides, the resulting values were used as a default to calculate the mass shifts expected from bioconjugation. Finally, these experiments also confirmed

the stability of the mutants during the bioconjugation and subsequent purification procedure.

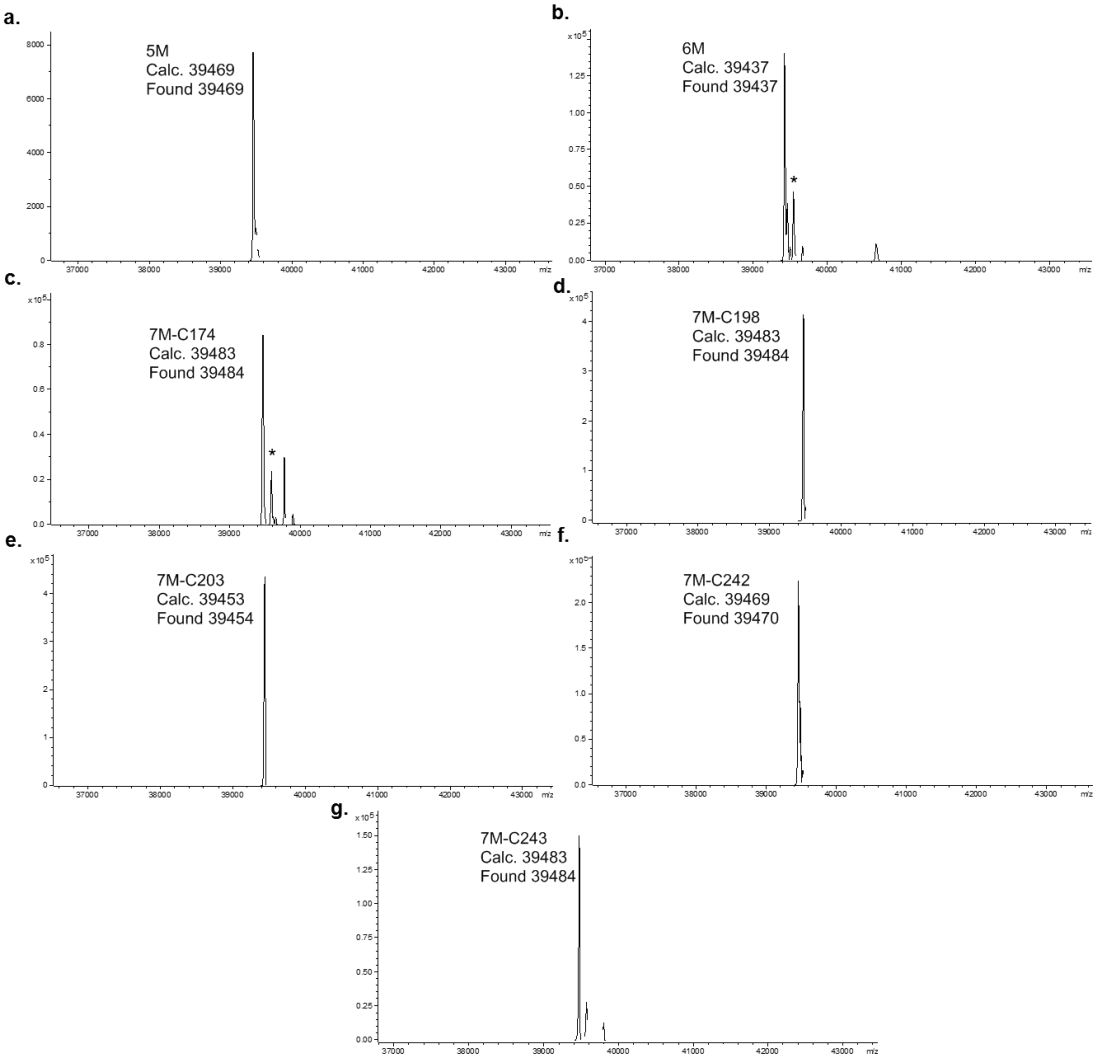


Figure 4.13. Deconvolution results of mass spectrometry analysis of a. TbADH 5M, b. TbADH 6M, c. 7M-C174, d. 7M-C198, e. 7M-C203, f. 7M-C242 and g. 7M-C243. The theorical values calculated through ExPASy and the experimental values found were showed as Calc and Found respectively. Peaks resulting from Tris ion adducts were outlined with *.

The bioconjugation process did not affect the protein integrity based on the mass spectrometry results. It was noteworthy that TbADH 6M and 7M-C174 showed an extra peak resulting of the addition of a Tris ion (+121 $g.mol^{-1}$). The origin of the ion was the buffer solution used to store the protein. However, a similar addition was described by Chait *et al.* with phosphate ion adducts (+98 $g.mol^{-1}$) and the origin of this adduct could be traced up to the cytosol.[226] Therefore, the +98 and +121 $g.mol^{-1}$ adducts were considered as ionized forms of the protein. Bioconjugation was then carried out starting with TbADH 5M and the different ligands (Figure 4.14).

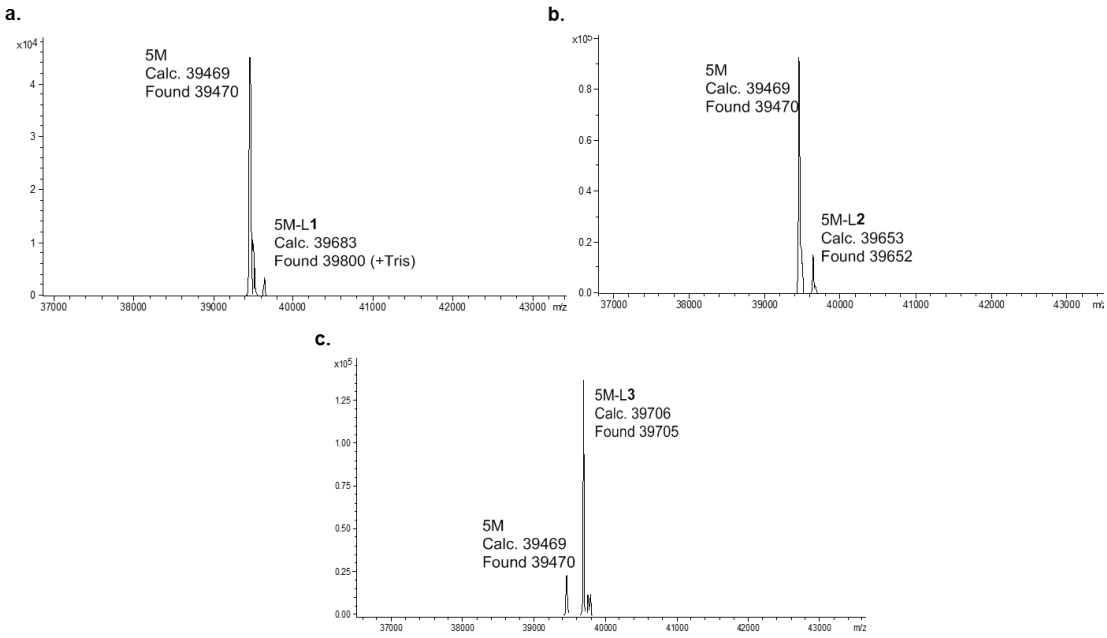


Figure 4.14. Deconvolution results of mass spectrometry analysis of TbADH 5M after bioconjugation with a) *N*-sulfonyl-ethylenediamine **L1**, b) bipyridine **L2** or c) phenanthroline **L3**. The theorical values calculated through ExPASy and the experimental values found were showed as Calc and Found respectively.

The bioconjugation procedure with sulfonamide and bipyridine both yielded a vast majority of unlabelled protein. However, the labelling procedure with phenanthroline yielded the desired chemo-enzymatic hybrid in an estimated 9:1 ratio to the unlabelled protein.

Although optimisation was performed using the sulfonamide ligand, bioconjugation results based on mass spectrometry indicated very poor labelling. These false positives could come from already oxidized thiols that could, therefore, not react with the reagent. To circumvent such situations, some researchers used a reducing agent to increase thiols reactivity towards Ellman's reagent. [227]

The sulfonamide and bipyridine ligands differed by their bulkiness. The bipyridine is more spacious than the sulfonamide moiety and the two-connected flat benzene rings increased spatial restriction. However, this structural difference yielded similar results by mass spectrometry. Thus, the shape of the ligand seemed to have little or no impact on the labelling.

On the other hand, the phenanthroline ligand, which was slightly bulkier than the bipyridine one, was able to react with the cysteine residue. The main difference between these two ligands was the reactive moiety. Indeed, both the sulfonamide and bipyridine ligands possessed an alkyl bromide while the phenanthroline one possessed an acyl bromide (Figure 4.15).

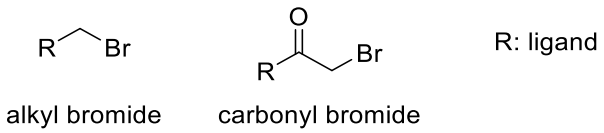


Figure 4.15. Structure of the two different reactive moieties inserted in the ligands to react with the thiol of the cysteine residue.

Carbonyl groups are known to be electron withdrawing groups (EWG). By pulling electrons away from the bromine, the carbon-bromine bond becomes weaker, hence increasing its reactivity. The difference of reactivity between the two moieties was thus considered the main criteria affecting the labelling.

Although it was not spotted during the labelling with TbADH 5M, other nucleophilic residues such as lysine or histidine, could potentially interfere with labelling. Therefore, a sixth mutation, C37A, was introduced into TbADH 5M to create a chassis without cysteine residue. The newly created TbADH 6M (C37A-H59A-D150A-C203S-C283A-C295A) was then labelled with the different ligands to evaluate the chemo-specificity of the labelling process (Figure 4.16).

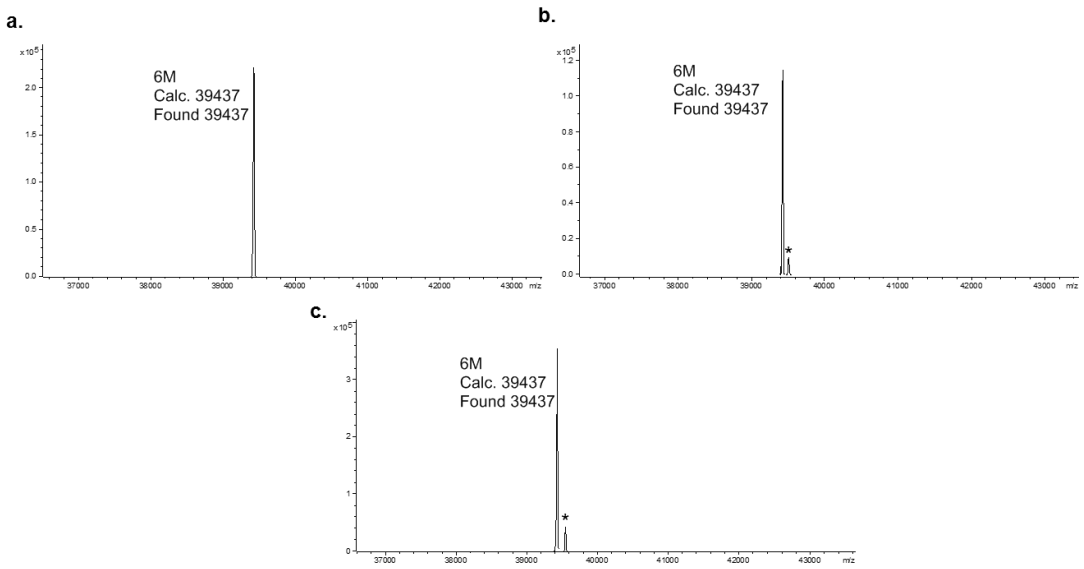


Figure 4.16. Deconvolution results of mass spectrometry analysis of TbADH 6M after bioconjugation with a) sulfonamide, b) bipyridine or c) phenanthroline. The theorical values calculated through ExPASy and the experimental values found were showed as Calc and Found respectively. Peaks resulting from Tris ion adducts were outlined with *.

As expected, no difference in molecular weight was observed with TbADH 6M when in presence of the ligands. Therefore, the mass shift observed with TbADH 5M was corresponding to the covalent bonding of the phenanthroline ligand with the available thiol of the residue.

Once the specificity of the labelling between the cysteine residue and the ligand was established, the process of labelling was then applied to the other mutants (Figure 4.17). Only sulfonamide and phenanthroline were later used to evaluate the mutants and their capability of reacting with the ligands. The former one was picked as it was the structure used to compute the cysteine positions and the latter due to its promising results from the labelling with TbADH 5M.

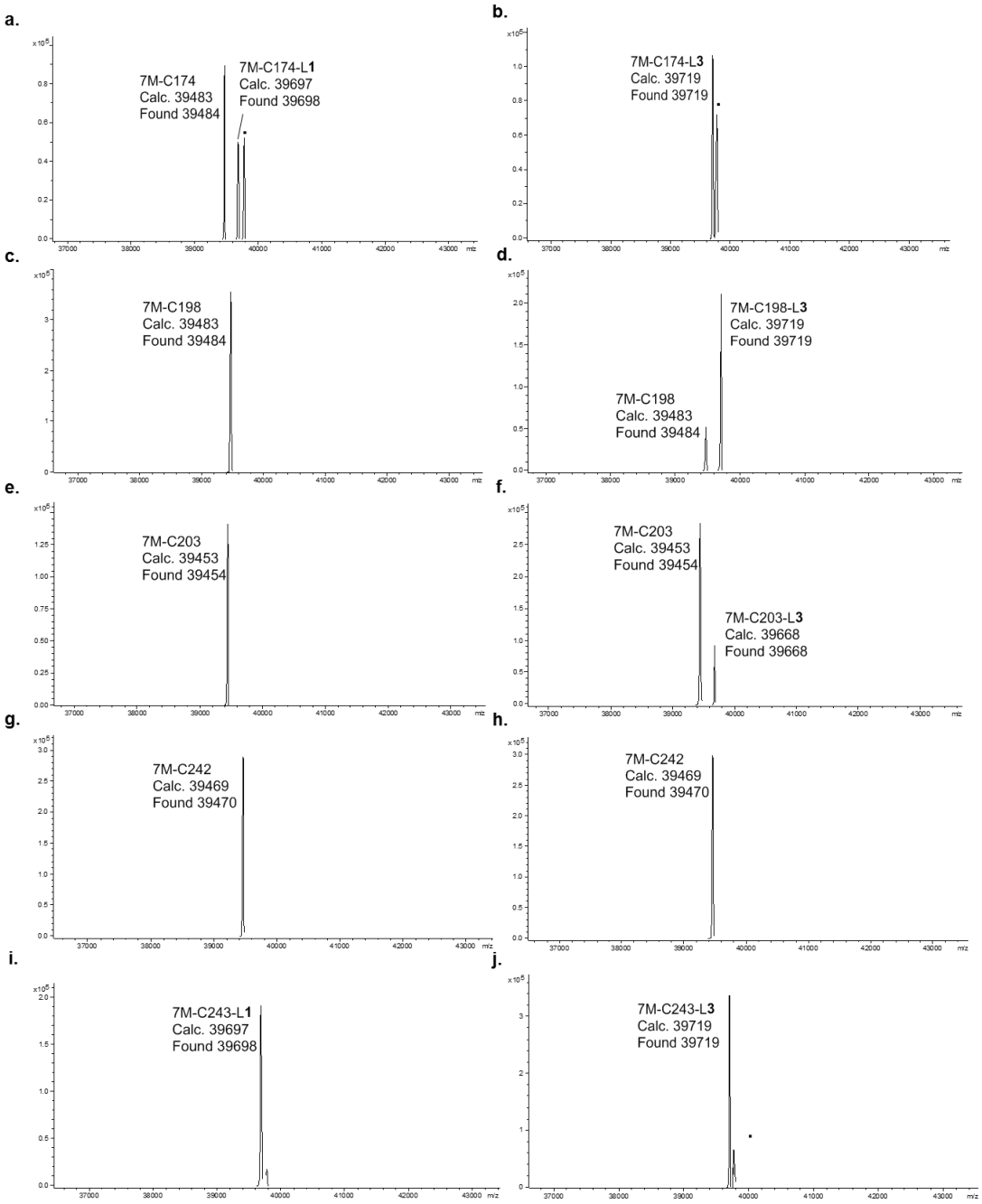


Figure 4.17. Deconvolution results of mass spectrometry analysis of 7M-C174 after bioconjugation with a) sulfonamide or b) phenanthroline, of 7M-C198 after bioconjugation with c) sulfonamide or d) phenanthroline, of 7M-C203 after bioconjugation with e) sulfonamide or f) phenanthroline, of 7M-C242 after bioconjugation with g) sulfonamide or h) phenanthroline, of 7M-C243 after bioconjugation with i) sulfonamide or j) phenanthroline. The theorical values calculated through ExPASy and the experimental values found were showed as Calc and Found respectively. Peaks resulting from Tris ion adducts were outlined with *.

The first observation made was about the better labelling observed with the phenanthroline ligand than the sulfonamide one. Indeed, the only proteins where the sulfonamide was able to bind the cysteine were 7M-C174 and 7M-C243. None of the other positions were able to offer enough availability for the reaction to occur, including position 7M-C242 which shared identical

interactions with the docked ligand **L1** than 7M-C243. Besides, positions 198 and 203 yielded labelled protein with 90 % and 20 % respectively (values obtained from the relative intensity of the peaks), when in contact with phenanthroline, while only the non-labelled mutants were observed in the presence of the sulfonamide ligand. These observations confirmed the difference of reactivity between the two ligands as a major effect on labelling efficiency under the same conditions.

As previously stated, the position 242 and 243, which were one residue apart, yielded completely opposite results. On one side, the thiol at position 242 was completely unreactive. The main argument about the lack of reactivity was the burial of the cysteine residue. However, the position 242 was well orientated within the protein cavity (Figure 4.7e) and the thiol could react with Ellman's reagent, discarding this eventuality. Crystallization of the mutant would provide additional information that might allowed to conclude on the lack of thiol reactivity at this position. On the other side, position 243 provided the best labelling results. When mixed with either sulfonamide or the phenanthroline ligand, full labelling was observed.

4.7 Summary and Conclusions

The overall aim of this study was to evaluate the position of the cysteine within the active site and to pinpoint positions where the bioconjugation between the ligands and the thiol were the best placed within the cofactor binding pocket for further development of the desired ArM. A rational approach was used, starting from a covalent docking study where 4 positions (174, 198, 242 and 243) were found suitable for experimental work, in addition to the active site cysteine C37 already evaluated in a previous study and cysteine C203 present in the cofactor cavity of the wild type. This was followed by the synthesis of 3 different ligands to evaluate the impact of the chemical structure upon bioconjugation.

After optimisation of the bioconjugation process, the various mutants were labelled individually with the 3 ligands. Three behaviours were expected based on computational results and polar interactions of the computed ligand **L1**. However, these predictions provided limited accuracy. Indeed, it was expected

that the mutant 7M-C242 would yield similar results as mutants 5M-C37 and 7M-C243 due to the similarity of the interactions involved, compared to $NADP^+$. Yet, this mutant displayed a non-reactive cysteine residue.

Therefore, 3 different reactivity of thiols were observed: a) the inaccessible cysteine within the mutant 7M-C242 where none of the ligands could react with the thiol, b) the mildly reactive cysteine residue within the mutants 7M-C198 and 7M-C203 where the reactivity of the ligand needed to be high enough to carry out the nucleophilic substitution, and c) the very reactive cysteine residue within the mutants 7M-C174 and C243 where both ligands could react with the thiol leading up to quantitative conversion of the mutant into the corresponding chemo-enzymatic hybrid.

In order to increase the positive outcome of bioconjugation with metal-based ligands, only the third reactivity of thiols depicted was selected as it was the only one where the labelling results were better than the published position 37. Hence, only mutant 7M-C174 and 7M-C243 were further studied. In particular, the mutant 7M-C243 was of great interest due to the outstanding results obtained through the bioconjugation process.

5 Artificial metalloenzymes for the reduction of nicotinamide derivatives

From the results of the previous chapter, mutants 7M-C174 and 7M-C243 were selected to build artificial metalloenzymes. The selection process described previously tested the feasibility of bioconjugation between proteins and metal-free bidentate ligands. Additionally, the mutant TbADH 5M was added as it was previously used to build an artificial metalloenzyme. The addition of this mutant provided reference values.

In this chapter, various artificial metalloenzymes were built and applied to the catalytic reduction of nicotinamide-containing chemicals, including natural cofactors NAD^+ and $NADP^+$. Rh- and Ir-based sulfonamide were selected for their reduction of ketones and imines whilst Rh- and Ir-based bipyridine and phenanthroline were selected for their reduction of nicotinamide derivatives. Substrate molecules should fit into the TbADH substrate pocket whilst the complexes should sit at the place of the cofactor. $NAD(P)^+$ cofactors were used as comparison. To initiate this study, metal-based ligands were synthesized.

5.1 Synthesis of metal-based ligands

From the metal-free ligands **L1**, **L2** and **L3**, a one-step reaction was performed to reach rhodium- and iridium-based catalysts. The reactions, called metalation, were all performed under the same conditions, regardless of the ligand or the metal used (Figure 5.1).

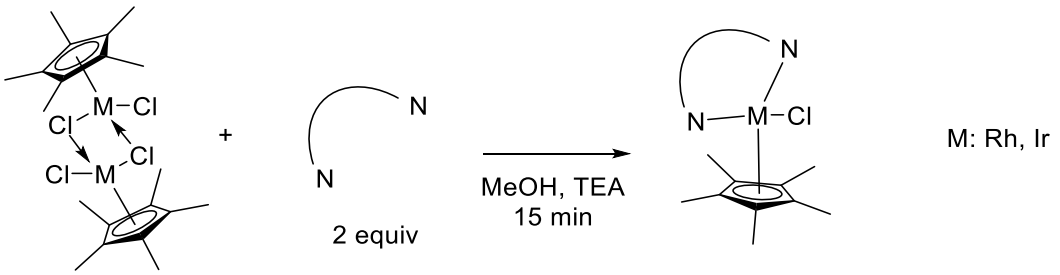
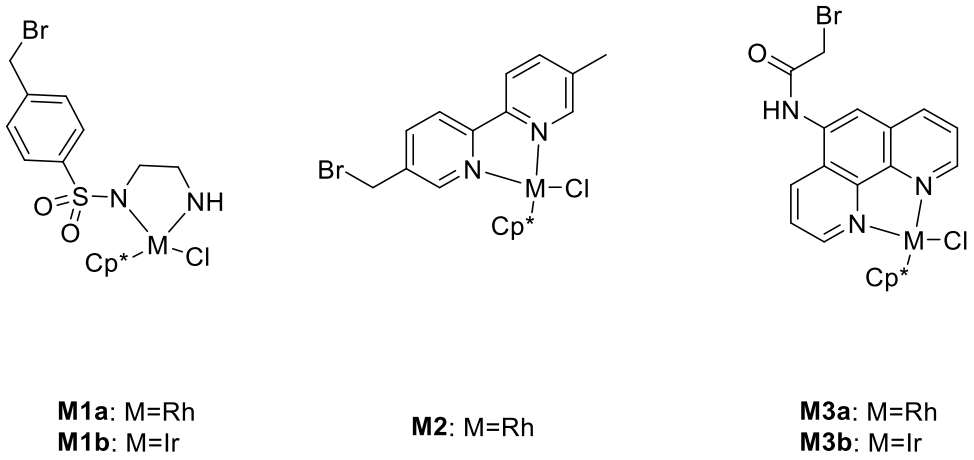


Figure 5.1. Overall representation of the metalation process.

Both metal precursors were coordinated dimers. Compared to the final compounds, the dimers were not soluble in methanol. This particularity also applied to the different ligands. Therefore, the progress of the reaction could be monitored from the flask as the suspension of the two reactants turned into

a clear, coloured solution. Five different combinations were developed; sulfonamide ligand **L1** with rhodium and iridium, bipyridine ligand **L2** with rhodium and phenanthroline ligand **L3** with rhodium and iridium (Figure 5.2). The bipyridine ligand **L2** was successfully obtained in relatively small amount, rhodium was therefore the only metal coordinated to this ligand. Once the reactions were finished, the products were recovered by precipitation.



M1a: M=Rh
M1b: M=Ir

M2: M=Rh

M3a: M=Rh
M3b: M=Ir

Figure 5.2. Structure of the different metal catalysts synthesized.

In the published report, TbADH 5M was combined with **M2** or **M3a** and the resulting artificial metalloenzyme was used to reduce $NADP^+$ into NADPH. This reaction was therefore used as a reference to compare the expected optimised mutants.

5.2 Reduction of $NADP^+$ using the metal complexes

Before conjugating the metal catalysts to the mutants, their capacity to perform the reduction of $NADP^+$ was first assessed (Figure 5.3). The aim was to discriminate metal catalysts that were not capable of reducing $NADP^+$ and only perform bioconjugation with the active catalysts.

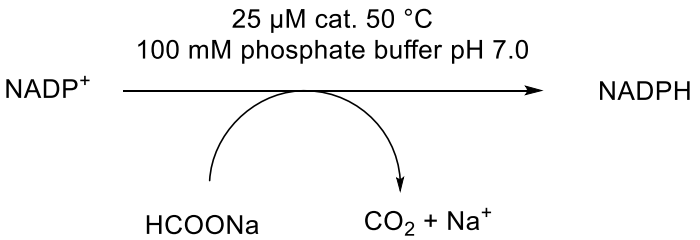


Figure 5.3. Reaction scheme of the reduction of $NADP^+$ by the different metal catalysts. Conditions: metal catalyst (25 µM), $NADP^+$ (420 µM) in sodium phosphate 100 mM buffer pH 7.0 at 50 ˚C.

The reaction was performed with every catalyst and turnover frequencies (TOF) were calculated from monitoring the appearance of NADPH at 340 nm (Table 5.1).

Table 5.1 Reduction of $NADP^+$ catalysed by metal catalysts. Conditions: catalyst (12.5 µM), $NADP^+$ (420 µM) in sodium phosphate 100 mM buffer pH 7.0 at 50 ˚C. The reaction was monitored at 340 nm for 1020 seconds. Each experiment was run in triplicate.

Catalyst	TOF (h^{-1})
M1a	4.13 ± 0.14
M2	193.8 ± 0.45
M3a	188.5 ± 0.93
M1b	111.1 ± 1.01
M3b	0.22 ± 0.06

According to the results obtained, the reactivity of metal catalysts depended on both the ligand and the metal ion used. The rhodium is highly reactive when coordinated to the bipyridine **M2** or phenanthroline **M3a**. However, the coordination with *N*-sulfonyl-ethylenediamine **M1a** yielded very low reactivity. On the other hand, when coordinating an iridium ion, ethylenediamine complex **M1b** yielded good results. When the iridium ion was complexed with phenanthroline however, the resulting catalyst **M3b** was inactive.

Compared to catalyst **M2** and **M3a**, the complex **M1a** was not charged, thus decreasing its solubility in water.[220] This solubility difference might have played a role in the lack of reactivity with this catalyst. On the other hand, the lack of reactivity from the catalyst **M3b** was expected as it was reported to be inefficient towards the reduction of NAD^+ compared to its Rh-based counterpart, **M3a** in this study. [228]

As a result, the catalysts **M1a** and **M3b** were not used further in the bioconjugation process due to their lack of reactivity towards the reduction of NADP+. The three other catalysts; **M3b**, **M2** and **M3a** were then used to build the corresponding artificial metalloenzymes.

5.3 Bioconjugation of metal catalysts with the different mutants

Using the previously optimised conditions for bioconjugation (i.e., 4 h, 37 ºC, 1 $mg.mL^{-1}$ (25 µM) of protein with 4 equivalents (100 µM) of ligands) resulted in precipitation of the proteins. Therefore, the bioconjugation with metal complexes were performed under reported conditions.

Following a published procedure where complexes **M2** and **M3a** were conjugated with mutant TbADH 5M,[217] each bioconjugation was performed for 1 h at room temperature by mixing each protein at a concentration of 4 $mg.mL^{-1}$ (100 µM) with 4 equivalents (400 µM) of complexes **M1b**, **M2** and **M3a**. As stated previously (section 4.6), protein concentration has little to no impact on bioconjugation efficiency. The main differences between the published conditions and the optimised conditions for this study were the time of exposure and the temperature. When combined, these parameters displayed a higher labelling efficiency with the ligand **L1**. By decreasing both parameters, it was therefore expected to reduce the interactions between the metal complexes and the protein, thus avoiding aggregation of proteins leading to precipitation.

While the bioconjugation with **M2** and **M3a** yielded the expected chemo-enzymatic hybrids, the conjugation with **M1b**, under these conditions, resulted in precipitation of the proteins in the sample regardless of the mutant used.

Therefore, optimisation of the conditions with **M1b** were investigated. The first variable to be changed was the concentration of protein. It was hypothesized that the initial concentration of 4 $mg.mL^{-1}$ was too high and therefore the amount of catalysts added (400 µM) was inducing precipitation by forming aggregates before homogenisation of the solution. The protein concentration was then lowered to 1 $mg.mL^{-1}$ and 100 µM (4 equivalents) of **M1b** were added to each protein sample. Unfortunately, precipitation occurred under these conditions.

Following the initial hypothesis, the concentration of **M1b** was reduced to 1 equivalent (25 µM) and was subsequently added to the protein samples at the lowest concentration. Once again, the proteins in each sample precipitated. A titration of **M1b** was finally performed with 1 $mg.mL^{-1}$ of protein concentration. The metal catalyst was added at various concentration (5, 10, 15, 20 and 25 µM). However, even with the lowest concentration of **M1b** (5 µM), precipitation of the proteins occurred. The only difference was the time needed to reach full precipitation, from 5 minutes at 25 µM to 30 minutes at 5 µM. The lack of solubility previously discussed with **M1a** (coming from the nature of the ligand)

might be the reason behind the precipitation observed, despite the modifications of the conditions attempted.

It was then decided to focus the effort on the artificial metalloenzymes successfully prepared. The hybrids were characterised by several biophysical methods: Ellman's assay, UV-Vis, ESI-MS and ICP-MS. In the next section, a complete set of analyses for all labelled mutants is provided. The first analysis performed was an Ellman's assay (Figure 5.4).

5.3.1 Ellman's assay of ArMs

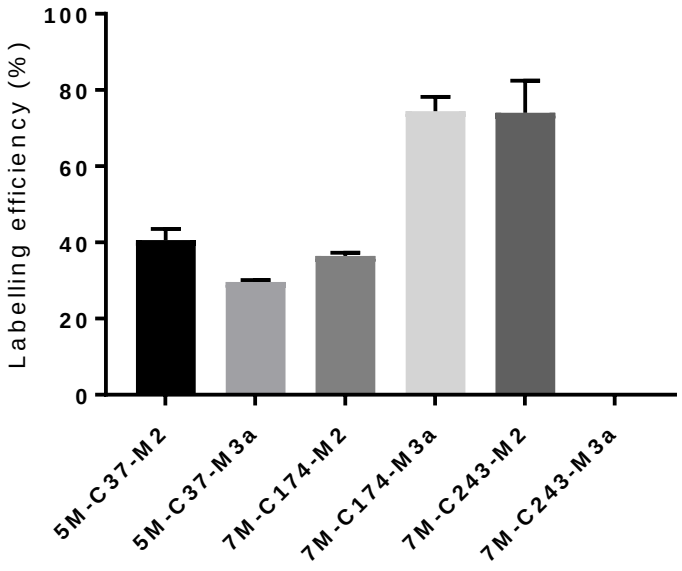


Figure 5.4. Percentage of labelled thiol in the artificial metalloenzymes resulting from the bioconjugation of 5M-C37, 7M-C174 and 7M-C243 with either catalyst **M2** or **M3a**. Results were normalized based on thiol accessibility for each mutant (section 4.4).

Interestingly, the bioconjugation depended more on the enzymatic scaffold than the catalyst used. Unexpectedly, 5M-C37 showed better bioconjugation with catalyst **M2** than **M3a**, with 42 and 29 % labelled thiols respectively while the labelling showed, on the ESI-MS, a better conjugation with ligand **L3** than **L2**. The opposite behaviour was observed with 7M-C174 with 38 and 76 % labelled thiols with **M2** and **M3a** respectively, in accordance with results of labelling with the ligands alone. 7M-C243 yielded 76 % labelled thiols with catalyst **M2**, as expected from the scaffold that exhibited the best results from bioconjugation with the ligands. However, the results obtained with 7M-C243-

M3a did not allowed any conclusion as they were out of the range of the assay. It is likely that this result was due to experimental error. However, due to the limited amount of hybrid prepared, a second assay was not possible. As this assay was used as a semi-quantitative test, more attention was put onto more accurate analyses to properly evaluate the quality of the bioconjugates.

5.3.2 UV-Vis analysis of ArMs

Analyses of the artificial metalloenzymes were then pursued. A spectral analysis was performed by UV-Vis on each hybrid, apoprotein and catalyst between 350 and 250 nm. Results were then superimposed to improve visual assessment of the bioconjugation process (Figure 5.5). A differential plot of the ArMs against each metal complexes is shown in Appendix 4.

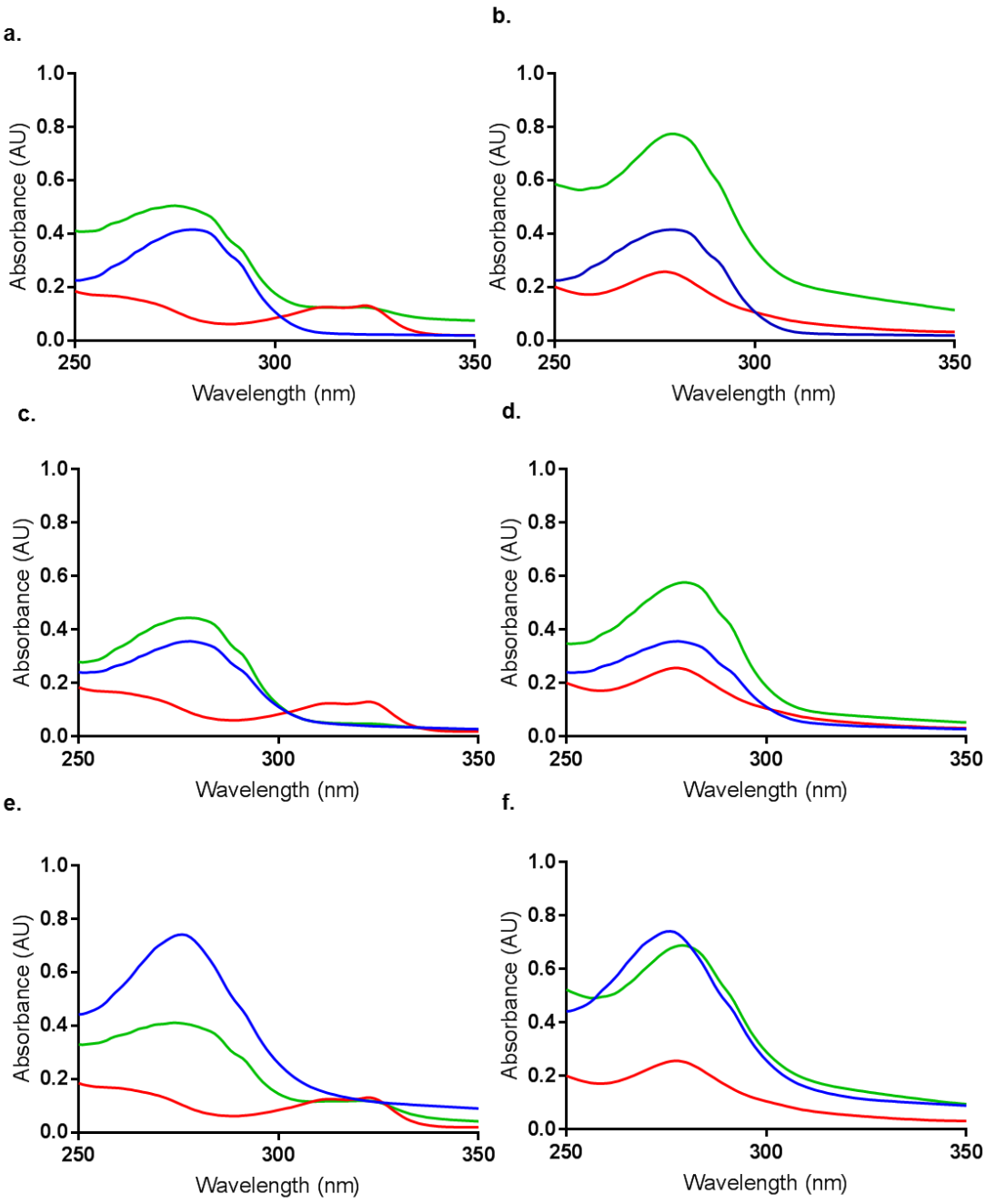


Figure 5.5. Superimposition of UV-Vis spectra of a, b) 5M-C37, c, d) 7M-C174 and e, f) 7M-C243 either in their apo forms (blue) or as artificial metalloenzymes (green), alongside with spectra of the metal catalysts a,c,e) **M2** and b,d,f) **M3a** (red). The spectra were recorded from 350 nm to 250 nm in Tris.HCl 100 mM buffer pH 8.0. Concentration of enzymes, metal catalysts and artificial metalloenzymes was 12.5 µM.

This set of analyses was performed to provide qualitative data on the bioconjugation process. Catalyst **M2** displayed a peak around 320 nm. Proteins, on the other hand, did not exhibit this peak. Therefore, it was expected to observe this peak in the resulting artificial metalloenzyme as an indication of catalyst binding. This expectation was fulfilled with mutant 5M-C37 and 7M-C243 where the two spectra, when superimposed, aligned at this

region. However, this peak was not observed with the mutant 7M-C174. This can whether be the result of a lack of binding from the catalyst, which would contradict the results from the Ellman's assay, or the embedded catalyst was buried within the active site in such a way that it can no longer interact with light.

The catalyst **M3a**, on the other hand solely displays a peak at 280 nm, which also corresponds to tryptophan absorption in the protein. However, when embedded into the enzyme, the resulting hybrid displayed, for all mutant, a slight shift towards red light from 277 nm to 280 nm. Additionally, the monitored absorbance from ArM 5M-C37-**M3a** and 7M-C174-**M3a** corresponded to the addition of both the mutant and the catalyst, free in solution. The lack of addition from the ArM 7M-C243-**M3a** could not be explained. Yet a shift of absorbance was observed, suggesting that the addition might have taken place.

5.3.3 ESI-MS of ArMs

The next set of analyses performed on the various hybrids was on an ESI-TOF mass spectrometer (Figure 5.6, Appendix 3). Similar to the bioconjugation with metal-free ligands in the previous chapter, the aim of these analyses was to observe if a mass shift corresponding to the addition of the catalyst to the enzyme was detected.

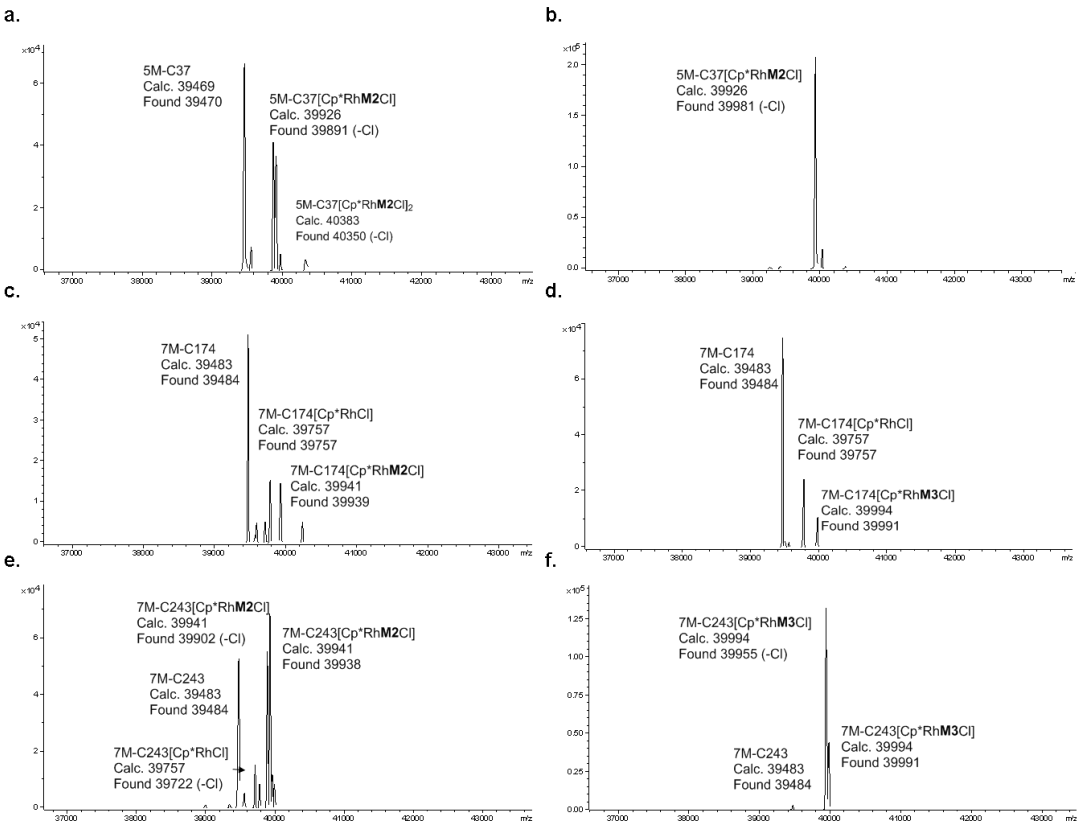


Figure 5.6 Deconvolution results of mass spectrometry analysis of a. b. 5M-C37, c. d. 7M-C174 and d. e. 7M-C243 after bioconjugation with catalysts **M2** (a. c. e.) or **M3a** (b. c. f.).

The mutant 5M-C37 yielded almost full bioconjugation with **M3a**, while half of the apoprotein was observed when conjugated with **M2**. Also, a slight amount of non-specific labelling was observed as a mass shift corresponding to the conjugation with two ligands was detected. The second bioconjugation was unspecific as each mutant was designed to hold a single reactive residue. Fortunately, the mutant 5M-C37 was the only one with which a second ligand conjugation was observed.

The mutant 7M-C174 was the least efficient in term of bioconjugation. With both metal complexes, the main species detected was the apoprotein. Nonetheless, the protein with the Cp*Rh conjugate, as well as with the full rhodium complexes **M2** and **M3a** were observed. The mass shift corresponding to the protein with the Cp*Rh might be the result of unspecific binding after dissociation of the metal complex from the bidentate ligand. This type of unspecific binding with rhodium complexes have previously been reported. [229] However, it was recognised that these results might impact further catalysis.

Finally, mutant 7M-C243 showed the best results out of the three protein scaffolds. Results of bioconjugation with **M3a** were similar to those obtained with 5M-C37, a very small amount of unlabelled protein was detected, and no unspecific binding was observed. When bioconjugated with catalyst **5**, the mutant mainly yielded the expected labelled protein. Some unspecific binding was also observed with the uncoordinated metal complex and less than a third of the protein detected was unlabelled.

Overall, regardless of the mutations, the artificial metalloenzyme developed with catalyst **M3a** displayed better results than those developed with catalyst **M2**. This might be the result of a better stability of the Rh-complex when coordinated with **M3a**, as most of the unspecific binding was found as a result of the Rh-complex dissociation from **M2**. Nucleophilic substitution occurring between the thiol and the bromoacetamide moiety were shown to be more efficient than with the alkyl bromide moiety. Thus, a better reactivity between the anchoring moiety and the thiol lead to less probability of Cp*Rh to dissociate.

As hypothesized, the position of the cysteine within the catalytic site played a major role in the success and yield of bioconjugation. So far, the mutant 7M-C243 seemed to display more potential than 5M-C37 while the mutant 7M-C174 yielded less efficient bioconjugation results.

5.3.4 ICP-MS of ArMs

Following the mass spectrometry analysis by electrospray, induced coupled plasma mass spectrometry (ICP-MS) was used to determine the metal content in each protein sample (Table 5.2). The aim was to accurately quantify the amount of Rh in each sample and observed whether there was a correlation with the previous mass spectrometry analysis.

Table 5.2. Results of the ICP-MS analysis. Each sample was diluted in 2% HNO_3 solution to reach a value of 80 ppb of Rh. Diluted samples were heat shocked to degrade the protein and free all metal ions in solution.

ArM	Rh content (%)
5M-C37-**M2**	90
5M-C37-**M3a**	77
7M-C174-**M2**	42
7M-C174-**M3a**	40
7M-C243-**M2**	57
7M-C243-**M3a**	75

The mutant 5M-C37 showed the best results in term of rhodium content. When labelled with **M2**, the protein exhibited both free enzyme and double labelled one alongside the expected single bioconjugation. The combination of both single and double labelled might explain the 90 % rhodium content in the protein sample. Surprisingly, the hybrid 5M-C37-**M3a** displayed a fairly pure, single labelled protein on the ESI-MS while the ICP-MS detected only 77 % rhodium content. These results were similar with the hybrid 7M-C243-**M3a** where 75 % rhodium content were detected and the ESI-MS spectra indicated a pure, single labelled artificial metalloenzyme.

These results could come from the limitation of the deconvolution process. Indeed, to avoid the deconvolution of the background noise from the raw spectra, a threshold was applied on the intensity of the peaks to be considered. This threshold might have hidden some unlabelled or partially labelled (only with the ligand as the metal ion would have dissociated from the complex). Nonetheless the similarity of the results proved the consistency of both methods and apparatus. Alternatively, a partial protein digestion could account for the underestimation of Rh content.

The mutant 7M-C174 yielded almost identical mass spectrometry spectra after bioconjugation with **M2** and **M3a**. These results were comparable in ICP-MS where 42 % and 40 % of rhodium content were respectively detected. Finally, the hybrid 7M-C243-**M2** displayed a slightly better bioconjugation rate on ESI-MS compared to 7M-C174-**M2**. This was confirmed by ICP-MS that was able to detect 57 % rhodium content in the protein sample.

Overall, the bioconjugation process yielded the desired hybrids with various success, as the metal complexes' presence was observed by UV-Vis within each ArM, with the exception of 7M-C174-**M2**. (Table 5.3). Whilst the ESI-MS results were in accordance with the ICP-MS results (for 5M-C37-**M2**, the higher Rh content come from Cp*Rh complexation), the results provided by Ellman's assay were inconsistent. Nonetheless, a prediction of the outcome of the catalysis was formulated, based on the results other than Ellman's assay, where mutants 5M-C37 and 7M-C243 should performed better than 7M-C174.

Table 5.3. Summary of the analytical results obtained from the ArMs. a) Data derived from relative peak intensity. n.d. not determined.

ArM	% labelling by Ellman estimation	Presence of metal complex peak (UV-Vis)	% labelling by ESI-MS [(a)]	% labelling by ICP-MS
5M-C37-**M2**	42	yes	53.8	90
5M-C37-**M3a**	29	yes	>99	77
7M-C174-**M2**	38	no	21.7	42
7M-C174-**M3a**	76	yes	13.6	40
7M-C243-**M2**	76	yes	52.7	57
7M-C243-**M3a**	n.d.	yes	>99	75

Once all the analyses were performed to assess, both qualitatively and quantitatively, the success of the bioconjugation, the reduction of $NADP^+$ was performed using the artificial metalloenzymes.

5.4 Reduction of NADP+ using artificial metalloenzymes

The conditions used to perform this reaction were similar to those used with the metal catalysts, at the exception of the loading concentration of the catalysts (Table 5.4, Appendix 5). While the concentration was 25 µM of metal catalysts, the biocatalysis counterpart used 12.5 µM which represented 0.5 mg of protein per reaction. The reason for this was to reduce the amount of protein necessary to perform all the experiments. Besides, the value of 12.5 µM corresponded to the protein content. Therefore, the TOF obtained was based on the protein sample concentration. These values were readjusted to metal content using the results from ICP-MS analysis to yield a TOF Rh value corresponding to metal complex reactivity.

Table 5.4. Reduction of $NADP^+$ catalysed by artificial metalloenzymes. Conditions: biocatalyst (12.5 µM), $NADP^+$ (420 µM) in sodium phosphate 100 mM buffer pH 7.0 at 50 ˚C. The reaction was monitored at 340 nm for 1020 seconds. Each experiment was run in triplicate. a) TOF protein is based on the protein sample. b) TOF Rh is adjusted to rhodium content based on results provided by ICP-MS. a. Published data from Morra *et al*.[217]

Catalyst	TOF protein (h^{-1})	TOF Rh (h^{-1})
Cp*Rh(C37-**M2**)Cl [a]		**59**
Cp*Rh(C37-**M2**)Cl	17.4 ± 0.04	19.3
Cp*Rh(C174-**M2**)Cl	8.8 ± 0.01	21.0
Cp*Rh(C243-**M2**)Cl	35.7 ± 0.34	62.6
Cp*Rh(C37-**M3a**)Cl [a]		**74**
Cp*Rh(C37-**M3a**)Cl	56.2 ± 0.45	73.0
Cp*Rh(C174-**M3a**)Cl	25.8 ± 0.05	64.5
Cp*Rh(C243-**M3a**)Cl	49.9 ± 0.13	66.5

It was expected to observe a decrease of activity due to the burial of the metal within the catalytic site of the enzyme, thus limiting the access to the reactive centre. Nonetheless, both hybrids containing 7M-C243 as an enzymatic scaffold displayed consistent results, comparable with reported activity. Hybrids containing complex **M3a** exhibited similar activity to reported data. With complex **M2**, 5M-C37 and 7M-C174 performed less than 7M-C243. Therefore, the position of the cysteine residue within the active site affected less the reaction than the nature of the ligand itself. Surprisingly, the mutant 7M-C174, which was expected to perform less, yielded similar activity to the either 5M-C37 or 7M-C243, based on the metal catalyst inserted.

Overall, complex **M3a** was the most suitable for this reaction as it provided consistent reactivity regardless of the anchoring position. Additionally, 7M-C234 was the most promiscuous scaffold as it showed similar reactivity regardless of the ligand. To evaluate the scope of the promiscuity observed, nicotinamide derivatives were tested under similar conditions.

5.5 Reduction of hydrophobic nicotinamide derivative compounds using metal complexes

All the different ArMs developed were able to reduce $NADP^+$ into NADPH to some extent. At the exception of mutant 5M-C37, the hybrids were designed to accommodate the metal complexes within the cofactor binding pocket, leading to the reduction of hydrophobic substrates. Thus, reduction of

nicotinamide derivatives, more hydrophobic than the natural cofactor, should yield better catalytic activity.

First, metal-catalysts were tested in solution to monitor the inherent reactivity of the catalysts towards the different substrates (Table 5.5). Only rhodium catalysts were used due to the difficulty to yield iridium-containing artificial metalloenzymes. Alongside **M2** and **M3a**, catalyst **M1a** was introduced into this experiment as a negative control. Indeed, this catalyst did not exhibit activity towards $NADP^+$ (section 5.2).

Three different scaffold were tested; NAD^+, another natural cofactor that could be used by the wild-type to some extent as a replacement for $NADP^+$,[194] Bn-NAD, a cofactor mimic developed by Hollman's team as an alternative to the natural cofactor with enoate reductases,[120] and Bn-NAD-Ph, a second cofactor mimic in which the structure of Bn-NAD was extended with a phenyl group attached to the nitrogen atom of the amide moiety. All three substrates possessed an oxidised nicotinamide ring that can be reduced in a similar fashion as $NADP^+$.

Table 5.5. Reduction of nicotinamide-containing compounds using the metal catalysts. Conditions: catalysts (25 µM), substrate (420 µM) in sodium phosphate 100 mM buffer pH 7.0 at 50 ˚C. The reaction was monitored at 340 nm (or 380 nm for Bn-NAD-Ph) for 120 seconds. Each experiment was run in triplicate. n.d.: not determined, results were below the threshold of detection.

Catalyst	Substrate	TOF (h^{-1})
Cp*RhCl-**M1a**	NAD+	n.d.
	Bn-NAD	14.9 ± 0.42
	Bn-NAD-Ph	29.9 ± 0.85
Cp*RhCl-**M2**	NAD+	181.7 ± 0.64
	Bn-NAD	90.2 ± 0.20
	Bn-NAD-Ph	382.1 ± 1.87
Cp*RhCl-**M3a**	NAD+	180.5 ± 0.68
	Bn-NAD	69.9 ± 0.51
	Bn-NAD-Ph	214.7 ± 1.38

As expected, results with NAD^+ were very similar to those with $NADP^+$. The two cofactors only differed by a single phosphate group attached to the ribose-adenosine part of the molecule. No changes in absorbance could be monitored with the catalyst **M1a** while very low activity (4.13 h^{-1}) was observed with

$NADP^+$. Likewise, results with catalysts **M2** and **M3a** were in the same range of activity, regardless of the natural cofactor used.

With the smaller and more hydrophobic substrates Bn-NAD and Bn-NAD-Ph, the catalyst **M1a** showed some activity, nevertheless, the results were still low compared to catalysts **M2** and **M3a**. These simpler structures might have facilitated the occurrence of the reaction. This was particularly visible with compound Bn-NAD-Ph, where both catalysts **M2** and **M3a** yielded higher activity, 382.1 and 214.7 h^{-1} respectively, than with $NADP^+$ as a substrate, 193.8 and 188.5 h^{-1} respectively. Although results with Bn-NAD were lower than with Bn-NAD-Ph, reaching up to a third of the activity with **M3a** (compared to $NADP^+$), they were still promising concerning substrate promiscuity. Overall, free in solution, the catalyst **5** seemed the most efficient one while the catalyst **M1a** displayed low to no activity depending on the substrate which confirmed its usage as a negative control in this experiment.

5.6 Reduction of nicotinamide derivatives compounds using artificial metalloenzymes

To perform the new sets of experiments, new batches of hybrids were required. Following the previously described analyses, these new hybrids went under similar processes. While all other analyses yielded very similar results, the metal-content obtained from ICP-MS differed slightly (Table 5.6).

Table 5.6. Results of the ICP-MS analysis. Each sample was diluted in 2% HNO_3 solution to reach a value of 80 ppb of Rh. Diluted samples were heat shocked to degrade the protein and free all metal ions in solution. Results of the former ICP-MS showed in parenthesis.

ArM	Rh content (%)
5M-C37-**M2**	100 (90)
5M-C37-**M3a**	42 (77)
7M-C174-**M2**	87 (42)
7M-C174-**M3a**	47 (40)
7M-C243-**M2**	50 (57)
7M-C243-**M3a**	67.5 (75)

Most of the hybrids yielded similar rhodium content compared to the previous bioconjugation. Nonetheless, two hybrids showed a metal content largely different from the previous samples. 5M-C37-**M3a** showed 42 % rhodium content in this new sample, which was below the previously observed 77 %.

7M-C174-**M2** showed 87 % rhodium content, corresponding to an increase by 2-fold of the previous set. Aside from an error in sample preparation, such as incomplete protein digestion, no other explanation was found about the change in metal content within these 2 hybrids. Nevertheless, the new results were used to calculate accurately the activity of the metal with the new substrates.

Using the same conditions as in section 5.4, the artificial metalloenzymes were tested for their substrate scope as they had previously shown their capability to reduce $NADP^+$. The first set of catalyses was performed with the enzymes conjugated with catalyst **M2** (Table 5.7).

Table 5.7. Reduction of nicotinamide-containing compounds using the artificial metalloenzymes conjugated with **M2**. Conditions: ArMs (12.5 µM), substrate (420 µM) in sodium phosphate 100 mM buffer pH 7.0 at 50 ˚C. The reaction was monitored at 340 nm (or 380 nm for Bn-NAD-Ph) for 1020 seconds. Each experiment was run in triplicate. Former $NADP^+$ data was shown as a reference.

Catalyst	Substrate	TOF protein (h^{-1})	TOF Rh (h^{-1})
Cp*Rh(C37-**M2**)Cl	$NADP^+$		**19.3**
	NAD^+	56.2 ± 0.44	56.2
	Bn-NAD	14.4 ± 0.47	14.4
	Bn-NAD-Ph	49.5 ± 1.6	49.5
Cp*Rh(C174-**M2**)Cl	$NADP^+$		**21.0**
	NAD^+	50.2 ± 0.31	57.6
	Bn-NAD	17.1 ± 0.47	19.6
	Bn-NAD-Ph	59.7 ± 1.3	68.5
Cp*Rh(C243-**M2**)Cl	$NADP^+$		**62.6**
	NAD^+	19.1 ± 0.04	38.5
	Bn-NAD	5.99 ± 0.17	12.1
	Bn-NAD-Ph	24.7 ± 0.36	49.5

The hybrids 5M-C37-**M2** and 7M-C174-**M2** showed better results with NAD^+ and Bn-NAD-Ph than with $NADP^+$. Concerning 7M-C174-**M2**, this behaviour can be the result of the greater metal content observed in the ICP-MS analysis. 7M-C243-**M2**, on the other hand, displayed less activity towards the various substrates, including NAD^+, compared to the $NADP^+$ cofactor. Surprisingly, this hybrid might exhibit the inherent selectivity of the protein scaffold for this cofactor, although to a lesser extent. This would, however, be in contradiction with the results of the covalent docking where the **L1** was shown to occupy the space of the cofactor. Unfortunately, mechanistic data are not yet available to provide a plausible explanation. Nevertheless, these 3 hybrids were able to

reduce the different substrates with activities behaving similarly as the metal catalysts free in solution. These results indicated a lack of impact from the protein scaffold on the substrate selectivity of the embedded metal catalyst, leading to the possible conclusion that Rh species might not be labelled or only partially labelled.

The second set of catalyses was performed with the mutants conjugated with catalyst **M3a** (Table 5.8). Surprisingly, the reduction reaction was, in most cases, less efficient with this catalyst than with **M2**.

Table 5.8. Reduction of nicotinamide-containing compounds using the artificial metalloenzymes conjugated with **M3a**. Conditions: ArMs (12.5 µM), substrate (420 µM) in sodium phosphate 100 mM buffer pH 7.0 at 50 ˚C. The reaction was monitored at 340 nm (or 380 nm for Bn-NAD-Ph) for 1020 seconds. Each experiment was run in triplicate. n.d.: not determined, results were below the threshold of detection. Former $NADP^+$ data was shown as a reference.

Catalyst	Substrate	TOF protein (h^{-1})	TOF Rh (h^{-1})
Cp*Rh(C37-**M3a**)Cl	$NADP^+$		**73.0**
	NAD^+	8.5 ± 0.04	20.1
	Bn-NAD	n.d.	-
	Bn-NAD-Ph	0.52 ± 0.04	1.2
Cp*Rh(C174-**M3a**)Cl	$NADP^+$		**64.5**
	NAD^+	15.4 ± 0.10	32.9
	Bn-NAD	0.69 ± 0.04	1.5
	Bn-NAD-Ph	2.54 ± 0.08	5.4
Cp*Rh(C243-**M3a**)Cl	$NADP^+$		**66.5**
	NAD^+	76.0 ± 0.87	112.6
	Bn-NAD	8.5 ± 3.4	12.6
	Bn-NAD-Ph	n.d.	-

When detected, the activities of the ArMs with the substrates Bn-NAD and Bn-NAD-Ph were very low. The best results obtained were with 7M-C243-**M3a**, yielding a TOF of 12.6 h^{-1} towards Bn-NAD. On the other hand, the activity was higher with NAD^+. 7M-C174 and 5M-C37 showed a drop of activity by 2 and 3 folds with 20.1 and 32.9 h^{-1} respectively, while 7M-C243-**M3a** displayed a TOF of 112.6 h^{-1}, corresponding to an increase of the activity by 2-fold, compared to $NADP^+$.

In the former set of catalysis with catalyst **M2**, the activity monitored was from unspecific binding of Rh species, resulting in a lack of substrate discrimination. The current set performed with catalyst **M3a**, however, exhibited a clear discrimination toward the nicotinamide derivatives. Furthermore, the catalytic

efficiency of the different ArMs varied significantly from one mutant to another, leading to the conclusion that unspecific binding of Rh species did not occurred with these ArMs or, at least, not in a significant amount. However, the accessibility of $NAD(P)^+$ cofactor within 7M-C243 remain unknown as the binding site for these chemicals should be occupied by the metal complex.

During the analytical process of the hybrids, it was pointed out that additional rhodium complexes were conjugated to the protein scaffold in an unspecific manner. These supplementary complexes might have been able to catalyse the monitored reduction of substrates, leading to the promising data presented above.

To evaluate the impact of unspecific binding onto catalysis, the mutant 6M was used to perform a bioconjugation with both catalysts **M2** and **M3a** and added to the subsequent catalytic reduction of $NADP^+$, the model reaction.

5.7 Evaluation of unspecific binding of the metal catalysts

The mutant TbADH 6M was used due to its proven inability to conjugate with the ligands to which the metal complexes were coordinated to (section 4.6). Therefore, the only reason why the hybrids might be created with this scaffold was unspecific binding of the metal catalyst (Table 5.9).

Table 5.9. Reduction of $NADP^+$ using TbADH 6M after bioconjugation with catalyst **M2** or **M3a**. Conditions: biocatalyst (12.5 µM), $NADP^+$ (420 µM) in 100 mM phosphate buffer pH 7.0 at 50 ˚C. The reaction was monitored at 340 nm for 1020 seconds. Each experiment was run in triplicate

Catalyst	TOF protein (h^{-1})
6M-**M2**	12.9 ± 0.08
6M-**M3a**	19.1 ± 0.10

The results of the catalysed reduction of $NADP^+$ with 6M-based ArMs were in accordance with the involvement of the unspecifically bound rhodium complexes with the reaction. Indeed, the 6M-**M2** hybrid yielded a TOF of 12.9 h^{-1}, similar to the results of 5M-C37-**M2** and 7M-C174-**M2** with TOF Rh values of 19.3 and 21 h^{-1} respectively. This catalyst was shown to provide unspecific binding throughout the analytical process.

On the other hand, the 6M-**M3a** hybrid displayed a TOF of 19.1 h^{-1}. Although it remained active, this value was lower by 3- to 4-fold to the other **M3a**-based ArMs. This proved the relatively efficient conjugation between the protein

scaffold and this catalyst. This also confirmed the substrate discrimination previously mentioned.

5.8 Effect of acids on compounds Bn-NAD and Bn-NAD-Ph

The activity provided previously with compounds Bn-NAD and Bn-NAD-Ph with ArMs were extracted from the linear evolution of the absorbance at the corresponding wavelength. However, after 500 seconds of monitoring the absorbance decreased progressively (Appendix 5). The by-product of the reaction was a release of carbon dioxide from formic acid after hydride exchange with the rhodium metal centre. It was thus hypothesized that the CO_2 released acidified the media and the two compounds were degrading under these acidic conditions, although pH variations were not performed before and after the catalysis.

To test this hypothesis, the reduced forms of Bn-NAD and Bn-NAD-Ph were used at maximum concentration reachable under the assay's condition, *i.e.* 420 µM. Phosphoric acid was then added progressively to the media and the absorbance at the corresponding wavelength was monitored (Figure 5.7). Phosphoric acid was chosen for this experiment as it was the conjugated acid to the phosphate ions composing the buffer solution. If the reduced forms of those two compounds were subjected to degradation in acidic conditions, a drop of absorbance should be observed.

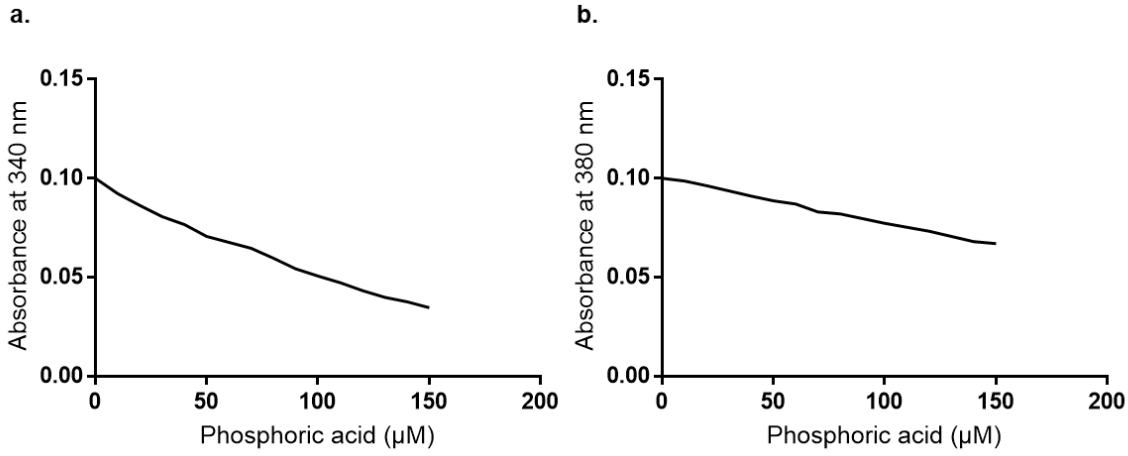


Figure 5.7. Impact of acidity of media on compounds Bn-NAD and Bn-NAD-Ph, normalized at 0.1 (UA). Conditions: substrate (420 µM) in 100 mM sodium phosphate buffer pH 7.0. Phosphoric acid was added progressively up to 150 µM and absorbance was monitored after each addition. Experiments were run in triplicate.

As predicted, the addition of phosphoric acid was directly correlated to a decrease of absorbance with either of the compounds. Therefore, the drop of absorbance observed after 500 seconds with the compounds Bn-NAD and Bn-NAD-Ph, might be correlated to the released of CO_2 from the activation step of the rhodium catalyst. However, a direct measure of the pH, before and after the catalysis, would be required to validate these results.

This degradation was however not observed with the metal catalyst free in solution. The degradation was monitored after 500 seconds with the ArMs while the reaction was only monitored for 120 seconds with the metal catalysts. Besides, the reduction reaction was faster with the catalysts free in solution. The fast release of CO_2 could have resulted in the by-product forming gas bubbles, lowering its concentration in solution and therefore reducing its impact on pH level.

5.9 Summary and Conclusions

Five metal catalysts were synthesized; **M1a**, **M1b**, **M2**, **M3a** and **M3b** as potential complexes to be coordinated with the selected protein scaffold from the previous chapter: 5M-C37, 7M-C174 and 7M-C243. Out of these 5 catalysts, 3 showed activity towards the reduction of $NADP^+$, the chosen model reaction. Therefore, the 3 active complexes **M1b**, **M2** and **M3a** underwent a bioconjugation process following published conditions. [217]

Only catalysts **M2** and **M3a** yielded the desired chemo-enzymatic hybrids under these conditions. Thus, the conditions were modified with **M1b** in attempt to yield the last ArMs. Despite various changes in conditions, the bioconjugation process resulted in full precipitation of the protein scaffold. Therefore, analyses of the hybrids were solely performed with **M2**- and **M3a**-conjugated ArMs.

The series of analyses consisted in an Ellman's assay to evaluate the amount of free thiol available in each protein sample, a UV-Vis analysis to observed the spectral changes in ArMs compared to their protein scaffolds, and 2 mass spectrometry analyses: ESI-MS to observe and quantify the resulting bioconjugates and ICP-MS to quantify the amount of metal within each protein sample. At the exception of Ellman's results, all the analyses were consistent

with each other, underlining the lack of accuracy of the Ellman's method. As stated previously, researchers carried out the assay under reducing conditions to improve the validity of this method. Nonetheless, the consistency of the sample preparation as well as the potential self-oxidation of the reagent probably account for the large variability of the results obtained. Hence, attention was focused on the other analyses.

This series of analyses underlined a better conjugation with catalyst **M3a** than **M2** that exhibited some unspecific binding, mainly due to dissociation of the rhodium complex from the ligand. Once the ArMs were analysed, they were tested upon reduction of $NADP^+$. Overall, the protein scaffold 7M-C243 performed better than the published 5M-C37, whilst 7M-C174 was the least efficient one with moderate activity monitored. As expected, the results of catalysis were lower with the ArMs than with the metal complexes free in solution due to the burial of the active complex within the protein cavity.

Following these exciting results, the substrate scope of the hybrids was evaluated. The metal catalysts were able to perform well with the various substrates, so did the ArMs. Interestingly, **M3a**-conjugated ArMs displayed high selectivity towards natural cofactors, displaying very low activity for the reduction of nicotinamide derivatives.

This raised a concerned on the role played by the unspecific binding of metal complexes observed earlier on. Thus, a control experiment was performed with the cysteine-deprived mutant 6M. Conjugation with both metal catalysts showed some activity towards the reduction of $NADP^+$. However, 6M-**5** exhibited similar activity to corresponding hybrids while 6M-**6a** displayed much lower activity, ca 3 to 4 times lower than the corresponding hybrids. This emphasized the impact of unspecific binding onto catalytic performances and raised an issue that could potentially be tackled in further research.

Finally, during the substrate scope experiments, a decrease in absorbance was monitored with the 2 unnatural substrates Bn-NAD and Bn-NAD-Ph after 500 seconds in the monitoring process. Due to the release of CO_2 as a by-product, resulting from the rhodium-complex activation by formate, it was

hypothesized that the medium was acidified as the reaction went on and degraded the product.

A control experiment was therefore put in place to monitor the changes in absorbance of the reduced form of these nicotinamide derivatives upon addition of phosphoric acid. As hypothesized, the absorbance dropped consequently of acid addition. These experiments could be validated by a direct measurement of the pH of the reaction, before and after the catalysis.

Although this study revealed a more suitable position for anchoring a metal complex within TbADH, *i.e.* position 243, more work needs to be done on the understanding of both the reaction mechanism and the substrate selectivity observed. Crystallization and the resulting 3D structure of such ArM could provide valuable information for further optimisation of the current building process, including the optimisation of the chemical scaffold.

6 Artificial metalloenzyme design by supramolecular binding

6.1 Background

The main drawback of the covalent binding approach for the design of artificial metalloenzyme is the requirement of a reactive residue that will act as an anchoring site for the metal catalyst to be introduced within the protein scaffold. By utilising supramolecular forces, a reactive residue is no longer needed. Among the features of ADHs, the cofactor binding site is the most promising one to provide supramolecular interactions directed toward the stabilisation of a supramolecular anchor. Indeed, these interactions already exist and are currently directed towards the nicotinamide cofactors NAD(P)H.

However, NAD(P)H molecules are very expensive; $854 and $231 per mmol of NADPH and NADH respectively in 2012.[141] This cost is mainly due to the complexity of the structure of these chemicals. Therefore, simpler designs were developed,[118, 120, 153] mimicking the nicotinamide ring of the cofactor as it's the part involved in the catalytic process. As an example, literature reported the use of the nicotinamide mimic Bn-NAD as a potent cofactor with the Xenobiotic enoate reductase A (XenA) from *Pseudomonas putida,* at the place of NADH.[119-120]

Enoate reductases (ERs) use two distinct cofactors for electron relay (Figure 6.1). NADH first provides a hydride to the oxidized form of flavin mononucleotide (FMN). The NAD^+ then leaves the catalytic site and the substrate replaces it. The reduced FMN will transfer the hydride to the substrate to regenerate its oxidized state, reducing, with the help of a water molecule, the targeted carbon-carbon double bond on the substrate.

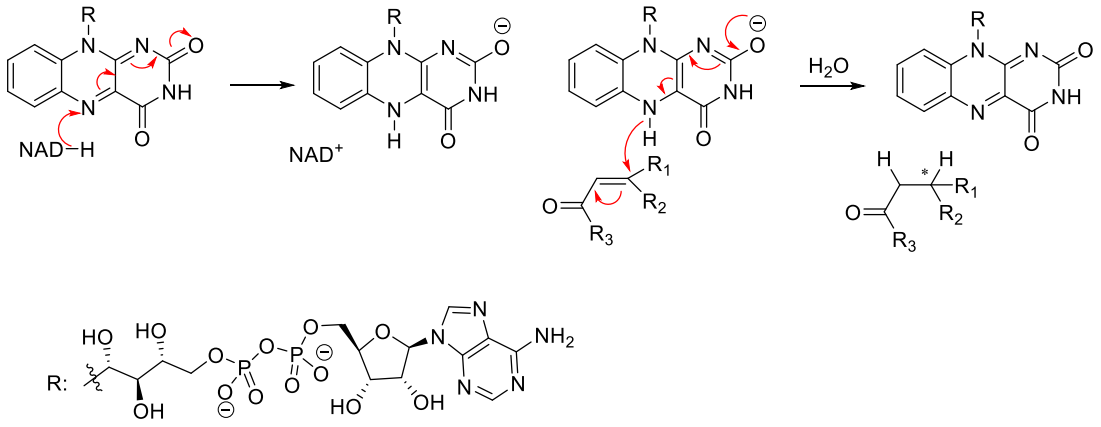


Figure 6.1. Simplified mechanism of FMN proton transfer using a nicotinamide cofactor as a hydride donor and an enone moiety as a substrate.

Based on previous work reported by Fish,[153] it was hypothesized that ADHs might also be able to use nicotinamide mimics at the place of NAD(P)H cofactors in ADHs. If so, they are expected to act either as hydride donors, by mimicking the cofactor capacity to transfer a hydride through the C_4 position of the nicotinamide ring, or to simply position themselves at the place of the cofactor and therefore behave similarly to inhibitors. The aim is to use these supramolecular structures as anchors to which a metal complex can be linked.

6.2 Expression and purification of wild-type His-HLADH and TbADH

Plasmids containing wild-type forms of TbADH and HLADH were available in the laboratory and were transformed into *E. coli* BL21(DE3) competent strains. Both proteins were expressed in *E. coli* according to previously described protocols (section 3.4.2) and then purified by affinity chromatography. The TbADH protein sequence contained an N-term Strep tag II (Trp-Ser-His-Pro-Gln-Phe-Glu-Lys), while the HLADH contained a C-term hexahistidine tag, hereafter referred as His-HLADH.

While the purification of TbADH was successfully achieved following the initial protocol, the process required optimisation for His-HLADH. Previous reports indicated EDTA in sodium phosphate 100 mM buffer pH 7.0 to be a suitable eluent for His-HLADH to remove the protein from the Ni^{2+}-agarose matrix of the column.[230] However, it appeared that at concentrations as high as 15 mM, EDTA was not able to displace the protein from the column, and higher concentrations of EDTA could have resulted in deterioration of the protein.

Therefore, imidazole was investigated as another chelating agent, in order to displace the bound protein out of the column. A final concentration of 500 mM of imidazole was used to purify His-HLADH (Appendix 6).

After purification, the protein concentration was 1 $mg.mL^{-1}$, determined by the Bradford method, and then the proteins were stored at -80 °C until further use. A total of 5 mg of His-HLADH and 17 mg of TbADH were obtained from 400 mL and 500 mL of culture medium, respectively.

The yield of 12.5 mg of purified His-HLADH per litre of culture corresponds to half of the typical value reported in literature (around 25 $mg.L^{-1}$ of culture). The reported results were based on the use of EDTA as a chelating agent rather than the imidazole used in this study. The change of chemical might be the reason behind the lower yield observed. On the other hand, the quantity of TbADH obtained from the purification process was comparable to the range of yields previously published.[194, 231]

Once the enzymes were purified, their respective activities were then assessed to be compared against literature as well as to provide values to be used as standards for further experiments.

6.3 Determination of the specific activity of His-HLADH and TbADH

The specific activity of His-HLADH for both the oxidation of ethanol and the reduction of acetaldehyde were determined by monitoring the respective formation or disappearance of the natural cofactor NADH at 340 nm, using UV-Vis spectrophotometry at room temperature (Table 6.1).

The specific activity of the enzyme was 0.86 $U.mg^{-1}$ for the oxidation and 9.1 $U.mg^{-1}$ for the reduction. Literature reported up to 1 $U.mg^{-1}$ for the oxidation and no data were provided for substrate reduction activity.[153, 201, 230] In comparison, the main commercial form of the enzyme was a freeze-dried preparation with a specific activity of 0.5 $U.mg^{-1}$ (oxidation of substrate). The results of activity were therefore considered in range and used as reference for further experiments.

The specific activity of TbADH was determined for the oxidation of (±)-2-butanol and for the reduction of 2-butanone, the natural substrates of this enzyme, by monitoring the formation or disappearance of the cofactor NADPH at 340 nm at 40 ˚C (Appendix 7). The specific activity was 74 $U.mg^{-1}$ for the oxidation of 2-butanol and 35 $U.mg^{-1}$ for the reduction of 2-butanone. This data was similar to previous literature reports.[204, 231-232]

Table 6.1. Determination of the specific activity of His-HLADH and TbADH for oxidation and reduction of their natural substrates. Conditions for His-HLADH: enzyme (25 µM), cofactors (1.5 mM) and substrates (200 mM) in 100 mM phosphate buffer pH 8.8 and 7.0 for ethanol and acetaldehyde respectively. Experiments run in triplicate and monitored at 340 nm for 400 seconds at room temperature. Conditions for TbADH: enzyme (2.5 µM), cofactors (1 mM) and substrates (20 mM) in 50 mM Tris HCl buffer pH 9.0 and 6.0 for 2-butanol and 2-butanone respectively. Experiments run in triplicate and monitored at 340 nm for 150 sec at 40 ˚C. (a) calculated from 400 mL (His-HLADH) and 500 mL (TbADH) cultures.

	Specific activity	Purification Yield [(a)] (mg of protein/ L of culture)
His-HLADH	0.86 $U.mg^{-1}$ *with ethanol* 9.1 $U.mg^{-1}$ *with acetaldehyde*	12.5
TbADH	74 $U.mg^{-1}$ *with 2-butanol* 35 $U.mg^{-1}$ *with 2-butanone*	34

Both enzymes showed specific activity in line with published data. Therefore, the next step was the synthesis of supramolecular anchor mimicking the nicotinamide ring of NAD(H) and NADP(H) cofactors.

6.4 Chemical synthesis

The development of an anchor capable of interacting in a supramolecular manner with ADHs was the starting point of this study. A complete anchoring system was initially designed (Figure 6.2). The design was composed of three distinct parts: a) a supramolecular anchor, b) a bidentate ligand to coordinate the desired metal ion and c) a linker. The enzymatic scaffold is NAD(P)-dependent, therefore the anchor was based on the nicotinamide mimic Bn-NAD. The ligand chosen was *N*-sulfonylethylenediamine as it was widely used in catalysis. Finally, the linker was designed upon the tosyl moiety used in Noyori's catalyst towards ATHs. This moiety was shown to be essential in the

stabilisation of the ethylenediamine-metal complex, including the addition of hydrophilicity to use the moiety in a ligand for the design of water soluble complexes.[100-103, 219-220]

From the initial structure, two substructures were extracted: the supramolecular anchor Bn-NAD and the anchor with a partial linker Bn-NAD-Ph.

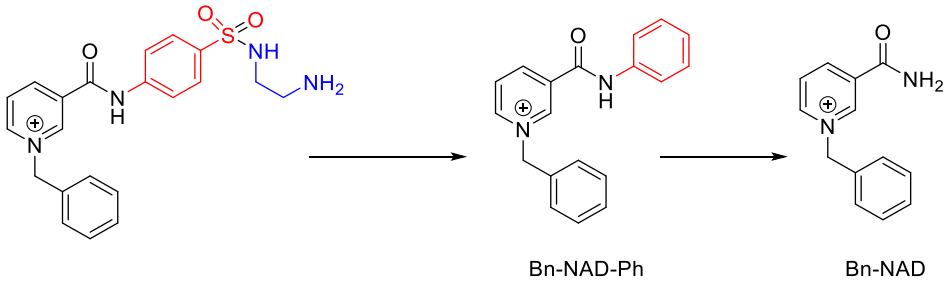
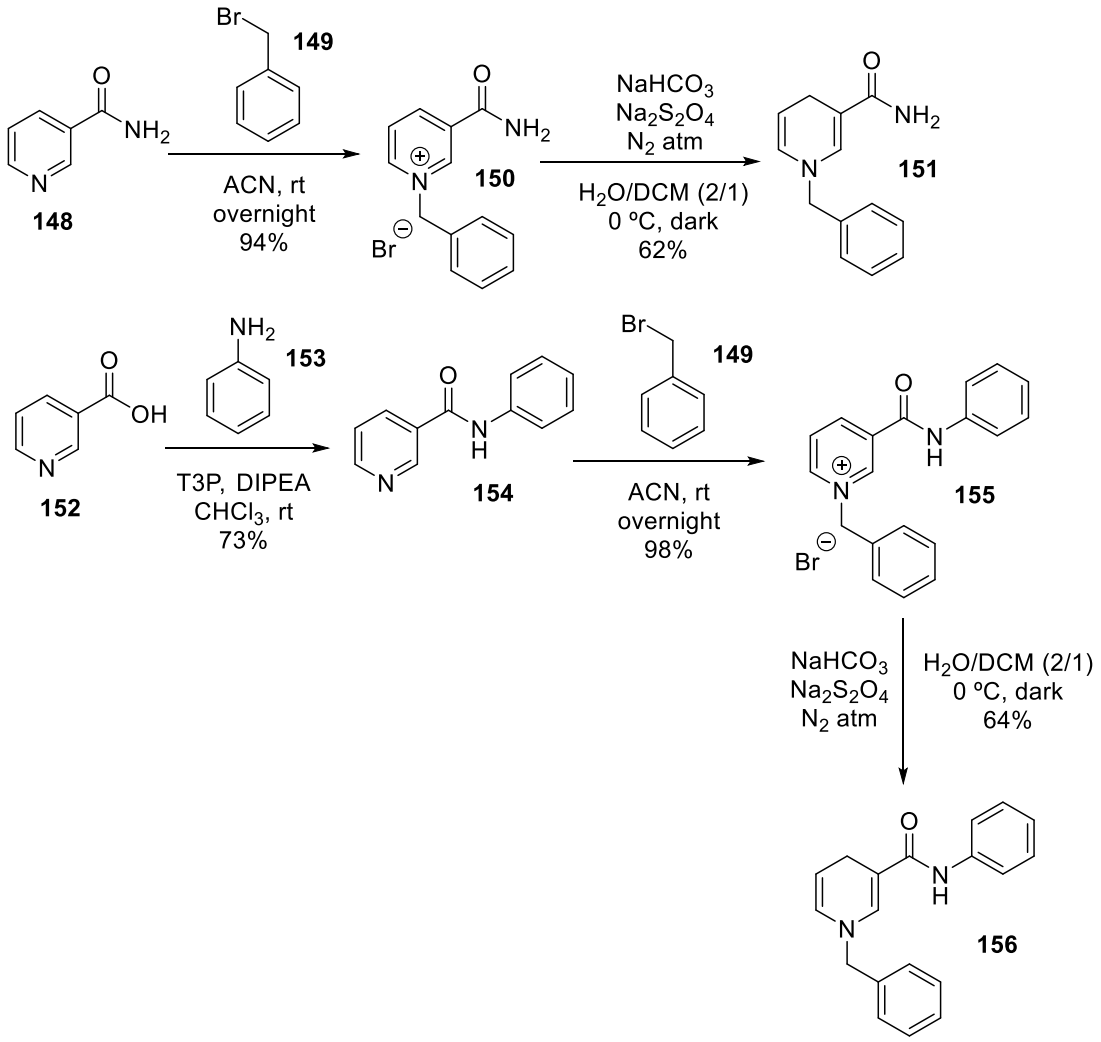


Figure 6.2. Structure of the expected ligand to coordinate with metal ions and the extracted substructures. The various parts of the ligand were highlighted as follow: bidentate coordination motif to the metal (blue), stabilisation linker (red) and supramolecular anchor (black).

Once the design of the metal catalyst was achieved, the anchors were then synthesised with and without the phenyl linker in order to determine the cofactor mimicking ability of the design within ADHs. The two anchors were synthesised, in both reduced and oxidised forms: benzyl nicotinamide (Bn-NAD) and its phenyl-substituted derivation (Bn-NAD-Ph). This yielded a total of 4 compounds in their oxidised (**150** and **155**) and reduced (**151** and **156**) forms (Scheme 6.1)



Scheme 6.1. Synthetic route to yield the desired nicotinamide derivatives. Overall yields; **150** (94 %), **151** (58 %), **155** (72 %) and **156** (46%).

To prepare the phenyl derivatives **155** and **156**, an amide coupling was first performed using propylphosphonic anhydride (T3P) as a coupling reagent, yielding the amide compound **154**. This method yielded a linear triphosphate by-product, easy to remove from solution *via* an aqueous work up. Both amides **148** and **154** were alkylated with benzyl bromide yielding the 2 desired scaffolds in their oxidised forms as bromide salts (**150**/**155**). These oxidised scaffolds were further reduced using sodium dithionite, to give the desired compounds **151** and **156**.

Once all the chemicals were synthesised and characterised by mass spectrometry and NMR, a UV-Vis spectrum analysis was performed to defined their optimal wavelength of absorption (λ_{opt}) and thereafter calculate their molar extinction coefficient (ε) at the aforementioned wavelength (Figure 6.3).

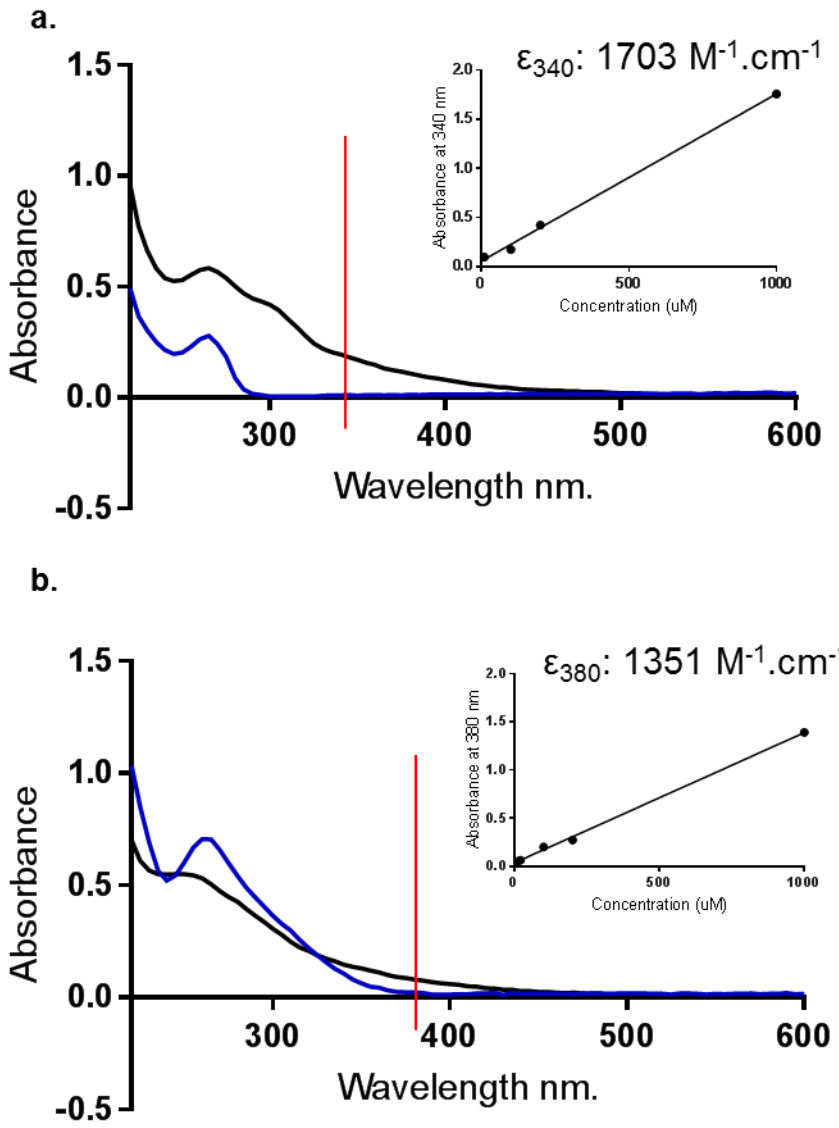


Figure 6.3. Spectra of a. Bn-NAD and b. Bn-NAD-Ph anchors in their oxidized (blue) and reduced (black) form. Conditions: anchor (100 µM) in 100 mM phosphate buffer pH 7.0. Optimal wavelength highlighted in red. Top right corner: molar extinction coefficient (ε) calculation and results for a. **150** and b. **155**.

Similarly, to the NAD^+/NADH couple (Figure 6.4), a difference was observed in light absorption between the oxidised and reduced forms of the mimics. However, the spectra obtained did not display any distinct band or peak, compared to the peak at 340 nm for NADH. With the Bn-NAD couple (**150**/**151**), the oxidised version of the mimic either absorbed less or no light compared to the reduced form. While for the Bn-NAD-Ph couple (**155**/**156**), between 260 and 320 nm, the oxidised form absorbed more light than its reduced counterpart. Therefore, each couple was evaluated differently, based on their own spectrum.

The Bn-NAD couple (**150**/**151**) yielded a reasonable range of wavelength to choose from. Whilst 295 nm offered the largest difference of absorbance, 340 nm was a preferred wavelength to compare the chemicals with NAD(P) cofactor under identical conditions. Unfortunately, this reasoning could not be applied to the Bn-NAD-Ph couple (**155**/**156**). Indeed, at this wavelength the compound **156** started to absorb light. Using a wavelength where both forms can absorb light would impact the precision of the method as it would be more difficult to isolate the behaviour of the light to a single chemical. Therefore, the more suitable 380 nm wavelength was chosen.

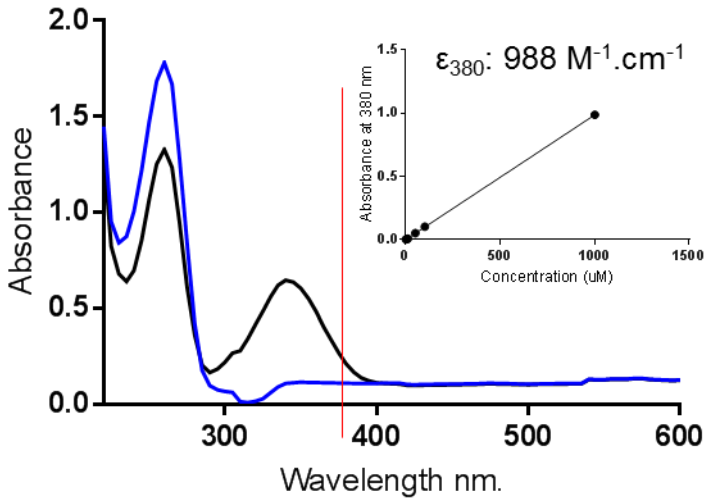


Figure 6.4. Spectra of NAD^+ (blue) and NADH (black). Conditions: cofactor (100 µM) in 100 mM phosphate buffer pH 7.0. Wavelength used for molar extinction coefficient calculations highlighted in red. Top right corner: molar extinction coefficient (ε) calculation and results of NADH.

Once the optimal wavelengths (λ_{opt}) were chosen for further experiment, their molar extinction coefficient (ε) was then calculated as the coefficient is wavelength dependent. The analysis yielded a coefficient of 1703 $M^{-1}.cm^{-1}$ for **150** at 340 nm and 1351 $M^{-1}.cm^{-1}$ for **155** at 380 nm. In comparison, NADH possesses a coefficient of 6220 $M^{-1}.cm^{-1}$ at 340 nm,[233] and of 988 $M^{-1}.cm^{-1}$ at 380 nm.

6.5 Determination of the activity of His-HLADH and TbADH using cofactor mimics

To evaluate the capability of the newly synthesized nicotinamide derivatives to act as cofactors, activity assays were carried out using UV-Vis spectroscopy

and HPLC analysis. If enzymatic activity with these compounds was monitored, it would be an indication of affinity between the proteins and the compound, including the capacity of the mimics to transfer hydride to the substrates *via* the Zn^{2+} ion.

Following the same procedure to evaluate the natural activity of each enzyme, the biocatalysis of natural substrates was monitored by UV-Vis at 340 nm with mimics **150**/**151** and at 380 nm with mimics **155**/**156**. Then a 24 h biotransformation was performed using each enzyme and the different cofactors in their reduced form. The product of the catalysis was analysed by chiral HPLC.

Figure 6.5 compares the specific activity of His-HLADH and TbADH with their natural cofactors and with the synthetic mimics, in both reduction and oxidation directions. The mimic **150** led to a lack of enzyme activity with both proteins. On the other hand, in the presence of the mimic **155**, 25 and 20% specific activity were retained for His-HLADH and TbADH respectively. However, the large variations monitored for HLADH indicated inconsistency, invalidating the conclusion with this enzyme.

The reduced form of both anchors (**151** and **156**) led to a significant drop of enzyme activity with a maximum of 8% activity retained with TbADH in the presence of compound **151**.

However, these preliminary results were encouraging because they suggested that reaction conditions could perhaps be optimised to increase activity with the mimics. Outside the scope of this project, this could be valuable in a context of biocatalytic application, assuming the enzyme has been optimised, the small percentage retained in some cases might be enough to be economically interesting.

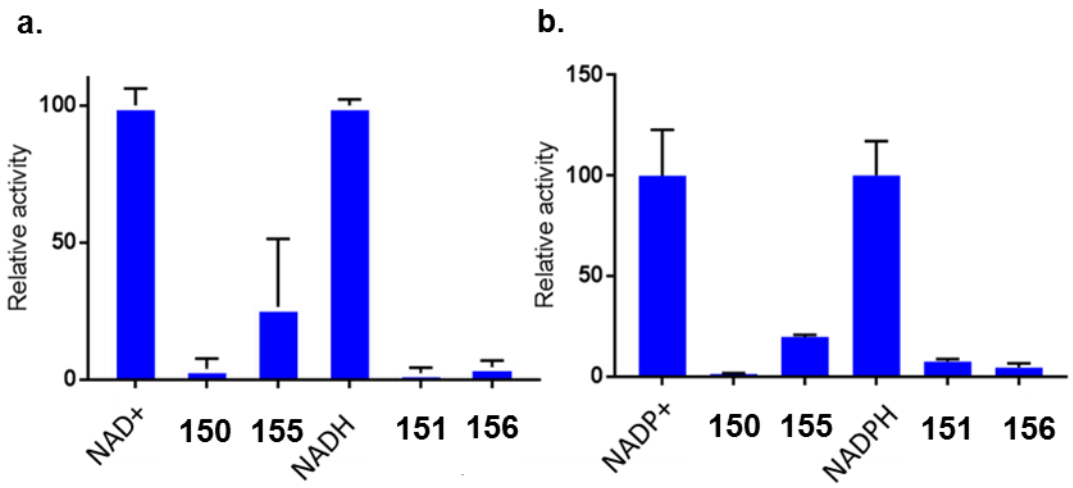


Figure 6.5. Specific activity of a) His-HLADH and b) TbADH with different mimics, relative to their natural corresponding cofactors. Cofactors and mimics (1 mM), ethanol / acetaldehyde (200 mM), (±)-2-butanol / 2-butanone (20 mM), His-HLADH (10 µg) in 100 mM phosphate buffer and TbADH (1 µg) in 50 mM Tris.HCl buffer, pH ranging from 6.0 to 9.0 and acetonitrile supplement 5% (v/v) with **151** and **156**. Reactions monitored at 340 nm for NAD (P) cofactors and mimics Bn-NAD (**150**/**151**), and at 380 nm for mimics Bn-NAD-Ph (**155**/**156**). Experiments run in triplicate a) at room temperature or b) at 40 °C.

According to the data presented above, the mimics are not suitable cofactors for alcohol dehydrogenases. A control without enzymes revealed no redox behaviour from the mimics under the assay's conditions. These results proved the stability of each compound under the conditions used.

However, it cannot be excluded that kinetics with such mimics were significantly slower than the kinetics of the natural cofactor and that the time period used to perform the assay was not appropriate. Therefore, another set of experiments was carried out during a longer period.

To assess whether the reaction was taking place with slow kinetics, catalytic assays were performed over a period of 24 h and were analysed by chiral HPLC (Appendix 8). The substrate, 4-phenyl-2-butanone, was used for these assays due to its low volatility compared to acetone and 2-butanone, which reduced the bias on measurement due to evaporation after a long period of time.

When the catalytic reaction to convert 4-phenyl-2-butanone into its corresponding (*S*)-alcohol was conducted, only natural cofactors, *i.e.* NADH and NADPH, were able to reduce the ketone with high yields (Figure 6.6). Although His-HLADH and TbADH possessed a natural preference for NADH and NADPH respectively, they were both able to yield the alcohol with the

other natural cofactor. This preference was almost unnoticeable with TbADH, which yielded a similar amount of product with both cofactors. Despite the time scale, the large protein concentration used, and the 4-fold excess of cofactor compared to substrate, only 40 % and 80 % conversion was reached with His-HLADH and TbADH respectively.

It was therefore hypothesized that an equilibrium was reached between the alcohol and the ketone. The ratio at which this equilibrium was reached depended on the catalyst used, explaining the difference of conversion observed between the two enzymes. Nonetheless, no alcohol molecules were detected using mimics **151** or **156**.

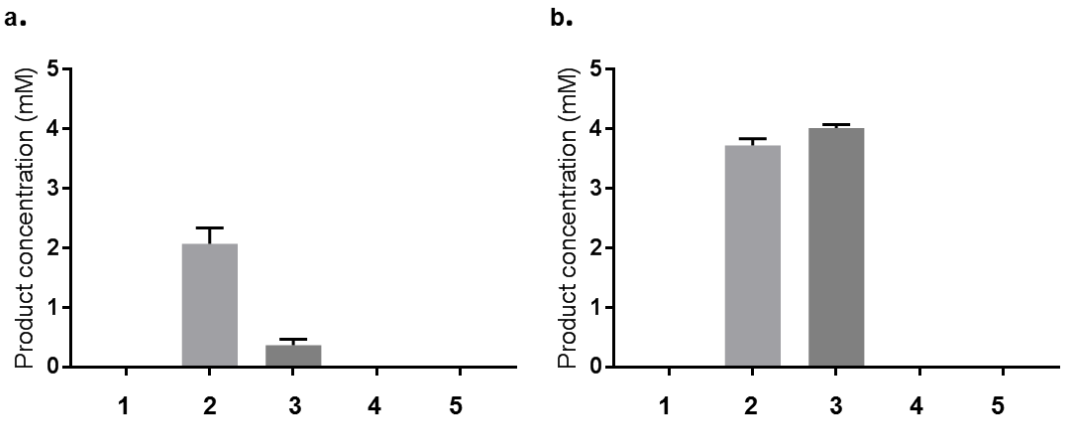


Figure 6.6. Reduction of 4-phenyl-2-butanone into (*S*)-4-phenyl-2-butanol during 24 h using a) His-HLADH at room temperature or b) TbADH at 37 ˚C. Conditions: His-HLADH (75 µM), TbADH (5 µM), cofactors (20 mM) and 4-phenyl-2-butanone (5 mM). 1: control without cofactor; 2: with NADH; 3: with NADPH; 4: with mimic **151**; 5: with mimic **156**. All experiments were run in triplicate.

Using similar conditions previously reported by Fish with HLADH, His-HLADH yielded similar amount of product with NADH as a cofactor. On the other hand, the mimics Bn-NAD and Bn-NAD-Ph were not able to yield any visible product.

However, in the published work, this particular experiment was performed with another NAD^+ mimic, β-nicotinamide mononucleotide (NMN, Figure 6.7).

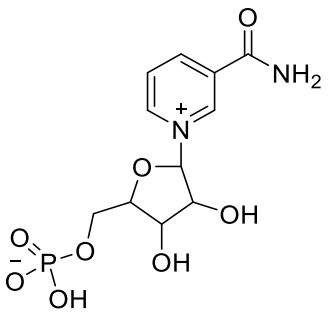


Figure 6.7. Representation of the NAD+ mimic β-nicotinamide mono nucleotide

Therefore, a similar experiment was conducted with this compound in order to compare our results with reported data (Figure 6.8, Appendix 8). The amount of substrate and cofactor used were comparable to those used in the published study; substrate, 2.99 mM (study) and 1.34 to 1.8 mM (this work), cofactor 2.99 mM (study) and 2 mM (this work). However, for enzyme concentration, it was decided to use amounts similar to those used for UV-Vis experiment in order to compare the results from the GC-FID to the behaviour observed so far with Bn-NAD and Bn-NAD-Ph. This resulted in a final concentration of enzyme of 0.5 µM for both His-HLADH and TbADH whilst the study performed the experiment with a protein concentration of 119 µM.

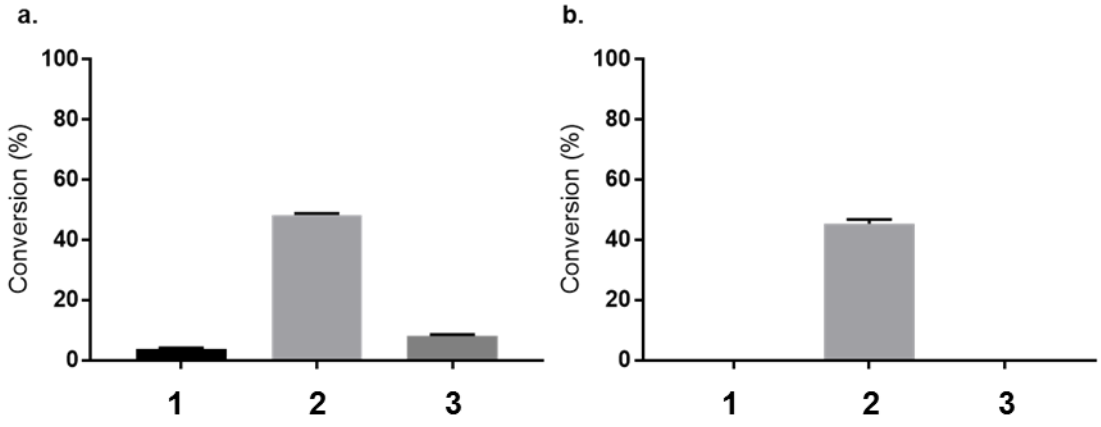


Figure 6.8. Results of the bioctalysed oxidation of a. 4-phenyl-2-butanol with His-HLADH and b. 2-pentanol with TbADH, 1: in the absence of cofactor, 2: in the presence of their natural cofactor or 3: the cofactor mimic β-nicotinamide mononucleotide (NMN). Conditions: 4-phenyl-2-butanol (1.34 mM), His-HLADH (0.5 µM) and cofactor (2 mM) in 100 mM sodium phosphate buffer pH 8.8. 2-pentanol (1.8 mM), TbADH (0.5 µM) and cofactor (2 mM) in 50 mM Tris.HCl buffer pH 9.0. Experiment were run in triplicate at room temperature for 24 h. Control experiments were performed under similar conditions as described at the exception of the addition of a cofactor.

In the reaction catalysed by His-HLADH, the conversion results obtained from the control and the mimic NMN were very similar with 3 and 8.3 % respectively. In the study published, the authors performed a complementary experiment to prove no natural cofactor was present within the commercial enzyme used. In this work, the low appearance of product in the control experiment showed that some NAD^+ was present in the batch used. Therefore, it was difficult to identify the cofactor mimic NMN as the sole reason for the product observed by GC-FID analysis. Moreover, the paper stated relatively similar yield between the cofactor and the mimic, with 56 and 53 % yield after 24 h respectively. Under the same conditions, the use of NAD^+ yielded 6-fold more product (48 %) than the mimic. Thus, in this experiment, the cofactor mimic was not considered responsible for the product observed, and could not be considered, in this situation, to act as a cofactor mimic.

This tendency was even more explicit in the experiment conducted with TbADH. With this enzyme, only the experiment using the natural cofactor $NADP^+$ yielded some product, 45 % after 24 h. Both the control reaction without cofactor and the experiment with NMN provided results with no detectable amount of product. Therefore, in this situation, NMN was not considered to act as a cofactor mimic.

The lack of (*S*)-alcohol product in the presence of derivatives **151** and **156** confirmed the inability of these compounds to mimic natural cofactors within alcohol dehydrogenases.

Compared to ERs, ADHs do not possess the FAD cofactor to act as a relay between the nicotinamide cofactor and the substrate. In this situation, the cofactor and the substrate are not present in the enzyme at the same time. This two-step process might have been the key component that allowed the Bn-NAD molecule to be a successful replacement for NADH in ERs.

Nonetheless, the lack of enzymatic activity in the presence of the mimics is not necessarily linked to a lack of affinity. Indeed, the derivatives might have interacted with the enzyme without the capacity to perform hydride transfer, resulting in these chemicals acting in a similar manner as protein inhibitors would.

6.6 Determination of the inhibitory potential of nicotinamide derivatives

Direct and indirect inhibitors are molecules that can bind into a protein active site where another molecule should (e.g. cofactor, ATP, substrate …), thus preventing the expected chemical reaction to occur.

The synthetic nicotinamide derivatives were expected to act similarly as the natural cofactor due to the presence of the nicotinamide functionality. However, the lack of activity previously shown do not preclude the structures to bind to the protein without getting involved in the reaction mechanism. This would result in an inhibition of the natural reaction in the presence of the mimics.

To determine whether the mimics inhibited the enzymes, a study was performed to quantify the inhibition of His-HLADH and TbADH activities, in the presence of nicotinamide derivatives. A range of concentration of mimics was mixed with the natural cofactor. Kinetics were performed following the evolution of the natural cofactor state. Once all sets were recorded, data was plotted in a logarithmic scale and a sigmoidal fit was computed to yield IC_{50} values that corresponded to the concentration of mimic required to inhibits half of the activity of the enzyme in the presence of its natural cofactor.

IC_{50} values of the different derivatives with His-HLADH were comprised between 3 and 5 mM (Table 6.2, Appendix 9), indicating very low inhibition of the protein. The inhibition was even weaker with TbADH, where mimic **151** was the only derivative to show a detectable interaction (IC_{50} below 10 mM).

Table 6.2. IC50 values of nicotinamide derivatives with His-HLADH and TbADH. NAD(P)H (300 mM), acetaldehyde and butan-2-one (10 mM), His-HLADH (10 µg) in 100 mM phosphate buffer pH 7.0 and TbADH (1 µg) in 50 mM Tris.HCl pH 6.0. NAD derivatives ranging from 10^{-10} to 10^{-2} M. Experiments run at room temperature in triplicate.

Enzyme	Mimic	IC_{50} (mM)
His-HLADH	**150**	4.7
	155	-
	151	3.4
	156	5.3
TbADH	**150**	>10
	155	>10
	151	8.1
	156	>10

When detected, inhibition of His-HLADH and TbADH were in the mM concentration range. These results were extremely high and highlighted a lack of impact on the biocatalysis from the derivatives. Besides, the oxidised form of the mimics yielded similar results as their reduced counterpart. This proved that no hydride was transferred between NAD(P)H and the oxidised mimics. This was the reflection of poor interaction between the synthetic mimics and the enzymes.

The high IC_{50} values resulting from the inhibition study coupled with the absence of enzyme activity previously confirmed demonstrated that the mimics were interacting neither with His-HLADH or TbADH at their cofactor anchoring site. Therefore, the mimics, under their current designs could not be considered suitable as anchors to build an artificial metalloenzyme using a supramolecular approach. However, to understand the lack of interaction previously stated, *in silico* studies were performed using docking techniques.

6.7 Molecular modelling study of ADHs and the cofactor mimics

Molecular modelling is a range of techniques that aimed at mimicking behaviour of molecules through computational calculation. Although those calculations can only estimate the reality, when combined with experimental data, they can bring useful information as well as a better understanding of molecular interactions.

Through docking techniques, molecular modelling was used to point out where the lack of interaction between the nicotinamide derivatives and the enzymes was coming from. Prior to any docking study, the cofactor of each enzyme was removed from their respective PDB files and re-docked into their corresponding emptied catalytic site to confirm the accuracy of the method used.

As highlighted in Figure 6.9 (a and b), HLADH possessed a NAD(H) binding pocket and a substrate binding pocket with a catalytic zinc ion in the centre. This configuration resulted in the coordination of the cofactor and the substrate with the Zn^{2+} ion during the catalysis (section 1.3.2.1).

The docking of mimics within HLADH showed that the compounds were positioned within the substrate binding pocket instead of the expected NAD(H)

binding pocket (Figure 6.9, c and d). The substrate pocket, more hydrophobic than the NAD(H) one, was probably accommodating the benzene rings of the different derivatives through hydrophobic interactions.

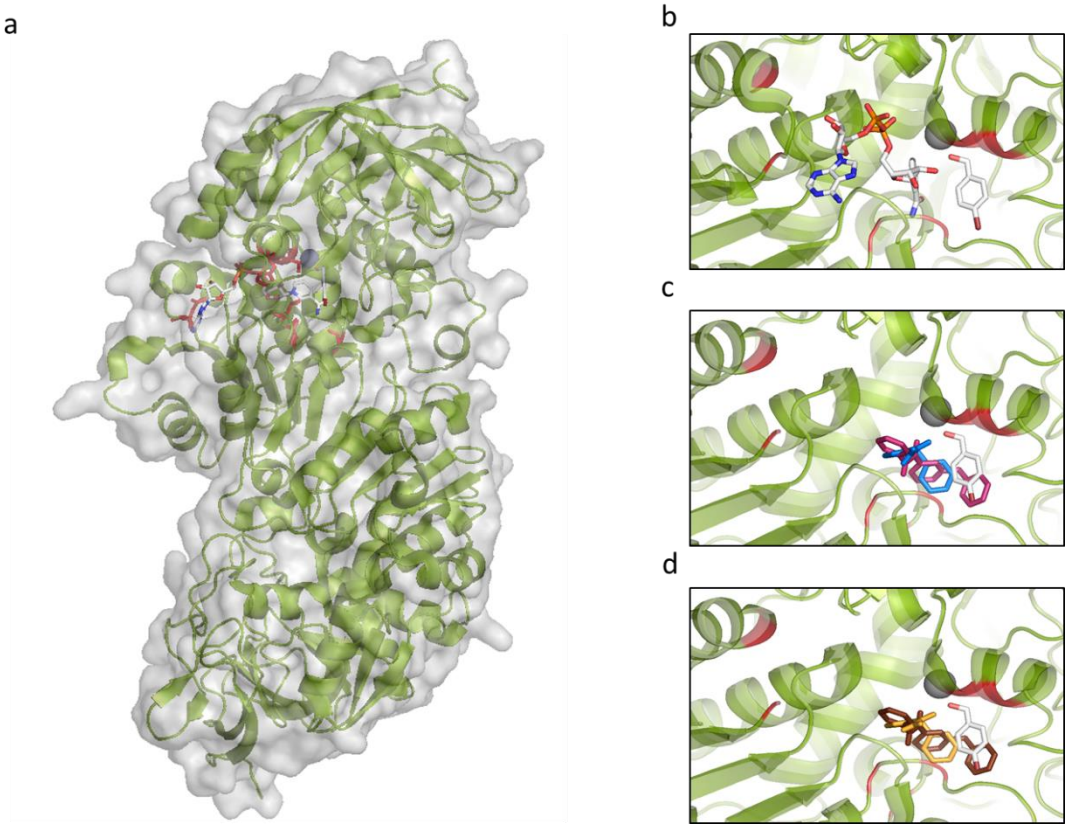


Figure 6.9. Structure of horse liver alcohol dehydrogenase (1HLD). a) General view of the enzyme in a dimeric assembly. b) Overview of the catalytic site including NAD^+ and *p*-bromobenzyl alcohol as cofactor and substrate respectively. c) Catalytic site with docking results of **150** (marine blue) and **155** (warm pink) showing superimposition with the substrate. d) Catalytic site with docking results of **151** (bright orange) and **156** (chocolate red) showing superimposition with the substrate. Amino acid residues interacting with NAD(H) (S48, H51, N223, V292, V294 and A317) are indicated in red.

The position of the mimics within the substrate pocket indicated some possible interactions via competition of the derivatives with the substrate instead of the cofactor, as initially hypothesized, thus explaining the lack of enzyme activity. However, the lack of inhibition previously observed showed that the possible interactions at the substrate pocket remained negligible.

The catalytic site of TbADH is similarly shaped to the one of HLADH, *i.e.* it contains a NADP(H) binding site, a substrate binding pocket and a Zn^{2+} ion in the centre (Figure 6.10, a and b). Compared to the previous results with HLADH, the nicotinamide mimics were docked around the nicotinamide ring of the NADP(H) (Figure 6.10, c and d). However, the nicotinamide ring, in all

cases was not superimposed to the ring of the cofactor, and the amide moiety in compound **150** and **151** was slightly reaching over the substrate pocket.

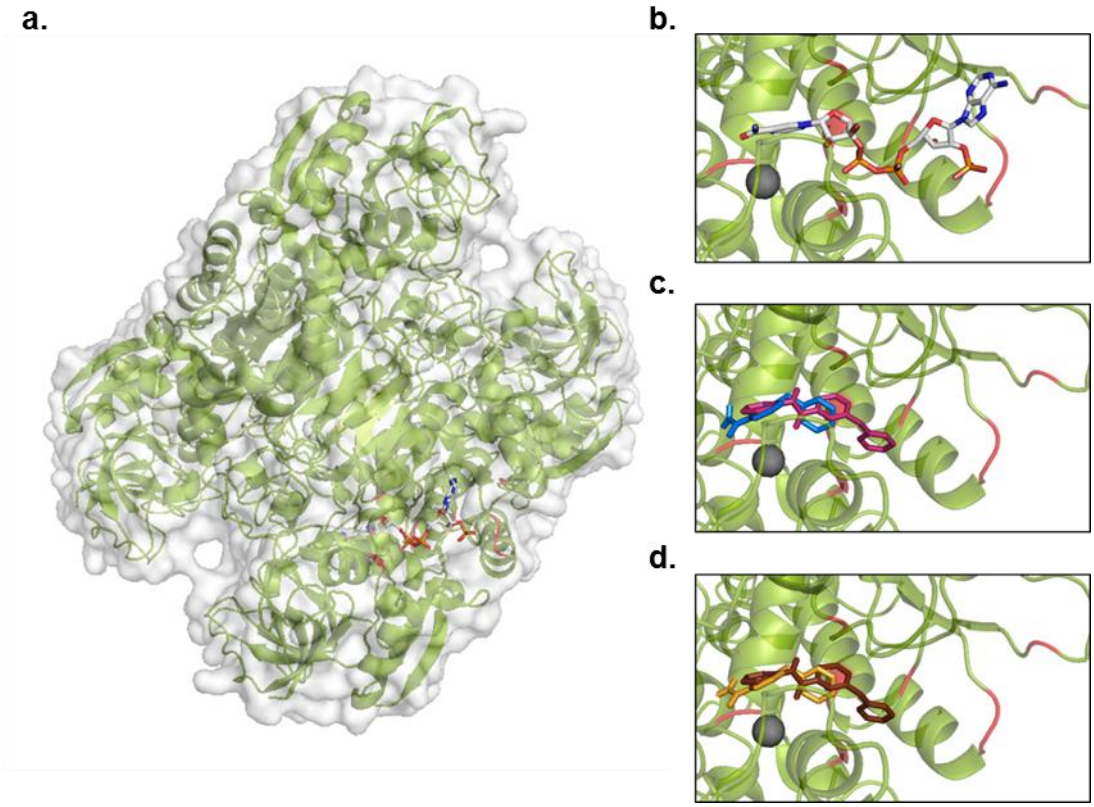


Figure 6.10. Structure of *Thermoanaerobacter brockii* alcohol dehydrogenase (1YKF). a) General view of the enzyme in a tetrameric assembly. b) Overview of the catalytic site including $NADP^+$ as cofactor. c) Catalytic site with docking results of **150** (marine blue) and **155** (warm pink). d) Catalytic site with docking results of **151** (bright orange) and **156** (chocolate red). Amino acid residues interacting with NADP(H) (T38, D150, I175, V178, S199, R200, Y218 and N266) are indicated in red.

Another hypothesis was that the mimics interacted with some residues at the other extremity of the NAD(P)H pocket, where the adenosine moiety was situated. This could have led to a supramolecular anchoring at the surface of the protein. Unfortunately, this hypothesis could not be evaluated using docking. A dynamic simulation would be required to estimate such interactions.

To conclude upon this study focused on the development of an artificial metalloenzyme in a supramolecular manner, the anchors that have been synthesized to mimic the nicotinamide ring of the natural cofactors NAD(H) and NADP(H) showed their inability to act as cofactors. Indeed, when put in solution with the enzyme and a substrate no reaction was monitored, nor product detected. The chemicals were not able to compete with the cofactors,

yielding little to no inhibition. Those results were then later confirmed by molecular modelling where it was shown that the substrate pocket of His-HLADH, more hydrophobic, was the preferred location for the synthetic anchors, while little is known about the interaction between the synthetic mimics and TbADH.

Based on those results, two approaches were considered to build *in silico* the desired artificial metalloenzyme and thus offer some perspective for further research. The first one was to redesign the anchor by replacing the benzyl moiety attached to the pyridinium nitrogen of the nicotinamide ring (later referred as N_1 position) and evaluating the impact of the new moieties on the positioning of the anchor candidates within the catalytic site of His-HLADH. The second approach was the search for another enzyme from the ADH superfamily that can accommodate the anchors already synthesized.

6.8 *In silico* evaluation of new designs for supramolecular anchors

As above-mentioned, the nicotinamide derivatives were sitting within the substrate pocket of His-HLADH due to higher hydrophobicity. By modifying the design of the anchors into a more hydrophilic compound, the chemicals should prefer the cofactor binding pocket instead, using existing interactions between the natural cofactor and the enzyme (Figure 6.11). The nicotinamide ring was decided to be maintain as this group interacts with the Zn^{2+} ion, therefore providing interactions to orientate the anchor and, by extension, the whole metal complex.

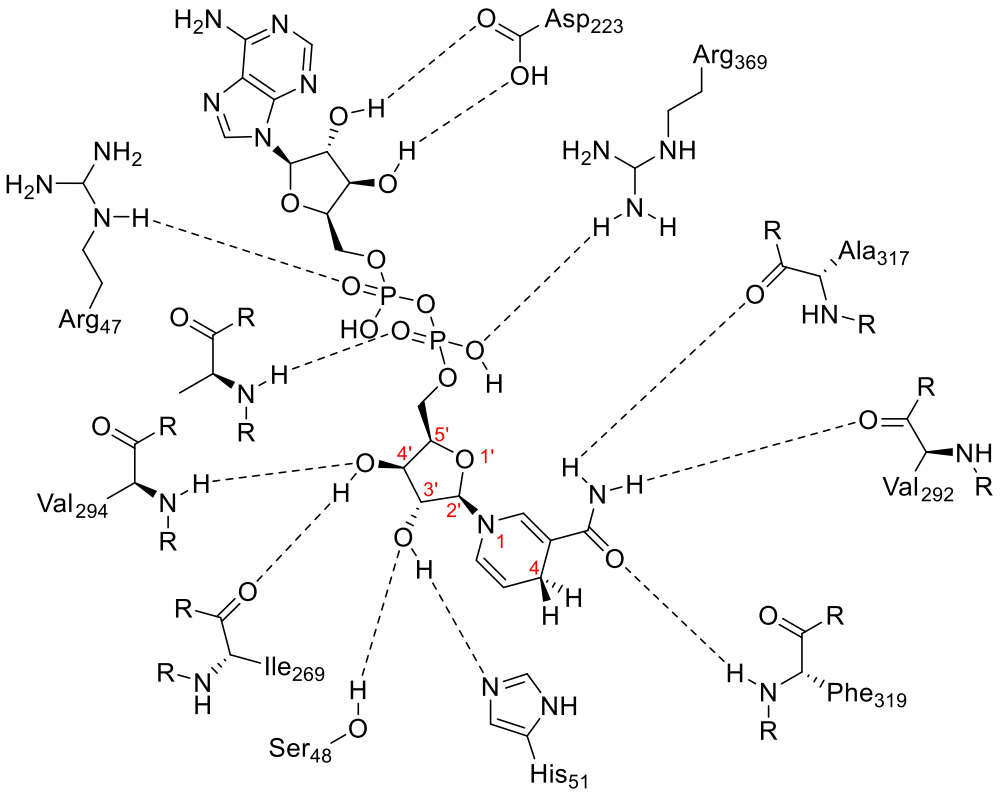


Figure 6.11. NADH interaction map with residues within HLADH cofactor binding pocket (PDB entry 4XD2). Numbering of relevant atoms is highlighted in red.

To optimise the design of the supramolecular anchors, the moiety attached in the N_1 position of the nicotinamide ring was modified *in silico* (Figure 6.12). To do so, 3 distinct parts were simultaneously evaluated: bulkiness, the distance between hydrophilic moieties and the N_1 position and the degree of hydrophilicity of the moieties introduced.

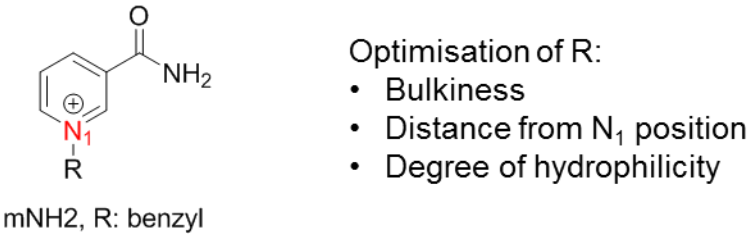


Figure 6.12. Highlight of the *in silico* evaluation for new nicotinamide derivative designs. Three different components were evaluated at the position N1 of the nicotinamide ring (red): the bulkiness of the moieties, the distance between the hydrophilic moieties and the N1 position and the degree of hydrophilicity of the moieties.

First, the benzyl group was replaced with smaller moieties to test the impact of steric hindrance on the positioning of the anchor. Thus, 4 aliphatic designs were made (Figure 6.13). A very short chain was introduced by using an alkyne moiety (**157**) or a nitrile one (**159**). Aliphatic chains were also introduced

as a 3-carbon length (**158**) or 4-carbon length (**160**). In both cases an alkene was added to the chain to limit the degree of freedom and therefore mimicked, to some extent, the constraints applied to the benzyl moiety.

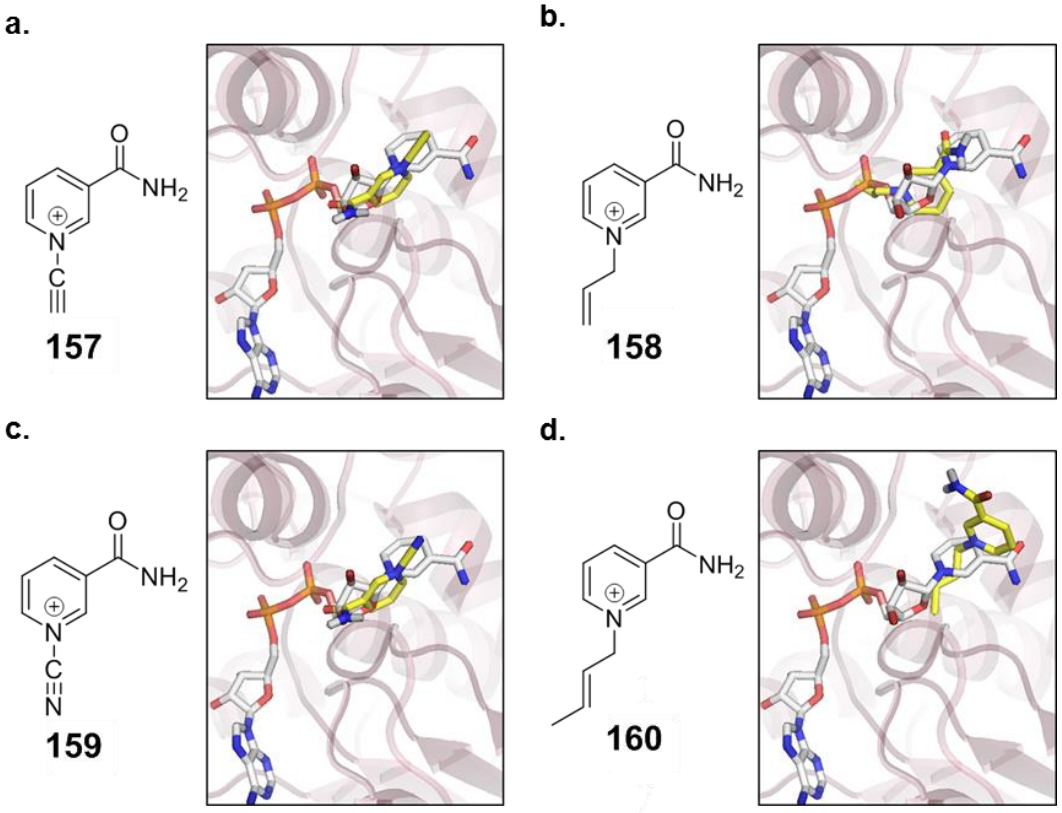


Figure 6.13. Docking results of HLADH (PDB 4XD2) with anchors designed to reduce steric hindrance. Anchors were coloured in yellow. Natural cofactor NAD was coloured in white. Oxygen, nitrogen and phosphorus atoms were highlighted in red, blue and orange respectively.

With all four, less hindered potential anchors, the compound was found within the cofactor pocket. This gave an indication on the importance of reducing bulkiness for reaching a better positioning. However, none of these designs were able to align with the nicotinamide ring of the cofactor. Compounds **157**, **158** and **159** showed a nicotinamide ring placed around the ribose moiety of the cofactor while the compound **160** was reaching towards the substrate pocket. This indicated the need to introduce a hydrophilic moiety for further improvement. Besides, the very short chain (alkyne **157** and nitrile **159**) yielded a “flipped” ring where the amide moiety was pointing towards the pyrophosphate of NADH. This implied that some length was required to stabilise the nicotinamide ring in a similar orientation as the natural one.

Following up to the impact of steric hindrance, hydrophilicity was introduced to potential anchors (Figure 6.14). This was performed by using hydroxylated alkyl chains at the place of the benzyl, with hydroxyl group(s) at different positions. It was hypothesized that these hydrogen-bond forming OH groups would stabilise the nicotinamide mimic at the position occupied by NAD(P)H, by interaction within the ribose binding site.

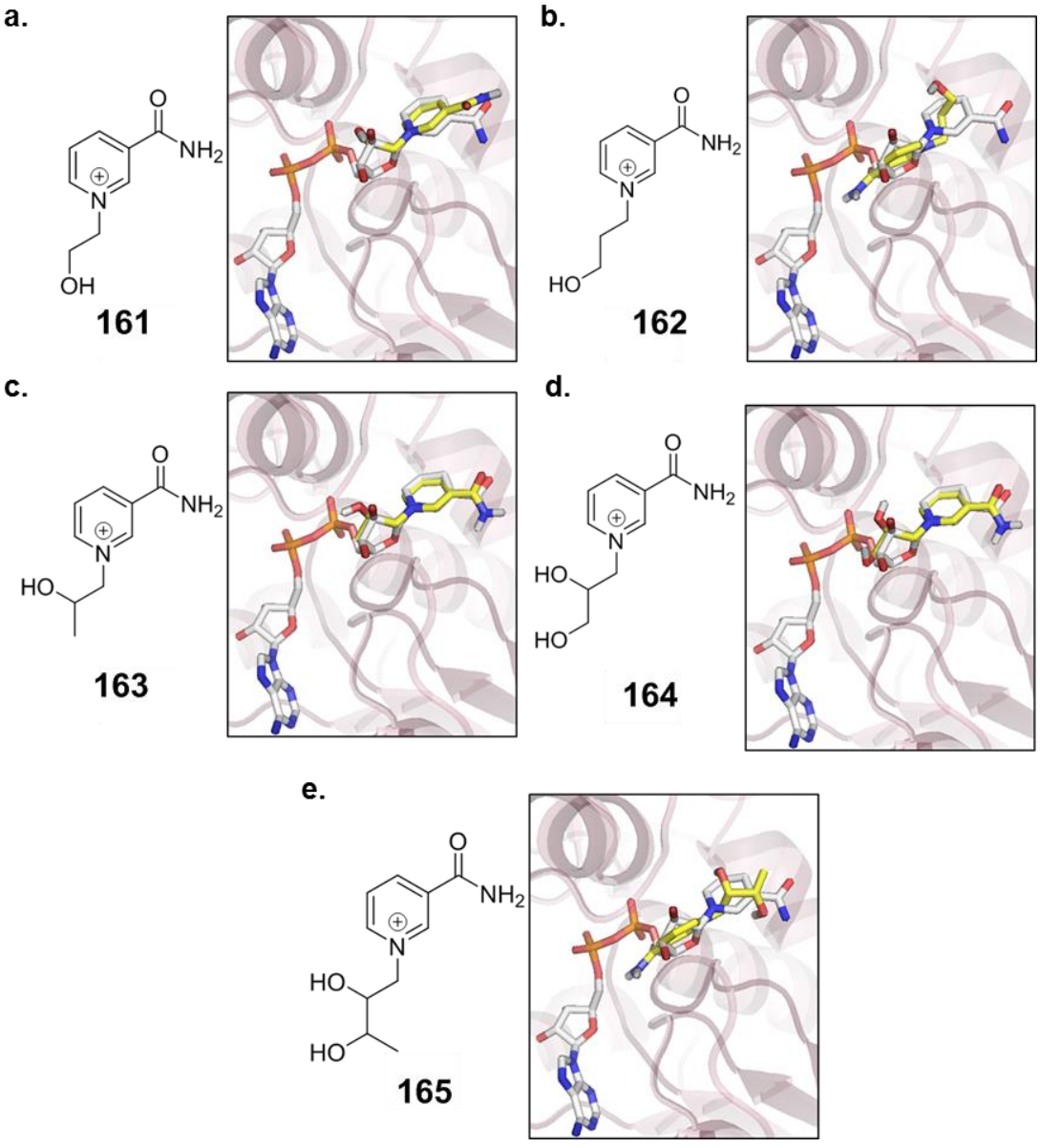


Figure 6.14. Docking results of HLADH (PDB 4XD2) with anchors designed to pinpoint hydrophilic interactions. Anchors were coloured in yellow. Natural cofactor NAD was coloured in white. Oxygen, nitrogen and phosphorus atoms were highlighted in red, blue and orange respectively.

Compounds **161** and **163** both yielded good superimposition of their nicotinamide ring with the one of the cofactors. On the other hand, compound

162 showed a hydroxyl group pointing towards the amide moiety of NADH while its nicotinamide ring was positioned around the ribose.

By the differences observed between **161**, **162** and **163**, the hydroxyl on the 3' carbon (**161** and **163**) led to an improved alignment with the cofactor compared to the same moiety place on the 4' carbon (**162**). With **161** and **163**, the position of the hydroxyl group was mimicking the hydroxyl in the 3' position of the ribose attached to the nicotinamide ring and was therefore found at this exact position on the result of the docking.

The added methyl on the design **163** confirmed that length is a key point to stabilise the potential anchor as it appeared superimposed to the cofactor structure. Length was already considered important by the end of the evaluation of steric hindrance impact and was now confirmed. When two hydroxyl groups were replacing the benzyl moiety within the structure **164,** the results were identical as the ones with **163**. According to these results, the 4' carbon might be a suitable position to add a hydroxyl group if present as a vicinal diol, as shown by the "flipped" ring positioning with **162**.

When compared to **164,** which is well superimposed to the cofactor, the potential anchor **165** exhibited a reverse positioning where the vicinal diol was located on the nicotinamide ring of the cofactor whilst its nicotinamide ring was located around the ribose. This change in positioning was due to a single methyl addition. To avoid such behaviour, the 4' carbon in position should not be branched.

The third part of this study aimed at comparing different degree of hydrophilicity in order to improve stability within the cofactor cavity (Figure 6.15). Three different moieties were evaluated and were put in contrast with results obtained from the hydroxyl **161**; carbonyl halide **166**, amide **167** and carboxylic acid **168**.

All these designs possessed a carbonyl moiety in the 3' position to compare with the carbon-oxygen single bond of the hydroxy group present in compound **161**. However, they were all linked to a different substituent that played a role in the resulting hydrophilicity.

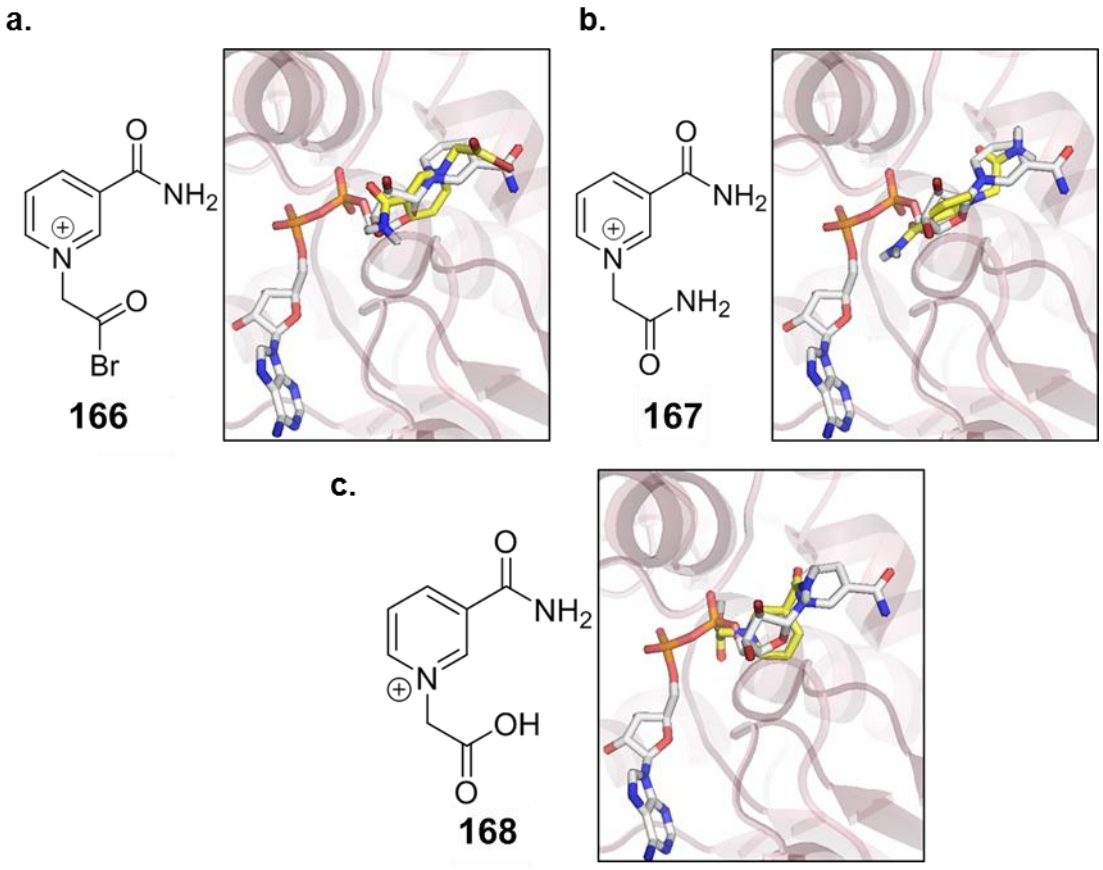


Figure 6.15. Docking results of HLADH (PDB 4XD2) with anchors designed to evaluate the impact of hydrophilicity. Anchors were coloured in yellow. Natural cofactor NAD was coloured in white. Oxygen, nitrogen and phosphorus atoms were highlighted in red, blue and orange respectively.

All three designs were more hydrophilic than **161** and unexpectedly, none of them could yield a positioning as good as compounds **161**, **163** and **164**. All the compounds **166**, **167** and **168** displayed a shift in positioning where the first phosphate group of the natural cofactor interacts with the enzymatic residues. The increased hydrophilicity might have resulted in mimicking the phosphate interactions rather than the ribose ones. This was particularly visible with the carboxylic acid **168**, which possessed the highest hydrophilicity.

The case of **166** was very interesting. This moiety being less hydrophilic than an amide moiety, the ring probably “flipped” to favour interactions around the ribose region, also indicating the role played by the furan ring to stabilise the cofactor within the active site.

At the end of this initial evaluation, the results were pointing towards a non-bulky, linear design with a hydroxyl moiety attached to the carbon in 3’ position.

Nevertheless, the study also showed the importance of the multiple interactions around the ribose. Consequently, a supplementary set of anchors was designed to simulate the ribose (Figure 6.16).

Two designs were made as a simple version of the ribose, the furan **169** and the dioxolane **171**. Then, bigger design using a pyran ring, more flexible than the initial benzyl ring, were inserted into compounds **170** and **172**. Finally, in the compound **173**, the hydroxyl in 3' position was turned into an ester and an extra pyran ring was added as an extension to evaluate the impact of the distance between the ring and the position N_1.

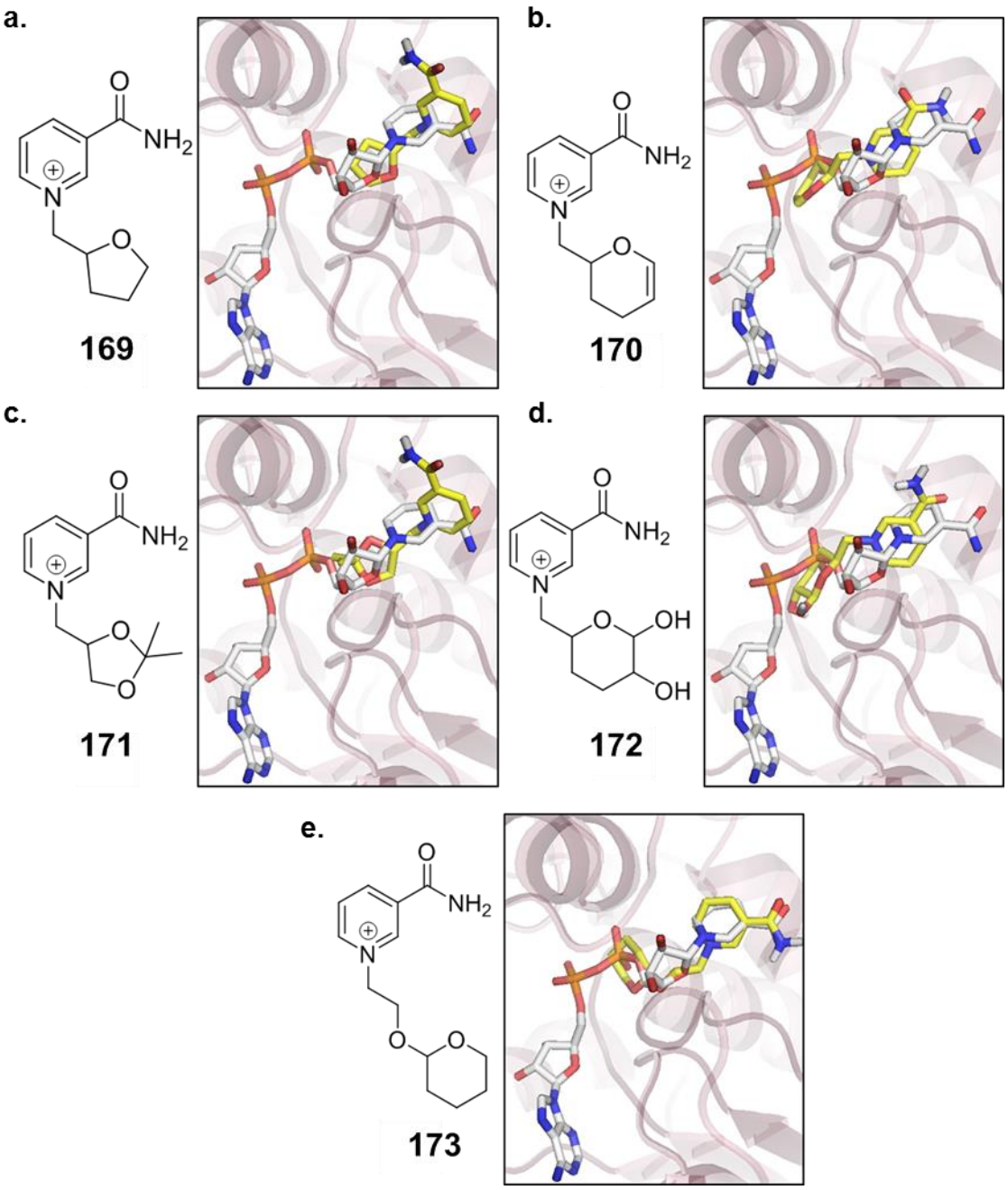


Figure 6.16. Docking results of HLADH (PDB 4XD2) with anchors designed to simulate the ribose of the cofactor. Anchors were coloured in yellow. Natural cofactor NAD was coloured in white. Oxygen, nitrogen and phosphorus atoms were highlighted in red, blue and orange respectively.

The simplified versions of the ribose, whether as a furan or a pyran ring, were probably too bulky and/or not hydrophilic enough as the anchors were not aligned with the nicotinamide ring of NADH anymore. Interestingly, the added hydroxyls groups in the design of **172** yielded a positioning around the phosphate group of the cofactor.

The last design, **173**, gave the best outcome. According to the result, the linear ether was the one which mimicked the 1’ oxygen atom in the ribose ring and the added pyran was therefore an extension of this design, which aimed at fitting at the phosphate group position in the cofactor.

Compared to the other compounds, the oxygen linked to the 3’ carbon within **173** was part of a hetero cycle. The ether moiety offers a larger degree of liberty compare to cycles, putting an emphasis on the importance of the interactions developed by this oxygen atom.

Based on all the previous results, 3 final designs were developed (Figure 6.17). They were all based on a linear chain as the degree of freedom provided could improve fitting. A hydroxyl moiety was added on the 3’ carbon as the presence of the ether function at the same position did not bring any benefit towards binding. Hydrogen bonding moieties, more hydrophilic than hydroxyl groups, were added to increase the chain length while providing interactions capable of mimicking those of a phosphate group.

The design **174** relied on the fact that sulphate group can easily mimic phosphate interactions due to the similar structure between the two moieties, whilst the diethylamide **175** and carboxylic acid **176** were chosen for their high hydrophilicity.

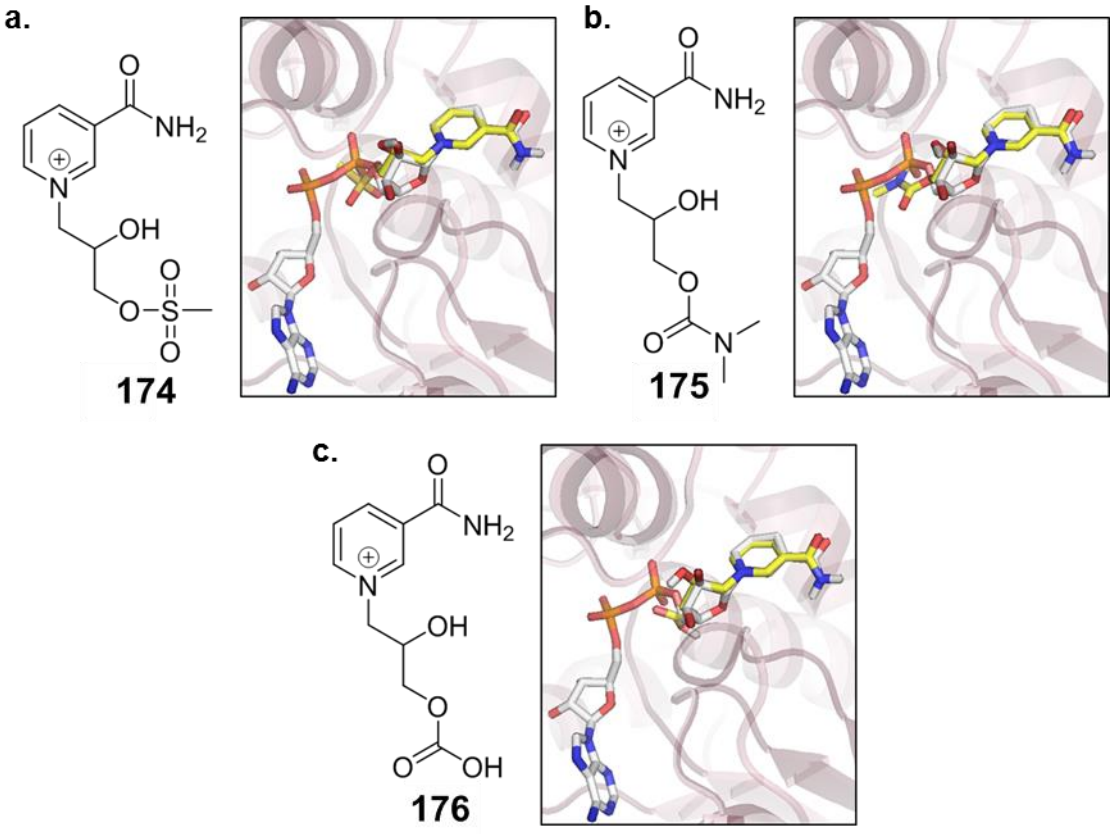


Figure 6.17. Docking results of HLADH (PDB 4XD2) with the final designs of supramolecular anchors. Anchors were coloured in yellow. Natural cofactor NAD was coloured in white. Oxygen, nitrogen and phosphorus atoms were highlighted in red, blue and orange respectively.

As expected, the nicotinamide ring, in all 3 designs, was very well superimposed with the one of NAD. The added hydroxyl group attached to the 3' carbon mimicked the interactions of the hydroxyl of the ribose in position 3', the oxygen attached to the 4' carbon mimicked the vicinal diol of the ribose and the extension of the chain was hydrophilic enough to mimic the phosphate group attached to the ribose.

Based on visual assessment, the 3 final designs displayed similar positioning within the catalytic site of HLADH. A retrosynthesis study was performed to evaluate the difficulty of these compounds to be synthesized (Figure 6.18). All three compounds can be reached with a 2-step synthesis from commercially available cheap materials, making them suitable alternatives to the expensive natural cofactor. These three designs were thus considered very good compounds that could be synthesized for further study involving *in vitro* experiments with HLADH.

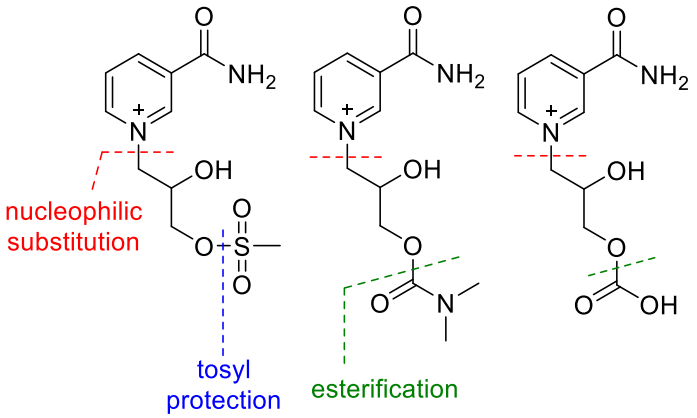


Figure 6.18. Highlight of the reactions required after the retrosynthesis process of potential anchors **174**, **175** and **176**.

As an alternative to the design and subsequent synthesis of these compounds for *in vitro* experimentation, a screening within the ADH family was also evaluated *in silico*. The aim was to find an ADH capable of accommodating the synthesized mimic Bn-NAD and Bn-NAD-Ph.

6.9 *In silico* screening of ADHs capable of accommodating anchors 150 and 151

The nicotinamide derivative Bn-NAD compound was shown to be a good alternative to nicotinamide cofactor with enoate reductase. The initial results obtained with HLADH and TbADH showed this chemical was not interacting with the proteins within their cofactor pocket, due to a relatively high hydrophobic design. Whilst designing more hydrophilic compounds was investigated to improve binding affinity, another alternative was to vary the biological scaffold. It was hypothesized that some ADHs could possibly accommodate this derivative at the place of their nicotinamide cofactor. This section aims at finding possible protein targets within the ADH superfamily to accommodate previously reported nicotinamide mimic Bn-NAD, using docking (Figure 6.19a).

From the Protein Data Bank (PDB), all ADHs structures were considered and a refining system was put in place using the following steps: a) only wild-type proteins were selected, as mutants can be later designed through optimisation to fit more specific requirements, b) only one ADH per species was evaluated, as the variations within the species were non-significant and c) the selected

ADHs were reported to be recombinantly expressed within a *E.coli* system to allow ease of experimental work.

Once the selection was achieved, each ADH protein sequence was aligned against the reference protein sequence of HLADH using the Basic Local Alignment Search Tool (BLAST) provided online by the National Centre for Biotechnology Information (NCBI). Proteins with more than 20% sequence homology to the reference were discarded as they were considered structurally too similar to HLADH which would lead to analogous results to those obtained throughout this chapter.

The remaining proteins were selected for docking of Bn-NAD inside the cofactor binding pocket (Appendix 10). The docking method was applied as follows: each PDB sequence was cleaned from non-amino acid chemicals (*i.e.* cofactors, ions, water, substrate …) using AutoDock Tool v4 software, then a grid box was built to create a docking space containing the Rossman fold motif present in every ADH. Finally, the 3D versions of NADPH and Bn-NAD, used previously, were docked into each grid box using AutoDock Vina software and the resulting docked ligands were analysed individually upon superimposition with the raw PDB structure of the corresponding protein.

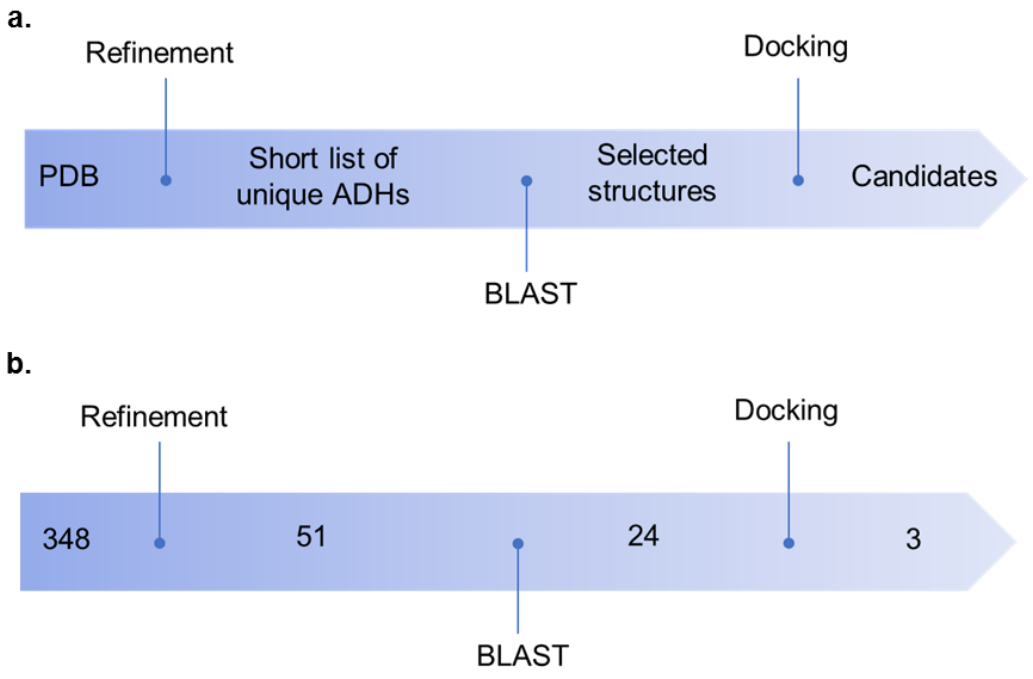


Figure 6.19. a. Representation and b. results of the ADH screening process.

To date, 348 alcohol dehydrogenases crystal structures were registered on the PDB website. Following the refinement system, 51 proteins were selected for sequence alignment against HLADH. The final 24 proteins that possessed less than 20% sequence homology to HLADH were then considered as potential candidates (Figure 6.19b).

One protein structure (PDB 3RF7) was only accepted by the software for viewing and was therefore discarded while the 23 remaining crystal structures were cleaned, and NADPH and Bn-NAD were docked within each ADH structure. The coordinates of each grid box were shown in (Appendix 10).

Out of the 23 structures used for docking only 3 were considered interesting candidates as nicotinamide derivative acceptors (Figure 6.19b). This was the result of a visual assessment where superimposition of the docked nicotinamide mimic with the crystallised cofactor was observed.

The 3 targets were all short-chain dehydrogenases/reductases (SDR) from various organisms: *Sphingobium yanoikuyae* DSM 6900 (4BMV), *Kluyveromyces polyspora* (5Z2X), and *Candida magnolia* (5MLN), later called SyADH, KpADH and CmADH respectively. The absence of a metal ion to catalyse the reaction was a particularity of SDRs. This absence left some supplementary space within the catalytic site at the edge between the cofactor and the substrate. This additional space might have benefited the anchors to sit at the place of the nicotinamide ring of the cofactor (Figure 6.20).

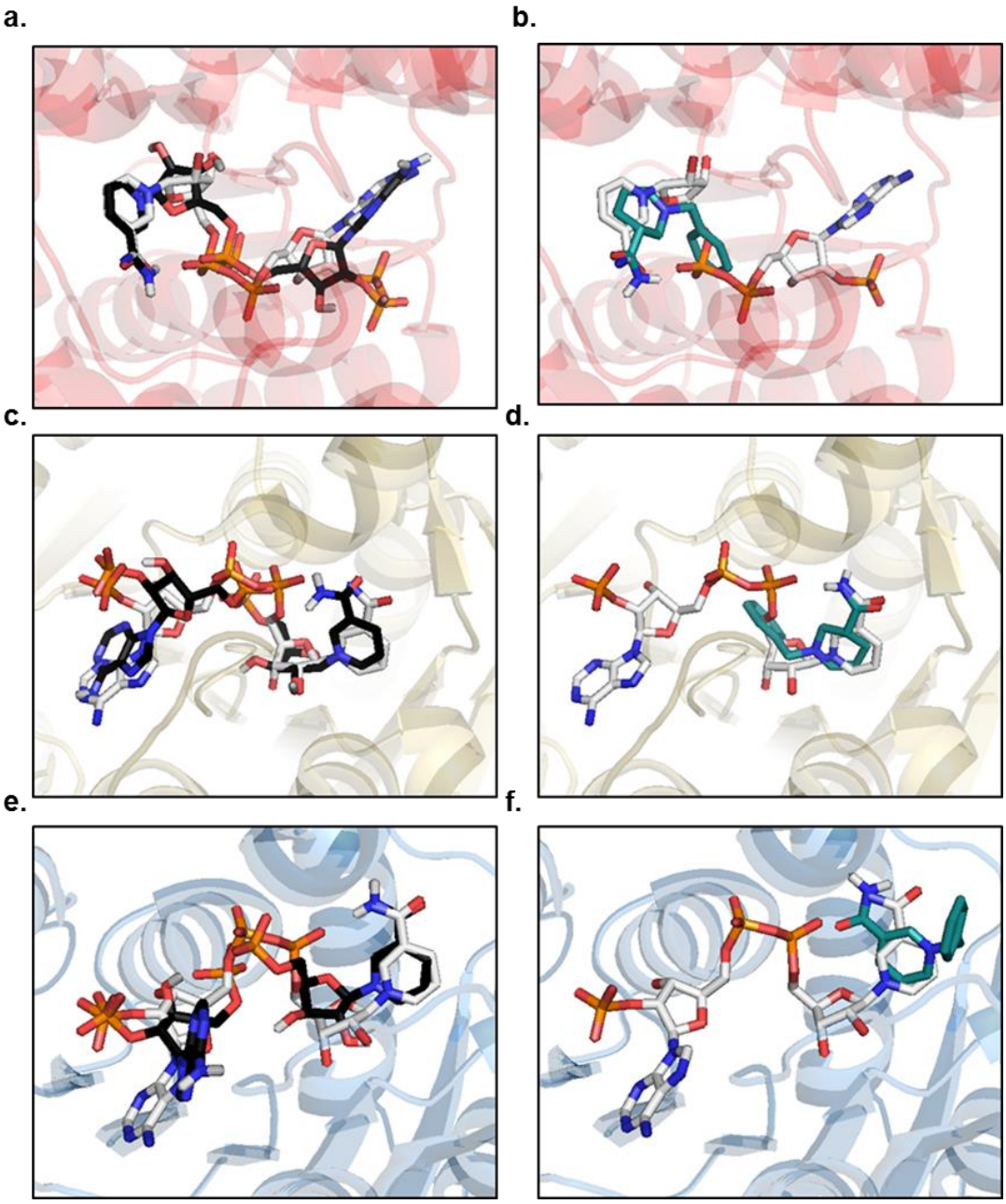


Figure 6.20. Docking results of the selected ADH candidates: a. b. SyADH, c.d. KpADH (yellow) and e. f. CmADH (blue) with NADPH (black) or Bn-NAD (turquoise). The natural cofactor for each structure was highlighted in white.

In all 3 cases (Figure 6.20 a, c and e), the redocked NADPH (in black) was spatially arranged in a similar fashion as the crystallized cofactor (in white). These results provided confidence on the accuracy of the method used. Although the nicotinamide ring of Bn-NAD with all candidates was mimicking the interactions of the natural cofactors (Figure 6.20 b, d and f), the extra benzene ring was better positioned with SyADH and KpADH, following the

cofactor. On the other hand, the benzene ring was pointing towards the substrate pocket within CmADH.

Out of the three enzymes, SyADH was the most studied one.[234-236] However, literature showed that the three candidates were accepting a large variety of bulky substrates (Figure 6.21).[237-238] This capability to accept these large, hydrophobic structures might be the reason behind the affinity results obtained *in silico*.

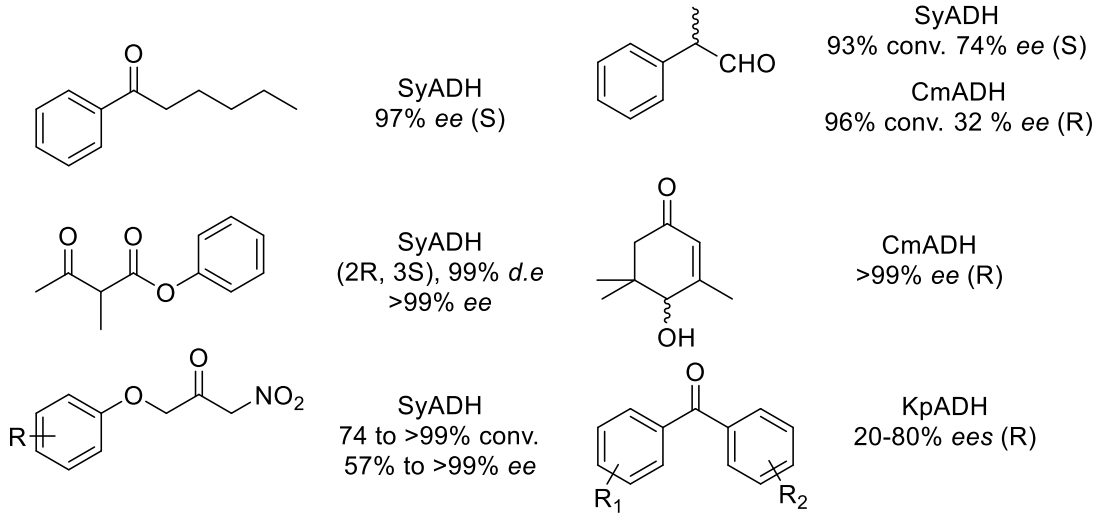


Figure 6.21. Various substrates depicted in literature for SyADH,[234] CmADH[237] and KpADH[238]. With each substrate is described the enzyme used and the reported results of the biocatalysis.

In conclusion, three ADHs (PDB entries 4BMV, 5Z2X and 5MLN) were found to be suitable to accommodate the previously designed and synthesized nicotinamide derivatives. Each of the enzymes was reported to show activity towards bulky substrates and evolved their structure to interact with large, more hydrophobic moieties. This study is thus providing a nice opportunity to pursue supramolecular anchoring design of artificial metalloenzyme based on nicotinamide-like scaffolds. *In vitro* experiments are however required to corroborate the results of this computational study.

6.10 Summary and Conclusions

To build an artificial metalloenzyme, a supramolecular approach was considered. Two enzymes, well documented, were selected: HLADH and TbADH. After the successful expression and purification of these enzymes, two scaffolds in both oxidized and reduced forms were designed as

supramolecular anchors that mimic nicotinamide cofactors NAD(H) and NADP(H): compounds Bn-NAD (**150**/**151**) and Bn-NAD-Ph (**155**/**156**).

The ability of the mimics to interact with each enzyme was then explored through activity and inhibition assays. The results from those studies led to the conclusion that no interactions occurred between the nicotinamide derivatives and the enzymes. To understand this lack of interaction a docking study was carried out, revealing that interactions occurred via hydrophobic forces. Those forces were, however, not applied within the cofactor pocket of the enzymes, as initially hypothesized.

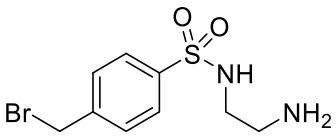
Finally, two distinct yet complementary approaches were used to identify, *in silico*, new targets for further research. The first approach focused on new chemical targets. The aim was to design new anchors capable of interacting with HLADH. The outcome of this approach was a general pattern to improve interaction with the enzyme at the nicotinamide ring space; a linear chain with one hydroxyl moiety at the 3'carbon followed by a more hydrophilic moiety. Also, 3 designs were identified that would require synthesis and activity assays to determine the accuracy of the models provided.

The second and final approach focused on new biological targets. The ADHs were composing a superfamily. It was then hypothesized that some other members of this family could accept the already synthesized anchors. Three potential enzymes from the SDR subfamily were found as potential acceptors.

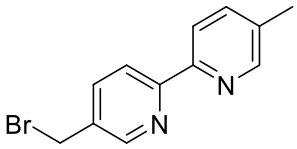
7 Overall discussion

The first objective of this thesis was the development of enzymatic scaffolds, based on TbADH, to covalently anchor ligands. A computational design approach was used to create a mutant library where the thiol bioconjugation handle was readily available for modification with the catalysts, and the validity of the computational models was assessed experimentally.

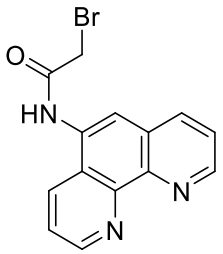
Various positions were picked throughout the NADPH binding pocket of the enzyme as a starting point of the *in silico* study. This study, developed with ligand **L1**, considered versatile for the coordination of complexes,[96, 98, 100-102] led to 4 positions to be mutated into cysteines. Another possible approach would have been to covalently dock bipyridine **L2** and/or phenanthroline **L3** at position 37, which were also investigated by others in our lab during the course of this thesis, and to compare the results with the study performed in this thesis. Given the rather limited reactivity of piano-stool complexes with these ligands, such an approach would have been more focused to the optimisation of NADPH (and derivatives) regeneration with ArMs, therefore disregarding the main objective of building a more general biocatalytic platform for transfer hydrogenation. Nonetheless, this could have led to different results similarly interesting.



L1



L2



L3

Throughout the design and the creation of the biological scaffold by site directed mutagenesis, Ellman's assay was used as a fast method to estimate the amount of bioconjugates yielded. With the apoprotein, the test showed 50-70 % thiol accessibility. Non-reducing conditions were used, compared to other researchers using dithiothreitol (DTT), β-mercaptoethanol (BME) or tris(2-carboxyethyl)phosphine (TCEP).[239] Such reducing conditions can be used prior to the bioconjugation to reduce all the cysteines, but they are not

compatible with the labelling step. Therefore, a purification step would have been required before the bioconjugation process to remove the reducing agent, leading to more intensive work to improve the accuracy of a quick method whilst more precise analyses were expected to be performed, providing more accurate and useful information, such as ESI- and ICP-MS.

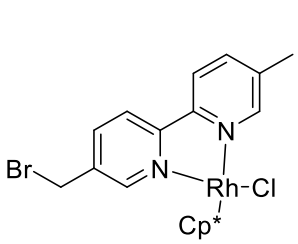
The bioconjugation process was optimised with TbADH 5M and the sulfonamide ligand **L1**. According to the results from the ESI-MS with the metal-free chemo-enzymatic hybrids, the optimisation could have been performed for each ligand individually and then compared to one another. However, the poor accuracy of the Ellman's assay did not preclude of better conditions if the optimisation was performed for each ligand.

Nevertheless, the bioconjugation results obtained by ESI-MS clearly demonstrated the efficiency of the acyl bromide over the alkyl bromide moiety, as labelling functionality of the ligands for the creation of a covalent bond with the enzyme. The sulfonamide ligand could have been synthesised with this more reactive moiety as it was hypothesised to be the most versatile of the three. Other moieties could have been investigated as well, such as maleimide or carbonylimidazole, which proved to be efficient warheads for thiol conjugation.[9] These moieties, however, would have extended the size of the ligands whilst the use, in this study, of acyl and alkyl bromide was to minimise their length. Nonetheless, some chemo-enzymatic hybrids were successfully achieved, including the 7M-C243 scaffold that exhibited full conjugation with both alkyl and acyl bromide-containing ligands.

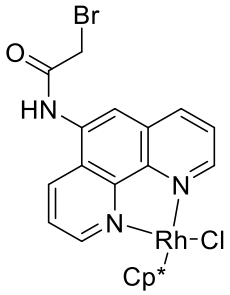
Metal complexes coordinated to the ligands were then synthesised, and 3 of them; **M1b**, **M2** and **M3a**, displayed activity towards the model reaction. These 3 complexes were then used to attempt the building of ArMs by covalent binding. When metal-complexes were used as bioconjugates, the complex **M1b** was not able to yield the ArM. Although optimisation was performed, the main reason hypothesised for the poor results was the lack of water solubility exhibited by the complex. The metal in suspension probably led to protein aggregation. TbADH is known to possess a high tolerance to organic solvent.[231] Addition of solvent, such as acetonitrile, might have helped the

solubilisation of this catalyst and improve the bioconjugation results. However, the aim of the ArMs, in the context of this study, was to provide a sustainable alternative to current methods for transfer hydrogenation and some of these reactions were already shown to be performed in water without co-solvent.[101, 103, 220]

The study then focused on the achieved ArMs, that aimed at reducing nicotinamide cofactors and derivatives, starting by analysing the amount of protein labelled with the catalysts. At the exception of Ellman's assay, shown to be inaccurate with our conditions, the various analyses were consistent with each other. A good example of consistency were the results of bioconjugation with ArM 7M-C243-**M2** where the metal complex was identified by UV-Vis, 53 % labelling was determined by ESI-MS and 57 % Rh content was detected by ICP-MS.



M2

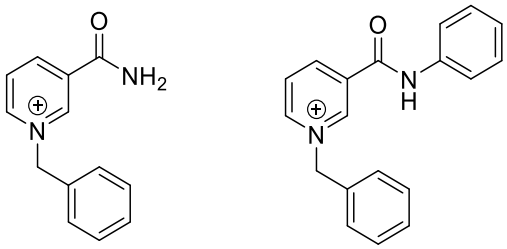


M3a

Furthermore, these results highlighted a less efficient conjugation between 5M-C174 and catalyst **M2**. This was monitored during the catalytic reduction of $NADP^+$ where the 7M-C174-**M2** displayed 3-fold less activity than published results from our group. This activity value was also shared with 5M-C37-**M2**, although the analyses showed a slightly improved bioconjugation compared to reported data. This could come from the observed dissociation of Cp*Rh from the complex with catalyst **M2** in both scaffolds. The dissociated specie could potentially bind more accessible residues, as a strong affinity of rhodium for histidines were reported.[240] Besides, the ligand **L3** seemed to coordinate in a stronger fashion with rhodium than ligand **L2** as no dissociation was observed with catalyst **M3a**. Overall, catalytic results were improved using the mutant 7M-C243 as a biological scaffold compared to the published 5M-C37.

Additional covalent docking with the metal complexes at the positions chosen by the end of the docking study could have provided valuable information. Unfortunately, due to the limitation of the software to compute Van der Waals and electrostatic forces for transition metals, the modelling was not performed. If achieved, NADPH could have been docked into the ArMs and provided a model to understand the behaviour observed with the ArMs towards the reduction of nicotinamide derivatives, including with the catalyst **M3a**. Indeed, the scaffold 7M-C243 should have allowed the metal complexes to sit within the cofactor binding pocket, therefore prohibiting the access to the natural cofactors. However, 7M-C243-**M3a** exhibited a strong activity towards the natural cofactor and none towards the nicotinamide mimic. Another approach to gain information would be the crystallisation of this ArM with and without soaking it with $NADP^+$. This would provide knowledge on the spatial arrangement of the metal complex and the substrate within the cavity of the enzyme, potentially allowing the formulation of a mechanism for the reaction observed. Similarly, the crystallisation of the other ArMs developed might shed a light on the unspecific binding described earlier. Information on the supplementary binding site(s) and their localisation on the protein scaffold as well as information on the nature of the specie bound (Cp*Rh or complexes) could be obtained.

The last part of this thesis was the use of the supramolecular approach to yield artificial metalloenzymes. HLADH and TbADH were used as wild-type, and their cofactor binding pocket was targeted as a site for supramolecular anchoring by using, to some extent, the already existing interactions between the nicotinamide cofactor and various residues. Bn-NAD, a reported structure to mimic $NAD(P)^+$ cofactor was used as a starting point.[120, 153] Additionally, a second structure (Bn-NAD-Ph) was also synthesised, based on the reported mimic, where a linker group was added for the subsequent addition of a metal complex if the approach was proved successful.



Bn-NAD Bn-NAD-Ph

The reported nicotinamide derivatives did not exhibit any capacity to transfer hydrides within the two ADHs evaluated. They were therefore expected to act as inhibitors, unfortunately, the results of the inhibition study revealed very poor inhibition. The docking study, however, revealed the propensity of the synthesised anchors to sit or point toward the substrate pocket. Nonetheless, these results were invalidated by the lack of inhibition. One hypothesis to explain the discordance between the inhibition assay and the docking study would be the existence of stronger interactions between the mimics and the surface of the proteins. To compute docking studies, a space is created *via* a grid to limit the calculation time. The grid was adjusted to the catalytic site of the enzymes therefore the potentially stronger interactions at the surface were discriminated as they were localised outside the calculation grid.

Another explanation, that also applied to the screening of new potential anchors, was the requirement of adenosine for the enzyme HLADH to be in the “active” form.[241] Presented in section 1.3.2.1, the binding of the cofactor modifies the form of HLADH into an active one where the substrate can enter. The form used for the computational studies was already active, as it was crystallised with the cofactor, which was removed *in silico*, probably leading to inaccurate results, including the potential interactions within the substrate pocket observed on the computational model. A rapid experimental work to evaluate this hypothesis would be to carry out HLADH activity assays with the already synthesised anchors and add adenosine in the solution as an “activator”. Another approach could have been the used of isothermal titration calorimetry (ITC). Aside from providing results on the existence of the interaction between the anchors and the proteins, the test provides quantitative results on the strength of the interactions, if detected.

Finally, as an alternative to the search *in silico* of new potential anchors, a second computational study was carried out to look for other ADHs capable of accommodating the already synthesised supramolecular anchors. Three SDRs were found to be suitable scaffold for the nicotinamide derivatives. Compared to the zinc-dependent enzymes, SDRs do not change their structure upon addition of a nicotinamide cofactor and the 3 enzymatic candidates resulting from the study were shown to accept relatively large and hydrophobic substrates, even more hydrophobic than the nicotinamide derivatives.[234-238] Therefore, these chemicals should fit into the cofactor binding pocket with more ease.

Another starting point of the supramolecular strategy would have been the use of ADHs that can accept both NADH and NADPH as cofactors, thus providing an initial promiscuity to accommodate chemicals in its cofactor binding pocket. Unfortunately, ADHs are all, in their wild-type form, specific toward one cofactor due to the additional interactions requires to interact with the 2' phosphate group of NADPH.[184] Protein engineering would be required to remove, or reduce, the cofactor specificity prior to usage as a potent scaffold for ArM *via* supramolecular anchoring.

8 Summary, conclusions and future work

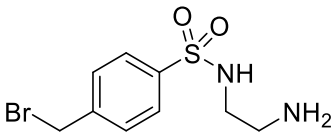
This thesis presents an attempt at developing ArMs for TH reactions by introducing d^6-piano stool complexes into ADHs. Two approaches to build ArMs were investigates; covalent and supramolecular anchoring of metal complexes within the cofactor binding pocket of the ADHs.

Mutants of *Thermoanaerobacter brockii* alcohol dehydrogenase (TbADH) were successfully achieved and subsequent bioconjugation with ligand and metal complexes yielded 5 different artificial metalloenzymes (ArMs). The capacity of these ArMs to perform the reduction of nicotinamide cofactors and their derivatives was then assessed, providing useful information about the role of the anchoring site within the enzymatic scaffold toward the conjugation and the catalytic efficiency. As an alternative, supramolecular anchor based on nicotinamide derivatives were synthesised and their capacity to act either as natural cofactors or inhibitors was assessed, leading to further study performed *in silico* by docking, indicating the need for further development to reduce the hydrophobicity of the anchoring structures.

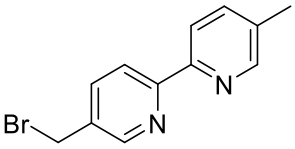
The evaluation of an anchoring position for the covalent binding of metal complexes in TbADH was outlined in Chapter 4. An initial study was carried out *in silico* to provide various positions throughout the cofactor binding site of TbADH where a residue could be mutated into a cysteine for nucleophilic substitution, leading to the creation of ArMs. Four positions; 174, 198, 242 and 243 were found to be suitable for the development of single cysteine mutants. Additionally, the position 37 and 203, represented by cysteines in the catalytic site of the wild-type enzyme were also used as anchoring positions. All six mutants were successfully engineered as well as a cysteine-deprive mutant for negative control. Finally, the accessibility of the newly introduced thiols was assessed. The Ellman's assay used to assess the accessibility was found to be inaccurate under the conditions used. Therefore, it could be envisaged to optimise the conditions of this assay.

Following the creation of the mutants, three ligands were synthesised; **L1**, **L2** and **L3**. The ligand **L1** was used as a versatile coordination motif for the creation of a biocatalytic platform while ligands **L2** and **L3** were previously

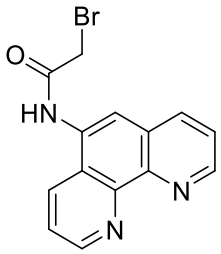
reported by our group as suitable conjugates with the chosen enzymatic scaffold.[217] The bioconjugation process was then optimised prior to be carry out with all the 6 mutants and 3 ligands individually. The results of the bioconjugation were assessed by ESI-MS. The results highlighted the impact of the reactive moiety of the ligands on the efficiency of the bioconjugation where the ligand bearing an acyl bromide was more efficient than the ones with an alkyl bromide. As the most versatile ligand **L1** was synthesised with an alkyl bromide, it could be interesting to evaluate the results of the bioconjugation with this ligand bearing an acyl bromide moiety instead. Nonetheless, the bioconjugation process lead to 2 interesting mutants for the bioconjugation with metal complexes; 7M-C174 and 7M-C243. To increase the number of potential mutants that could reach this stage, a new iteration of covalent docking could also be performed with the ligands **L2** and **L3**.



L1

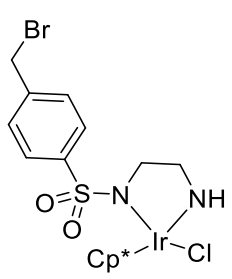


L2

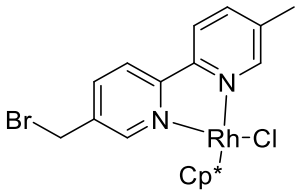


L3

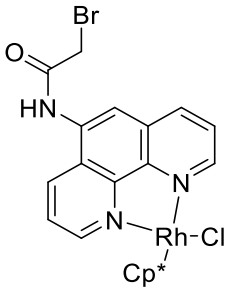
In Chapter 5, the two mutants that exhibited good bioconjugation with the ligands, as well as the mutant with a single cysteine at position 37 to act as a reference, were used as scaffold for the insertion of metal complexes. Five different metal complexes were synthesised by metalation of the previous ligands with either Rh- or Ir-based complexes. Three of these catalysts displayed activity towards the reduction of $NADP^+$ into NADPH, the model reaction; **M1b**, **M2** and **M3a**. Unfortunately, only 2 catalysts were successfully conjugated to the various enzymes, the last one, catalyst **M1b**, being poorly soluble in water. A bioconjugation with a co-solvent could be carried out to evaluate the impact of the solubility on the efficiency of the conjugation with this catalyst.



M1b



M2



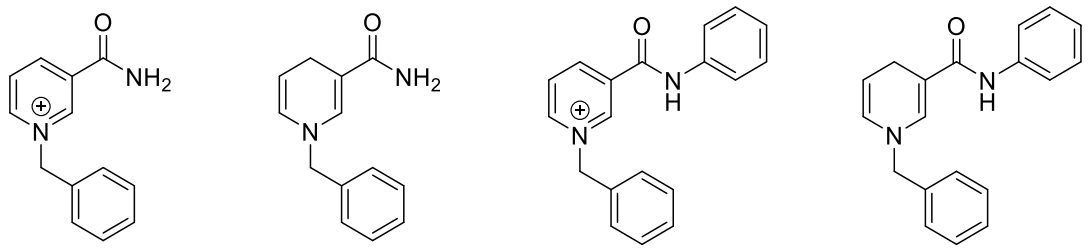
M3a

The resulting ArMs were analysed using various biophysical methods. The results of these analyses were consistent at the exception of the Ellman's assay, previously shown to be carried out in suboptimal conditions. However, the dissociation of Cp*Rh complexes from ligand **L2** was observed by ESI-MS and ICP-MS within some ArMs, possibly binding at the surface of the protein by coordination with histidine residues. Overall the results were consistent, and the ArMs were tested on the model reaction while considering the dissociation of Cp*Rh as a potential interference by catalysing the reaction outside the desired enzymatic pocket in a non-specific manner. With catalyst **M2**, the ArMs performed less than reported in literature. This indicates that the dissociation did not interfere directly with the catalysis but rather indirectly by reducing the amount of ArM produced, thus lowering the catalytic activity of the species. However, with catalyst **M3a**, the results were similar to the published data.

After the assessment of the catalytic activity of the ArMs with the model reaction, a new batch was prepared, and their substrate scope evaluated on the same reaction with nicotinamide derivatives. However, after 500 seconds in the monitoring of the reaction, degradation of the product was observed. It was hypothesised that the CO_2 released as a by-product of the activation of the metal centre was acidifying the solution, degrading the product. This hypothesis was evaluated by an assay performed on the product where degradation was observed, correlated to the amount of acid added to the solution. A direct pH measurement would, however, be required to confirm the results of the assay.

The new ArMs displayed a very good substrate scope with catalyst **M2**. At first, these results were considered very promising. On the other hand, the substrate scope with catalyst **M3a** was limited to natural cofactor. While the results with catalyst **M2** could be explained by unspecific binding and catalysis from the dissociated Cp*Rh species, the catalyst **M3a** was not expected, with the mutant 7M-C174 and 7M-C243, to exhibit a discrimination towards the derivatives but rather towards the natural cofactor due to the presence of the catalyst within the cofactor binding pocket. To understand the observed behaviour, tedious covalent docking with metal complexes could be performed, followed by a docking study with $NADP^+$ and its derivatives in the ArM model. As an alternative, crystallisation of the ArMs and soaking with the various nicotinamide-containing compounds could provide useful information on the spatial arrangement of the metal catalyst as well as some insight of a reaction mechanism.

Finally, in Chapter 6, a supramolecular approach was considered to develop ArMs. Two wild-type enzymatic scaffolds were evaluated; HLADH and TbADH. While the later was expressed and purified successfully according to published procedures, His-HLADH was not purified using the reported methodology. Therefore, the purification conditions were changed from 15 mM EDTA to 500 mM imidazole in order to displace the enzyme from the column. Once the enzymes were purified and their natural activity assessed, two supramolecular anchors, based on nicotinamide derivatives, were synthesised in both oxidised and reduced forms, yielding a total of 4 anchors.



Bn-NAD Bn-NAD-Ph

Initially, the capacity of the anchor to mimic the natural cofactors $NAD(P)^+/H$ was assessed *via* an activity assay with the enzyme and its natural substrate. Unfortunately, the anchors could not transfer hydride, as expected from their

structure, and no product could be observed. However, a report showed that, in the case of HLADH, adenosine played an important role in the activation of the enzyme to provide accessibility for the substrate molecule.[241] A second activity assay, including adenosine in the solution, could be carry out to evaluate the impact of the "inactive" form of the enzyme of the results.

Nevertheless, it was hypothesised that the derivatives could act as inhibitors, explaining the lack of enzymatic activity observed with the enzymes. The inhibition assay was also unsuccessful, leading to the conclusion that these chemicals were not interacting with the enzymes. Thus, a docking study was carried out. The study revealed a hydrophobic character from the derivatives, more likely to interact with the enzyme within the substrate binding pocket rather than the expected cofactor binding cavity. An experimental study using isothermal titration calorimetry (ITC) could be performed to confront the results from the docking. However, these results do not correlate with the lack of inhibitory potential of the anchors. Although it was expected a competition with the cofactor, a competition with the substrate would have been detected similarly under the conditions used. Therefore, a more plausible explanation is the limitation of the docking technique that requires a predetermined space to perform the calculation. This space was adjusted around the catalytic site. Therefore, the results did not provide any information concerning interactions of the derivatives at the surface of the enzyme.

Following the unsuccessful results obtained in Chapter 6 so far, two distinct *in silico* studies were performed. The first one was to evaluate various structures of potential anchors and their impact on the docking results. Different factors were evaluated leading to 3 potential anchors. These anchors would need to be synthesised and tested by an activity assay to compare the validity of the docking results. If the results are conclusive, further research can be performed by adding a linker and a coordination site to introduce metal-complexes.

The second study aimed at evaluating different enzymatic scaffold from the ADH family. After refining the possible candidates from the plethora of ADHs available, docking was performed with the mimic **150**, yielding 3 ADHs. These

enzymes were part of the SDR subfamily that do not possess catalytic metal ions. Furthermore, these enzymes were reported to accommodate bulky substrates, potentially more hydrophobic than the mimic. To confirm the results of this study, the ADHs should be expressed, purified and their activity with the derivative assessed.

In conclusion, this thesis provided foundation work for the development of an artificial metalloenzyme from a nicotinamide-dependent scaffold. Continuous improvement of molecular modelling conjugated with crystallisation will provide useful information to understand the catalytic behaviour of the current ArMs developed, potentially leading to a biocatalytic platform for transfer hydrogenation reaction. In parallel, further experimental work in the supramolecular anchoring strategy could lead to robust ArMs, capable of competing with current chemical and bio-catalysts.

9 References

1. Teplyakov, A.; Polyakov, K.; Obmolova, G.; Strokopytov, B.; Kuranova, I.; Osterman, A.; Grishin, N.; Smulevitch, S.; Zagnitko, O.; Galperina, O.; Matz, M.; Stepanov, V., Crystal structure of carboxypeptidase T from Thermoactinomyces vulgaris. *European Journal of Biochemistry* **1992,** *208* (2), 281-288.
2. Arfin, S. M.; Kendall, R. L.; Hall, L.; Weaver, L. H.; Stewart, A. E.; Matthews, B. W.; Bradshaw, R. A., Eukaryotic methionyl aminopeptidases: two classes of cobalt-dependent enzymes. *Proceedings of the National Academy of Sciences* **1995,** *92* (17), 7714-7718.
3. Chang, C. M.; Klema, V. J.; Johnson, B. J.; Mure, M.; Klinman, J. P.; Wilmot, C. M., Kinetic and structural analysis of substrate specificity in two copper amine oxidases from Hansenula polymorpha. *Biochemistry* **2010,** *49* (11), 2540-2550.
4. Yun, D.; Dey, M.; Higgins, L. J.; Yan, F.; Liu, H.-w.; Drennan, C. L., Structural Basis of Regiospecificity of a Mononuclear Iron Enzyme in Antibiotic Fosfomycin Biosynthesis. *Journal of the American Chemical Society* **2011,** *133* (29), 11262-11269.
5. Ha, N.-C.; Oh, S.-T.; Sung, J. Y.; Cha, K. A.; Lee, M. H.; Oh, B.-H., Supramolecular assembly and acid resistance of Helicobacter pylori urease. *Nature Structural Biology* **2001,** *8* (6), 505-509.
6. Rowsell, S.; Pauptit, R. A.; Tucker, A. D.; Melton, R. G.; Blow, D. M.; Brick, P., Crystal structure of carboxypeptidase G2, a bacterial enzyme with applications in cancer therapy. *Structure* **1997,** *5* (3), 337-347.
7. Lewis, J. C., Artificial Metalloenzymes and Metallopeptide Catalysts for Organic Synthesis. *ACS Catalysis* **2013,** *3* (12), 2954-2975.
8. Schwizer, F.; Okamoto, Y.; Heinisch, T.; Gu, Y.; Pellizzoni, M. M.; Lebrun, V.; Reuter, R.; Köhler, V.; Lewis, J. C.; Ward, T. R., Artificial Metalloenzymes: Reaction Scope and Optimization Strategies. *Chemical Reviews* **2018,** *118* (1), 142-231.
9. Pàmies, O.; Diéguez, M.; Bäckvall, J.-E., Artificial Metalloenzymes in Asymmetric Catalysis: Key Developments and Future Directions. *Advanced Synthesis & Catalysis* **2015,** *357* (8), 1567-1586.
10. Yamamura, K.; Kaiser, E. T., Studies on the oxidase activity of copper(II) carboxypeptidase A. *Journal of the Chemical Society, Chemical Communications* **1976,** (20), 830-831.
11. Liljas, A.; HÅKansson, K.; Jonsson, B. H.; Xue, Y., Inhibition and catalysis of carbonic anhydrase. *European Journal of Biochemistry* **1994,** *219* (1-2), 1-10.
12. Okrasa, K.; Kazlauskas, R. J., Manganese-Substituted Carbonic Anhydrase as a New Peroxidase. *Chemistry - A European Journal* **2006,** *12* (6), 1587-1596.
13. Jing, Q.; Okrasa, K.; Kazlauskas, R. J., Stereoselective Hydrogenation of Olefins Using Rhodium-Substituted Carbonic Anhydrase—A New Reductase. *Chemistry - A European Journal* **2009,** *15* (6), 1370-1376.
14. Jing, Q.; Kazlauskas, R. J., Regioselective Hydroformylation of Styrene Using Rhodium-Substituted Carbonic Anhydrase. *ChemCatChem* **2010,** *2* (8), 953-957.

15. Podtetenieff, J.; Taglieber, A.; Bill, E.; Reijerse, E. J.; Reetz, M. T., An Artificial Metalloenzyme: Creation of a Designed Copper Binding Site in a Thermostable Protein. *Angewandte Chemie International Edition* **2010,** *49* (30), 5151-5155.
16. Bos, J.; Fusetti, F.; Driessen, A. J. M.; Roelfes, G., Enantioselective Artificial Metalloenzymes by Creation of a Novel Active Site at the Protein Dimer Interface. *Angewandte Chemie International Edition* **2012,** *51* (30), 7472-7475.
17. Bos, J.; García-Herraiz, A.; Roelfes, G., An enantioselective artificial metallo-hydratase. *Chemical Science* **2013,** *4* (9), 3578-3582.
18. Bos, J.; Browne, W. R.; Driessen, A. J. M.; Roelfes, G., Supramolecular Assembly of Artificial Metalloenzymes Based on the Dimeric Protein LmrR as Promiscuous Scaffold. *Journal of the American Chemical Society* **2015,** *137* (31), 9796-9799.
19. Bersellini, M.; Roelfes, G., Multidrug resistance regulators (MDRs) as scaffolds for the design of artificial metalloenzymes. *Organic & Biomolecular Chemistry* **2017,** *15* (14), 3069-3073.
20. Drienovská, I.; Alonso-Cotchico, L.; Vidossich, P.; Lledós, A.; Maréchal, J.-D.; Roelfes, G., Design of an enantioselective artificial metallo-hydratase enzyme containing an unnatural metal-binding amino acid. *Chemical Science* **2017,** *8* (10), 7228-7235.
21. Villarino, L.; Splan, K. E.; Reddem, E.; Alonso-Cotchico, L.; Gutiérrez de Souza, C.; Lledós, A.; Maréchal, J.-D.; Thunnissen, A.-M. W. H.; Roelfes, G., An Artificial Heme Enzyme for Cyclopropanation Reactions. *Angewandte Chemie International Edition* **2018,** *57* (26), 7785-7789.
22. Drienovská, I.; Mayer, C.; Dulson, C.; Roelfes, G., A designer enzyme for hydrazone and oxime formation featuring an unnatural catalytic aniline residue. *Nature Chemistry* **2018,** *10* (9), 946-952.
23. Alonso-Cotchico, L.; Sciortino, G.; Vidossich, P.; Rodríguez-Guerra Pedregal, J.; Drienovská, I.; Roelfes, G.; Lledós, A.; Maréchal, J.-D., Integrated Computational Study of the Cu-Catalyzed Hydration of Alkenes in Water Solvent and into the Context of an Artificial Metallohydratase. *ACS Catalysis* **2019,** *9* (5), 4616-4626.
24. Mayer, C.; Dulson, C.; Reddem, E.; Thunnissen, A.-M. W. H.; Roelfes, G., Directed Evolution of a Designer Enzyme Featuring an Unnatural Catalytic Amino Acid. *Angewandte Chemie International Edition* **2019,** *58* (7), 2083-2087.
25. Roelfes, G., LmrR: A Privileged Scaffold for Artificial Metalloenzymes. *Accounts of Chemical Research* **2019,** *52* (3), 545-556.
26. Drienovská, I.; Rioz-Martínez, A.; Draksharapu, A.; Roelfes, G., Novel artificial metalloenzymes by in vivo incorporation of metal-binding unnatural amino acids. *Chemical Science* **2015,** *6* (1), 770-776.
27. Ory, J. J.; Mazhary, A.; Kuang, H.; Davies, R. R.; Distefano, M. D.; Banaszak, L. J., Structural characterization of two synthetic catalysts based on adipocyte lipid-binding protein. *Protein Engineering, Design and Selection* **1998,** *11* (4), 253-261.
28. Yang, H.; Srivastava, P.; Zhang, C.; Lewis, J. C., A General Method for Artificial Metalloenzyme Formation through Strain-Promoted Azide–Alkyne Cycloaddition. *ChemBioChem* **2014,** *15* (2), 223-227.

29. Levine, H. L.; Kaiser, E. T., Oxidation of dihydronicotinamides by flavopapain. *Journal of the American Chemical Society* **1978,** *100* (24), 7670-7677.
30. Otsuki, T.; Nakagawa, Y.; Kaiser, E. T., Synthesis and characterization of covalent flavin–papain complexes with sulphur in the sulphide and sulphone oxidation states. *Journal of the Chemical Society, Chemical Communications* **1978,** (11), 457-459.
31. Kaiser, E.; Lawrence, D., Chemical mutation of enzyme active sites. *Science* **1984,** *226* (4674), 505-511.
32. Reetz, M. T.; Rentzsch, M.; Pletsch, A.; Maywald, M., Towards the Directed Evolution of Hybrid Catalysts. *CHIMIA International Journal for Chemistry* **2002,** *56* (12), 721-723.
33. Reetz, M. T.; Rentzsch, M.; Pletsch, A.; Taglieber, A.; Hollmann, F.; Mondière, R. J. G.; Dickmann, N.; Höcker, B.; Cerrone, S.; Haeger, M. C.; Sterner, R., A Robust Protein Host for Anchoring Chelating Ligands and Organocatalysts. *ChemBioChem* **2008,** *9* (4), 552-564.
34. Talbi, B.; Haquette, P.; Martel, A.; de Montigny, F.; Fosse, C.; Cordier, S.; Roisnel, T.; Jaouen, G.; Salmain, M., (η6-Arene) ruthenium(ii) complexes and metallo-papain hybrid as Lewis acid catalysts of Diels–Alder reaction in water. *Dalton Transactions* **2010,** *39* (24), 5605-5607.
35. Haquette, P.; Talbi, B.; Barilleau, L.; Madern, N.; Fosse, C.; Salmain, M., Chemically engineered papain as artificial formate dehydrogenase for NAD(P)H regeneration. *Organic & Biomolecular Chemistry* **2011,** *9* (16), 5720-5727.
36. Laan, W.; Muñoz, B. K.; Heeten, R. d.; Kamer, P. C. J., Artificial Metalloenzymes through Cysteine-Selective Conjugation of Phosphines to Photoactive Yellow Protein. *ChemBioChem* **2010,** *11* (9), 1236-1239.
37. Davies, R. R.; Distefano, M. D., A Semisynthetic Metalloenzyme Based on a Protein Cavity That Catalyzes the Enantioselective Hydrolysis of Ester and Amide Substrates. *Journal of the American Chemical Society* **1997,** *119* (48), 11643-11652.
38. Sacchettini, J. C.; Meininger, T. A.; Lowe, J. B.; Gordon, J. I.; Banaszak, L. J., Crystallization of rat intestinal fatty acid binding protein. Preliminary X-ray data obtained from protein expressed in Escherichia coli. *Journal of Biological Chemistry* **1987,** *262* (11), 5428-30.
39. Sacchettini, J. C.; Gordon, J. I.; Banaszak, L. J., Crystal structure of rat intestinal fatty-acid-binding protein: Refinement and analysis of the Escherichia coli-derived protein with bound palmitate. *Journal of Molecular Biology* **1989,** *208* (2), 327-339.
40. Xu, Z.; Bernlohr, D. A.; Banaszak, L. J., Crystal structure of recombinant murine adipocyte lipid-binding protein. *Biochemistry* **1992,** *31* (13), 3484-3492.
41. LaLonde, J. M.; Bernlohr, D. A.; Banaszak, L. J., X-ray Crystallographic Structures of Adipocyte Lipid-Binding Protein Complexed with Palmitate and Hexadecanesulfonic Acid. Properties of Cavity Binding Sites. *Biochemistry* **1994,** *33* (16), 4885-4895.
42. Reiner, T.; Jantke, D.; Marziale, A. N.; Raba, A.; Eppinger, J., Metal-Conjugated Affinity Labels: A New Concept to Create Enantioselective Artificial Metalloenzymes. *ChemistryOpen* **2013,** *2* (2), 50-54.
43. Davies, R. R.; Kuang, H.; Qi, D.; Mazhary, A.; Mayaan, E.; Distefano, M. D., Artificial metalloenzymes based on protein cavities: Exploring the effect

of altering the metal ligand attachment position by site directed mutagenesis. *Bioorganic & Medicinal Chemistry Letters* **1999,** *9* (1), 79-84.
44. Jarvis, A. G.; Obrecht, L.; Deuss, P. J.; Laan, W.; Gibson, E. K.; Wells, P. P.; Kamer, P. C. J., Enzyme Activity by Design: An Artificial Rhodium Hydroformylase for Linear Aldehydes. *Angewandte Chemie International Edition* **2017,** *56* (44), 13596-13600.
45. Doble, M. V.; Jarvis, A. G.; Ward, A. C. C.; Colburn, J. D.; Götze, J. P.; Bühl, M.; Kamer, P. C. J., Artificial Metalloenzymes as Catalysts for Oxidative Lignin Degradation. *ACS Sustainable Chemistry & Engineering* **2018,** *6* (11), 15100-15107.
46. Mayer, C.; Gillingham, D. G.; Ward, T. R.; Hilvert, D., An artificial metalloenzyme for olefin metathesis. *Chemical Communications* **2011,** *47* (44), 12068-12070.
47. Sauer, D. F.; Bocola, M.; Broglia, C.; Arlt, M.; Zhu, L. L.; Brocker, M.; Schwaneberg, U.; Okuda, J., Hybrid Ruthenium ROMP Catalysts Based on an Engineered Variant of β-Barrel Protein FhuA ΔCVFtev: Effect of Spacer Length. *Chemistry – An Asian Journal* **2015,** *10* (1), 177-182.
48. Garber, S. B.; Kingsbury, J. S.; Gray, B. L.; Hoveyda, A. H., Efficient and Recyclable Monomeric and Dendritic Ru-Based Metathesis Catalysts. *Journal of the American Chemical Society* **2000,** *122* (34), 8168-8179.
49. Gessler, S.; Randl, S.; Blechert, S., Synthesis and metathesis reactions of a phosphine-free dihydroimidazole carbene ruthenium complex. *Tetrahedron Letters* **2000,** *41* (51), 9973-9976.
50. Flenniken, M. L.; Willits, D. A.; Brumfield, S.; Young, M. J.; Douglas, T., The Small Heat Shock Protein Cage from Methanococcus jannaschii Is a Versatile Nanoscale Platform for Genetic and Chemical Modification. *Nano Letters* **2003,** *3* (11), 1573-1576.
51. Flenniken, M. L.; Liepold, L. O.; Crowley, B. E.; Willits, D. A.; Young, M. J.; Douglas, T., Selective attachment and release of a chemotherapeutic agent from the interior of a protein cage architecture. *Chemical Communications* **2005,** (4), 447-449.
52. Gułajski, Ł.; Śledź, P.; Lupa, A.; Grela, K., Olefin metathesis in water using acoustic emulsification. *Green Chemistry* **2008,** *10* (3), 271-274.
53. Philippart, F.; Arlt, M.; Gotzen, S.; Tenne, S. J.; Bocola, M.; Chen, H. H.; Zhu, L.; Schwaneberg, U.; Okuda, J., A Hybrid Ring-Opening Metathesis Polymerization Catalyst Based on an Engineered Variant of the β-Barrel Protein FhuA. *Chemistry - A European Journal* **2013,** *19* (41), 13865-13871.
54. Carey, J. R.; Ma, S. K.; Pfister, T. D.; Garner, D. K.; Kim, H. K.; Abramite, J. A.; Wang, Z.; Guo, Z.; Lu, Y., A Site-Selective Dual Anchoring Strategy for Artificial Metalloprotein Design. *Journal of the American Chemical Society* **2004,** *126* (35), 10812-10813.
55. Zhang, J.-L.; Garner, D. K.; Liang, L.; Chen, Q.; Lu, Y., Protein scaffold of a designed metalloenzyme enhances the chemoselectivity in sulfoxidation of thioanisole. *Chemical Communications* **2008,** (14), 1665-1667.
56. Zhang, J. L.; Garner, D. K.; Liang, L.; Barrios, D. A.; Lu, Y., Noncovalent Modulation of pH-Dependent Reactivity of a Mn–Salen Cofactor in Myoglobin with Hydrogen Peroxide. *Chemistry - A European Journal* **2009,** *15* (30), 7481-7489.

57. Hayashi, T.; Hisaeda, Y., New Functionalization of Myoglobin by Chemical Modification of Heme-Propionates. *Accounts of Chemical Research* **2002,** *35* (1), 35-43.
58. Ozaki, S.-i.; Yang, H.-J.; Matsui, T.; Goto, Y.; Watanabe, Y., Asymmetric oxidation catalyzed by myoglobin mutants. *Tetrahedron: Asymmetry* **1999,** *10* (1), 183-192.
59. Ohashi, M.; Koshiyama, T.; Ueno, T.; Yanase, M.; Fujii, H.; Watanabe, Y., Preparation of Artificial Metalloenzymes by Insertion of Chromium(III) Schiff Base Complexes into Apomyoglobin Mutants. *Angewandte Chemie International Edition* **2003,** *42* (9), 1005-1008.
60. Oohora, K.; Meichin, H.; Kihira, Y.; Sugimoto, H.; Shiro, Y.; Hayashi, T., Manganese(V) Porphycene Complex Responsible for Inert C–H Bond Hydroxylation in a Myoglobin Matrix. *Journal of the American Chemical Society* **2017,** *139* (51), 18460-18463.
61. Dydio, P.; Key, H. M.; Nazarenko, A.; Rha, J. Y.-E.; Seyedkazemi, V.; Clark, D. S.; Hartwig, J. F., An artificial metalloenzyme with the kinetics of native enzymes. *Science* **2016,** *354* (6308), 102-106.
62. Mirts, E. N.; Petrik, I. D.; Hosseinzadeh, P.; Nilges, M. J.; Lu, Y., A designed heme-[4Fe-4S] metalloenzyme catalyzes sulfite reduction like the native enzyme. *Science* **2018,** *361* (6407), 1098-1101.
63. Zunszain, P. A.; Ghuman, J.; Komatsu, T.; Tsuchida, E.; Curry, S., Crystal structural analysis of human serum albumin complexed with hemin and fatty acid. *BMC Structural Biology* **2003,** *3* (1), 6.
64. Rousselot-Pailley, P.; Bochot, C.; Marchi-Delapierre, C.; Jorge-Robin, A.; Martin, L.; Fontecilla-Camps, J. C.; Cavazza, C.; Ménage, S., The Protein Environment Drives Selectivity for Sulfide Oxidation by an Artificial Metalloenzyme. *ChemBioChem* **2009,** *10* (3), 545-552.
65. Ricoux, R.; Allard, M.; Dubuc, R.; Dupont, C.; Maréchal, J.-D.; Mahy, J.-P., Selective oxidation of aromatic sulfide catalyzed by an artificial metalloenzyme: new activity of hemozymes. *Organic & Biomolecular Chemistry* **2009,** *7* (16), 3208-3211.
66. Allard, M.; Dupont, C.; Robles, V. M.; Doucet, N.; Lledós, A.; Maréchal, J. D.; Urvoas, A.; Mahy, J. P.; Ricoux, R., Incorporation of Manganese Complexes into Xylanase: New Artificial Metalloenzymes for Enantioselective Epoxidation. *ChemBioChem* **2012,** *13* (2), 240-251.
67. Green, N. M., Avidin. In *Advances in Protein Chemistry*, Anfinsen, C. B.; Edsall, J. T.; Richards, F. M., Eds. Academic Press: 1975; Vol. 29, pp 85-133.
68. Wilson, M. E.; Whitesides, G. M., Conversion of a protein to a homogeneous asymmetric hydrogenation catalyst by site-specific modification with a diphosphinerhodium(I) moiety. *Journal of the American Chemical Society* **1978,** *100* (1), 306-307.
69. Lin, C.-C.; Lin, C.-W.; Chan, A. S. C., Catalytic hydrogenation of itaconic acid in a biotinylated Pyrphos–rhodium(I) system in a protein cavity. *Tetrahedron: Asymmetry* **1999,** *10* (10), 1887-1893.
70. Collot, J.; Gradinaru, J.; Humbert, N.; Skander, M.; Zocchi, A.; Ward, T. R., Artificial Metalloenzymes for Enantioselective Catalysis Based on Biotin−Avidin. *Journal of the American Chemical Society* **2003,** *125* (30), 9030-9031.

71. Skander, M.; Humbert, N.; Collot, J.; Gradinaru, J.; Klein, G.; Loosli, A.; Sauser, J.; Zocchi, A.; Gilardoni, F.; Ward, T. R., Artificial Metalloenzymes: (Strept)avidin as Host for Enantioselective Hydrogenation by Achiral Biotinylated Rhodium−Diphosphine Complexes. *Journal of the American Chemical Society* **2004,** *126* (44), 14411-14418.
72. Klein, G.; Humbert, N.; Gradinaru, J.; Ivanova, A.; Gilardoni, F.; Rusbandi, U. E.; Ward, T. R., Tailoring the Active Site of Chemzymes by Using a Chemogenetic-Optimization Procedure: Towards Substrate-Specific Artificial Hydrogenases Based on the Biotin–Avidin Technology. *Angewandte Chemie International Edition* **2005,** *44* (47), 7764-7767.
73. Skander, M.; Malan, C.; Ivanova, A.; Ward, T. R., Chemical optimization of artificial metalloenzymes based on the biotin-avidin technology: (S)-selective and solvent-tolerant hydrogenation catalysts via the introduction of chiral amino acid spacers. *Chemical Communications* **2005,** (38), 4815-4817.
74. Rusbandi, U. E.; Lo, C.; Skander, M.; Ivanova, A.; Creus, M.; Humbert, N.; Ward, T. R., Second Generation Artificial Hydrogenases Based on the Biotin-Avidin Technology: Improving Activity, Stability and Selectivity by Introduction of Enantiopure Amino Acid Spacers. *Advanced Synthesis & Catalysis* **2007,** *349* (11-12), 1923-1930.
75. Pierron, J.; Malan, C.; Creus, M.; Gradinaru, J.; Hafner, I.; Ivanova, A.; Sardo, A.; Ward, T. R., Artificial Metalloenzymes for Asymmetric Allylic Alkylation on the Basis of the Biotin–Avidin Technology. *Angewandte Chemie International Edition* **2008,** *47* (4), 701-705.
76. Mao, J.; Ward, T. R., Artificial Metalloenzymes for Enantioselective Catalysis Based on the Biotin-Avidin Technology. *CHIMIA International Journal for Chemistry* **2008,** *62* (12), 956-961.
77. Lo, C.; Ringenberg, M. R.; Gnandt, D.; Wilson, Y.; Ward, T. R., Artificial metalloenzymes for olefin metathesis based on the biotin-(strept)avidin technology. *Chemical Communications* **2011,** *47* (44), 12065-12067.
78. Kajetanowicz, A.; Chatterjee, A.; Reuter, R.; Ward, T. R., Biotinylated Metathesis Catalysts: Synthesis and Performance in Ring Closing Metathesis. *Catalysis Letters* **2014,** *144* (3), 373-379.
79. Hyster, T. K.; Knörr, L.; Ward, T. R.; Rovis, T., Biotinylated Rh(III) Complexes in Engineered Streptavidin for Accelerated Asymmetric C–H Activation. *Science* **2012,** *338* (6106), 500-503.
80. Pordea, A.; Mathis, D.; Ward, T. R., Incorporation of biotinylated manganese-salen complexes into streptavidin: New artificial metalloenzymes for enantioselective sulfoxidation. *Journal of Organometallic Chemistry* **2009,** *694* (6), 930-936.
81. Ward, T. R., Artificial Metalloenzymes Based on the Biotin−Avidin Technology: Enantioselective Catalysis and Beyond. *Accounts of Chemical Research* **2011,** *44* (1), 47-57.
82. Steinreiber, J.; Ward, T. R., Artificial Metalloenzymes for Enantioselective Catalysis Based on the Biotin–Avidin Technology. In *Bio-inspired Catalysts*, Ward, T. R., Ed. Springer Berlin Heidelberg: Berlin, Heidelberg, 2009; pp 93-112.
83. Haak, R. M.; Berthiol, F.; Jerphagnon, T.; Gayet, A. J. A.; Tarabiono, C.; Postema, C. P.; Ritleng, V.; Pfeffer, M.; Janssen, D. B.; Minnaard, A. J.; Feringa, B. L.; de Vries, J. G., Dynamic Kinetic Resolution of Racemic β-

Haloalcohols: Direct Access to Enantioenriched Epoxides. *Journal of the American Chemical Society* **2008,** *130* (41), 13508-13509.
84. Köhler, V.; Wilson, Y. M.; Dürrenberger, M.; Ghislieri, D.; Churakova, E.; Quinto, T.; Knörr, L.; Häussinger, D.; Hollmann, F.; Turner, N. J.; Ward, T. R., Synthetic cascades are enabled by combining biocatalysts with artificial metalloenzymes. *Nature Chemistry* **2012,** *5*, 93.
85. Liang, A. D.; Serrano-Plana, J.; Peterson, R. L.; Ward, T. R., Artificial Metalloenzymes Based on the Biotin–Streptavidin Technology: Enzymatic Cascades and Directed Evolution. *Accounts of Chemical Research* **2019,** *52* (3), 585-595.
86. Reetz, M. T.; Peyralans, J. J. P.; Maichele, A.; Fu, Y.; Maywald, M., Directed evolution of hybrid enzymes: Evolving enantioselectivity of an achiral Rh-complex anchored to a protein. *Chemical Communications* **2006,** (41), 4318-4320.
87. Knoevenagel, E.; Bergdolt, B., Ueber das Verhalten des Δ2.5-Dihydroterephtalsäuredimethylesters bei höheren Temperaturen und in Gegenwart von Palladiummohr. *Berichte der deutschen chemischen Gesellschaft* **1903,** *36* (3), 2857-2860.
88. Wang, D.; Astruc, D., The Golden Age of Transfer Hydrogenation. *Chemical Reviews* **2015,** *115* (13), 6621-6686.
89. Meerwein, H.; Schmidt, R., Ein neues Verfahren zur Reduktion von Aldehyden und Ketonen. *Justus Liebigs Annalen der Chemie* **1925,** *444* (1), 221-238.
90. Verley, A., Sur l'echange de groupements fonctionnels entre deux molecules. Passage de la fonction alcool a la fonction aldehyde et inversement. *Bull. Soc. Chim. Fr* **1925,** *37*, 537-542.
91. Trocha-Grimshaw, J.; Henbest, H. B., Catalysis of the transfer of hydrogen from propan-2-ol to αβ-unsaturated ketones by organoiridium compounds. A carbon–iridium compound containing a chelate keto-group. *Chemical Communications (London)* **1967,** (11), 544-544.
92. McPartlin, M.; Mason, R., The structure of a bis(dimethyl sulphoxide)iridium(III) complex containing a metal–carbon σ-bond. *Chemical Communications (London)* **1967,** (11), 545-546.
93. Sasson, Y.; Blum, J., Homogeneous catalytic transfer-hydrogenation of α,β-unsaturated carbonyl compounds by dichlorotris(triphenylphosphine)ruthenium (II). *Tetrahedron Letters* **1971,** *12* (24), 2167-2170.
94. Blum, J.; Sasson, Y.; Iflah, S., Hydrogen transfer from formyl compounds to α,β-unsaturated ketones catalyzed by Ru, Rh and Ir complexes. *Tetrahedron Letters* **1972,** *13* (11), 1015-1018.
95. Sasson, Y.; Blum, J., Dichlorotris(triphenylphosphine)ruthenium-catalyzed hydrogen transfer from alcohols to saturated and .alpha.,.beta.-unsaturated ketones. *The Journal of Organic Chemistry* **1975,** *40* (13), 1887-1896.
96. Noyori, R.; Hashiguchi, S., Asymmetric Transfer Hydrogenation Catalyzed by Chiral Ruthenium Complexes. *Accounts of Chemical Research* **1997,** *30* (2), 97-102.
97. Noyori, R.; Sandoval, C. A.; Muniz, K.; Ohkuma, T., Metal-ligand bifunctional catalysis for asymmetric hydrogenation. *Philos Trans A Math Phys Eng Sci* **2005,** *363* (1829), 901-12; discussion 1035-40.

98. Ikariya, T.; Murata, K.; Noyori, R., Bifunctional transition metal-based molecular catalysts for asymmetric syntheses. *Org Biomol Chem* **2006,** *4* (3), 393-406.
99. Vineyard, B. D.; Knowles, W. S.; Sabacky, M. J.; Bachman, G. L.; Weinkauff, D. J., Asymmetric hydrogenation. Rhodium chiral bisphosphine catalyst. *Journal of the American Chemical Society* **1977,** *99* (18), 5946-5952.
100. Canivet, J.; Suss-Fink, G., Water-soluble arene ruthenium catalysts containing sulfonated diamine ligands for asymmetric transfer hydrogenation of [small alpha]-aryl ketones and imines in aqueous solution. *Green Chemistry* **2007,** *9* (4), 391-397.
101. Wang, C.; Li, C.; Wu, X.; Pettman, A.; Xiao, J., pH-Regulated Asymmetric Transfer Hydrogenation of Quinolines in Water. *Angewandte Chemie International Edition* **2009,** *48* (35), 6524-6528.
102. Tang, Y.; Li, X.; Lian, C.; Zhu, J.; Deng, J., Synthesis of a water-soluble cationic chiral diamine ligand bearing a diguanidinium and application in asymmetric transfer hydrogenation. *Tetrahedron: Asymmetry* **2011,** *22* (14–15), 1530-1535.
103. Wang, L.; Zhou, Q.; Qu, C.; Wang, Q.; Cun, L.; Zhu, J.; Deng, J., Efficient asymmetric transfer hydrogenation of N-sulfonylimines on water. *Tetrahedron* **2013,** *69* (31), 6500-6506.
104. List, B., Proline-catalyzed asymmetric reactions. *Tetrahedron* **2002,** *58* (28), 5573-5590.
105. Mayer, S.; List, B., Asymmetric Counteranion-Directed Catalysis. *Angewandte Chemie International Edition* **2006,** *45* (25), 4193-4195.
106. Yang, J. W.; List, B., Catalytic Asymmetric Transfer Hydrogenation of α-Ketoesters with Hantzsch Esters. *Organic Letters* **2006,** *8* (24), 5653-5655.
107. Michrowska, A.; List, B., Concise synthesis of ricciocarpin A and discovery of a more potent analogue. *Nature Chemistry* **2009,** *1* (3), 225-228.
108. Northrup, A. B.; MacMillan, D. W. C., The First General Enantioselective Catalytic Diels−Alder Reaction with Simple α,β-Unsaturated Ketones. *Journal of the American Chemical Society* **2002,** *124* (11), 2458-2460.
109. Huang, Y.; Walji, A. M.; Larsen, C. H.; MacMillan, D. W. C., Enantioselective Organo-Cascade Catalysis. *Journal of the American Chemical Society* **2005,** *127* (43), 15051-15053.
110. Ouellet, S. G.; Walji, A. M.; Macmillan, D. W. C., Enantioselective Organocatalytic Transfer Hydrogenation Reactions using Hantzsch Esters. *Accounts of Chemical Research* **2007,** *40* (12), 1327-1339.
111. Zheng, C.; You, S.-L., Transfer hydrogenation with Hantzsch esters and related organic hydride donors. *Chemical Society Reviews* **2012,** *41* (6), 2498-2518.
112. Williams, R. E.; Bruce, N. C., 'New uses for an Old Enzyme' – the Old Yellow Enzyme family of flavoenzymes. *Microbiology* **2002,** *148* (6), 1607-1614.
113. Peters, C.; Kölzsch, R.; Kadow, M.; Skalden, L.; Rudroff, F.; Mihovilovic, M. D.; Bornscheuer, U. T., Identification, Characterization, and Application of Three Enoate Reductases from Pseudomonas putida in In Vitro Enzyme Cascade Reactions. *ChemCatChem* **2014,** *6* (4), 1021-1027.
114. Hulley, M. E.; Toogood, H. S.; Fryszkowska, A.; Mansell, D.; Stephens, G. M.; Gardiner, J. M.; Scrutton, N. S., Focused Directed Evolution of

Pentaerythritol Tetranitrate Reductase by Using Automated Anaerobic Kinetic Screening of Site-Saturated Libraries. *ChemBioChem* **2010,** *11* (17), 2433-2447.
115. Spiegelhauer, O.; Dickert, F.; Mende, S.; Niks, D.; Hille, R.; Ullmann, M.; Dobbek, H., Kinetic Characterization of Xenobiotic Reductase A from Pseudomonas putida 86. *Biochemistry* **2009,** *48* (48), 11412-11420.
116. Spiegelhauer, O.; Mende, S.; Dickert, F.; Knauer, S. H.; Ullmann, G. M.; Dobbek, H., Cysteine as a Modulator Residue in the Active Site of Xenobiotic Reductase A: A Structural, Thermodynamic and Kinetic Study. *Journal of Molecular Biology* **2010,** *398* (1), 66-82.
117. Spiegelhauer, O.; Werther, T.; Mende, S.; Knauer, S. H.; Dobbek, H., Determinants of Substrate Binding and Protonation in the Flavoenzyme Xenobiotic Reductase A. *Journal of Molecular Biology* **2010,** *403* (2), 286-298.
118. Paul, C. E.; Gargiulo, S.; Opperman, D. J.; Lavandera, I.; Gotor-Fernández, V.; Gotor, V.; Taglieber, A.; Arends, I. W. C. E.; Hollmann, F., Mimicking Nature: Synthetic Nicotinamide Cofactors for C═C Bioreduction Using Enoate Reductases. *Organic Letters* **2013,** *15* (1), 180-183.
119. Geddes, A.; Paul, C. E.; Hay, S.; Hollmann, F.; Scrutton, N. S., Donor–Acceptor Distance Sampling Enhances the Performance of "Better than Nature" Nicotinamide Coenzyme Biomimetics. *Journal of the American Chemical Society* **2016,** *138* (35), 11089-11092.
120. Knaus, T.; Paul, C. E.; Levy, C. W.; de Vries, S.; Mutti, F. G.; Hollmann, F.; Scrutton, N. S., Better than Nature: Nicotinamide Biomimetics That Outperform Natural Coenzymes. *Journal of the American Chemical Society* **2016,** *138* (3), 1033-1039.
121. Löw, S. A.; Löw, I. M.; Weissenborn, M. J.; Hauer, B., Enhanced Ene-Reductase Activity through Alteration of Artificial Nicotinamide Cofactor Substituents. *ChemCatChem* **2016,** *8* (5), 911-915.
122. Joerg H. Schrittwiser, S. V., and Wolfgang Kroutil, Biocatalytic Imine Reduction and Reductive Amination of Ketones. In *Advanced Synthesis and Catalysis*, May 7, 2015 ed.; 2015; Vol. 357, pp 1665-1685.
123. De-Eknamkul, W.; Zenk, M. H., Enzymic formation of (R)-reticuline from 1,2-dehydroreticuline in the opium poppy plant. *Tetrahedron Letters* **1990,** *31* (34), 4855-4858.
124. Wallwey, C.; Matuschek, M.; Xie, X.-L.; Li, S.-M., Ergot alkaloid biosynthesis in Aspergillus fumigatus: Conversion of chanoclavine-I aldehyde to festuclavine by the festuclavine synthase FgaFS in the presence of the old yellow enzyme FgaOx3. *Organic & Biomolecular Chemistry* **2010,** *8* (15), 3500-3508.
125. Adams, E.; Frank, L., Metabolism of Proline and the Hydroxyprolines. *Annual Review of Biochemistry* **1980,** *49* (1), 1005-1061.
126. Vaijayanthi, T.; Chadha, A., Asymmetric reduction of aryl imines using Candida parapsilosis ATCC 7330. *Tetrahedron: Asymmetry* **2008,** *19* (1), 93-96.
127. Mitsukura, K.; Suzuki, M.; Tada, K.; Yoshida, T.; Nagasawa, T., Asymmetric synthesis of chiral cyclic amine from cyclic imine by bacterial whole-cell catalyst of enantioselective imine reductase. *Organic & Biomolecular Chemistry* **2010,** *8* (20), 4533-4535.
128. Mitsukura, K.; Suzuki, M.; Shinoda, S.; Kuramoto, T.; Yoshida, T.; Nagasawa, T., Purification and Characterization of a Novel (<I>R</I>)-Imine

Reductase from <I>Streptomyces</I> sp. GF3587. *Bioscience, Biotechnology, and Biochemistry* **2011,** *75* (9), 1778-1782.
129. Leipold, F.; Hussain, S.; Ghislieri, D.; Turner, N. J., Asymmetric Reduction of Cyclic Imines Catalyzed by a Whole-Cell Biocatalyst Containing an (S)-Imine Reductase. *ChemCatChem* **2013,** *5* (12), 3505-3508.
130. Rodríguez-Mata, M.; Frank, A.; Wells, E.; Leipold, F.; Turner, N. J.; Hart, S.; Turkenburg, J. P.; Grogan, G., Structure and Activity of NADPH-Dependent Reductase Q1EQE0 from Streptomyces kanamyceticus, which Catalyses the R-Selective Reduction of an Imine Substrate. *ChemBioChem* **2013,** *14* (11), 1372-1379.
131. Hussain, S.; Leipold, F.; Man, H.; Wells, E.; France, S. P.; Mulholland, K. R.; Grogan, G.; Turner, N. J., An (R)-Imine Reductase Biocatalyst for the Asymmetric Reduction of Cyclic Imines. *ChemCatChem* **2015,** *7* (4), 579-583.
132. Grogan, G.; Turner, N. J., InspIRED by Nature: NADPH-Dependent Imine Reductases (IREDs) as Catalysts for the Preparation of Chiral Amines. *Chemistry – A European Journal* **2016,** *22* (6), 1900-1907.
133. Dürrenberger, M.; Heinisch, T.; Wilson, Y. M.; Rossel, T.; Nogueira, E.; Knörr, L.; Mutschler, A.; Kersten, K.; Zimbron, M. J.; Pierron, J.; Schirmer, T.; Ward, T. R., Artificial Transfer Hydrogenases for the Enantioselective Reduction of Cyclic Imines. *Angewandte Chemie International Edition* **2011,** *50* (13), 3026-3029.
134. Gamenara, D.; Domínguez de María, P., Enantioselective imine reduction catalyzed by imine reductases and artificial metalloenzymes. *Organic & Biomolecular Chemistry* **2014,** *12* (19), 2989-2992.
135. Hestericová, M.; Heinisch, T.; Alonso-Cotchico, L.; Maréchal, J.-D.; Vidossich, P.; Ward, T. R., Directed Evolution of an Artificial Imine Reductase. *Angewandte Chemie International Edition* **2018,** *57* (7), 1863-1868.
136. Raines, D. J.; Clarke, J. E.; Blagova, E. V.; Dodson, E. J.; Wilson, K. S.; Duhme-Klair, A.-K., Redox-switchable siderophore anchor enables reversible artificial metalloenzyme assembly. *Nature Catalysis* **2018,** *1* (9), 680-688.
137. Sello, G.; Orsini, F., Alcohol and 1,2-Diol Dehydrogenases: Synthetic Use in the Preparation of Chiral Alcohols by Carbonyl Reduction. *Mini-Reviews in Organic Chemistry* **2006,** *3* (1), 37-47.
138. Hollmann, F.; Arends, I. W. C. E.; Holtmann, D., Enzymatic reductions for the chemist. *Green Chemistry* **2011,** *13* (9), 2285-2314.
139. Letondor, C.; Humbert, N.; Ward, T. R., Artificial metalloenzymes based on biotin-avidin technology for the enantioselective reduction of ketones by transfer hydrogenation. *Proceedings of the National Academy of Sciences of the United States of America* **2005,** *102* (13), 4683-4687.
140. Madern, N.; Queyriaux, N.; Chevalley, A.; Ghasemi, M.; Nicolotti, O.; Ciofini, I.; Mangiatordi, G. F.; Salmain, M., Piano-stool d6-rhodium(III) complexes of chelating pyridine-based ligands and their papain bioconjugates for the catalysis of transfer hydrogenation of aryl ketones in aqueous medium. *Journal of Molecular Catalysis B: Enzymatic* **2015,** *122*, 314-322.
141. Truppo, M. D., 7.4 Cofactor Recycling for Enzyme Catalyzed Processes. In *Comprehensive Chirality*, Carreira, E. M.; Yamamoto, H., Eds. Elsevier: Amsterdam, 2012; pp 46-70.

142. Hollmann, F.; Schmid, A., Electrochemical Regeneration of Oxidoreductases for Cell-free Biocatalytic Redox Reactions. *Biocatalysis and Biotransformation* **2004,** *22* (2), 63-88.
143. Hollmann, F.; Hofstetter, K.; Schmid, A., Non-enzymatic regeneration of nicotinamide and flavin cofactors for monooxygenase catalysis. *Trends in Biotechnology* **2006,** *24* (4), 163-171.
144. Yuan, R.; Watanabe, S.; Kuwabata, S.; Yoneyama, H., Asymmetric Electroreduction of Ketone and Aldehyde Derivatives to the Corresponding Alcohols Using Alcohol Dehydrogenase as an Electrocatalyst. *The Journal of Organic Chemistry* **1997,** *62* (8), 2494-2499.
145. Hilt, G.; Jarbawi, T.; Heineman, W. R.; Steckhan, E., An Analytical Study of the Redox Behavior of 1,10-Phenanthroline-5,6-dione, its Transition-Metal Complexes, and its N-Monomethylated Derivative with regard to their Efficiency as Mediators of NAD(P)+ Regeneration. *Chemistry - A European Journal* **1997,** *3* (1), 79-88.
146. Wu, H.; Tian, C.; Song, X.; Liu, C.; Yang, D.; Jiang, Z., Methods for the regeneration of nicotinamide coenzymes. *Green Chemistry* **2013,** *15* (7), 1773-1789.
147. Willner, I.; Mandler, D., Enzyme-catalysed biotransformations through photochemical regeneration of nicotinamide cofactors. *Enzyme and Microbial Technology* **1989,** *11* (8), 467-483.
148. Taglieber, A.; Schulz, F.; Hollmann, F.; Rusek, M.; Reetz, M. T., Light-Driven Biocatalytic Oxidation and Reduction Reactions: Scope and Limitations. *ChemBioChem* **2008,** *9* (4), 565-572.
149. Sengupta, A.; Sunder, A. V.; Sohoni, S. V.; Wangikar, P. P., The effect of CO2 in enhancing photosynthetic cofactor recycling for alcohol dehydrogenase mediated chiral synthesis in cyanobacteria. *Journal of Biotechnology* **2019,** *289*, 1-6.
150. Steckhan, E.; Herrmann, S.; Ruppert, R.; Thömmes, J.; Wandrey, C., Continuous Generation of NADH from NAD⊕ and Formate Using a Homogeneous Catalyst with Enhanced Molecular Weight in a Membrane Reactor. *Angewandte Chemie International Edition in English* **1990,** *29* (4), 388-390.
151. Steckhan, E.; Herrmann, S.; Ruppert, R.; Dietz, E.; Frede, M.; Spika, E., Analytical study of a series of substituted (2,2'-bipyridyl)(pentamethylcyclopentadienyl)rhodium and -iridium complexes with regard to their effectiveness as redox catalysts for the indirect electrochemical and chemical reduction of NAD(P)+. *Organometallics* **1991,** *10* (5), 1568-1577.
152. Lo, H. C.; Leiva, C.; Buriez, O.; Kerr, J. B.; Olmstead, M. M.; Fish, R. H., Bioorganometallic Chemistry. 13. Regioselective Reduction of NAD+ Models, 1-Benzylnicotinamde Triflate and β-Nicotinamide Ribose-5'-methyl Phosphate, with in Situ Generated [Cp*Rh(Bpy)H]+: Structure−Activity Relationships, Kinetics, and Mechanistic Aspects in the Formation of the 1,4-NADH Derivatives. *Inorganic Chemistry* **2001,** *40* (26), 6705-6716.
153. Lo, H. C.; Fish, R. H., Biomimetic NAD+ Models for Tandem Cofactor Regeneration, Horse Liver Alcohol Dehydrogenase Recognition of 1,4-NADH Derivatives, and Chiral Synthesis. *Angewandte Chemie International Edition* **2002,** *41* (3), 478-481.
154. Lutz, J.; Hollmann, F.; Ho, T. V.; Schnyder, A.; Fish, R. H.; Schmid, A., Bioorganometallic chemistry: biocatalytic oxidation reactions with biomimetic

NAD+/NADH co-factors and [Cp*Rh(bpy)H]+ for selective organic synthesis. *Journal of Organometallic Chemistry* **2004,** *689* (25), 4783-4790.
155. Lo, H. C.; Ryan, J. D.; Kerr, J. B.; Clark, D. S.; Fish, R. H., Bioorganometallic chemistry: Co-factor regeneration, enzyme recognition of biomimetic 1,4-NADH analogs, and organic synthesis; tandem catalyzed regioselective formation of N-substituted-1,4-dihydronicotinamide derivatives with [Cp*Rh(bpy)H]+, coupled to chiral S-alcohol formation with HLADH, and engineered cytochrome P450s, for selective C-H oxidation reactions. *Journal of Organometallic Chemistry* **2017,** *839*, 38-52.
156. Bradshaw, C. W.; Hummel, W.; Wong, C. H., Lactobacillus kefir alcohol dehydrogenase: a useful catalyst for synthesis. *The Journal of Organic Chemistry* **1992,** *57* (5), 1532-1536.
157. Nakamura, K.; Matsuda, T., Asymmetric Reduction of Ketones by the Acetone Powder of Geotrichum candidum. *The Journal of Organic Chemistry* **1998,** *63* (24), 8957-8964.
158. Bastos, F. d. M.; dos Santos, A. G.; Jones, J.; Oestreicher, E. G.; Pinto, G. F.; Paiva, L. M. C., Three different coupled enzymatic systems for in situ regeneration of NADPH. *Biotechnology Techniques* **1999,** *13* (10), 661-664.
159. Bastos, F. M.; França, T. K.; Machado, G. D. C.; Pinto, G. F.; Oestreicher, E. G.; Paiva, L. M. C., Kinetic modelling of coupled redox enzymatic systems for in situ regeneration of NADPH. *Journal of Molecular Catalysis B: Enzymatic* **2002,** *19-20*, 459-465.
160. Aalbers, F. S.; Fraaije, M. W., Design of Artificial Alcohol Oxidases: Alcohol Dehydrogenase–NADPH Oxidase Fusions for Continuous Oxidations. *ChemBioChem* **2019,** *20* (1), 51-56.
161. Tishkov, V. I.; Popov, V. O., Catalytic mechanism and application of formate dehydrogenase. *Biochemistry (Moscow)* **2004,** *69* (11), 1252-1267.
162. Bommarius, A. S.; Schwarm, M.; Drauz, K., Biocatalysis to amino acid-based chiral pharmaceuticals—examples and perspectives. *Journal of Molecular Catalysis B: Enzymatic* **1998,** *5* (1), 1-11.
163. Slusarczyk, H.; Felber, S.; Kula, M. R.; Pohl, M., Stabilization of NAD-dependent formate dehydrogenase from Candida boidinii by site-directed mutagenesis of cysteine residues. *European Journal of Biochemistry* **2000,** *267* (5), 1280-1289.
164. Mayol, O.; David, S.; Darii, E.; Debard, A.; Mariage, A.; Pellouin, V.; Petit, J.-L.; Salanoubat, M.; de Berardinis, V.; Zaparucha, A.; Vergne-Vaxelaire, C., Asymmetric reductive amination by a wild-type amine dehydrogenase from the thermophilic bacteria Petrotoga mobilis. *Catalysis Science & Technology* **2016,** *6* (20), 7421-7428.
165. Yanto, Y.; Yu, H.-H.; Hall, M.; Bommarius, A. S., Characterization of xenobiotic reductase A (XenA): study of active site residues, substrate spectrum and stability. *Chemical Communications* **2010,** *46* (46), 8809-8811.
166. Zhang, Y.; Yao, P.; Cui, Y.; Wu, Q.; Zhu, D., One-Pot Enzymatic Synthesis of Cyclic Vicinal Diols from Aliphatic Dialdehydes via Intramolecular C−C Bond Formation and Carbonyl Reduction Using Pyruvate Decarboxylases and Alcohol Dehydrogenases. *Advanced Synthesis & Catalysis* **2018,** *360* (21), 4191-4196.
167. Li, H.; Xiao, W.; Xie, P.; Zheng, L., Co-immobilization of enoate reductase with a cofactor-recycling partner enzyme. *Enzyme and Microbial Technology* **2018,** *109*, 66-73.

168. Howe, G. W.; van der Donk, W. A., Temperature independent kinetic isotope effects as evidence for a Marcus-like model of hydride tunneling in phosphite dehydrogenase. *Biochemistry* **2019**.
169. Assil-Companioni, L.; Schmidt, S.; Heidinger, P.; Schwab, H.; Kourist, R., Hydrogen-Driven Cofactor Regeneration for Stereoselective Whole-Cell C=C Bond Reduction in Cupriavidus necator. *ChemSusChem* **2019,** *12* (11), 2361-2365.
170. Bornadel, A.; Hatti-Kaul, R.; Hollmann, F.; Kara, S., A Bi-enzymatic Convergent Cascade for ε-Caprolactone Synthesis Employing 1,6-Hexanediol as a 'Double-Smart Cosubstrate'. *ChemCatChem* **2015,** *7* (16), 2442-2445.
171. Vallee, B. L.; Hoch, F. L., Yeast Alcohol Dehydrogenase, A Zinc Metalloenzyme. *Journal of the American Chemical Society* **1955,** *77* (3), 821-822.
172. Wills, C.; Martin, T., Alteration in the redox balance of yeast leads to allyl alcohol resistance. *FEBS Letters* **1980,** *119* (1), 105-108.
173. Wang, S.; Nie, Y.; Xu, Y.; Zhang, R.; Ko, T.-P.; Huang, C.-H.; Chan, H.-C.; Guo, R.-T.; Xiao, R., Unconserved substrate-binding sites direct the stereoselectivity of medium-chain alcohol dehydrogenase. *Chemical Communications* **2014,** *50* (58), 7770-7772.
174. Mansell, D. J.; Toogood, H. S.; Waller, J.; Hughes, J. M. X.; Levy, C. W.; Gardiner, J. M.; Scrutton, N. S., Biocatalytic Asymmetric Alkene Reduction: Crystal Structure and Characterization of a Double Bond Reductase from Nicotiana tabacum. *ACS catalysis* **2013,** *3* (3), 370-379.
175. Kato-Noguchi, H., Wounding stress induces alcohol dehydrogenase in maize and lettuce seedlings. *Plant Growth Regulation* **2001,** *35* (3), 285-288.
176. Stavrinides, A. K.; Tatsis, E. C.; Dang, T.-T.; Caputi, L.; Stevenson, C. E. M.; Lawson, D. M.; Schneider, B.; O'Connor, S. E., Discovery of a Short-Chain Dehydrogenase from Catharanthus roseus that Produces a New Monoterpene Indole Alkaloid. *ChemBioChem* **2018,** *19* (9), 940-948.
177. Peng, H.-P.; Chan, C.-S.; Shih, M.-C.; Yang, S. F., Signaling Events in the Hypoxic Induction of Alcohol Dehydrogenase Gene in Arabidopsis. *Plant Physiology* **2001,** *126* (2), 742-749.
178. Anthony, C.; Zatman, L., The microbial oxidation of methanol. The alcohol dehydrogenase of Pseudomonas sp. M27. *Biochemical Journal* **1965,** *96* (3), 808-812.
179. Kersters, K.; De Ley, J., Primary and secondary alcohol dehydrogenases from Gluconobacter. In *Methods in Enzymology*, Academic Press: 1966; Vol. 9, pp 346-354.
180. Jornvall, H.; Hoog, J.-O., Nomenclature of Alcohol Dehydrogenases. *Alcohol and Alcoholism* **1995,** *30* (2), 153-161.
181. Staab, C. A.; Hellgren, M.; Höög, J.-O., Medium- and short-chain dehydrogenase/reductase gene and protein families. *Cellular and Molecular Life Sciences* **2008,** *65* (24), 3950.
182. Farrés, J.; Moreno, A.; Crosas, B.; Peralba, J. M.; Allali-Hassani, A.; Hjelmqvist, L.; Jörnvall, H.; Parés, X., Alcohol Dehydrogenase of Class IV (σσ-ADH) from Human Stomach. *European Journal of Biochemistry* **1994,** *224* (2), 549-557.
183. Ursprung, H.; Leone, J., Alcohol dehydrogenases: A polymorphism in Drosophila melanogaster. *Journal of Experimental Zoology* **1965,** *160* (2), 147-154.

184. Reid, M. F.; Fewson, C. A., Molecular Characterization of Microbial Alcohol Dehydrogenases. *Critical Reviews in Microbiology* **1994,** *20* (1), 13-56.
185. Smidt, O. D.; Preez, J. C. D.; Albertyn, J., The alcohol dehydrogenases of Saccharomyces cerevisiae: a comprehensive review. *FEMS Yeast Research* **2008,** *8* (7), 967-978.
186. Wang, N.; Shi, H.; Yao, Q.; Zhou, Y.; Kang, L.; Chen, H.; Chen, K., Cloning, expression and characterization of alcohol dehydrogenases in the silkworm Bombyx mori. *Genetics and Molecular Biology* **2011,** *34*, 240-243.
187. Benach, J.; Atrian, S. l.; Gonzàlez-Duarte, R.; Ladenstein, R., The refined crystal structure of Drosophila lebanonensis alcohol dehydrogenase at 1.9 å resolution11Edited by R. Huber. *Journal of Molecular Biology* **1998,** *282* (2), 383-399.
188. Benach, J.; Atrian, S. l.; Gonzàlez-Duarte, R.; Ladenstein, R., The catalytic reaction and inhibition mechanism of Drosophila alcohol dehydrogenase: observation of an enzyme-bound NAD-ketone adduct at 1.4 Å resolution by X-ray crystallography11Edited by R. Huber. *Journal of Molecular Biology* **1999,** *289* (2), 335-355.
189. Persson, B.; Krook, M.; JÖRnvall, H., Characteristics of short-chain alcohol dehydrogenases and related enzymes. *European Journal of Biochemistry* **1991,** *200* (2), 537-543.
190. Persson, B.; Kallberg, Y.; Bray, J. E.; Bruford, E.; Dellaporta, S. L.; Favia, A. D.; Duarte, R. G.; Jörnvall, H.; Kavanagh, K. L.; Kedishvili, N.; Kisiela, M.; Maser, E.; Mindnich, R.; Orchard, S.; Penning, T. M.; Thornton, J. M.; Adamski, J.; Oppermann, U., The SDR (short-chain dehydrogenase/reductase and related enzymes) nomenclature initiative. *Chemico-Biological Interactions* **2009,** *178* (1), 94-98.
191. Kallberg, Y.; Oppermann, U.; Jörnvall, H.; Persson, B., Short-chain dehydrogenases/reductases (SDRs). *European Journal of Biochemistry* **2002,** *269* (18), 4409-4417.
192. Filling, C.; Berndt, K. D.; Benach, J.; Knapp, S.; Prozorovski, T.; Nordling, E.; Ladenstein, R.; Jörnvall, H.; Oppermann, U., Critical Residues for Structure and Catalysis in Short-chain Dehydrogenases/Reductases. *Journal of Biological Chemistry* **2002,** *277* (28), 25677-25684.
193. Kavanagh, K. L.; Jörnvall, H.; Persson, B.; Oppermann, U., Medium- and short-chain dehydrogenase/reductase gene and protein families. *Cellular and Molecular Life Sciences* **2008,** *65* (24), 3895.
194. Korkhin, Y.; Kalb, A. J.; Peretz, M.; Bogin, O.; Burstein, Y.; Frolow, F., NADP-dependent bacterial alcohol dehydrogenases: crystal structure, cofactor-binding and cofactor specificity of the ADHs of Clostridium beijerinckii and Thermoanaerobacter brockii11Edited by R. Huber. *Journal of Molecular Biology* **1998,** *278* (5), 967-981.
195. Raj, S. B.; Ramaswamy, S.; Plapp, B. V., Yeast Alcohol Dehydrogenase Structure and Catalysis. *Biochemistry* **2014,** *53* (36), 5791-5803.
196. Wills, C.; Kratofil, P.; Londo, D.; Martin, T., Characterization of the two alcohol dehydrogenases of Zymomonas mobilis. *Archives of Biochemistry and Biophysics* **1981,** *210* (2), 775-785.
197. Scopes, R. K., An iron-activated alcohol dehydrogenase. *FEBS Letters* **1983,** *156* (2), 303-306.

198. Moon, J.-H.; Lee, H.-J.; Park, S.-Y.; Song, J.-M.; Park, M.-Y.; Park, H.-M.; Sun, J.; Park, J.-H.; Kim, B. Y.; Kim, J.-S., Structures of Iron-Dependent Alcohol Dehydrogenase 2 from Zymomonas mobilis ZM4 with and without NAD+ Cofactor. *Journal of Molecular Biology* **2011,** *407* (3), 413-424.
199. Williamson, V. M.; Paquin, C. E., Homology of Saccharomyces cerevisiae ADH4 to an iron-activated alcohol dehydrogenase from Zymomonas mobilis. *Molecular and General Genetics MGG* **1987,** *209* (2), 374-381.
200. Eklund, H.; Plapp, B. V.; Samama, J. P.; Brändén, C. I., Binding of substrate in a ternary complex of horse liver alcohol dehydrogenase. *Journal of Biological Chemistry* **1982,** *257* (23), 14349-58.
201. Johansson, A.; Mosbach, K.; Månsson, M.-O., Horse Liver Alcohol Dehydrogenase can Accept NADP+ as Coenzyme in High Concentrations of Acetonitrile. *European Journal of Biochemistry* **1995,** *227* (1-2), 551-555.
202. Olson, L. P.; Luo, J.; Almarsson, Ö.; Bruice, T. C., Mechanism of Aldehyde Oxidation Catalyzed by Horse Liver Alcohol Dehydrogenase. *Biochemistry* **1996,** *35* (30), 9782-9791.
203. Lee, C.; Bedgar, D. L.; Davin, L. B.; Lewis, N. G., Assessment of a putative proton relay in Arabidopsis cinnamyl alcohol dehydrogenase catalysis. *Organic & Biomolecular Chemistry* **2013,** *11* (7), 1127-1134.
204. Kleifeld, O.; Shi, S. P.; Zarivach, R.; Eisenstein, M.; Sagi, I., The conserved Glu-60 residue in Thermoanaerobacter brockii alcohol dehydrogenase is not essential for catalysis. *Protein Science* **2003,** *12* (3), 468-479.
205. Benner, S. A., The stereoselectivity of alcohol dehydrogenases: A sterochemical imperative? *Experientia* **1982,** *38* (5), 633-637.
206. Cahn, R. S.; Ingold, C.; Prelog, V., Specification of Molecular Chirality. *Angewandte Chemie International Edition in English* **1966,** *5* (4), 385-415.
207. You, K.-s.; Arnold, L. J.; Allison, W. S.; Kaplan, N. O., Enzyme stereospecificities for nicotinamide nucleotides. *Trends in Biochemical Sciences* **1978,** *3* (4), 265-268.
208. Williams, T. N.; Van Den Driessche, G. A.; Valery, A. R. B.; Fourches, D.; Freeman, H. S., Toward the Rational Design of Sustainable Hair Dyes Using Cheminformatics Approaches: Step 2. Identification of Hair Dye Substance Database Analogs in the Max Weaver Dye Library. *ACS Sustainable Chemistry & Engineering* **2018,** *6* (11), 14248-14256.
209. Trott, O.; Olson, A. J., AutoDock Vina: Improving the speed and accuracy of docking with a new scoring function, efficient optimization, and multithreading. *Journal of Computational Chemistry* **2010,** *31* (2), 455-461.
210. Ban, F.; Dalal, K.; Li, H.; LeBlanc, E.; Rennie, P. S.; Cherkasov, A., Best Practices of Computer-Aided Drug Discovery: Lessons Learned from the Development of a Preclinical Candidate for Prostate Cancer with a New Mechanism of Action. *Journal of Chemical Information and Modeling* **2017,** *57* (5), 1018-1028.
211. Grate, J. W.; Mo, K. F.; Daily, M. D., Triazine-Based Sequence-Defined Polymers with Side-Chain Diversity and Backbone–Backbone Interaction Motifs. *Angewandte Chemie International Edition* **2016,** *55* (12), 3925-3930.
212. Huo, H.; Zhou, Z.; Zhang, A.; Wu, L., Ruthenium(II)-catalyzed transfer hydrogenation of aldehydes with new water-soluble monotosylated

ethylenediamines as ligands. *Research on Chemical Intermediates* **2012,** *38* (1), 261-268.
213. Ipe, B. I.; Yoosaf, K.; Thomas, K. G., Functionalized Gold Nanoparticles as Phosphorescent Nanomaterials and Sensors. *Journal of the American Chemical Society* **2006,** *128* (6), 1907-1913.
214. Steinbrecher, T.; Zhu, C.; Wang, L.; Abel, R.; Negron, C.; Pearlman, D.; Feyfant, E.; Duan, J.; Sherman, W., Predicting the Effect of Amino Acid Single-Point Mutations on Protein Stability—Large-Scale Validation of MD-Based Relative Free Energy Calculations. *Journal of Molecular Biology* **2017,** *429* (7), 948-963.
215. Olsson, M. H. M.; Søndergaard, C. R.; Rostkowski, M.; Jensen, J. H., PROPKA3: Consistent Treatment of Internal and Surface Residues in Empirical pKa Predictions. *Journal of Chemical Theory and Computation* **2011,** *7* (2), 525-537.
216. Harder, E.; Damm, W.; Maple, J.; Wu, C.; Reboul, M.; Xiang, J. Y.; Wang, L.; Lupyan, D.; Dahlgren, M. K.; Knight, J. L.; Kaus, J. W.; Cerutti, D. S.; Krilov, G.; Jorgensen, W. L.; Abel, R.; Friesner, R. A., OPLS3: A Force Field Providing Broad Coverage of Drug-like Small Molecules and Proteins. *Journal of Chemical Theory and Computation* **2016,** *12* (1), 281-296.
217. Morra, S.; Pordea, A., Biocatalyst–artificial metalloenzyme cascade based on alcohol dehydrogenase. *Chemical Science* **2018,** *9* (38), 7447-7454.
218. Peng, B.; Liu, C.; Li, Z.; Day, J. J.; Lu, Y.; Lefer, D. J.; Xian, M., Slow generation of hydrogen sulfide from sulfane sulfurs and NADH models. *Bioorganic & Medicinal Chemistry Letters* **2017,** *27* (3), 542-545.
219. Wu, J.; Wang, F.; Ma, Y.; Cui, X.; Cun, L.; Zhu, J.; Deng, J.; Yu, B., Asymmetric transfer hydrogenation of imines and iminiums catalyzed by a water-soluble catalyst in water. *Chemical Communications* **2006,** (16), 1766-1768.
220. Li, L.; Wu, J.; Wang, F.; Liao, J.; Zhang, H.; Lian, C.; Zhu, J.; Deng, J., Asymmetric transfer hydrogenation of ketones and imines with novel water-soluble chiral diamine as ligand in neat water. *Green Chemistry* **2007,** *9* (1), 23-25.
221. Haraguchi, N.; Tsuru, K.; Arakawa, Y.; Itsuno, S., Asymmetric transfer hydrogenation of imines catalyzed by a polymer-immobilized chiral catalyst. *Organic & Biomolecular Chemistry* **2009,** *7* (1), 69-75.
222. Peretz, M.; Bogin, O.; Tel-Or, S.; Cohen, A.; Li, G.; Chen, J.-S.; Burstein, Y., Molecular Cloning, Nucleotide Sequencing, and Expression of Genes Encoding Alcohol Dehydrogenases From the ThermophileThermoanaerobacter brockiiand the MesophileClostridium beijerinckii. *Anaerobe* **1997,** *3* (4), 259-270.
223. Ellman, G. L., Tissue sulfhydryl groups. *Archives of Biochemistry and Biophysics* **1959,** *82* (1), 70-77.
224. Yang, Y.; Tong, X.; Luo, G.; Shu, Y.; Zheng, Y., Comparative Analysis of Crystal Structures between 2,2′-Bipyridine and

6,6′-Dimethyl-2,2′-Bipyridine Supported CuSCF3 Complexes: An Unusual

Coordination Transition from Mononuclear to Binuclear Mode. *Asian Journal of Chemistry* **2019,** *31* (9), 2121-2124.

225. Ziessel, R.; Hissler, M.; Ulrich, G., Synthesis of Polydendate Acyclic and Macrocyclic Polyamine Ligands Bearing 2,2′-Bipyridine or 2,2′-Bipyridine N,N′-Dioxide Moieties. *Synthesis* **1998,** *1998* (09), 1339-1346.
226. Chowdhury, S. K.; Katta, V.; Beavis, R. C.; Chait, B. T., Origin and Removal of Adducts (Molecular Mass = 98 u) Attached to Peptide and Protein Ions in Electrospray Ionization Mass Spectra. *Journal of the American Society for Mass Spectrometry* **1990,** *1* (5), 382-388.
227. Mosaddegh, B.; Takalloo, Z.; Sajedi, R. H.; Shirin Shahangian, S.; Hassani, L.; Rasti, B., An inter-subunit disulfide bond of artemin acts as a redox switch for its chaperone-like activity. *Cell Stress and Chaperones* **2018,** *23* (4), 685-693.
228. Canivet, J.; Süss-Fink, G.; Štěpnička, P., Water-Soluble Phenanthroline Complexes of Rhodium, Iridium and Ruthenium for the Regeneration of NADH in the Enzymatic Reduction of Ketones. *European Journal of Inorganic Chemistry* **2007,** *2007* (30), 4736-4742.
229. Trynda-Lemiesz, L.; Pruchnik, F. P., Studies on the interaction between human serum albumin and (Rh 2 (OAc) 2 (bpy) 2 (H 2 O) 2)(OAc) 2. *Journal of Inorganic Biochemistry $V 66* **1997,** (3), 187-192.
230. Quaglia, D.; Irwin, J. A.; Paradisi, F., Horse Liver Alcohol Dehydrogenase: New Perspectives for an Old Enzyme. *Molecular Biotechnology* **2012,** *52* (3), 244-250.
231. Olofsson, L.; Nicholls, I. A.; Wikman, S., TBADH activity in water-miscible organic solvents: correlations between enzyme performance, enantioselectivity and protein structure through spectroscopic studies. *Organic & Biomolecular Chemistry* **2005,** *3* (5), 750-755.
232. Lamed, R. J.; Zeikus, J. G., Novel NADP-linked alcohol–aldehyde/ketone oxidoreductase in thermophilic ethanologenic bacteria. *Biochemical Journal* **1981,** *195* (1), 183-190.
233. Ben, D. R., *Data for Biochemical Research (3rd ed.)* Clarendon Press: Oxford, 1985.
234. Man, H.; Kędziora, K.; Kulig, J.; Frank, A.; Lavandera, I.; Gotor-Fernández, V.; Rother, D.; Hart, S.; Turkenburg, J. P.; Grogan, G., Structures of Alcohol Dehydrogenases from Ralstonia and Sphingobium spp. Reveal the Molecular Basis for Their Recognition of 'Bulky–Bulky' Ketones. *Topics in Catalysis* **2014,** *57* (5), 356-365.
235. Lavandera, I.; Oberdorfer, G.; Gross, J.; de Wildeman, S.; Kroutil, W., Stereocomplementary Asymmetric Reduction of Bulky–Bulky Ketones by Biocatalytic Hydrogen Transfer. *European Journal of Organic Chemistry* **2008,** *2008* (15), 2539-2543.
236. Lavandera, I.; Kern, A.; Resch, V.; Ferreira-Silva, B.; Glieder, A.; Fabian, W. M. F.; de Wildeman, S.; Kroutil, W., One-Way Biohydrogen Transfer for Oxidation of sec-Alcohols. *Organic Letters* **2008,** *10* (11), 2155-2158.
237. Tavanti, M.; Parmeggiani, F.; Castellanos, J. R. G.; Mattevi, A.; Turner, N. J., One-Pot Biocatalytic Double Oxidation of α-Isophorone for the Synthesis of Ketoisophorone. *ChemCatChem* **2017,** *9* (17), 3338-3348.
238. Zhou, J.; Wang, Y.; Xu, G.; Wu, L.; Han, R.; Schwaneberg, U.; Rao, Y.; Zhao, Y.-L.; Zhou, J.; Ni, Y., Structural Insight into Enantioselective Inversion of an Alcohol Dehydrogenase Reveals a "Polar Gate" in Stereorecognition of

Diaryl Ketones. *Journal of the American Chemical Society* **2018,** *140* (39), 12645-12654.
239. Winther, J. R.; Thorpe, C., Quantification of thiols and disulfides. *Biochimica et Biophysica Acta (BBA) - General Subjects* **2014,** *1840* (2), 838-846.
240. Vohidov, F.; Knudsen, S. E.; Leonard, P. G.; Ohata, J.; Wheadon, M. J.; Popp, B. V.; Ladbury, J. E.; Ball, Z. T., Potent and selective inhibition of SH3 domains with dirhodium metalloinhibitors. *Chemical Science* **2015,** *6* (8), 4778-4783.
241. Sicsic, S.; Durand, P.; LangrenÉ, S.; Goffic, F. L. E., Activity of NMN+, nicotinamide ribose and analogs in alcohol oxidation promoted by horse-liver alcohol dehydrogenase. *European Journal of Biochemistry* **1986,** *155* (2), 403-407.

10 Appendices

Appendix 1. Site directed mutagenesis

The DNA sequence of the 2 genes used for site directed mutagenesis in Chapter 4 are shown below. The different features are highlighted as follow: restriction sites in green, start and stop codons in blue, the N-terminus strep-tag in brown, the mutations applied to gene in red and the C-terminus his-tag in italic.

TbADH 5M sequence

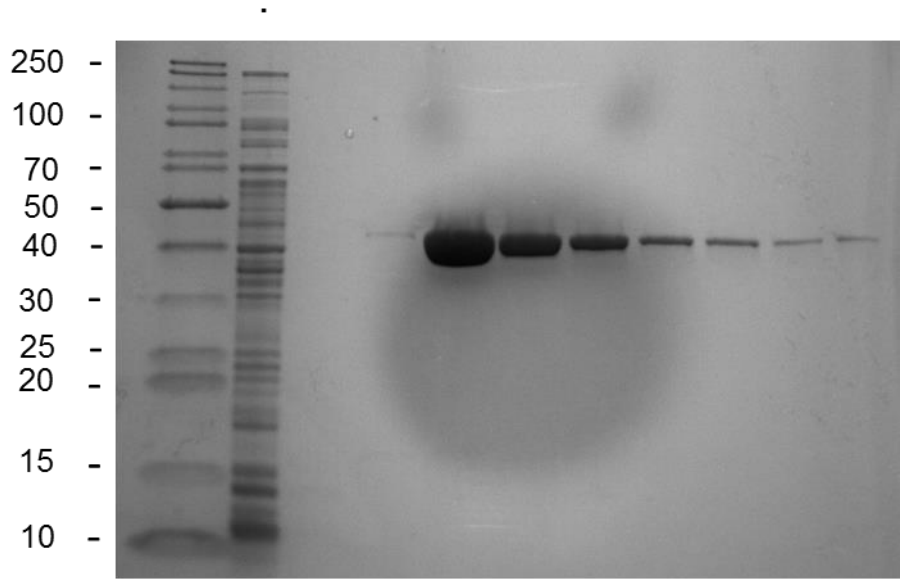
AGAAGCTAACTTCCCCTCTAGAATAATTTTGTTTAACTTTAAGAAGGAGA
TATACATATGTGGAGCCACCCGCAGTTCGAAAAATCTTCTGGTCTGGTT
CCGCGTGGATCCATGAAGGGCTTCGCGATGCTGAGCATTGGTAAGGTT
GGCTGGATCGAGAAAGAAAAACCGGCTCCGGGTCCGTTCGACGCTATC
GTGCGTCCGCTGGCTGTTGCGCCGTGCACCTCTGACATCCATACCGTT
TTCGAGGGTGCGATCGGTGAGCGCCACAACATGATCCTGGGTGCCGAA
GCGGTGGGCGAGGTTGTTGAAGTTGGCTCTGAGGTGAAAGACTTTAAG
CCGGGTGATCGTGTTGTTGTTCCGGCAATCACCCCGGACTGGCGTACT
TCCGAAGTTCAGCGCGGCTACCACCAGCACTCTGGCGGTATGCTGGCG
GGTTGGAAATTCTCCAACGTTAAGGACGGCGTGTTCGGCGAGTTCTTC
CATGTGAACGACGCTGACATGAACCTGGCGCACCTGCCGAAGGAAATC
CCGCTGGAAGCGGCGGTTATGATTCCGGCTATGATGACTACTGGTTTC
CATGGTGCAGAGCTGGCAGACATTGAGCTGGGTGCAACCGTTGCGGTT
CTGGGTATCGGTCCGGTTGGCCTGATGGCGGTGGCTGGTGCGAAACT
GCGTGGTGCGGGTCGTATCATCGCGGTTGGTTCTCGTCCGGTGAGCGT
TGATGCTGCTAAATACTACGGTGCGACCGACATTGTTAACTACAAAGAC
GGTCCGATCGAATCTCAGATTATGAACCTGACCGAGGGCAAAGGCGTG
GACGCAGCGATTATCGCAGGTGGTAACGCGGATATCATGGCGACCGCT
GTTAAAATCGTTAAACCGGGTGGTACTATTGCGAACGTGAACTATTTCG
GTGAAGGCGAAGTGCTGCCGGTGCCGCGTCTGGAATGGGGTGCTGGT
ATGGCACATAAGACCATTAAAGGTGGTCTGGCTCCGGGCGGTCGTCTG
CGCATGGAACGTCTGATTGACCTGGTTTTCTACAAACGTGTTGACCCGT
CTAAACTGGTTACCCACGTGTTCCGTGGTTTCGACAACATCGAAAAGGC
TTTTATGCTGATGAAGATAAACCGAAAGATCTGATCAAACCGGTGGTT
ATCCTGGCGTAACTCGAG*CACCACCACCACCACCAC*TGAGATCCGGCT
GCTAACAAAGCCCGAAAGAAGCGTACGTC

TbADH 6M sequence

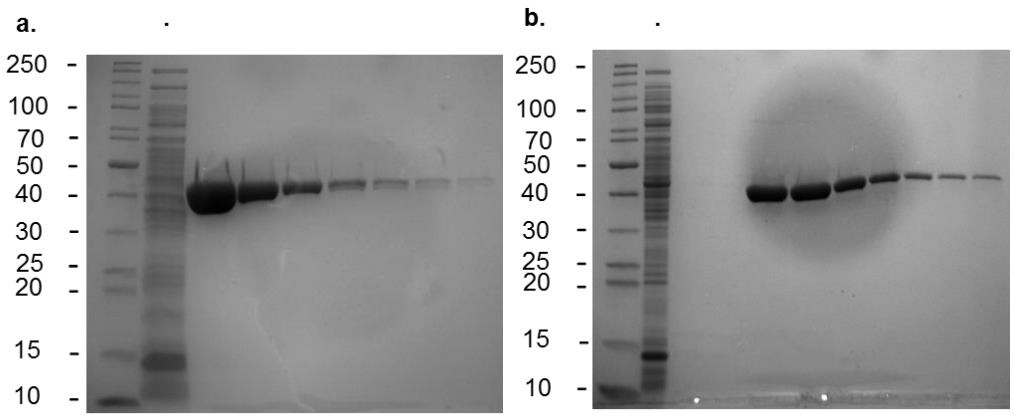
GATAGCCGAAACTTCCCCTCTAGAATAATTTTGTTTTAACTTTAAGAAGG
AGATATACATATGTGGAGCCACCCGCAGTTCGAAAAATCTTCTGGTCTG
GTTCCGCGTGGATCCATGAAGGGCTTCGCGATGCTGAGCATTGGTAAG
GTTGGCTGGATCGAGAAAGAAAAACCGGCTCCGGGTCCGTTCGACGCT
ATCGTGCGTCCGCTGGCTGTTGCGCCGGCAACCTCTGACATCCATACC

GTTTTCGAGGGTGCGATCGGTGAGCGCCACAACATGATCCTGGGTGCC
GAAGCGGTGGGCGAGGTTGTTGAAGTTGGCTCTGAGGTGAAAGACTTT
AAGCCGGGTGATCGTGTTGTTGTTCCGGCAATCACCCCGGACTGGCGT
ACTTCCGAAGTTCAGCGCGGCTACCACCAGCACTCTGGCGGTATGCTG
GCGGGTTGGAAATTCTCCAACGTTAAGGACGGCGTGTTCGGCGAGTTC
TTCCATGTGAACGACGCTGACATGAACCTGGCGCACCTGCCGAAGGAA
ATCCCGCTGGAAGCGGCGGTTATGATTCCGGCTATGATGACTACTGGT
TTCCATGGTGCAGAGCTGGCAGACATTGAGCTGGGTGCAACCGTTGCG
GTTCTGGGTATCGGTCCGGTTGGCCTGATGGCGGTGGCTGGTGCGAAA
CTGCGTGGTGCGGGTCGTATCATCGCGGTTGGTTCTCGTCCGGTGAGC
GTTGATGCTGCTAAATACTACGGTGCGACCGACATTGTTAACTACAAAG
ACGGTCCGATCGAATCTCAGATTATGAACCTGACCGAGGGCAAAGGCG
TGGACGCAGCGATTATCGCAGGTGGTAACGCGGATATCATGGCGACCG
CTGTTAAAATCGTTAAACCGGGTGGTACTATTGCGAACGTGAACTATTT
CGGTGAAGGCGAAGTGCTGCCGGTGCCGCGTCTGGAATGGGGTGCTG
GTATGGCACATAAGACCATTAAAGGTGGTCTGGCTGGTATGGCACATAA
GACCATTAAAGGTGGTCTGGCTCCGGGCGGTCGTCTGCGCATGGAACG
TCTGATTGACCTGGTTTTCTACAAACGTGTTGACCCGTCTAAACTGGTTA
CCCACGTGTTCCGTGGTTTCGACAACATCGAAAAGGCTTTTATGCTGATT
GAAAGATAAACCGAAAGATCTGATCAAACCGGTGGTTATCCTGGCGTAA
CTCGAG*CACCACCACCACCACCAC*TGAGATCCGGCTGCTAACAAAGCC
CGAAAGAAGCGTACGTC

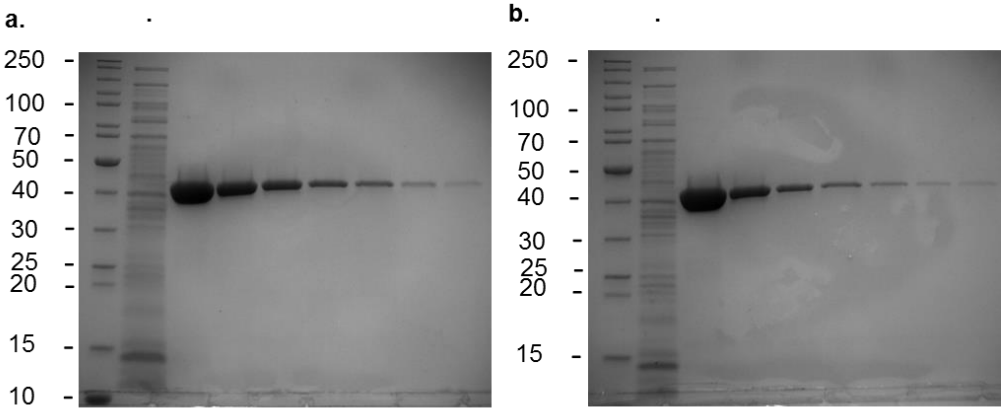
Appendix 2.SDS-PAGE of mutants



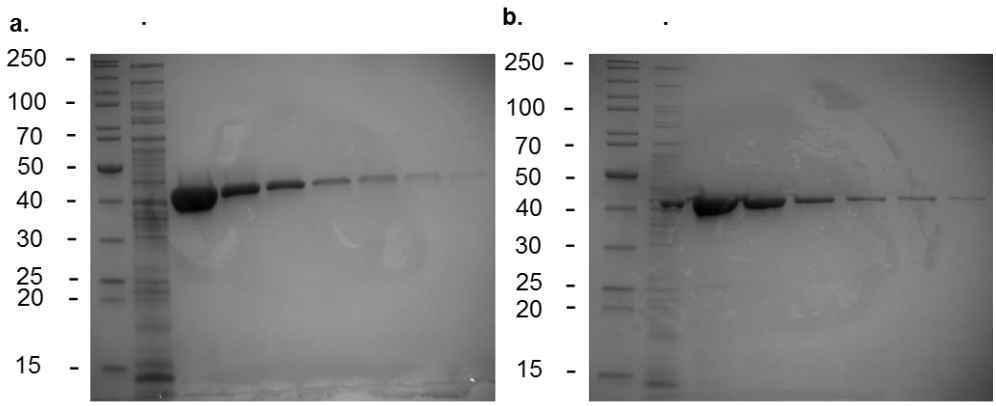
SDS-PAGE of the mutant 5M-C37. The different protein sizes of the ladder were depicted on the left side of the gel. The lane containing the flow through of each purification was outlined with the "·".



SDS-PAGE of the mutants a. TbADH 6M and b. 7M-C174. The different protein sizes of the ladder were depicted on the left side of each gel. The lane containing the flow through of each purification was outlined with the "·".

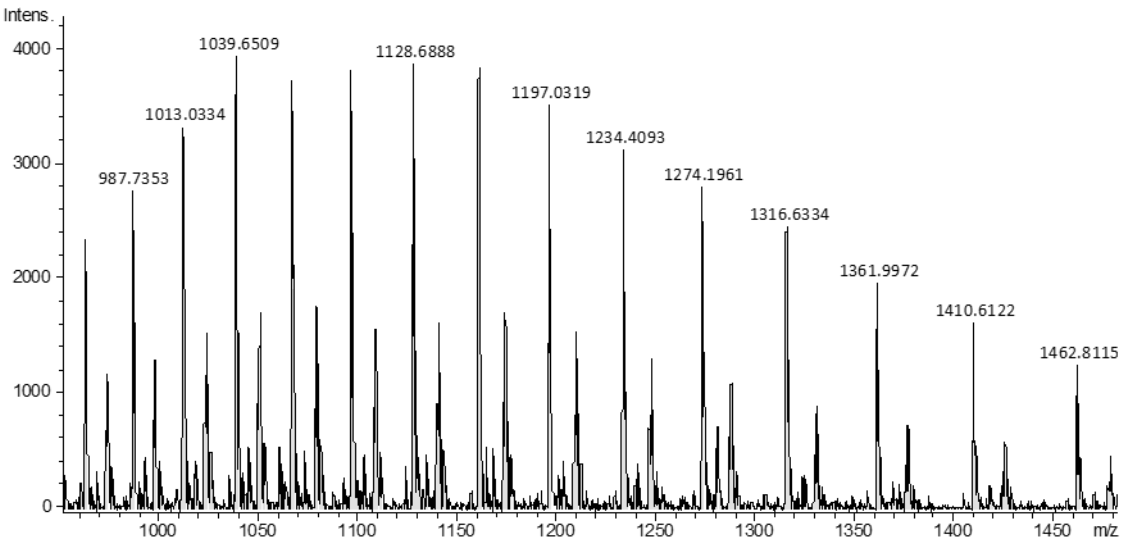


SDS-PAGE of the mutants a. 7M-C198 and b. 7M-C203. The different protein sizes of the ladder were depicted on the left side of each gel. The lane containing the flow through of each purification was outlined with the "·".

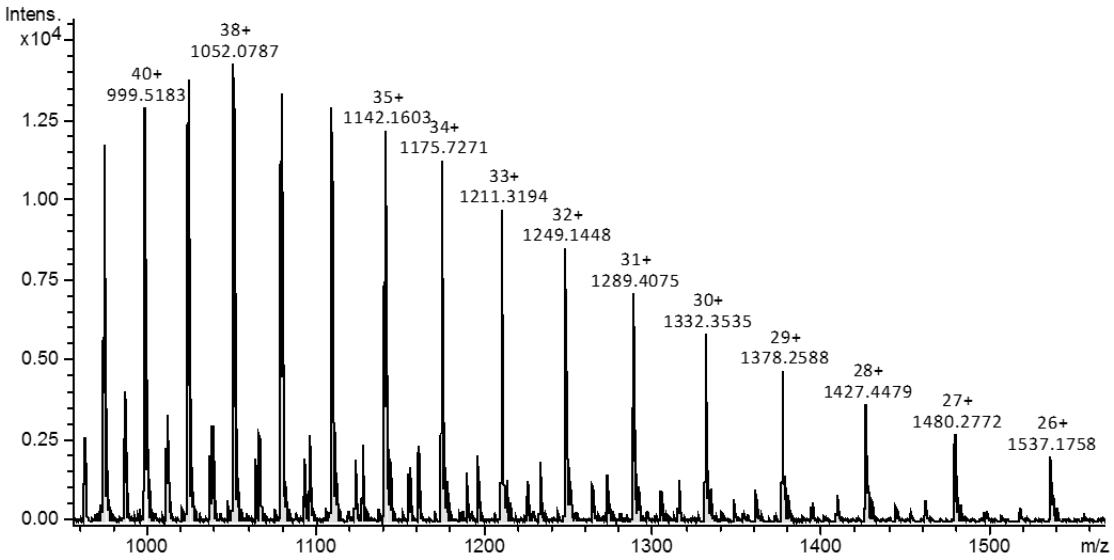


SDS-PAGE of the mutants a. 7M-C242 and b. 7M-C243. The different protein sizes of the ladder were depicted on the left side of each gel. The lane containing the flow through of each purification was outlined with the "·".

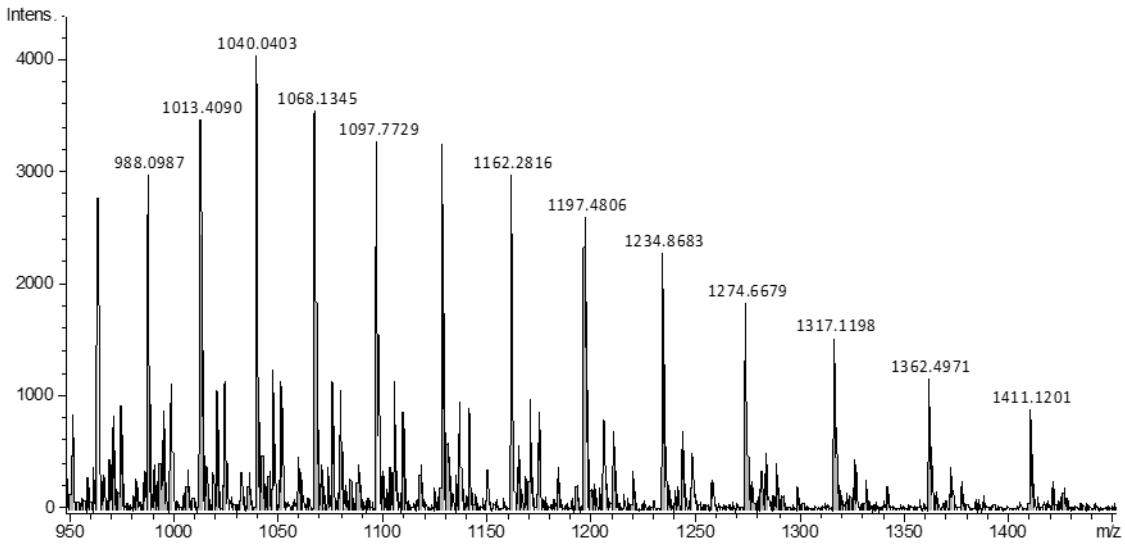
Appendix 3. Non deconvoluted ESI-MS spectra of ArMs



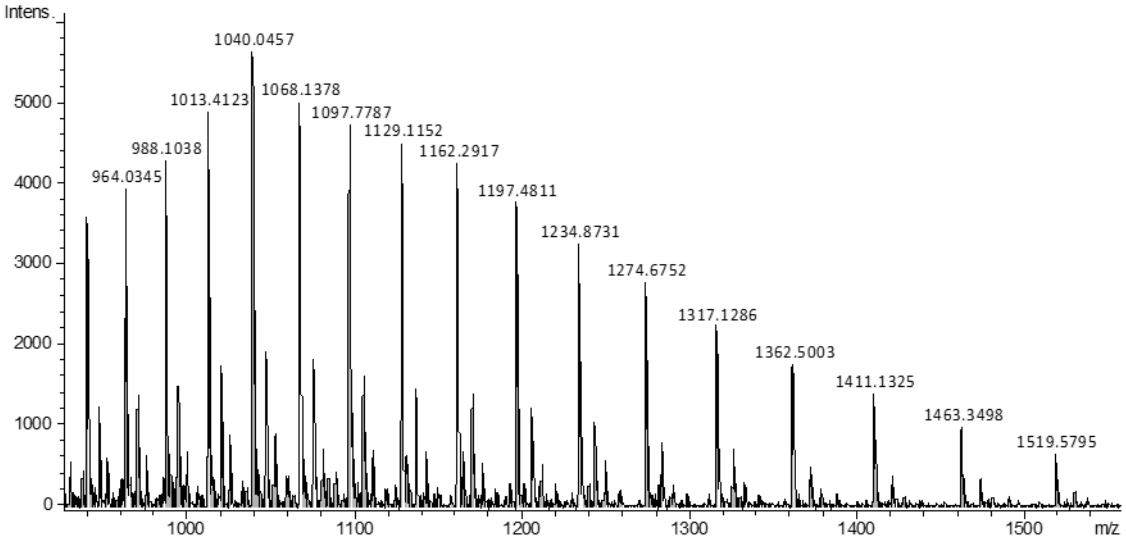
Non-deconvoluted spectrum of 5M-C37-**M2**. The ratio m/z for the main species is presented for each peak.



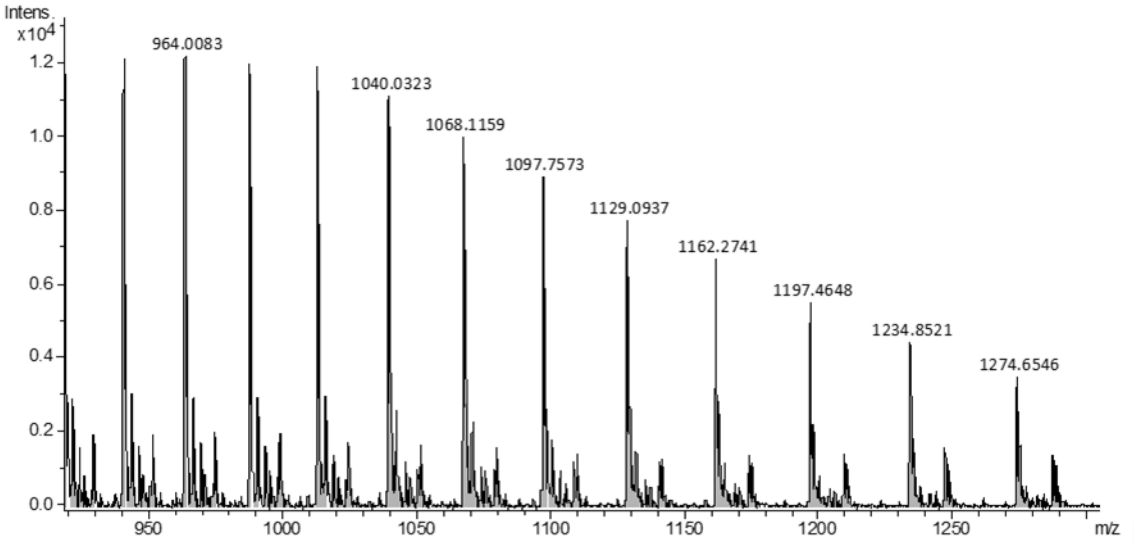
Non-deconvoluted spectrum of 5M-C37-**M3a**. The ratio m/z for the main species is presented for each peak.



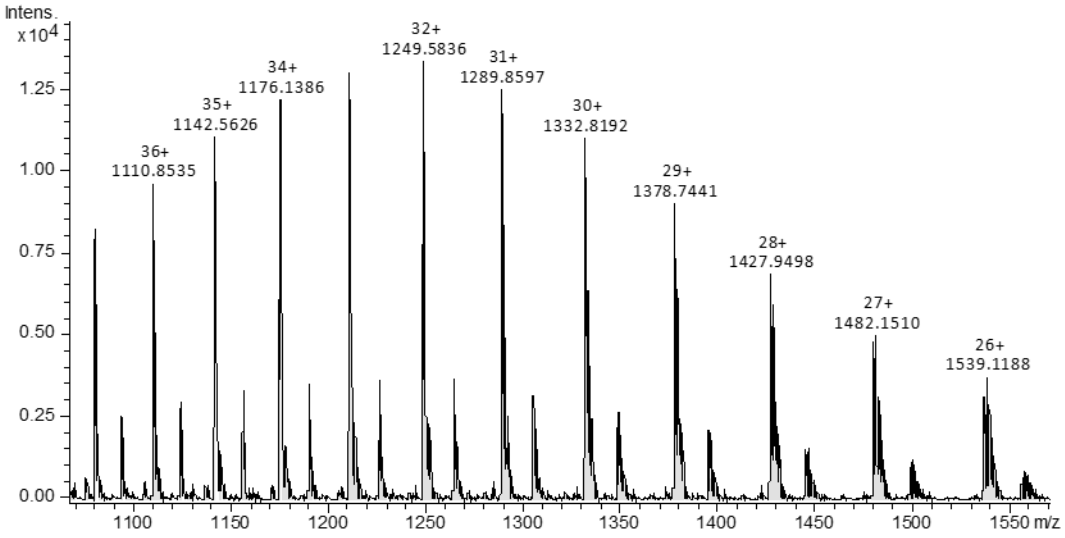
Non-deconvoluted spectrum of 7M-C174-**M2**. The ratio m/z for the main species is presented for each peak.



Non-deconvoluted spectrum of 7M-C174-**M3a**. The ratio m/z for the main species is presented for each peak.

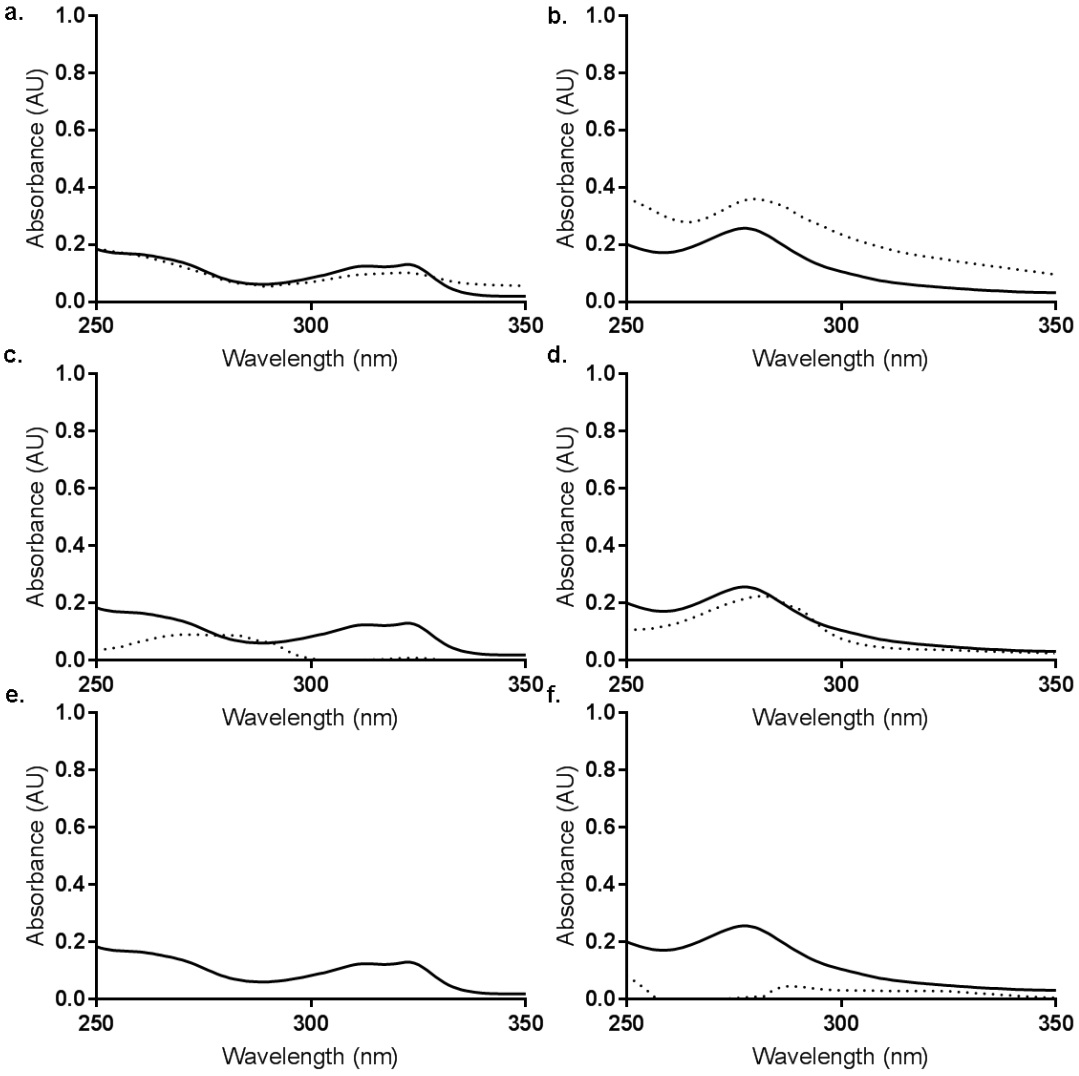


Non-deconvoluted spectrum of 7M-C243-**M2**. The ratio m/z for the main species is presented for each peak.



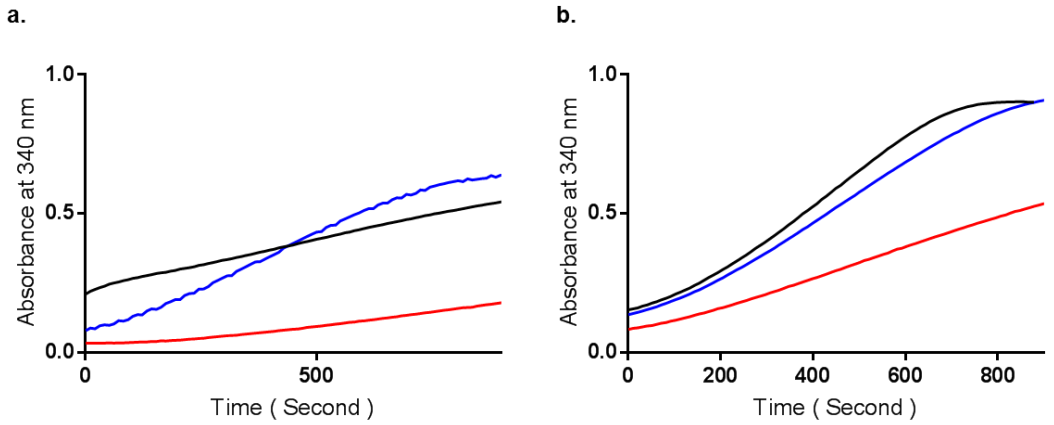
Non-deconvoluted spectrum of 7M-C243-**M3a**. The ratio m/z for the main species is presented for each peak.

Appendix 4. Plot spectra of ArMs and metal complexes

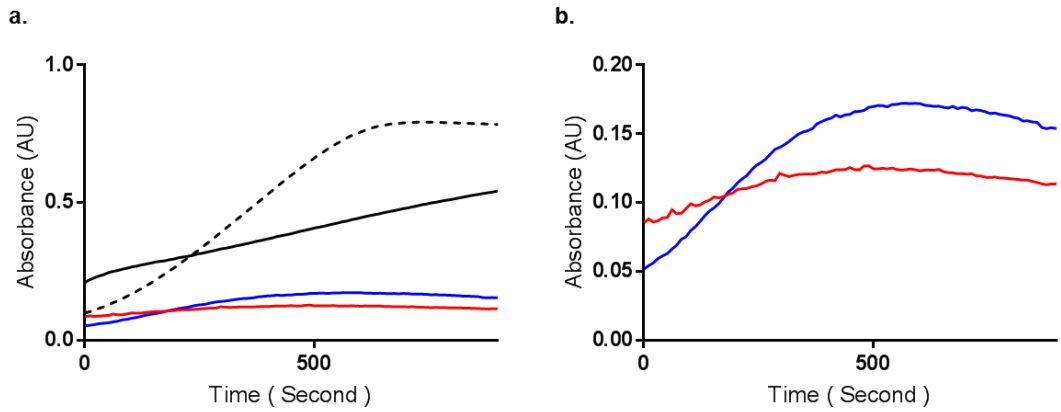


Difference spectra of each ArMs against the embedded metal catalyst (dotted line) by comparison with the metal catalyst alone (full line). On the left side, the catalyst is **M2** and on the ride side the catalyst is **M3a**. a,b) 5M-C37, c,d) 7M-C174 and e,f) 7M-C243.

Appendix 5. Reduction of $NADP^+$ and nicotinamide derivatives catalysed by ArMs

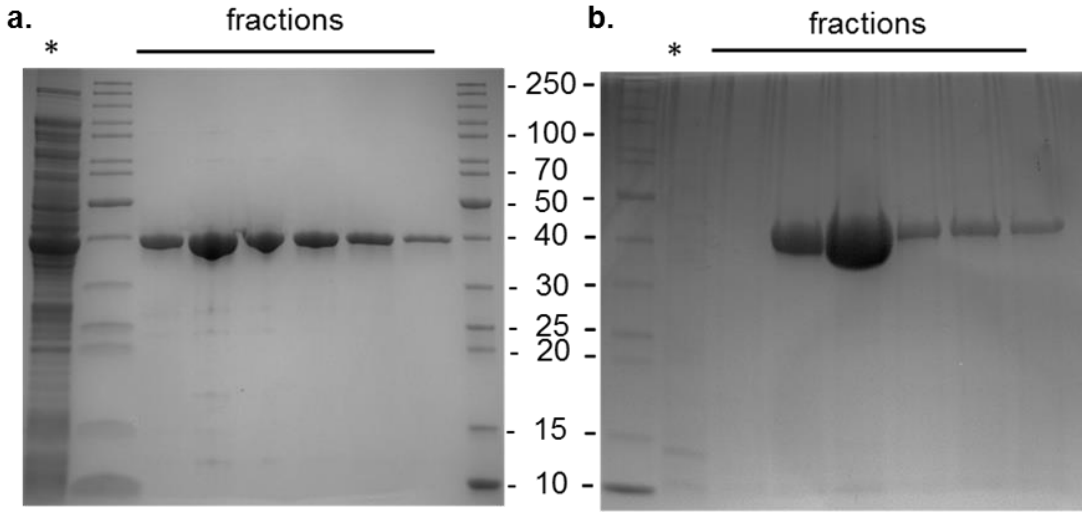


Reduction of $NADP^+$ by ArMs with catalyst a. **M2** and b. **M3a**. Conditions: biocatalyst (12.5 µM), $NADP^+$ (420 µM) in sodium phosphate 100 mM buffer pH 7.0 at 50 ˚C. The reaction was monitored at 340 nm for 1020 seconds. The enzymatic scaffolds are highlighted as follow: 5M-C37 in black, 7M-C174 in red and 7M-C243 in blue.



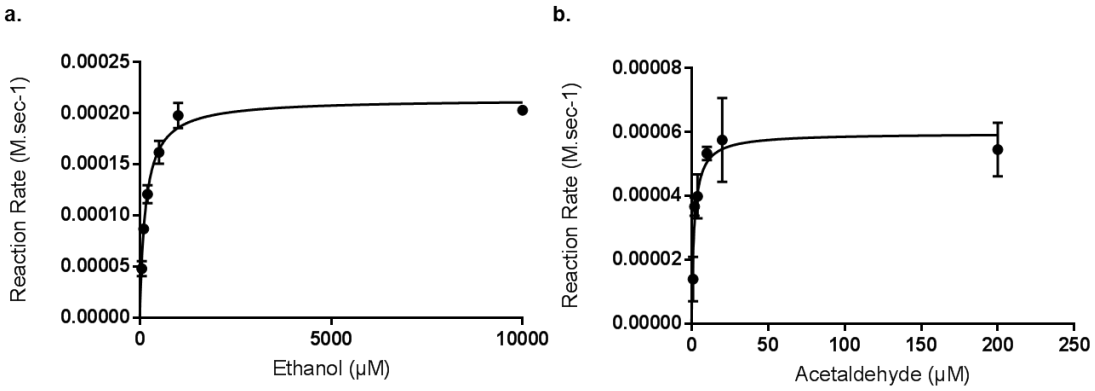
Reduction of nicotinamide-containing compounds catalysed by 5M-C37-**M2**. Conditions: biocatalyst (12.5 µM), nicotinamide derivative (420 µM) in sodium phosphate 100 mM buffer pH 7.0 at 50 ˚C. The reaction was monitored at 340 nm for 1020 seconds. The nicotinamide cofactors and derivatives are highlighted as follow: $NADP^+$ in black, NAD^+ in black dotted line, Bn-NAD in red and Bn-NAD-Ph in blue. A zoom of the left figure is shown in the right side, exhibiting the product degradation recorded after 500 seconds.

Appendix 6. SDS-PAGE of wild-type HLADH and TbADH

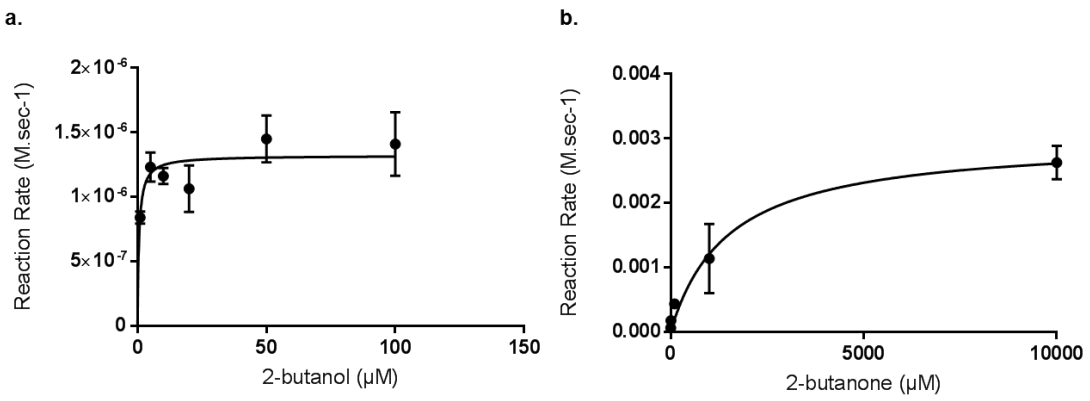


SDS-PAGE after purification of a. His-HLADH and b. TbADH. The different protein sizes of the ladder were depicted between the two gels. The lane containing the flow through of each purification was outlined with the *.

Appendix 7. Michaelis-Menten kinetics of the substrates of wild-type HLADH and TbADH

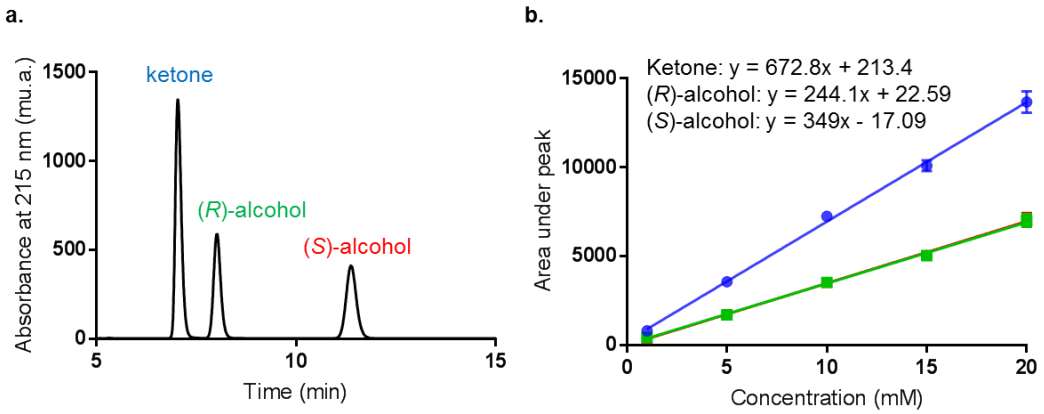


Michaelis-Menten of ethanol (left) and acetaldehyde (right) with His-HLADH where the specific activities were extracted from. Conditions: ethanol (concentration range from 50 µM to 10 mM), His-HLADH (25 µM), NAD^+ (1.5 mM) in sodium phosphate 100 mM buffer pH 8.8 and acetaldehyde (concentration range from 1 to 200 µM), His-HLADH (25 µM), NADH (1.5 mM) in sodium phosphate 100 mM buffer pH 7.0. The reactions were monitored at room temperature for 120 seconds at 340 nm. Each experiment was run in triplicate.

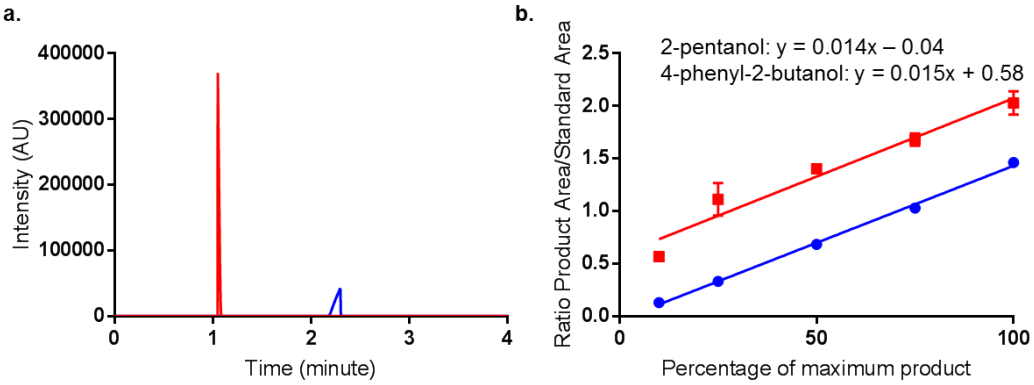


Michaelis-Menten of 2-butanol (left) and 2-butanone (right) with TbADH where the specific activities were extracted from. Conditions: 2-butanol (concentration range from 1 to 100 µM), TbADH (2.5 µM), $NADP^+$ (1 mM) in Tris.HCl 50 mM buffer pH 9.0 and 2-butanone (concentration range from 10 µM to 10 mM), TbADH (2.5 µM), NADPH (1 mM) in Tris.HCl 50 mM buffer pH 6.0. The reactions were monitored at 40 °C for 120 seconds at 340 nm. Each experiment was run in triplicate.

Appendix 8. Calibration curves exploited for HPLC and GC-FID

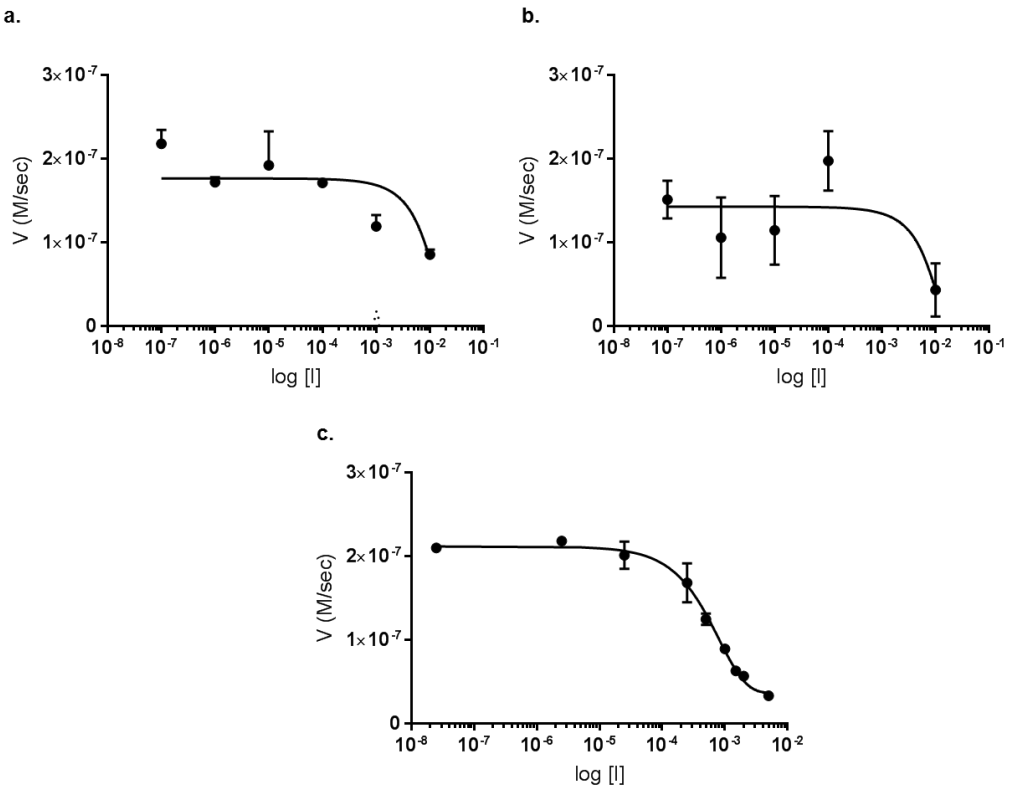


Results of a run in chiral HPLC with of 4-phenyl-2-butanone and ± 4-phenyl-2-butanol (left) and the corresponding calibration curve of the compounds (right). Conditions of the calibrations: each compound was injected after extraction with *n*-hexane from sodium phosphate 100 mM pH 7.0 or Tris.HCl 50 mM pH 6.0 buffered solution at a concentration ranging from 1 to 20 mM. Each experiment was run in triplicate. The run with all the compounds was performed at 20 mM concentration.



Results of a run in GC-FID (left) with 2-pentanol (blue) and 4-phenyl-2-butanol (red) and the corresponding calibration curve for each compound (right). Conditions of the calibration: 2-pentanol (concentration range 0.18 to 1.8 mM), in Tris.HCl 50 mM buffer pH 9.0 and 4-phenyl-2-butanol (concentration range 0.14 to 1.34 mM) in sodium phosphate 100 mM pH 8.8 were extracted in *n*-hexane then injected into the apparatus. Each experiment was run in triplicate. The run was performed at 1.8 mM with 2-pentanol and 1.34 mM with 4-phenyl-2-butanol.

Appendix 9. Inhibition kinetics of His-HLADH with mimics 150, 151 and 156



Sigmoidal plot of inhibition kinetics of a. **150**, b. **151** and c. **156** with HLADH. Conditions: acetaldehyde (10 mM), His-HLADH (25 µM), NADH (0.3 mM), **150**/**151** (concentration ranging from 10-7 to 10-2 M) or **156** (concentration ranging from 10-10 to 10-2 M) in sodium phosphate 100 mM buffer pH 7.0. The experiments were monitored at room temperature for 120 seconds at 340 nm. Each experiment was run in triplicate.

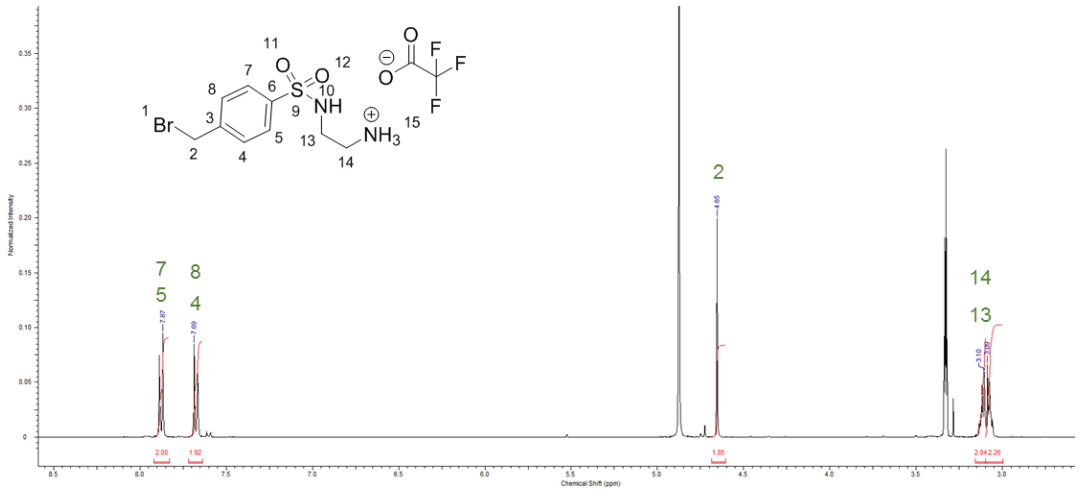
Appendix 10. Grid coordinates of ADHs docking study

PDB entry	x coordinate	y coordinate	z coordinate	x size	y size	z size
1a4u	18.788	-2.141	1.338	30	30	30
1e3e	96.221	29.526	28.999	24	20	24
1m2w	60.964	80.863	37.831	24	40	28
1mg5	-2.635	-2.2	33.478	18	36	20
1w6s	5.599	22.511	-15.177	26	28	30
1yqd	54.836	115.988	31.041	24	28	24
3gaz	80.651	-44.014	-59.421	40	40	40
3goh	37.496	6.69	14.486	40	40	40
3iv7	28.294	31.104	34.294	50	34	34
3l77	-36.304	-15.43	-16.978	22	22	24
3owo	15.34	-14.876	2.813	26	24	26
4bmn	41.412	17.745	47.087	30	36	30
4bms	-15.833	-26.333	19.556	32	30	32
4bmv	23.836	-13.31	87.441	24	20	28
4fr2	3.428	-8.628	21.685	40	40	40
4quk	12.083	-1.304	-5.904	34	40	38
4rf4	112.647	-1.208	50.151	26	28	28
4ure	11.561	-2.246	14.473	28	26	30
5mln	15.593	60.595	23.067	40	40	40
5tt1	-11.427	-0.224	21.266	32	36	32
5uzx	-17.694	6.861	3.667	34	30	32
5z2x	-52.068	122.475	-0.209	24	20	32
6c7l	6.862	-32.216	-8.498	22	18	24
6c49	14.684	14.791	36.07	26	26	30
6hlf	2.785	19.71	14.421	28	28	30

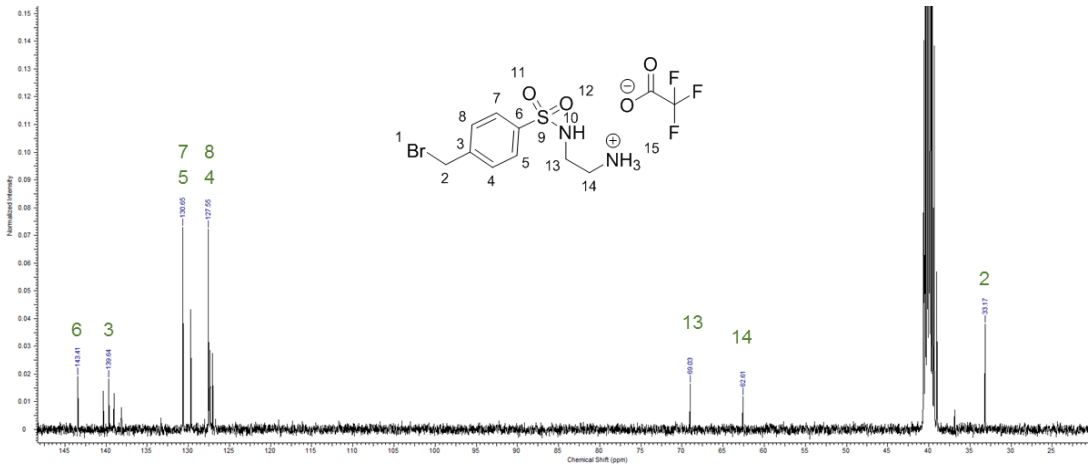
The PDB entry and corresponding grid coordinates of the various ADHs used for the screening *in silico* of a new biological scaffold to accommodate mimic Bn-NAD for the design of ArMs using a supramolecular approach.

Appendix 11. ^{1}H, ^{13}C NMR and MS spectra of the ligands and complexes synthesised

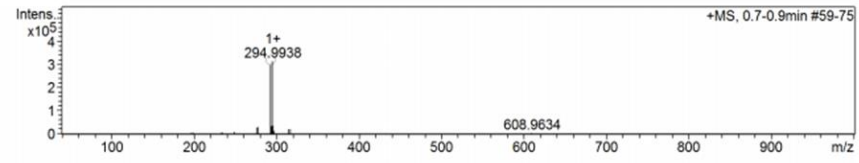
^{1}H NMR *N*-(2-aminoethyl)-4-(bromoethyl)benzenesulfonamide, **L1**



^{13}C NMR *N*-(2-aminoethyl)-4-(bromoethyl)benzenesulfonamide, **L1**

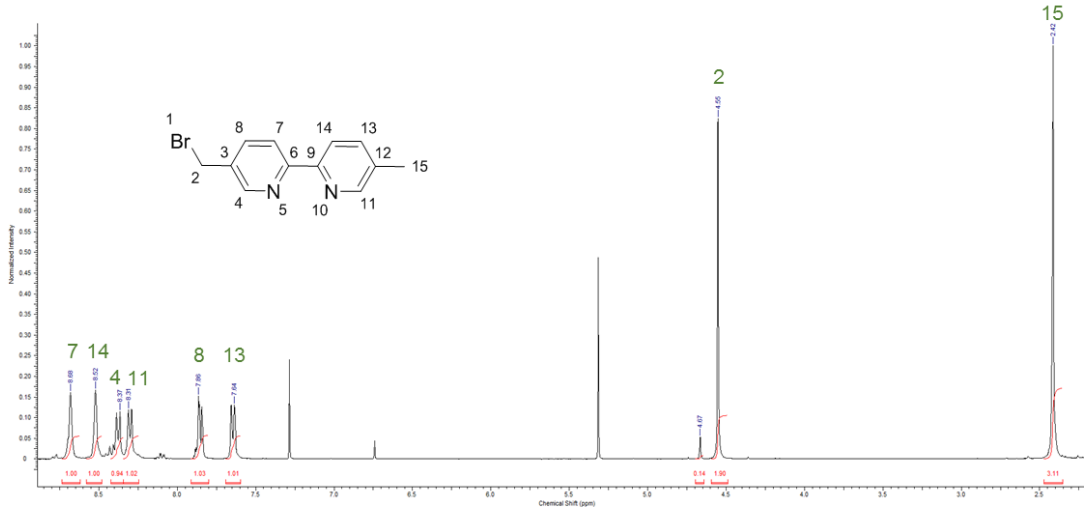


ESI-MS *N*-(2-aminoethyl)-4-(bromoethyl)benzenesulfonamide, **L1**

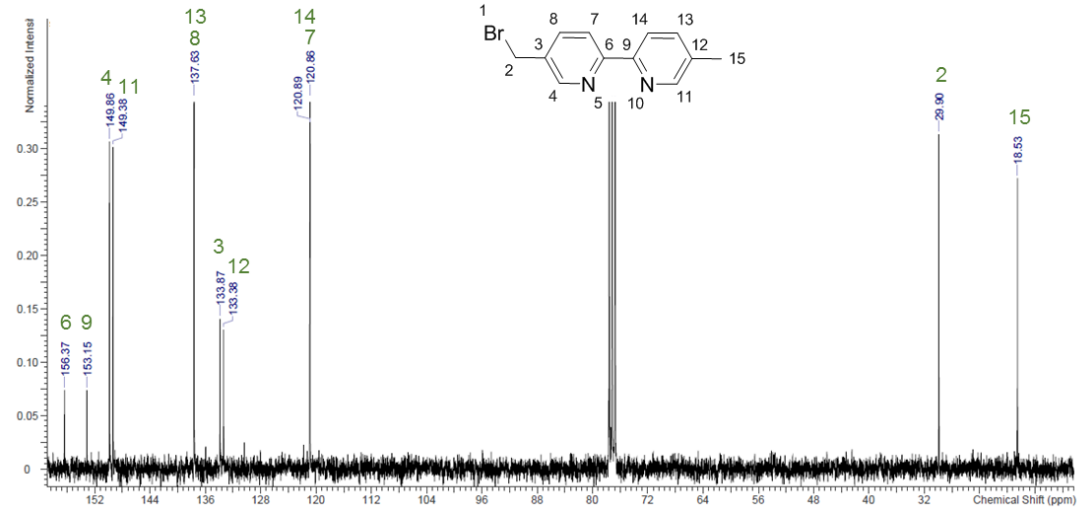


#	m/z	I %	
1	196.9705	2.2	
2	198.9684	2.1	
3	218.9289	1.0	
4	232.9251	2.3	
5	234.9238	2.2	
6	249.0459	3.6	
7	251.0420	1.3	
8	275.9682	9.5	
9	276.9709	1.1	
10	277.9665	10.0	
11	278.9696	1.1	
12	292.9957	94.7	←
13	293.9977	11.1	
14	294.9938	100.0	←
15	295.9956	11.5	
16	296.9904	5.0	
17	314.9763	6.9	
18	316.9747	7.2	
19	586.9813	1.4	
20	608.9634	1.8	

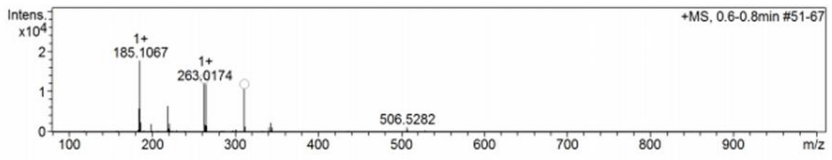
^{1}H NMR 5-(bromomethyl)-5'-2,2'-bipyridine, **L2**



^{13}C NMR 5-(bromomethyl)-5'-2,2'-bipyridine, **L2**

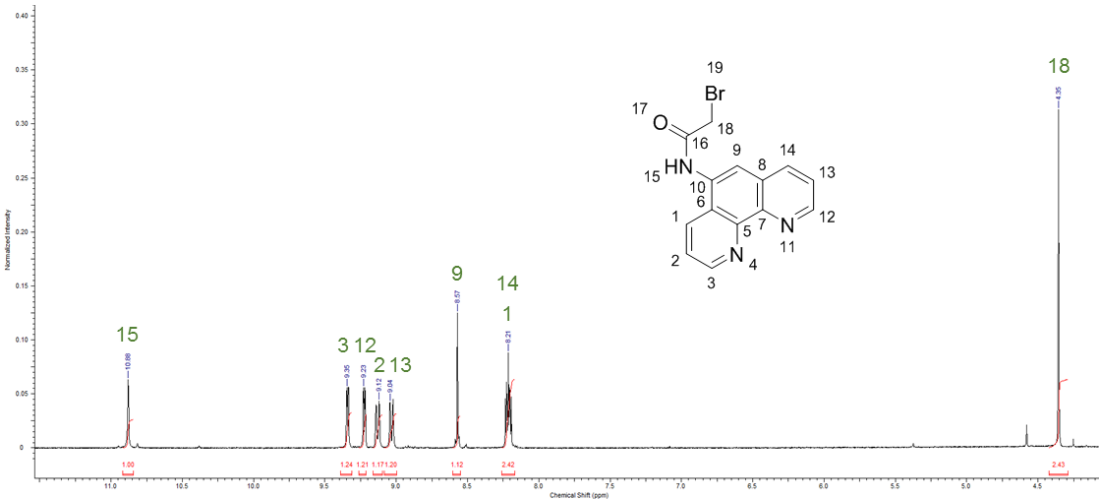


ESI-MS 5-(bromomethyl)-5'-2,2'-bipyridine, **L2**

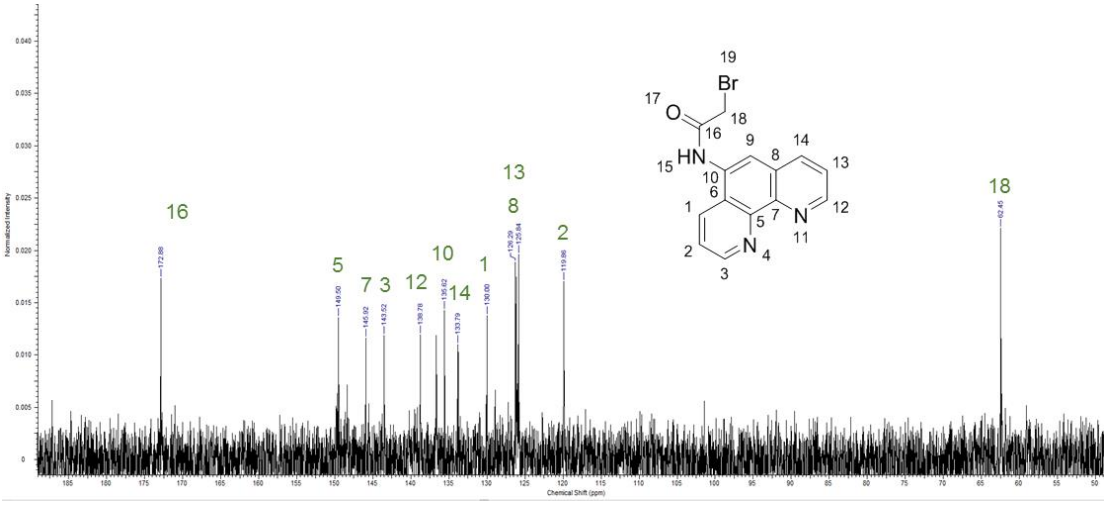


#	m/z	I %	
1	183.0914	2.8	
2	184.0990	32.7	
3	185.1067	100.0	
4	186.1100	13.4	
5	190.1243	2.5	
6	199.0863	11.1	
7	219.0678	36.3	
8	220.0697	5.0	
9	221.0646	11.8	
10	263.0174	67.8	←
11	264.0195	9.8	
12	265.0151	67.0	←
13	266.0182	9.0	
14	301.1406	3.6	
15	311.0032	60.2	
16	312.0060	7.6	
17	340.9272	6.7	
18	342.9254	12.7	
19	344.9293	6.5	
20	506.5282	6.4	

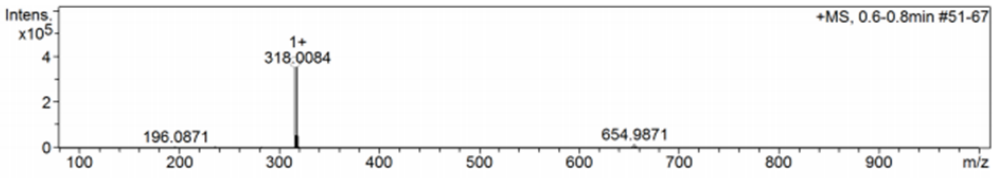
^{1}H NMR 5-(2'-bromo)-acetamido-1,10-phenantrholine, **L3**



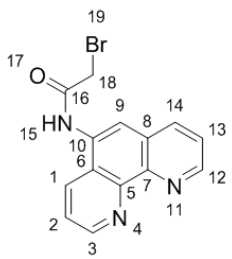
^{13}C NMR 5-(2'-bromo)-acetamido-1,10-phenantrholine, **L3**



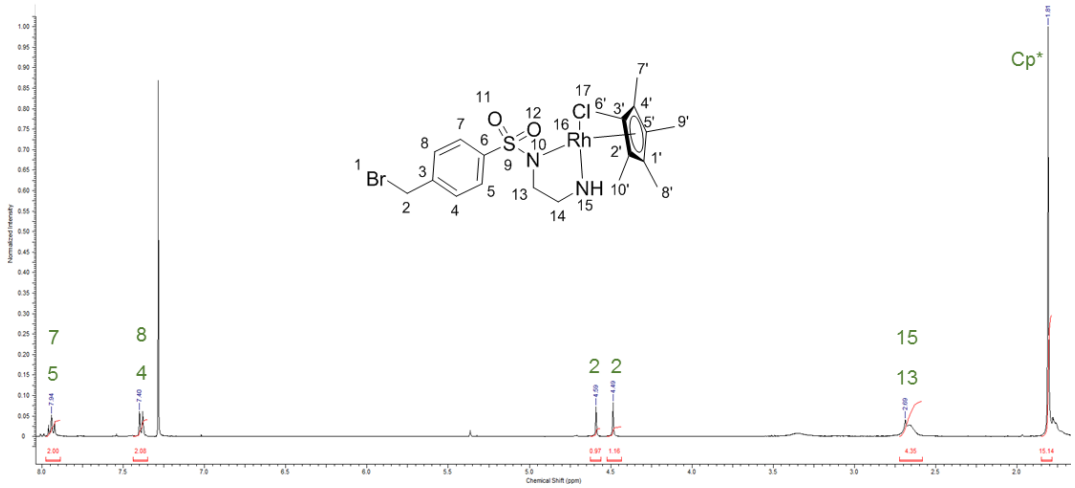
ESI-MS 5-(2'-bromo)-acetamido-1,10-phenantrholine, **L3**



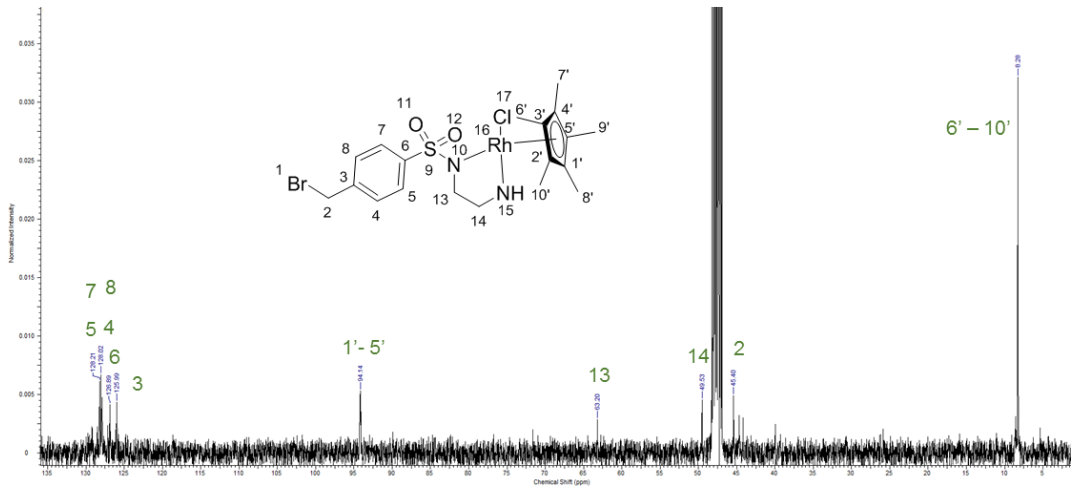
#	m/z	I %	
1	195.0792	1.4	
2	196.0871	2.5	
3	236.0816	2.3	
4	268.1079	1.5	
5	282.2787	1.7	
6	316.0099	99.4	←
7	317.0122	16.0	
8	318.0084	100.0	←
9	319.0100	15.2	
10	320.0100	1.5	
11	337.9897	1.4	
12	339.9876	1.4	
13	633.0064	1.1	
14	652.9918	2.4	
15	654.9871	5.0	
16	655.9911	1.6	
17	656.9881	2.4	
18	657.9881	0.7	
19	969.9879	0.9	
20	971.9853	1.0	



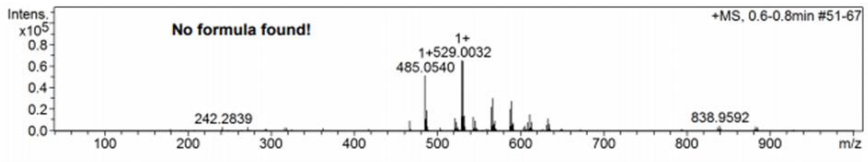
^{1}H NMR Cp*Rh(*N*-(2-aminoethyl)-4-(bromoethyl)benzenesulfonamide) chloride, **M1a**



^{13}C NMR Cp*Rh(*N*-(2-aminoethyl)-4-(bromoethyl)benzenesulfonamide) chloride, **M1a**

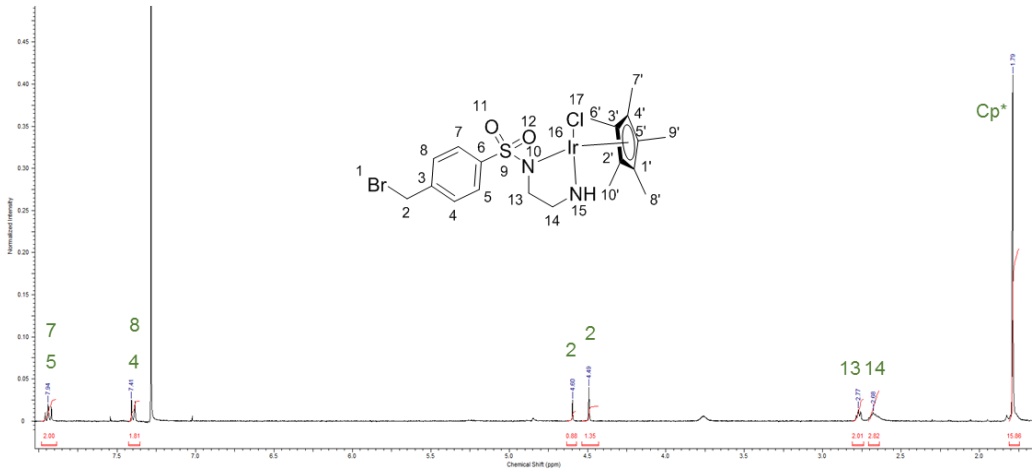


ESI-MS Cp*Rh(*N*-(2-aminoethyl)-4-(bromoethyl)benzenesulfonamide) chloride, **M1a**

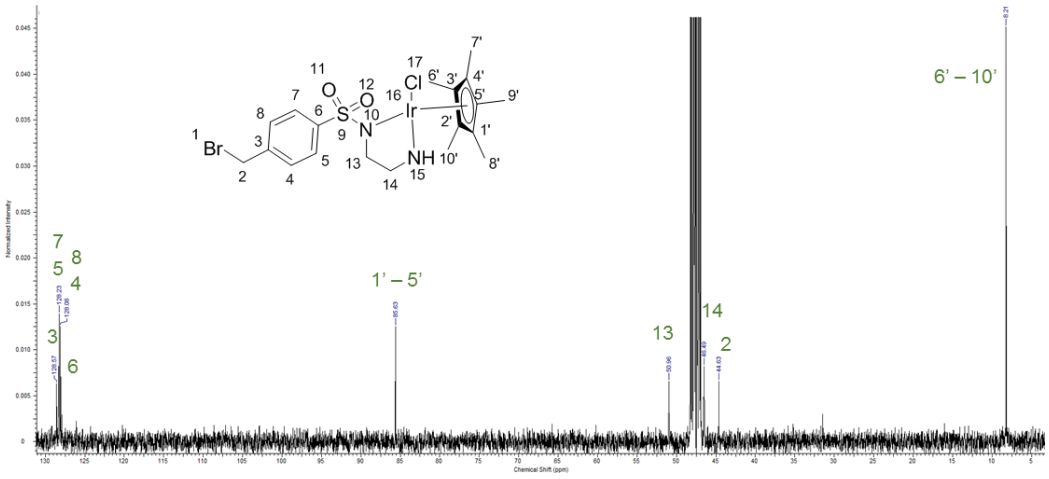


#	m/z	I %
1	467.0856	14.5
2	485.0540	78.5
3	486.0562	17.0
4	487.0508	29.5
5	521.0293	18.2
6	523.0269	12.9
7	529.0032	100.0
8	530.0056	20.6
9	531.0015	99.6
10	532.0034	22.1
11	543.0113	20.0
12	545.0088	14.7
13	564.9793	34.2
14	566.9772	46.5
15	568.9762	14.8
16	586.9608	31.5
17	588.9590	42.8
18	610.9263	23.9
19	612.9244	12.7
20	632.9081	17.6

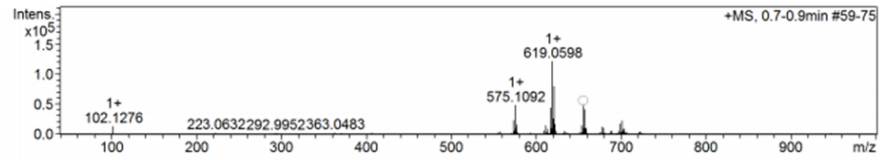
^{1}H NMR Cp*Ir(*N*-(2-aminoethyl)-4-(bromoethyl)benzenesulfonamide) chloride, **M1b**



^{13}C NMR Cp*Ir(*N*-(2-aminoethyl)-4-(bromoethyl)benzenesulfonamide) chloride, **M1b**

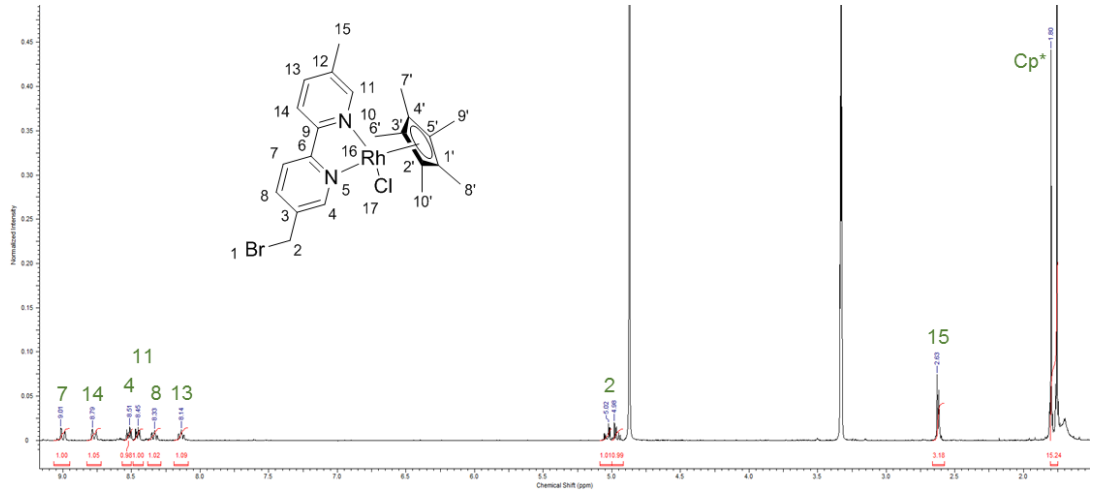


ESI-MS Cp*Ir(*N*-(2-aminoethyl)-4-(bromoethyl)benzenesulfonamide) chloride, **M1b**

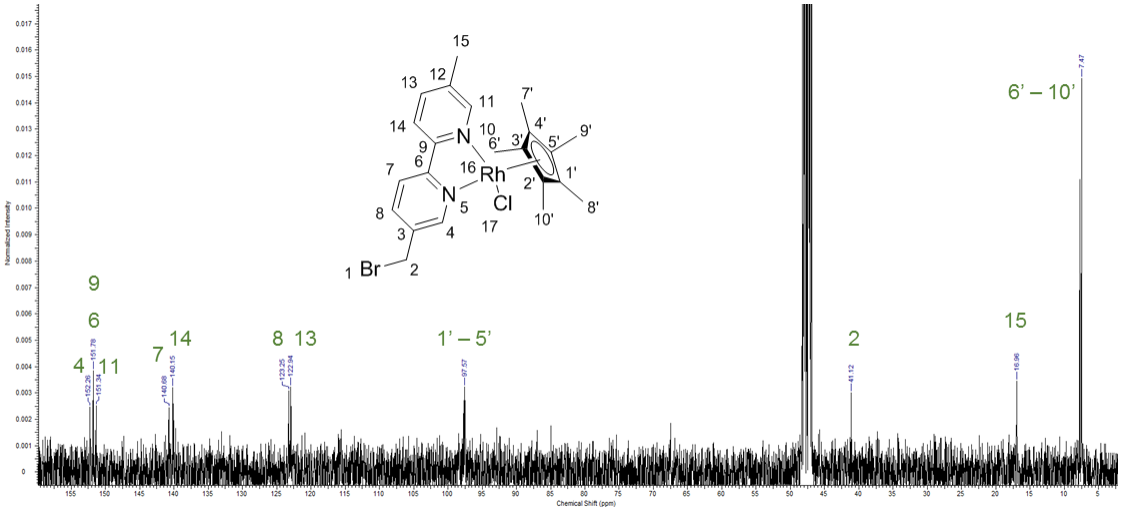


#	m/z	I %	
1	102.1276	11.1	
2	573.1087	19.6	
3	575.1092	40.1	
4	576.1117	8.9	
5	577.1080	13.5	
6	611.0848	12.5	
7	617.0589	36.3	
8	619.0598	100.0	←
9	620.0615	21.7	
10	621.0586	65.7	←
11	622.0601	13.8	
12	653.0425	12.3	
13	655.0336	39.5	
14	656.0372	8.9	
15	657.0340	34.1	
16	659.0310	8.9	
17	677.0158	10.5	
18	679.0149	9.0	
19	698.9837	14.7	
20	700.9848	19.1	

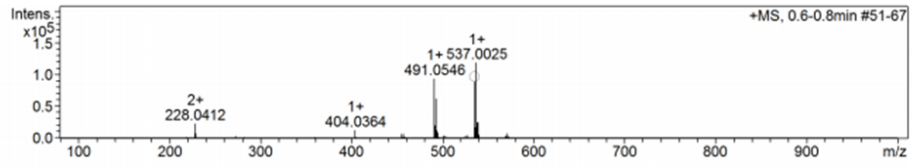
^{1}H NMR Cp*Rh(5-(bromomethyl)-5'-2,2'-bipyridine) chloride, **M2**



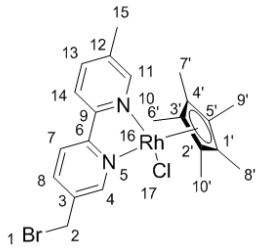
^{13}C NMR Cp*Rh(5-(bromomethyl)-5'-2,2'-bipyridine) chloride, **M2**



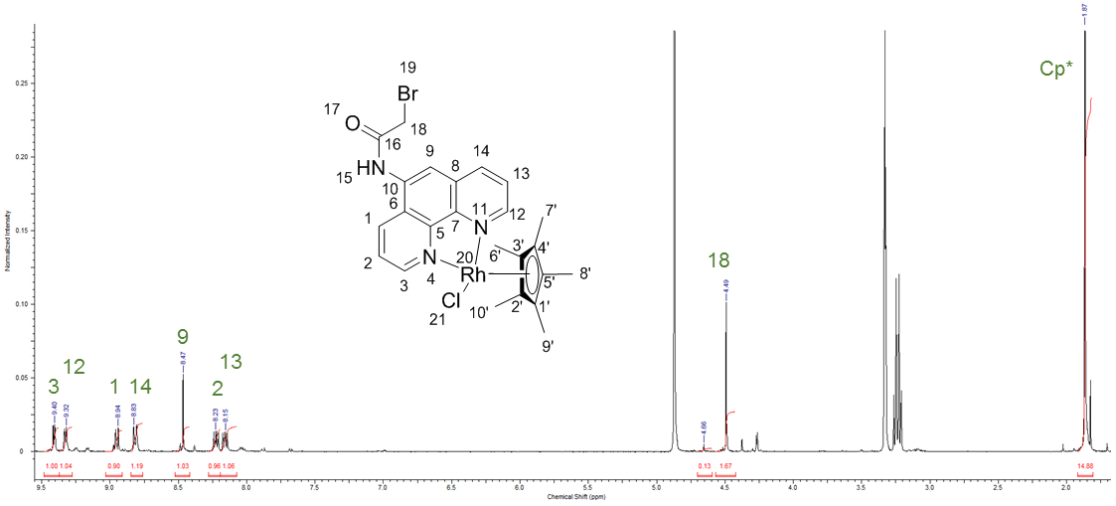
ESI-MS Cp*Rh(5-(bromomethyl)-5'-2,2'-bipyridine) chloride, **M2**



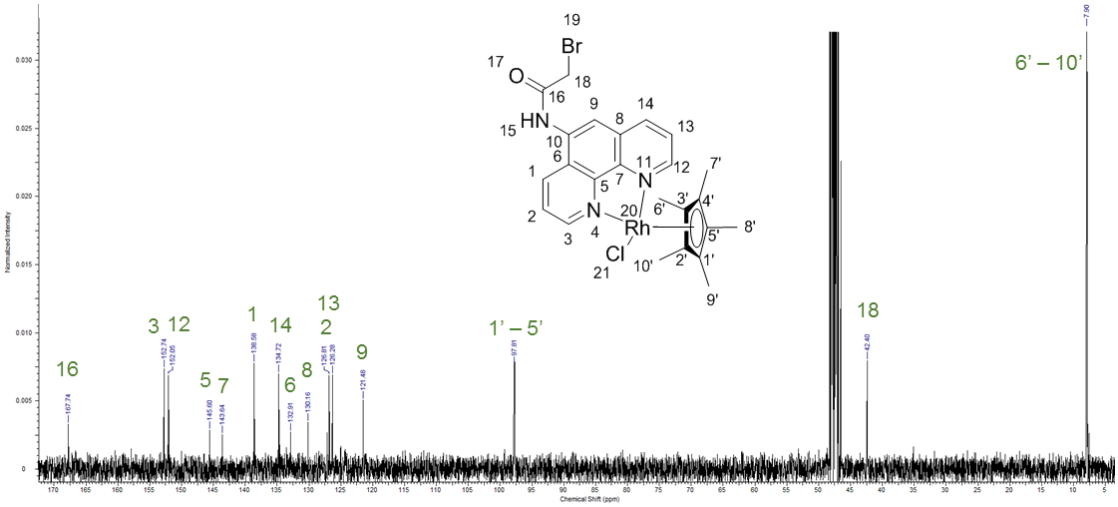
#	m/z	I %	
1	228.0412	19.1	
2	228.5428	4.7	
3	229.0402	6.5	
4	404.0364	10.5	
5	455.0748	5.9	
6	457.0839	5.6	
7	491.0546	78.8	
8	492.0547	16.8	
9	493.0512	52.4	
10	494.0523	10.3	
11	495.0463	7.7	
12	525.0113	3.8	
13	527.0103	3.9	
14	535.0034	74.7	←
15	536.0047	14.8	
16	537.0025	100.0	←
17	538.0021	21.4	
18	538.9989	21.3	
19	539.9992	4.8	
20	570.9613	6.6	



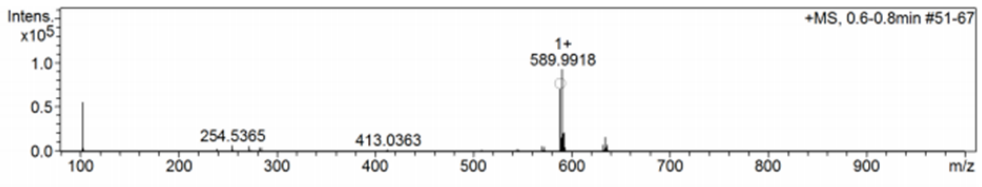
^{1}H NMR Cp*Rh(5-(2'-bromo)-acetamido-1,10-phenantrholine) chloride, **M3a**



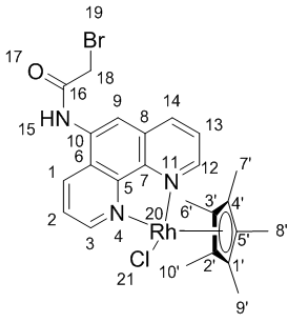
^{13}C NMR Cp*Rh(5-(2'-bromo)-acetamido-1,10-phenantrholine) chloride, **M3a**



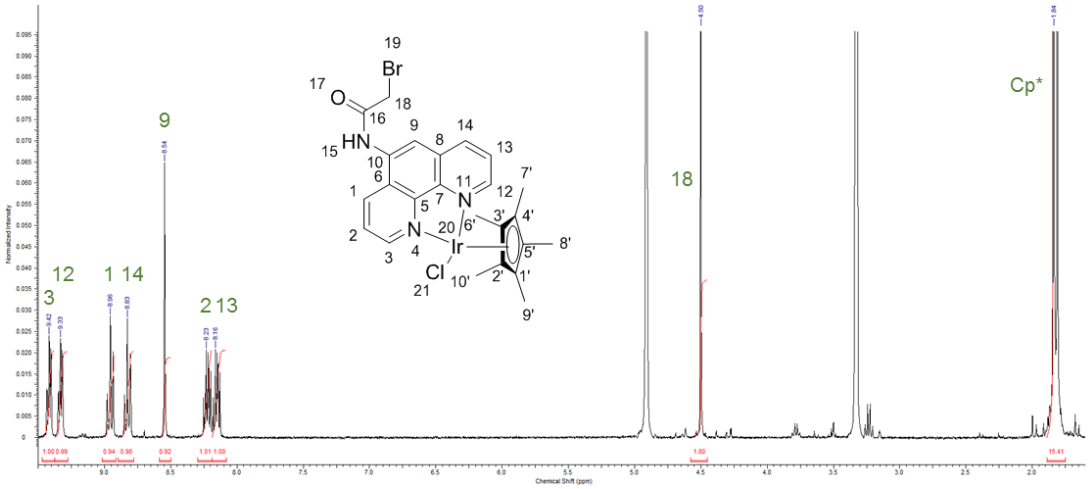
ESI-MS Cp*Rh(5-(2'-bromo)-acetamido-1,10-phenantrholine) chloride, **M3a**



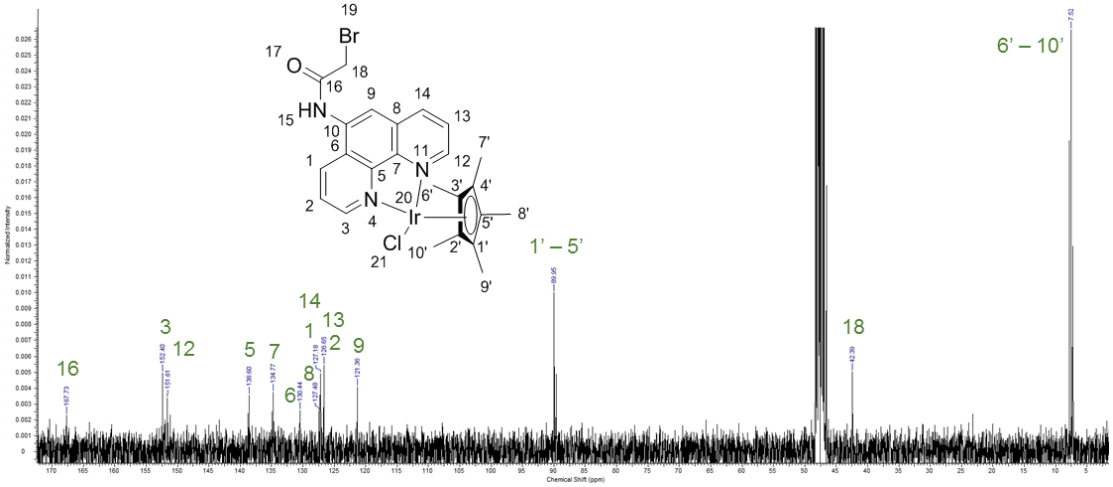
#	m/z	I %
1	102.1291	59.9
2	103.1316	4.0
3	239.2242	3.6
4	254.5365	7.8
5	272.0584	6.5
6	283.1740	5.0
7	285.1723	4.6
8	544.0424	3.0
9	570.0238	6.4
10	572.0239	5.8
11	587.9930	76.1
12	588.9949	17.0
13	589.9918	100.0
14	590.9938	22.7
15	591.9887	23.2
16	592.9918	5.2
17	631.9397	8.1
18	633.9386	17.7
19	634.9427	4.5
20	635.9390	8.0



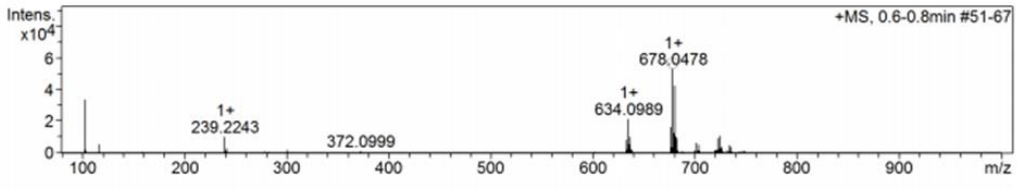
^{1}H NMR Cp*Ir(5-(2'-bromo)-acetamido-1,10-phenantrholine) chloride, **M3b**



^{13}C NMR Cp*Ir(5-(2'-bromo)-acetamido-1,10-phenantrholine) chloride, **M3b**

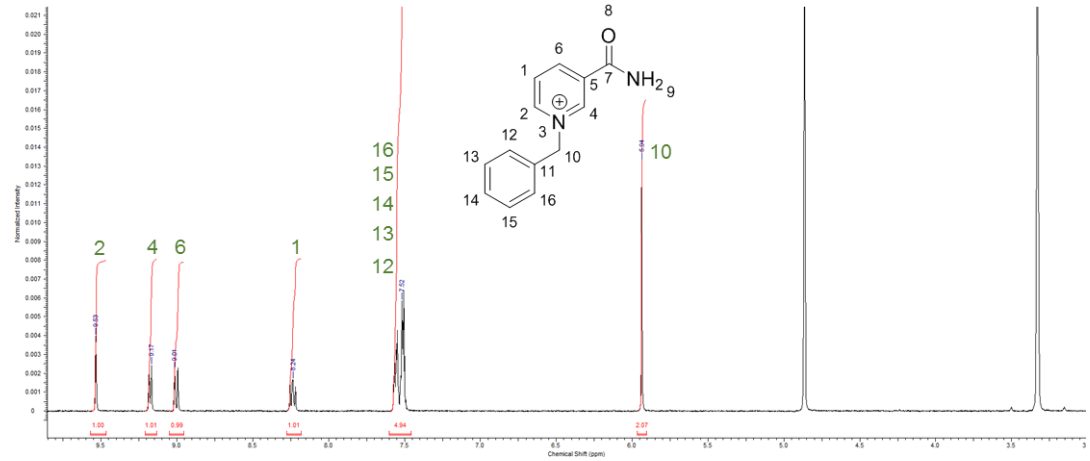


ESI-MS Cp*Ir(5-(2'-bromo)-acetamido-1,10-phenantrholine) chloride, **M3b**

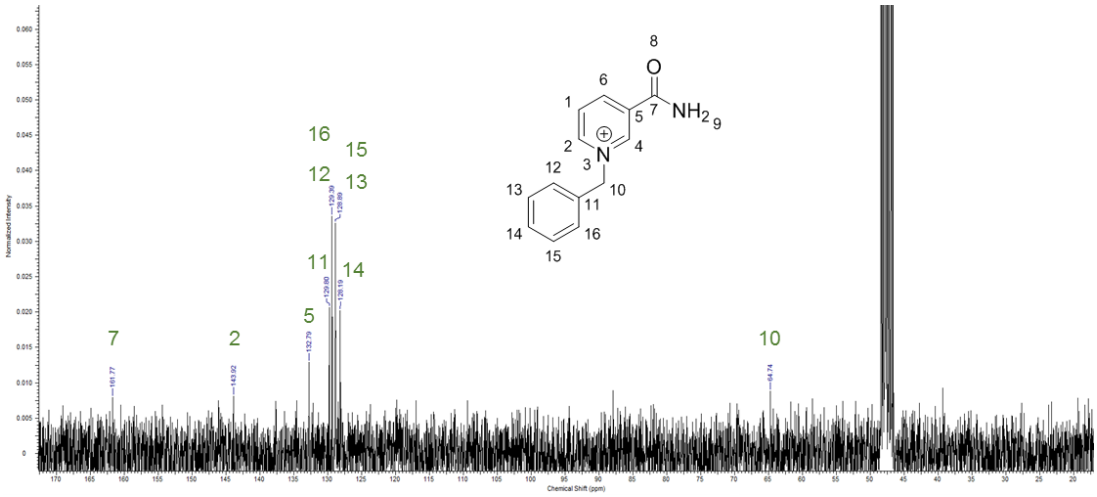


#	m/z	I %
1	102.1289	63.4
2	116.1187	10.5
3	239.2243	19.4
4	632.0979	15.7
5	634.0989	40.6
6	635.1013	10.7
7	636.0975	19.5
8	676.0497	30.9
9	678.0478	100.0
10	679.0522	24.4
11	680.0469	80.1
12	681.0495	20.1
13	682.0439	17.4
14	701.1689	12.3
15	703.1696	10.3
16	721.9950	17.7
17	723.9964	20.4
18	725.9927	7.4
19	733.1982	9.6
20	735.1983	7.5

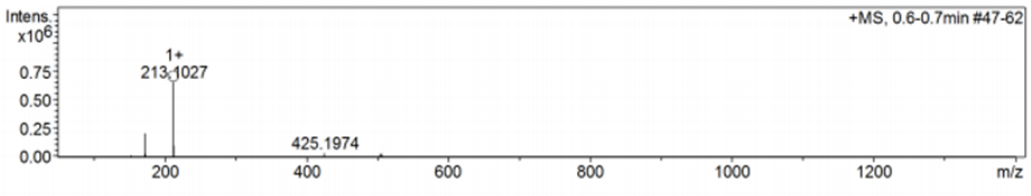
^{1}H NMR 1-benzyl-3-carboxamide-pyridinium, **150**



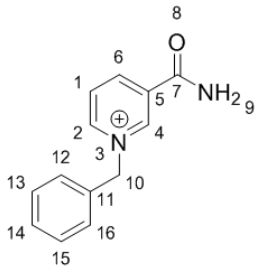
^{13}C NMR 1-benzyl-3-carboxamide-pyridinium, **150**



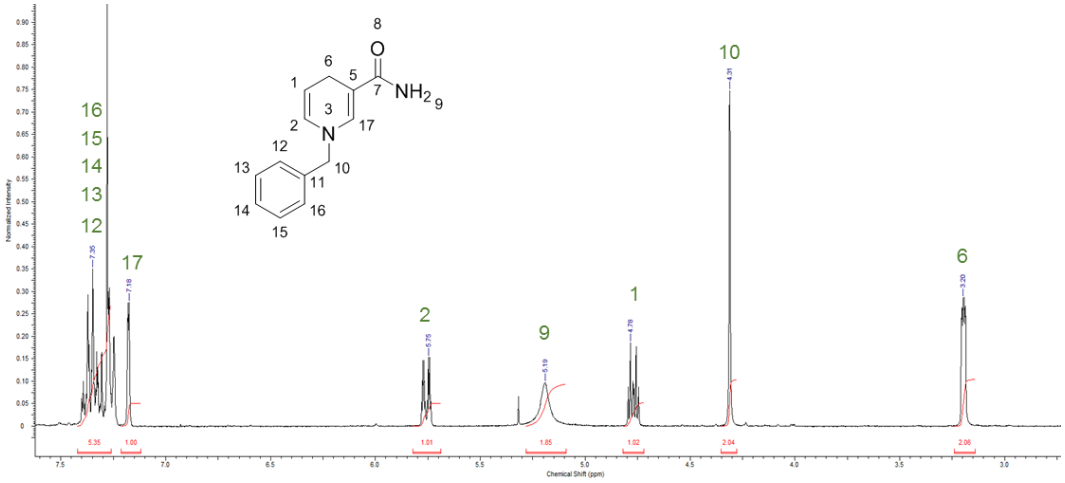
ESI-MS 1-benzyl-3-carboxamide-pyridinium, **150**



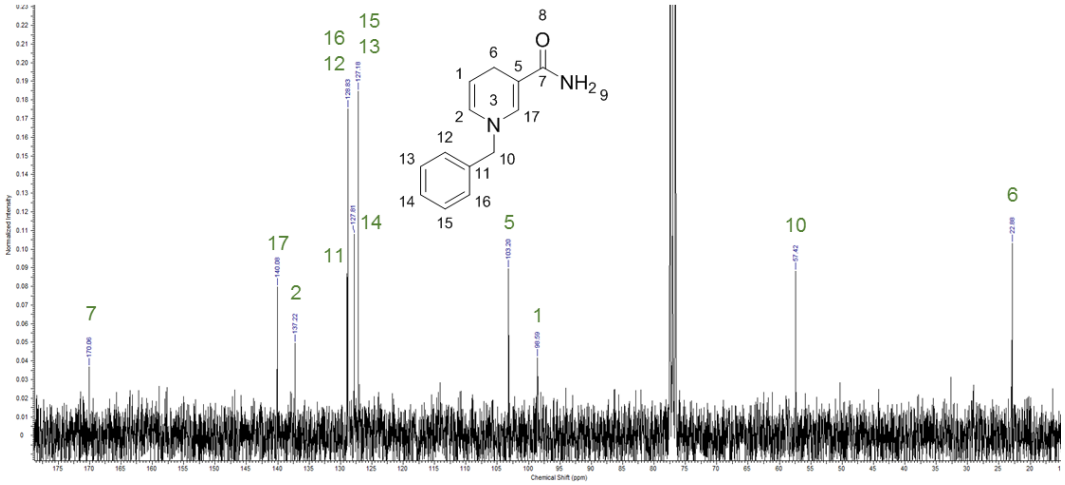
#	m/z	I %
1	153.1384	2.3
2	172.1807	31.7
3	173.1836	3.7
4	213.1027	100.0
5	214.1054	15.3
6	215.1082	1.3
7	225.1966	1.0
8	235.0846	1.5
9	242.2845	1.2
10	279.0932	0.7
11	425.1974	4.6
12	426.2005	1.5
13	447.1790	0.8
14	505.1230	4.5
15	506.1258	1.3
16	507.1212	4.5
17	508.1235	1.4
18	637.2927	1.2
19	717.2203	1.3
20	719.2194	1.4



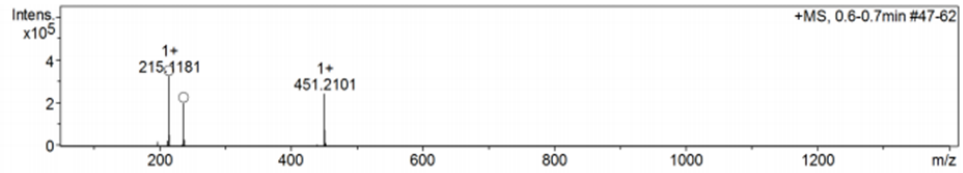
^{1}H NMR 1-benzyl-3-carboxamide-1,4-dihydropyridine, **151**



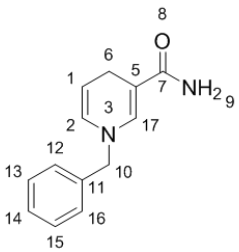
^{13}C NMR 1-benzyl-3-carboxamide-1,4-dihydropyridine, **151**



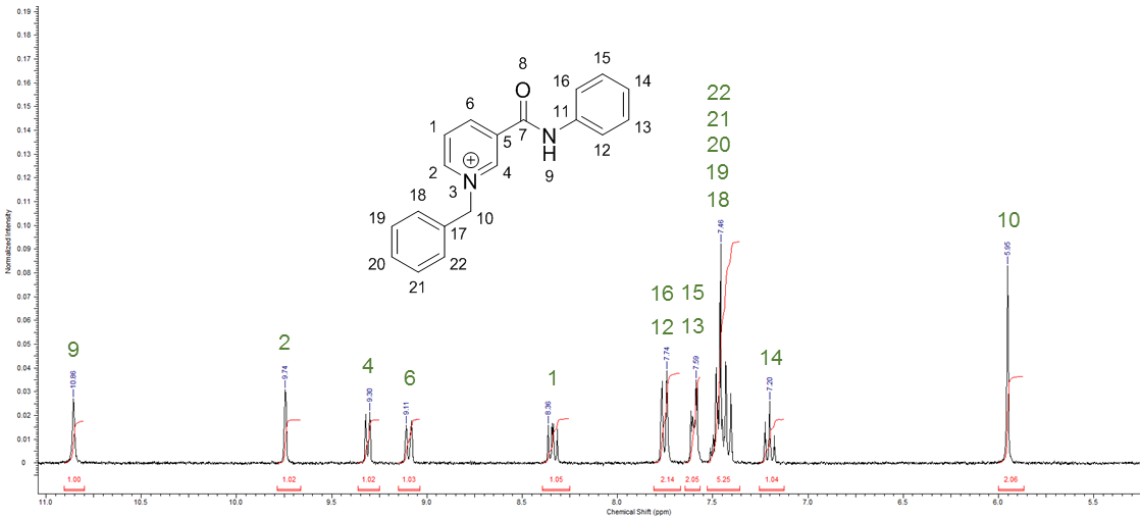
ESI-MS 1-benzyl-3-carboxamide-1,4-dihydropyridine, **151**



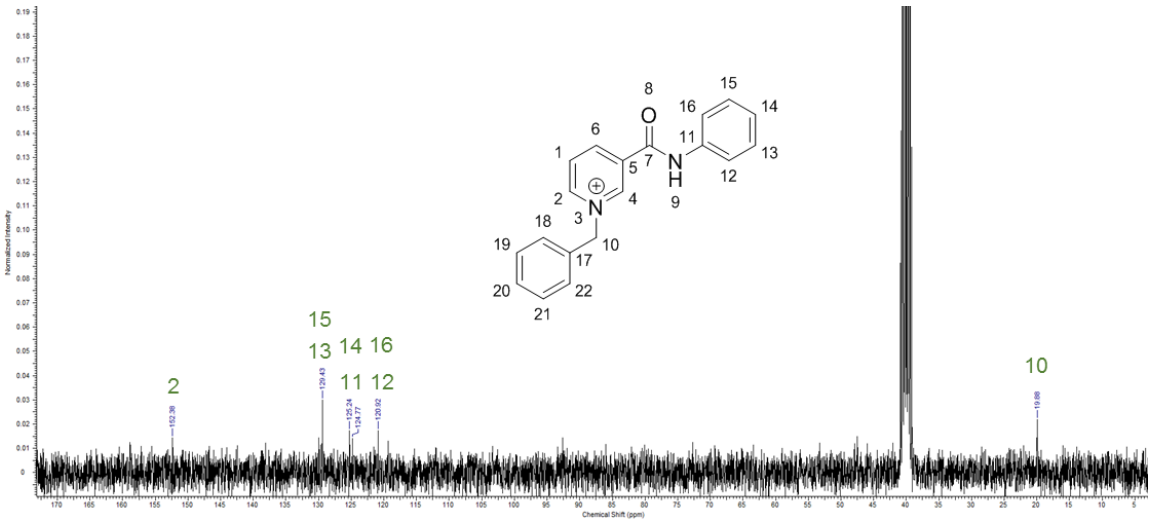
#	m/z	I %
1	198.0913	6.1
2	199.0944	0.9
3	213.1020	7.9
4	214.1050	1.4
5	215.1181	100.0
6	216.1210	15.7
7	217.1239	1.4
8	235.0839	1.8
9	237.1001	61.8
10	238.1031	9.4
11	305.0882	0.8
12	440.2124	1.8
13	440.7149	1.3
14	448.2018	1.5
15	448.7057	0.9
16	451.2101	74.8
17	452.2134	23.2
18	453.2156	3.8
19	497.1879	0.9
20	519.1961	1.1



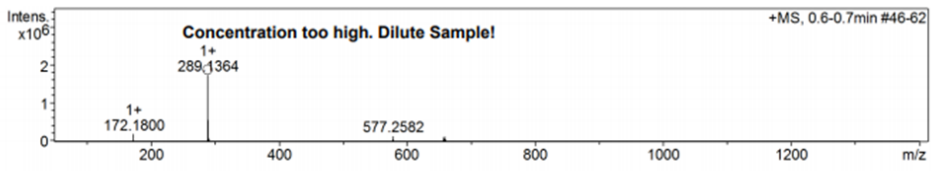
^{1}H NMR *N*-phenyl-1-benzyl-3-carboxamide-pyridinium, **155**



^{13}C NMR *N*-phenyl-1-benzyl-3-carboxamide-pyridinium, **155**

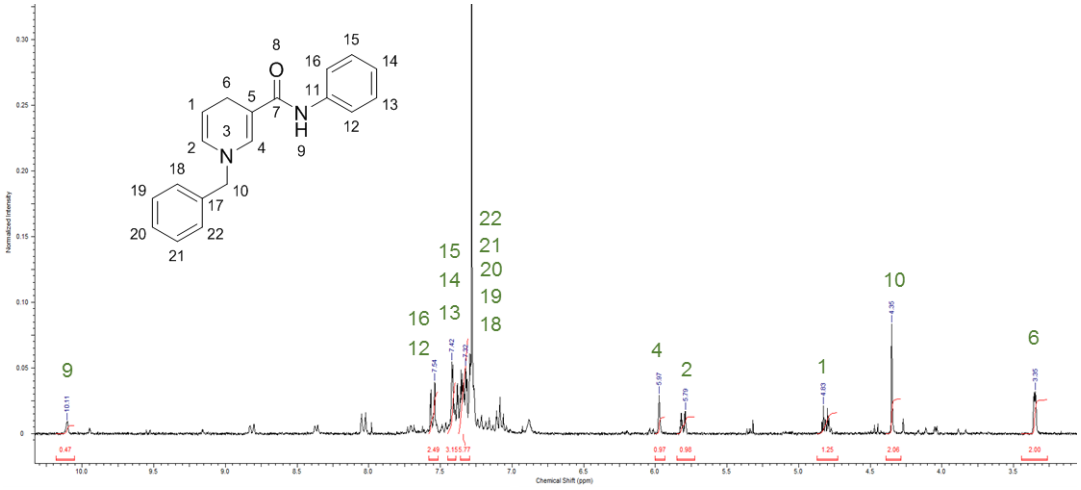


ESI-MS *N*-phenyl-1-benzyl-3-carboxamide-pyridinium, **155**

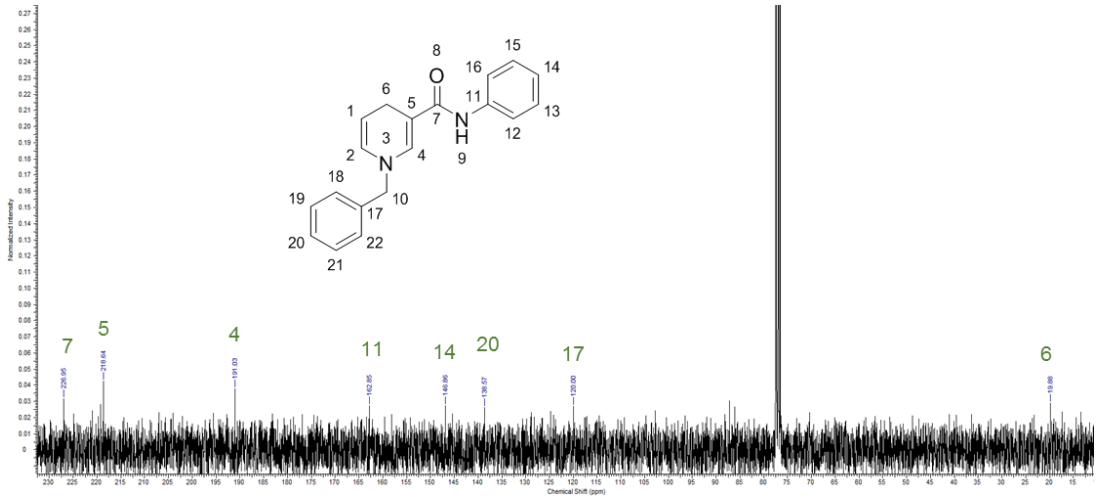


#	m/z	I %
1	153.1373	0.9
2	172.1800	10.9
3	173.1827	1.3
4	289.1364	100.0
5	289.3323	0.9
6	289.5246	0.7
7	289.9804	1.0
8	290.1372	32.0
9	291.1398	3.7
10	311.1157	1.2
11	379.1802	0.6
12	577.2582	7.6
13	578.2614	3.3
14	579.2644	0.7
15	599.2403	0.5
16	657.1848	6.4
17	658.1879	2.8
18	659.1838	6.7
19	660.1864	2.7
20	661.1901	0.6

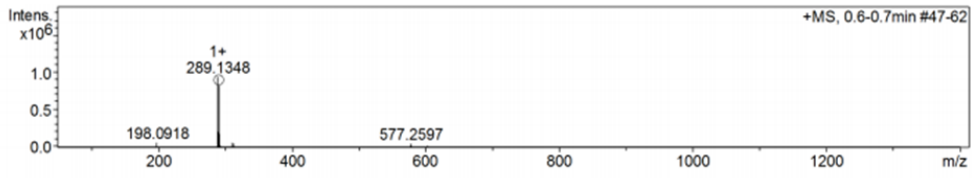
^{1}H NMR *N*-phenyl-1-benzyl-3-carboxamide-1,4-dihydropyridine, **156**



^{13}C NMR *N*-phenyl-1-benzyl-3-carboxamide-1,4-dihydropyridine, **156**



ESI-MS *N*-phenyl-1-benzyl-3-carboxamide-1,4-dihydropyridine, **156**



#	m/z	I %
1	198.0918	6.3
2	199.0944	0.9
3	289.1348	100.0
4	289.7074	0.3
5	290.1372	22.3
6	291.1497	88.0
7	292.1528	19.4
8	293.1560	2.2
9	311.1157	6.4
10	312.1191	1.4
11	313.1312	4.7
12	314.1343	0.9
13	577.2597	5.4
14	578.2625	2.3
15	579.2672	0.6
16	599.2415	1.2
17	600.2452	0.5
18	601.2549	0.4
19	603.2727	2.0
20	604.2764	0.8